

This item was submitted to [Loughborough's Research Repository](#) by the author.
Items in Figshare are protected by copyright, with all rights reserved, unless otherwise indicated.

Effect of osteonal microstructure on crack propagation: a computational study

PLEASE CITE THE PUBLISHED VERSION

PUBLISHER

Loughborough University

LICENCE

CC BY-NC-ND 4.0

REPOSITORY RECORD

Wang, Mayao. 2020. "Effect of Osteonal Microstructure on Crack Propagation: A Computational Study".
Loughborough University. <https://doi.org/10.26174/thesis.lboro.11822670.v1>.

Effect of Osteonal Microstructure on Crack Propagation: A Computational Study

By

Mayao Wang

A Doctoral Thesis

Submitted in partial fulfilment of the requirements for the award of

Doctor of Philosophy of Loughborough University

Oct 2018

© by Mayao Wang 2018

Abstract

Bone is a biological tissue with a highly hierarchical structure, playing a significant role in supporting body and protecting the organs. Ageing and degenerative bone diseases such as osteoporosis could cause a loss of bone mineral and change its micromorphology, leading to greater risk of fracture and limited functionalities. At micro-scale, cortical bone could be treated as natural composite material with four main constituents, namely, osteons, Haversian canals, cement lines and interstitial matrix. Changing the heterogeneous distributions of microstructural constituents alters local distributions of stresses and strains as well as propagation of cracks in case of fracture. Previous researches (Bernhard et al., 2013) on crack propagation in cortical bone focused on a relationship between the variation of micro-constituents and mechanical properties. However, a study of the effect of morphological variations originating from different population groups, including those affected by pathological conditions such as osteoporosis, on fracture resistance of cortical bone was not performed. Mechanical behaviour and crack-propagation characteristics for different population groups are still difficult to predict using experimental methods. Computational approaches including a cohesive-element (CE) method and an extended finite-element method (X-FEM) (Li, Abdel-Wahab, Demirci, & Silberschmidt, 2013a) are popular techniques for simulation of crack initiation/propagation thanks to their computational efficiency in modelling discontinuities and singularities in bone interior. However, the CE approach must define a single pre-path for crack propagation in the model while the standard XFEM-based technique used in commercial software cannot produce bifurcation and intersection of cracks and is limited to one crack per simulation domain, in contrast to real-life observations.

The aim of this PhD project is to investigate the effect of morphology and

mechanical properties of microstructural constituents on crack propagation in various groups of cortical bone by development and implementation of the improved cohesive-element method and a special MATLAB program.

Numerical models of cortical-bone tissues with randomly distributed microstructural constituents were developed for four groups including young, senior, diseased (osteoporosis) and treated. They were based on the data collected for osteonal morphometric parameters from experimental images produced with a dedicated MATLAB program. Another MATLAB program was also developed to insert cohesive elements at the edges of solid elements, so that the model could generate multiple cracks instead of a single crack. This MATLAB program was also adapted to calculate the crack lengths in various microstructural constituents of the cortical bone models. The mesh-sensitivity test and validation for the developed models of the cortical bone were implemented to guarantee the reliability of the simulation tools. In order to analyse the effect of morphology of microstructural constituents of the cortical bone, two kinds of loading condition including (i) uniaxial tension without notch and (ii) compact tension with a single notch were employed to assess the crack growth in the cortical-bone models. Mechanical properties of three microstructural constituents were changed in the developed models, to analyse their effect on crack propagation in the cortical bone models.

The results of this study demonstrated the importance of the micromorphology of cortical bones on crack-propagation process and the higher strain-energy release rate of the osteons. Meanwhile, the crack propagation in the cement lines and uncracked ligament bridging were two significant phenomena enhancing toughness of the cortical bone during crack growth.

Keywords: cortical bone, micromorphology, crack propagation, cohesive

element, multi-crack

Acknowledgements

During my PhD study, I must thank for the support and encouragement of my family and friends, because this journey was rather challenging. I don't know whether I could have completed my PhD study, if I don't have them in my life. But I still enjoyed my PhD study, because I was interested in my research topic and I believe that my study may improve the quality of life.

First and foremost, I would like to thank my supervisors Prof. Vadim Silberschmidt and Dr Simin Li for their patient and professional encouragement and guidance during my PhD study. Especially, I sincerely thank Prof. Vadim Silberschmidt for the understanding, encouragement, support and suggestions, thanks to his guidance I could complete this research. I also appreciate Dr Simin Li's support, especially the understanding of simulation methods. I am deeply grateful to Dr Qiang Liu for his patient help and the support with the Abaqus technique. With his help I could overcome many technique difficulties. I also thank Dr Xing Gao for his help with the random-structure generation.

Secondly, I would like to thank Jiahan Tang, Jianglong Guo, Tianyang Qiu and Yuchen Zhao for their help in my life in UK.

Last but not the least, I would like to gratefully thank my parents, Shunhua Wang and Lixin Zhang for their unconditional love, support and belief during the whole PhD journey. Without them, it is not possible for me to complete this research.

List of Publications

Journal Paper

Wang, M.¹, Li, S.¹, Scheidt, A. V., Qwamizadeh, M., Busseb, B., & Silberschmidt, V. V. (2019) Numerical study of crack initiation and growth in human cortical bone: effect of micro-morphology. *Engineering Fracture Mechanics*. (under review)

Conference papers

Wang, M., Zimmermann, E. A., Riedel, C., Busseb, B., Li, S., & Silberschmidt, V. V. (2017). Effect of micro-morphology of cortical bone tissue on fracture toughness and crack propagation. *Procedia Structural Integrity*, 6, 64-68.

Wang, M., Gao, X., Abdel-Wahab, A., Li, S., Zimmermann, E. A., Riedel, C. & Silberschmidt, V. V. (2015). Effect of micromorphology of cortical bone tissue on crack propagation under dynamic loading. In *EPJ Web of Conferences* (Vol. 94, p. 03005). EDP Sciences.

Li, S., Wang, M., Gao, X., Zimmermann, E. A., Riedel, C., Busseb, B., Silberschmidt, V. V. (2015). Fracture processes in cortical bone: Effect of microstructure. In: *Proceedings of the XLIII Summer School - Conference "Advanced Problems in Mechanics APM 2015"*, St. Petersburg, 22-27 June, 2015, St. Petersburg, 188-209.

Wang, M., Gao, X., Abdel-Wahab, A., Zimmermann, E. A., Riedel, C., Busseb, B., Silberschmidt, V. V. (2014). Effect of micromorphology of cortical bone tissue on crack propagation: XFEM analysis. In: *Micromech 2014. Advanced in Micromechanics of Materials. Book of Abstracts of the International Conference on Advances in Micromechanics of Materials*, 8-11 July 2014, Rzeszów, Poland. G. Mishuris, I. Sevostianov, F. Stachowicz (eds.). Rzeszów, 105-106. ISBN: 978-83-7199-942-9.

Wang, M., Gao, X., Abdel-Wahab, A., Zimmermann, E. A., Riedel, C., Busseb, B., Silberschmidt, V. V. (2015). Effect of micromorphology on crack growth in cortical bone tissue: X-FEM study. In: ICM12. Book of Abstracts, Karlsruhe Institute of Technology, 254.

Wang, M., Gao, X., S. Li, Zimmermann, E. A., Riedel, C., Busseb, B., Silberschmidt, V. V. (2015). Effect of micromorphology of cortical bone tissue on crack propagation under quasi-static and dynamic loading: X-FEM Studies. In: ICAM3D International Conference in Advanced Manufacturing for Multifunctional Miniaturised Devices, 3–4 June 2015, Loughborough, UK. Conference Proceedings, 99-100. ISBN 978-194327810-7.

Li, S., Wang, M., Gao, X., Zimmermann, E. A., Riedel, C., Busseb, B., Silberschmidt, V. V. (2015). Fracture processes in cortical bone: Effect of microstructure. In: XLIII International Conference “Advanced Problems in Mechanics APM 2015” Book of Abstracts, June 22-27, 2015, St. Petersburg, Russia, 99-100. ISBN 978-5-91753-103-8.

Li, S., Wang, M., Du, J., Silberschmidt, V. V. (2016) Computational analysis of fracture and healing processes in cortical bone tissue. In: Proc. of the 12th World Congress on Computational Mechanics & the 6th Asia-Pacific Congress on Computational Mechanics, 24-29 July 2016, Seoul, Korea, 586.

Li, S., Wang, M., Silberschmidt, V. V. (2018). Finite-element analysis of fracture toughness of bovine cortical bone: effect of osteonal micro-morphology. In: 22nd European Conference on Fracture - ECF22 Loading and Environment Effects on Structural Integrity. Book of Abstracts. Belgrade, Serbia, 26 - 31 August 2018. DIVK, Belgrade, 162.

Wang, M., Li, S., E.A. Zimmermann, Zimmermann, E. A., Riedel, C., Busseb, B., Silberschmidt, V. V. (2018). Effect of bone micromorphology on multiple crack propagation: Finite-element analysis. - In: Proceedings of the V Virtual Physiological Human conference VPH2018, 5-7 September 2018, Zaragoza, Spain, 119.

List of conferences

Mathematical and Computer Simulations in Mechanics of Solids and Structures (MCM) (2017).

8th International Symposium on Mechanics of Materials (2015).

8th International Symposium on Mechanics of Materials and Structures' summer school (2015).

Micromech 2014, Advanced in Micromechanics of Materials (2014).

12th International Conference on the Mechanical Behavior of Materials (ICM12) (2015).

International Conference in Advanced Manufacturing for Multifunctional Miniaturised Devices (ICAM3D) (2015).

XLIII International Conference "Advanced Problems in Mechanics APM 2015" (2015).

Proc. of the 12th World Congress on Computational Mechanics & the 6th Asia-Pacific Congress on Computational Mechanics (2016)

22nd European Conference on Fracture - ECF22 Loading and Environment Effects on Structural Integrity (2018).

Proceedings of the V Virtual Physiological Human conference VPH2018 (2018).

Contents

Abstract	I
Acknowledgements	IV
List of Publications	V
List of conferences	VII
Chapter 1- Introduction	1
1.1 Research background.....	1
1.2 Aim and objectives.....	2
1.3 Thesis outline and key findings	4
Chapter 2 Bone morphology.....	6
2.1 Introduction	6
2.2 Hierarchical structure of bone	6
2.2.1 Nanoscale.....	6
2.2.2 Microscale	9
2.2.3 Macroscale	11
2.3 Bone as a living material	15
2.4 Effect of age and disease on hierarchical structure of bone	18
2.4.1 Effect of age and disease on bone at nano-level	19
2.4.2 Effect of age and disease on bone at microscale	22
2.5 Summary.....	26
Chapter 3 Bone mechanics.....	27
3.1 Introduction	27
3.2 Anisotropic elastic properties of cortical bone	27

3.2.1 Elastic modulus of cortical bone.....	29
3.2.2 Poisson's ratio of cortical bone	30
3.3 Factors affecting elastic properties of cortical bone	31
3.4 Effect of age and disease on elastic properties of cortical bone.....	33
3.4 Fracture toughening mechanisms of cortical bone	36
3.4.1 Intrinsic toughening mechanism.....	36
3.4.2 Extrinsic toughening mechanism	39
3.4.3 Fracture toughness	42
3.5 Effect of age and disease on fracture toughness of cortical bone ..	44
3.6 summary	48
Chapter 4 Modelling of bone.....	50
4.1 introduction	50
4.2 Macroscale bone models.....	50
4.2.1 Elastic model.....	50
4.2.2 Viscoelastic model.....	51
4.3 Microstructure based model	54
4.4 Fracture mechanics based models of bone.....	59
4.4.1 Linear elastic fracture mechanics model.....	60
4.4.2 Cohesive model	60
4.4.3 Extended finite element method model	64
4.5 Summary.....	69
Chapter 5 Methodology for Finite Element Simulation.....	70
5.1 Finite element model setup	70

5.2 Cohesive element model generation process	71
5.3 Calculate the percentage of the crack length in microstructural constituents.....	75
5.4 Mesh sensitivity study	76
5.4.1 Uniaxial tension	77
5.4.2 Compact tension.....	81
5.5 Conclusion.....	85
Chapter 6 Simulation of crack initiation and growth in human cortical bone: effects of osteonal morphology	86
6.1 Introduction	86
6.2 Materials and Measurement	87
6.3 Model specification	92
6.4. Result and Analysis	93
6.4.1 Morphological variation	93
6.4.2 Mechanical properties.....	96
6.5 Discussion	108
6.6 Conclusion.....	111
Chapter 7- Effect of Micro-morphology of Cortical Bone Tissue on Fracture Toughness and Crack Propagation in Compact-tension Simulation	112
7.1 Introduction	112
7.2 Models generation.....	114
7.3 Results	116
7.4 Discussion	126

7.5. Conclusion.....	129
Chapter 8 Effect of Fracture Toughness of Micro-constituents of Cortical bone on Crack Propagation	130
8.1 Introduction	130
8.2 Methodology	132
8.3 Simulation Results	134
8.3.1 Effect of fracture toughness of interstitial matrix and osteon on initiation and growth slope of stress intensity factors.....	134
8.3.2 Effect of fracture toughness of interstitial matrix and osteon on fracture mechanics.....	140
8.4 Discussion	154
8.5 Conclusion.....	156
Chapter 9- Conclusions and future work.....	158
9.1 General conclusion	158
9.2 Future work.....	162
9.2 Limitations of the current work.....	165
References	166

Chapter 1- Introduction

1.1 Research background

The area of biomaterials such as bone increasingly attracts researchers in academia and industry. Bones have both unique biological and engineering features, being a natural material that differs from traditional engineering materials. In biological terms, bone is the main component of a human skeleton system. It is important for supporting and protecting organs of the body; producing red and white blood cells to transfer nutrition and provide resistance to viruses, and storing minerals for the whole body. In engineering terms, bone has a hierarchical structure and unique anisotropic and heterogeneous mechanical properties. Its unique structure provides human with sufficient support in their daily life.

According to the recent investigations, osteoporosis and age factors are the main reasons for bone fracture, influencing the quality of life. In UK, three million people suffer from osteoporosis. Accordingly, it is a common sense that a broken bone affects the life of a people; one in two women and one in five men aged over 50 suffers from it. Generally, a conventional treatment is to use medicine to restrain a bone resorption process to decrease a bone's material-losing rate. The mineral density of bone, assessed by dual-energy X-ray absorptiometry, is used to diagnose a bone health condition. However, this method is inadequate to predict fracture risk, because the loading capacity of bone is determined by its hierarchical structure that including osteons, Haversian canals, interstitial matrix and cement lines. Therefore, recent research was focused on bone fracture accounting for its hierarchical structure to evaluate the fracture risk exactly.

The experiment to detect the effect of osteonal microstructure of cortical bone on crack propagation is a method, but it could not be used to monitor the crack propagation during loading for fixed specific factors of morphology or mechanical properties to investigate their effects separately. Recently, a finite-element (FE) simulations method, including extended finite-element method (x-fem) and cohesive-element method (CE), has become popular in current research used for crack-propagation prediction for various materials. But the deficiencies of them restrict to generate the multiple cracks based on local strain or stress concentration in cortical bone.

To the author's knowledge, modelling of bones of different groups with multiple cracks is rarely researched. Accordingly, this study could increase the understanding of the effect of morphology of bone on its fracture in different groups.

1.2 Aim and objectives

Aim

The aim of this PhD project is to study the effect of osteonal microstructure of cortical bone, including micro-morphology and fracture toughness for various groups of patients (young, aged, diseased and treated) on the fracture process. The microstructural features of human cortical bone tissues were acquired from a project partner and were analyzed for the development of advanced, group-specific computational models of human cortical bone, including the random distribution and heterogeneous mechanical properties of its microstructure components. It is hoped that the result of this project will be used as a scientific tool to improve our understanding of the fracture process of bone tissue in various groups of people, and ultimately underpin future studies to reduce an

injury rate related to the bone fracture.

Objectives

The objectives of this PhD project are as follows:

1. To analyze micrographs of human cortical bone from different groups including young, aged, diseased and treated (obtained from a Germany partner), to evaluate the statistical features of spatial distribution of its microstructure and parameters of independent Haversian systems.
2. To develop the parametric finite-element models of different types of microstructural human cortical bone using a MATLAB program based on the obtained statistical data.
3. To develop a special cohesive-element method using a MATLAB program to generate random multiple cracks in microstructured cortical bone based on strain concentration
4. To test the mesh sensitivity and validate the developed numerical models
5. To simulate the fracture process of four studied types of human cortical bone without pre-notch but with the same mechanical properties of their constituents under uniaxial tension loading conditions using the developed advanced computational models.
6. To simulate the fracture process of different types of human cortical bone with a pre-notch and the same mechanical properties under corresponding to the test compact tension conditions using the developed advanced computational models.
7. To analyze the effect of mechanical properties of the bone constituents with

the same morphology of osteonal microstructure on the fracture process in human cortical bone with a pre-notch using the developed numerical tools.

1.3 Thesis outline and key findings

The present thesis consists of nine chapters and their outlines are as follow:

Chapter 2: Bone morphology

A literature review chapter is given to discuss the morphology of bone at various structural hierarchical levels and the effect of age and diseased on it.

Chapter 3: Bone mechanics

A literature review chapter focuses on the mechanical properties of bone at various length scales and the effect of age and diseased on them.

Chapter 4: Modelling bone

A literature review chapter presents different modelling techniques used to simulate the fracture process in bone.

Chapter 5: Methodology

In this chapter, the process used to develop a MATLAB program for generation of the finite element model, insertion of cohesive elements into the edges of finite element and detection of the crack length under loading. The mesh-sensitivity test and the validation of the developed model employing previous experimental results is also presented.

Chapter 6: Simulation of crack initiation and growth in human cortical bone: effects of micro-morphology

This chapter introduces the effect of micro-morphology of osteonal

microstructure of cortical bone on crack initiation and growth under uniaxial loading conditions without a pre-notch. The results demonstrate and quantify the difference of micro-morphology of osteonal microstructures in four groups including young, senior, diseased and treated. The characteristics of osteonal microstructure of the young group allows it to have tough mechanical behaviour.

Chapter 7: Effect of micro-morphology of cortical bone tissue on fracture toughness and crack propagation in compact-tension simulation

In this chapter, a pre-notch was inserted into the developed models of four group's bones. The R-curve results of compact-tension models of four groups showed that the characteristic features of the osteonal microstructure of the young group resulted in more crack attracted by the cement lines and uncracked-ligament bridging that could toughen the cortical bone.

Chapter 8: Effect of fracture toughness of osteonal microstructure of cortical bone on fracture behaviour

In this chapter, the effect of fracture toughness of osteonal microstructure of cortical bone on fracture behaviour was investigated with the same models but with various levels of fracture toughness of constituents of osteonal microstructure. The R-curve results demonstrated that the higher fracture toughness of the osteons could improve the quality of cortical bone.

Chapter 9: Conclusion and future work

The conclusion and future work of this thesis are introduced in this chapter.

Chapter 2 Bone morphology

2.1 Introduction

The skeleton system, which is composed of bone tissue, cartilages, ligaments and other tissues, is significant for the human. Especially, the characteristic of hardness and rigidity of the bone tissue could support the human body, facilitate movement, and protect the internal organs. Bone tissue as a biological material could also store the healing cells, repair the damaged area and change the mass, shape and properties to adapt to various situations (S. Cowin & Telega, 2003). These mechanical and biological functions are caused by the complex and hierarchical structure of bone.

Therefore, this chapter focuses on the detail of hierarchical structure, cell biology of bone and the effect of age and disease on the bone to understand how they provide the structural and biological functions.

2.2 Hierarchical structure of bone

2.2.1 Nanoscale

At nanoscale, bone is composed of an organic matrix, mineral phase and water.

Mineral

Hydroxyapatite crystals is the basic unit of bone mineral. These nanocrystals comprise approximately 65% of bones mass (S. Cowin & Telega, 2003) and 33-43% of bone volume (Olszta et al., 2007). The mineral phase provided strength and stiffness of bone. Therefore, the bone mineral density (BMD) test is a traditional method to predict deterioration and fracture risk of bone. The size of mineral is controversial because of the different measurement techniques. At the

early stage, the transmission electron microscopy (TEM) and small angle X-ray scattering were applied to measure the dimensions of crystal. The lengths, widths and thickness of plate-shaped crystal are approximately 40-60 nm, 20-30 nm and 1.5-4 nm, respectively (P. Fratzl et al., 1992; Wachtel & Weiner, 1994; Ziv & Weiner, 1994). While the minerals had larger dimensions measured by the atomic force microscopy (AFM) or small and wide angle X-ray scattering, that the width and length were approximately 30-350 nm (Hassenkam et al., 2004; Tong et al., 2003; Turunen et al., 2016). Schwarcz et al. (2014) employed dark-field TEM to measure the dimensions of mineral crystal. The lengths, widths and thickness of plate-shaped crystal were approximately 28 nm, 5.8 nm and 5-6nm, respectively.

Organic matrix

Organic matrix is composed of mainly type-I collagen (90%) and small amounts of non-collagenous proteins (10%). It occupies approximately 35% of the total mass (S. Cowin & Telega, 2003) and 32–44% of bone volume (Olszta et al., 2007). The collagen matrix contributes to the ductile and fracture toughness of bone. Collagen molecules, called tropocollagen, are group together in a quarter-staggered arrangement forming collagen fibril with 80-100 nm in diameter (Garnero, 2015). The quarter-staggered arrangement results in 40 nm periodic gaps (Landis et al., 1993). The mineral crystal inside the collagen fibrils is called intra-fibrillar mineral, while it coating the collagen fibrils is called extra-fibrillar mineral (Fig.2.1). The osteopontin, sialoprotein, osteonectin, and osteocalcin are the components of non-collagenous proteins. Non-collagenous protein serves as important regulators of bone mineralization process (Boskey et al., 1998; Poundarik et al., 2011) and acts as 'glue' to bond the mineral and collagen together (Boskey et al., 1998; Hang et al., 2014). Some studies reported that

non-collagenous protein was an essential role in toughness of bone (Poundarik et al., 2015; Wang et al., 2018).

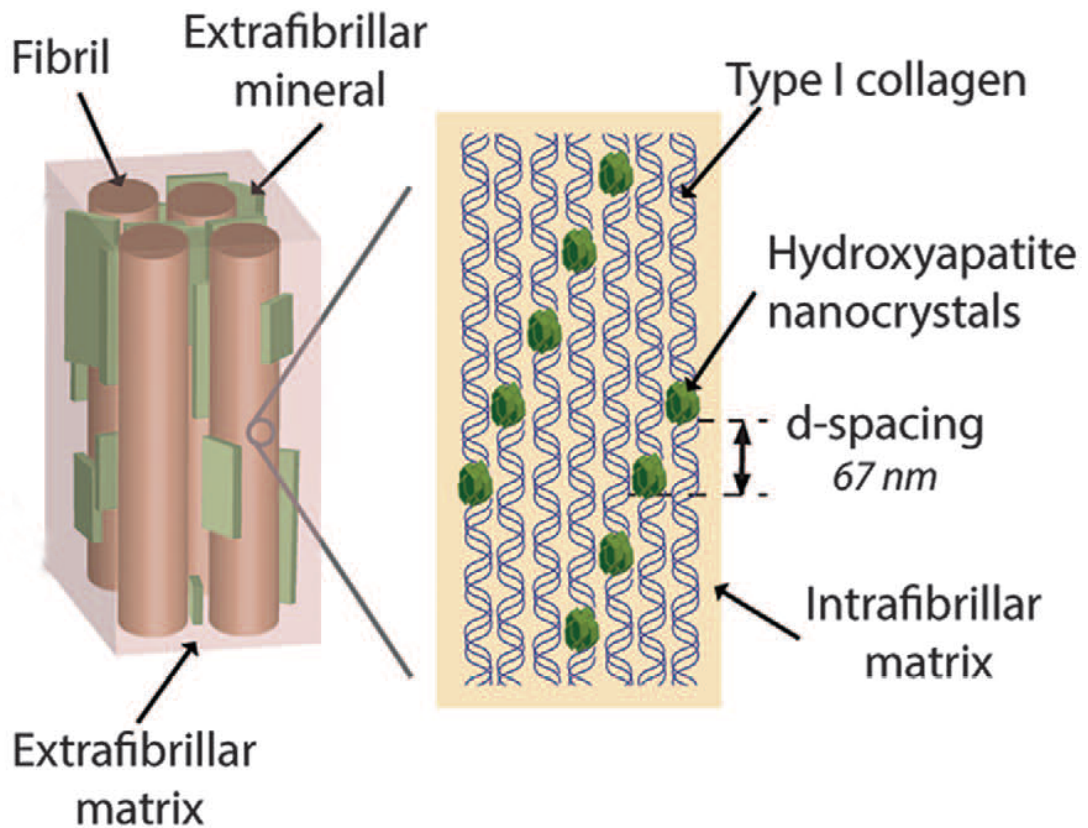


Figure 2.1. Schematic illustration of the structure of collagen fibrils (Zimmermann et al., 2015).

Water

Water located within collagen fibrils is an essential component of bone tissue. It takes up to about 15-25% of bone volume (Olszta et al., 2007). Water is either loosely bound between collagen (Bella et al., 1995; Brodsky & Persikov, 2005) and mineral phases or chains of tropocollagen (Davies et al., 2014). It contributes to the ductility or plasticity of bone (Currey, 2012).

2.2.2 Microscale

At microscale, lamellae and lacunae. Lamellae is a sheet-like structure with approximately 3-7 μm in thickness. It is composed of highly organized collagen fibrils bundles and apatite crystals (Currey, 2003). In lacunae, osteocyte, a kind of bone cell, are located inside it. The cells in bone could communicate with each other via canaliculi.

According to the lamellae organization manner, the cortical bone could be divided into osteon (Haversian system), interstitial matrix and Circumferential lamella (Fig.2.2).

Osteon

Osteon with about 200-300 μm in diameter and up to 100 in length, forms from lamella arranging into concentric cylinders along the main axis of the bone. The Haversian canal with 50-90 μm in diameter is inside the center of the osteon's and parallel to the bone's main axis. The channels inside osteon, normally perpendicular to the bone's central axis is called Volkmann canals, for communication of Haversian canals (Tobergte & Curtis, 2013). Both two types of channel contain blood vessels and nerves system inside it. Osteon has a lower stiffness comparing with the surrounding matrix. Because osteon in bone needs long time (months or even years) to complete mineralization, it is a less mineralized constituent in bone. (Currey, 2012). But it acts as a barrier responsible for protecting the blood vessel from crack destroying by keeping the perimeter of the canal (Mohsin et al., 2006; Wagermaier et al., 2015). The cement line with about 2-5 μm in thickness surrounds osteons as a layer separating the interstitial matrix and osteon. The cement line appears in the Haversian system when the osteoclast has completed the erosional activity and before new osteon

is implanted into the raw surface. The functions and components of the cement line are not clear. At early study, cement line was a mineral deficit structure but with amounts of sulfur by back-scattered electron imaging (BSE) and X-ray microprobe analysis (Schaffler et al., 1987). On the other hand, Skedros et al. (2005) had opposite results that the cement lines were actually a mineral rich and collagen deficient structure. In addition, in Skedros et al. (2005) and McKee & Nanci (1996) study, the cement lines had non-collagen protein such as osteopontin, glycosaminoglycans, osteocalcin, so that it had local adhesive and modulus mismatch function. The latest results from Milovanovic (2018), presented that the cement lines are the hypermineralized structure with consistently higher calcium content than their corresponding osteons based on quantitative backscattered electron images results. The cement line was a significant structure for bone to deflect a crack from osteons or promote the crack initiation from it (Rho et al., 1998 and Sabet et al., 2016).

Interstitial matrix

The matrix lied between osteons is called interstitial matrix, which consists of remnants of old osteonal or circumferential lamella. Interstitial matrix has a similar lamellar structure to that of the osteon, but it is a higher mineralised lamellar structure comparing with osteon (Jae Young Rho et al., 1998).

Circumferential lamella

Circumferential lamellae could be found at the outer or inner of cross-section of bone tissue. The circumferential lamellae are responsible for bone growth on specific surfaces (Shea & Miller, 2005).

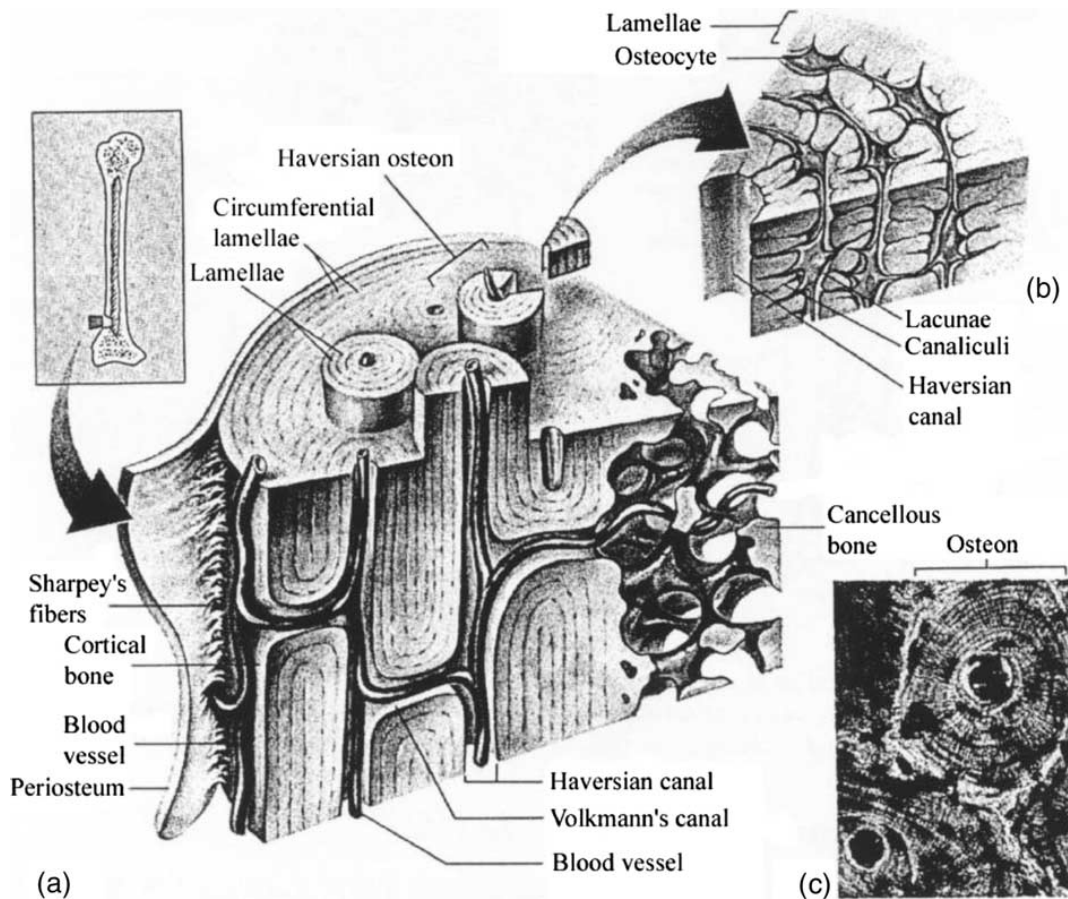


Figure 2.2. Microstructures of cortical bone. (a) 3D sketch of cortical bone, (b) one piece of a Haversian system, (c) Haversian system under microscopy (Doblaré et al., 2004)

2.2.3 Macroscale

At macroscale, from the macroscopic point of view, a long bone can be divided into cortical bone and trabecular bone that could be distinguished according to their porosity.

Trabecular bone, also called cancellous or spongy bone, has more porosity (75-95%) than that of cortical bone (Jee, 2001). It could be found in cuboidal bones, flat bones and at the ends of long bones. The pores of trabecular bone are interconnected and filled with marrow. In trabecular bone, the lamellae assemble into trabeculae which are in the form of rods or struts. Trabecula consists of trabecular packets which have a crescent shape and are about 50 mm thick and

1 mm long (Jasiuk et al., 2015). Its soft structure could be for shock absorption and joint connection.

On the other hand, the porosity of cortical bone or called compact bone is approximately between 5%-10% (Jee, 2001). Cortical bone could be found at the exterior surface and the diaphysis. The cortical bone has osteon, interstitial matrix and circumferential matrix according to the lamella organization manner in the previous section. Its primary function is responsible for bearing the loading of the body and maintains the movement of the human because of its rigid structure, so it is greatly significant for human in the daily life. Cortical bone has a lower metabolic rate per unit of volume comparing with trabecular bone, which will change significantly due to bone mineral density losing.

From the histological point of view, bone can be divided into woven bone and lamellar bone characterized by the orientations of fibril bundles.

Woven bone

Woven bone is characterized by randomly oriented fibril bundles (Fig 2.3). It could be found in embryonic bones and fracture callus (Wagermaier et al., 2015). It forms from static osteogenesis, that the immovable stationary osteoblast rapidly deposit osteoid in all direction (Ferretti et al., 2002). This process results in the random arrangement of the fibril bundles. The rapid growth rate makes woven bone weak, but it allows bone in animals to have fast growth and fixed the fracture site. Also, woven bone is substituted by lamellar bone through remodelling process (Zhang et al., 2012).

Lamellar bone

Lamellar bone has a plywood structure, consists of multiple parallel layers (lamella) (Fig. 2.4). The fibril bundles are oriented in same direction in each

lamella, while, the orientations of them are different between adjacent lamella (Wagermaier et al., 2015; Weiner & Wagner, 1998) This unique structure makes the lamellar bone are considered as asymmetry material that it has better stiffness and toughness in various directions than that of the woven bone. The osteoblasts slowly move on the osteogenic surface and deposit osteoid to form the lamellar bone. Lamellar bone can be formed by the remodelling of pre-existing bone (Wagermaier et al., 2015).

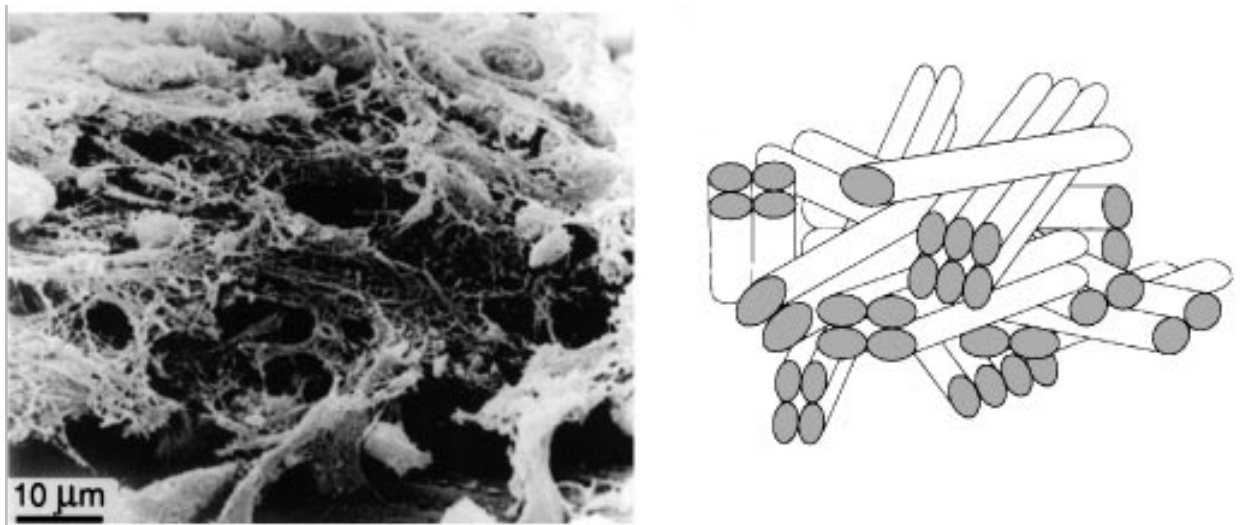


Figure 2.3. Images and lamella arrangement of woven bone (Weiner & Wagner, 1998).

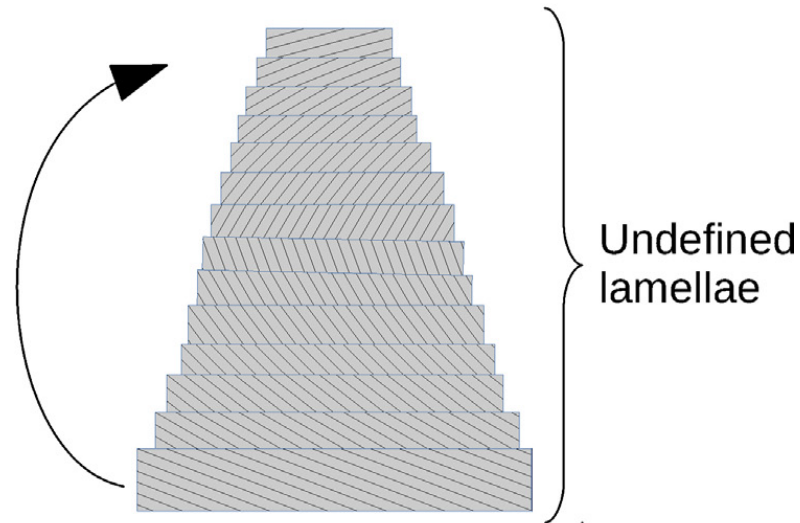


Figure 2.4. Twisted plywood model of lamellar bone (Mitchell & van Heteren, 2016).

Fibrolamellar

Fibrolamellar bone also called plexiform bone or laminar bone is found particularly in large mammals or need fast growth animals, such as bovine and ovine, while it sometime could be found in humans. It forms around the blood vessels on the periosteal surface of the bone. Then, a thin layer of porous and hypercalcified bone (transition area) grow close to the plexiform area. Finally, porous bone is slowly replaced by lamellar bone. This process results in the sandwich-like structure of bone (Fig. 2.5) (Barrera et al., 2016; Currey, 2012; Hillier & Bell, 2007). Fibrolamellar bone has a fast growth rate (about 80-100 μm per day) that is satisfied with the necessity of large and fast-growing animals (Barrera et al., 2016). However, fibrolamellar bone with a brick-like configuration of structural units is stronger bone comparing with the lamellar bone when loaded along the longitudinal direction. While it is weak bone when loaded on the other directions (Currey, 2003).

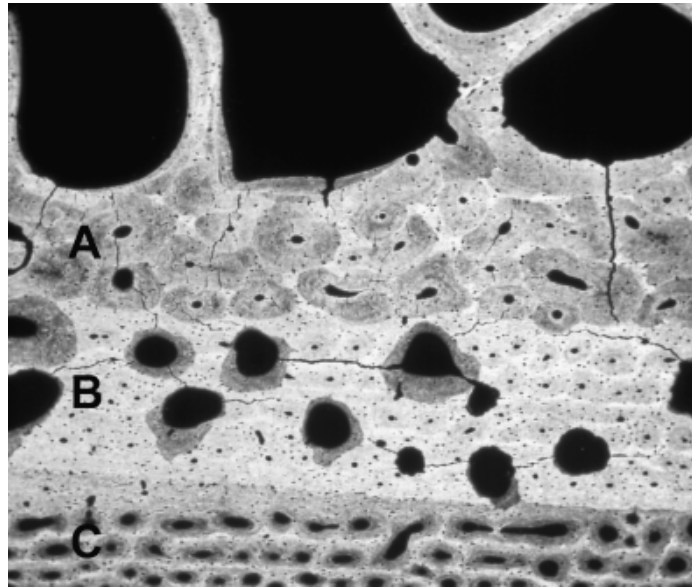


Figure 2.5. Backscattered electron image illustrating types of sheep cortical bone. (A) Haversian bone (endosteal zone), (B) transition area between Haversian bone and plexiform bone (mesosteal zone), (C) plexiform bone (periosteal zone). Field width: 2.5 mm (Hillier & Bell, 2007).

2.3 Bone as a living material

The hierarchical structure of bone results in that bone as a biological material has either mechanical functions or physiological functions. Three different functions of bone are as following:

Mineral homeostasis: Bone stores calcium, phosphate, sodium and magnesium inside it. These ions are responsible for blood clotting, nerve impulse transmission and chemical signalling.

Hematopoiesis: The void in the centre of long bones, called intramedullary canal, stores marrow which generate the red blood cell for the body.

Mechanical: Bone protects vital internal organs such as brain and heart, and transmits the force between segments for mobility of body.

Bone is a living material that is continuously undergoing remodelling and repair. Bone remodelling occurs throughout adult life and relies on the coupled and balanced processes of bone formation and resorption. This process will take 90-130 days to fix the fracture area (Ishtiaq et al., 2015). It maintains skeletal integrity that bone's cells resorb and replace the fracture area. Every basic multicellular unit (BMU) performs in this process, including osteoblasts, osteoclasts, bone lining cells and osteocytes (Fig.2.6).

Osteoblasts has forty days of a life span. It is a significant cell to form the bone matrix. When osteoblasts reach the end of their functional life, they may become osteocytes and lining cells, or they may die (Muschler et al., 2004). The periosteum layer or stromal tissue of bone marrow generate the osteoblasts.

Osteocytes forms from osteoblast which stops secreting osteoid and become osteocyte in the newly forming bone. The short axis of each lacuna is oriented parallel to the thickness of the lamella (Currey, 2003). Osteocytes are considered as the mechanosensor cells that could regulate the bone remodelling process (Cowin et al., 1991; Lanyon, 1993).

Osteoclasts are huge multinucleated cells. It has a function that could resorb old or damaged bone. The bone marrow generates osteoclast, which could be found on the surface of the cortical bone or trabecular bone or within cortical bone. Osteoclasts secrete acids and proteolytic enzymes, which could dissolve mineral salt and digest the organic matrix of bone (Muschler et al., 2004).

Bone lining cells also form from osteoblast not buried in new bone. They could be found on the surface when bone formation is completed but they could be reactivated by chemical signal and mechanical stimuli.

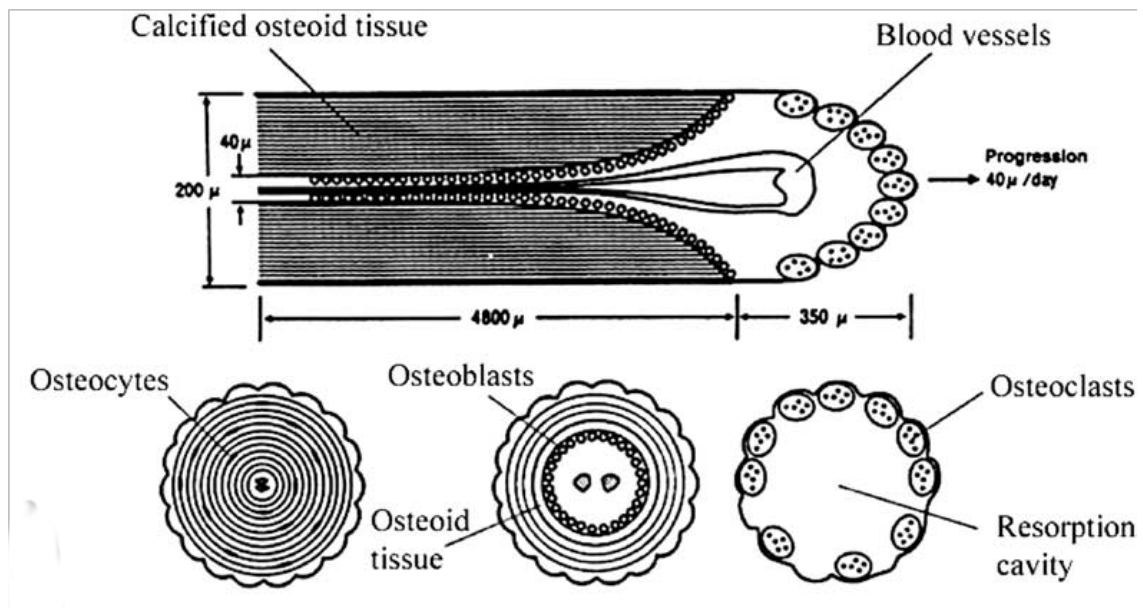


Figure 2.6. Cells in cortical bone during the remodelling process in cortical bone (Muschler et al., 2004).

The remodelling process could be divided into three processes including resorption, reversal and formation. At the early stage, the osteocytes die at the area of micro-damage and provide signal for the remodelling process on the fracture surface. The partially differentiated mononuclear pro-osteoclasts moves to the bone surface and then they become multinucleated osteoclasts. After the completion of resorption, there is a reversal phase when mononuclear cells appear on the bone surface. These cells provide the signals for differentiation and migration of osteoblast and create the surface for osteoblast to begin bone formation. After osteoblast laying down the bone, the bone formation phase launches until the resorbed bone is replaced by the new bone. When the formation phase is complete, osteoblasts become osteocyte and lining cells or may die. The stages of bone remodelling have different lengths. Resorption phase probably lasts for about two weeks. The reversal phase may take up to four or five weeks. The formation process needs the most extended times (4 months) until the new bone is completely formed (Hadjidakis & Androulakis, 2006;

Ishtiaq et al., 2015).

2.4 Effect of age and disease on hierarchical structure of bone

Both the quantity and quality of the human bone begin to deteriorate after reaching peak bone mass with age (Heaney et al., 2000). Some bone diseases also have a similar effect on the bone, such as Paget's disease, osteogenesis imperfecta and osteoporosis (Ishtiaq et al., 2015). The deterioration of bone enhances the risk of fracture, which influence the daily life of the human.

Paget's disease increases bone remodelling, bone hypertrophy and abnormal bone structure. The bones with Paget's disease have the high bone density and bone size, but this kind of bone has a high risk of bone fracture. The speed of remodelling process is increased, so the bone does have organized collagen fibres instead of the woven bone with poor mechanical properties. (Garnero, 2015).

Osteogenesis imperfecta is a disease that affect both mineralized and non-mineralized tissue of the bone. Osteogenesis imperfecta results in a decrease of bone formation. The low bone mass and trabecular thickness could be observed in the bone with this disease (Rauch et al., 2000).

Osteoporosis is the most common bone disease in humans. It is a major public health problem. Osteoporosis could result in the wrist, hip and vertebra fracture. Over 3 million people suffer from this disease in the UK and more than 500000 people have bone fragility fractures due to osteoporosis every year (NHS, 2015). This disease could result in the low bone mass, deterioration of bone tissue and disruption structure (Cosman et al., 2014). The prevalence of osteoporosis in the human will increase with age and women have a higher risk of osteoporosis than men (NHS, 2015). The dual-energy X-ray absorptiometry (DXA) could be used

to diagnose the osteoporosis based on measuring the mineral density (BMD) of bone. The bone with low mineral density results from a remodelling imbalance that the resorption rate is higher than the formation rate caused by the osteoporosis. A common treatment for osteoporosis is a class of drug called bisphosphonates which could inhibit bone resorption.

2.4.1 Effect of age and disease on bone at nano-level

Age and disease affect the bone at nano-level by various factors in different components, including mineral phase (mineral content and crystal size), collagen phase (collagen content and collagen crosslinks) and water (water bound).

Mineral phase

In the early stage, the bone mineral density in aged and osteoporotic cortical bone attracted the researchers. The patients with osteoporosis have lower bone mineral density, therefore, whether the bone mineral content or bone mineral density change with age was studied in the early stage. Laval (1983) measured the bone mineral density of cortical bone. The results presented that the bone mineral density decreased with age. But Hui et al. (1988) tested 521 women cortical bone (age from 45 to 80 years). In this paper, there was no evidence that age would increase or decrease bone mineral content. In addition, McCalden (1993) tested 235 cortical bone specimens (age from 20 to 102 years). The author did not find the correlation between mineral content and ageing. Then, Currey (1996) continued to study the effect aging on the mineral content which has a positive relationship with age, but the large overlap in bone mineral content existed between young and age group (25-80 years). In this paper, The age group had a large range in bone mineral density. The quantitative backscattered electron was also used to study the bone mineral density of four kinds of human

cortical bone, such as young, aged, osteoporosis and treated (bisphosphonate treatment). The authors showed that the young and aged groups had higher bone mineral density than that of the osteoporotic and treated groups, while there was no significant difference between young and aged group (Milovanovic et al., 2015). As a result, it was not clear whether age could affect the bone mineral density or bone mineral content. The changes in mineral crystal size with age and disease were also investigated. Burnell (1980) and Holden (1995) used X-ray diffraction method to tested the rat and human bone's mineral crystal size and concluded that the crystal size increased with age. Fratzl et al. (1991) compared the sizes of the mineral crystals of young and old rat bone by using small-angle X-ray scattering method. The thickness of mineral crystal could increase to 3 nm with age increasing. However, the study (Simmons, 1991) presented that age could not affect the size of the mineral crystal. Milovanovic et al. (2014) used atomic force microscopy to analyse the osteoporotic and healthy old bones. The size of mineral crystal in the osteoporotic bone was larger than that of the healthy old bone. In conclusion, the bone mineral density and mineral crystal size measurement are two good methods to identify the health and diseased cortical bone, whereas, the relationship between bone mineral phase and age is still not clear.

Collagen phase

The collagen contents in aged and diseased bone were interesting topic to be investigated. At early stage, the collagen content significantly decreased with age (20-100 years) (A. J. Bailey et al., 1999). In addition, Mitsuru et al. (2006) pointed out that the total collagen contents of bone increased with age (0-20 years), while it significantly decreased with age (over 20 years). However, Wang et al. (2002) pointed that there was a significant difference of collagen contents between the

young bone (19-49 years) and the middle aged bone (50-69 years); The elderly bone (over 70 years) had no difference comparing with other two kinds of bones. Silva et al. (2006) measured the collagen contents in normal and osteoporotic mouse bone. The collagen content of the osteoporotic bone was lower than that of the normal bone.

Enzymatic crosslinks and non-enzymatic crosslinks as bonds could connect the collagen molecules or fibrils together (Bailey et al., 1998). Some studies (Gourion-Arsiquaud et al., 2009; Wang et al., 2002; Zioupos et al, 1999) demonstrated that the enzymatic crosslinks in age and young bone stay at a constant level. However, Zioupos et al. (1999) found that the non-enzymatic glycation, resulting in the formation of non-enzymatic crosslinks, significantly increase with age. The similar results showed that the content of non-enzymatic crosslinks significantly increased with age (Odetti et al., 2005). The results from Saito et al. (1997) indicated that the content of non-enzymatic crosslinks in bone with 50 years of age was four to ten higher than that in bone with ten years of age. In terms of osteoporotic bone, this diseased bone had lower enzymatic crosslinks and higher non-enzymatic crosslinks than that of the healthy bone (Oxlund et al., 1996; Mitsuru et al., 2006; Mitsuru et al., 2006). However, the bone samples in these studies were trabecular bone.

The collagen contents of the healthy and diseased bone are significantly different. It relates to the mineral content influenced by the increasing age but the relationship between these two parameters is still unclear, while the non-enzymatic crosslink increased with the increasing age or disease.

Water

Nuclear Magnetic Resonance (NMR) is utilized to measure the mobile water and bound water in cortical bone. Pore water is in microstructure such as Haversian

canal, canaliculi and lacunae. While bound water is in a nanostructure to glue collagen and mineral (Nyman et al., 2008) . Nyman (2008) found that the young bone (21- 55 years) had less bound water, but there was slightly increase in the amounts of pore water with age (41-105 years) in human cortical bone (Fig.2.7) The reduction in bound water with age also could be found in rat bones(Uppuganti et al., 2016).

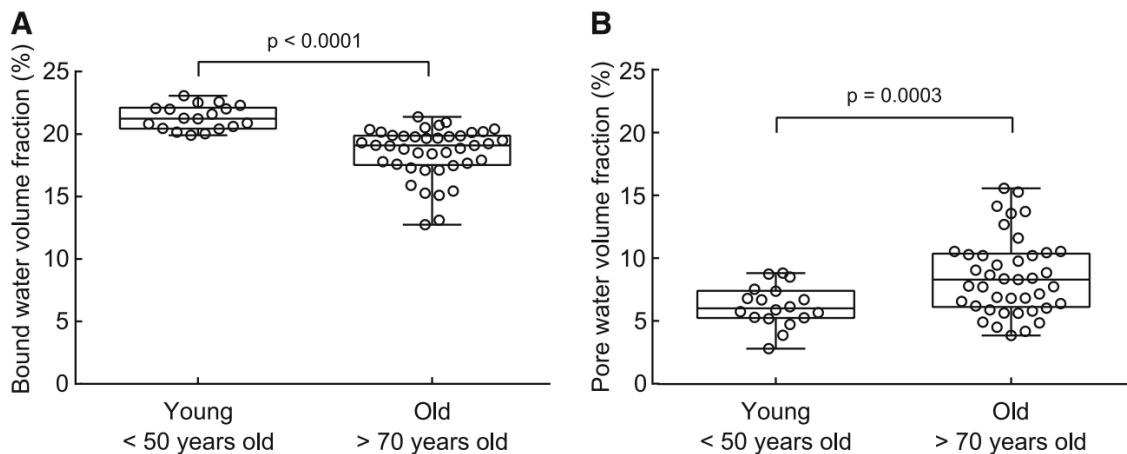


Figure 2.7. Bound water per bone volume (A), Pore water per bone volume (B): young (n=18, 21-51 years), old (n=41, 70-105 years) (Nyman et al., 2008).

2.4.2 Effect of age and disease on bone at microscale

Age and disease could change the characteristics of microstructure in bone, including the volumetric fraction and features of porosity and osteon, which reflecting the imbalance remodelling process. The imbalance remodelling process of age and disease is that the resorption rate is higher than the formation rate (Karen L. Bell et al., 2001; Parfitt, 1998).

Porosity

The porosity of bone significantly increases because of age and disease. McCalden (1993) analysed the micro-image of cortical bone's cross-section to

investigate the change in the porosity with age. There was a marked increase in porosity with age for female bone. The young bone might have smaller osteon than that of the aged bone. The nuclear magnetic resonance was employed to study the change in the porosity of cortical bone due to age. This technique could measure the volume of porosity. The volume fraction of porosity significantly increased with age in this study (Wang & Ni, 2003). The change in the area of porosity with age was also introduced by Bousson et al. (2001) and Thompson (1980). The mean value of the area of porosity had a positive correlation with age and there was more large porosity exist in old bone. The giant canal in the cortical bone is called resorption cavity caused by the uncontrol of osteoclast resorbing the osteon (Parfitt, 1998). The percentage of the resorption cavity increased with age in female cortical bone, while there was no significant difference in male cortical bone (Karen L. Bell et al., 2001). The osteoporosis bone had more extra large canals (172-385 μm) and giant canal (over 385 μm) in the anterior and inferior region of cortical bone than of the healthy old bone (K. L. Bell et al., 1999). Therefore, the age and disease result in the large volumetric fraction of porosity, particularly the giant canal in cortical bone.

Osteon

In 1974, Black et al. (1974) measured the size of osteon on the cross-section of cortical bone. The results presented that the area of the Haversian canals and osteons increased with age. However, the results studied by Evans (1976) and Britz et al.(2009) showed that the young bone had larger osteons comparing with the old bone. In addition, Evans (1976) pointed out that the area of osteonal bone and interstitial matrix decreased with age. The size of osteons in the osteoporotic bone was studied by Bell et al. (2000). The results indicated that the osteoporotic bone had a large number of composite osteons (comprised of several osteons)

while small osteonal bone area. In recent study, Bernhard (2013) divided the people into four groups, such as young group, aged group, osteoporotic group and bisphosphonate group, to quantify the difference of Haversian system between each group. The results presented that the young group had the largest diameter of osteon ($233.14 \pm 23.25 \mu\text{m}$) and the lowest size of Haversian canal ($56.03 \pm 10.17 \mu\text{m}$) in the four groups. The bisphosphonate group had the higher diameter of osteon ($215.78 \pm 20.38 \mu\text{m}$) than that of the osteoporotic group ($179.7 \pm 15.35 \mu\text{m}$) and slightly higher values than that of the old group ($193.35 \pm 10.98 \mu\text{m}$)(Fig 2.8). In conclusion, aged and diseased bones have the smaller osteon areas than that of the young group.

The nanostructure and microstructure of bone could be influenced by age and diseased as introduced in previous sections. In previous study, the characteristics of porosity and osteon were investigated by using various test methods. However, there is still a lack of data of osteonal morphology in four groups, including young group, aged group, diseased group (osteoporosis) and treated group (bisphosphonate), to establish the statistical simulation models. The cortical bone models with microstructural constituents, including osteons, cement lines, Haversian canal and interstitial area, could be utilized to study the mechanical behaviour of bone.

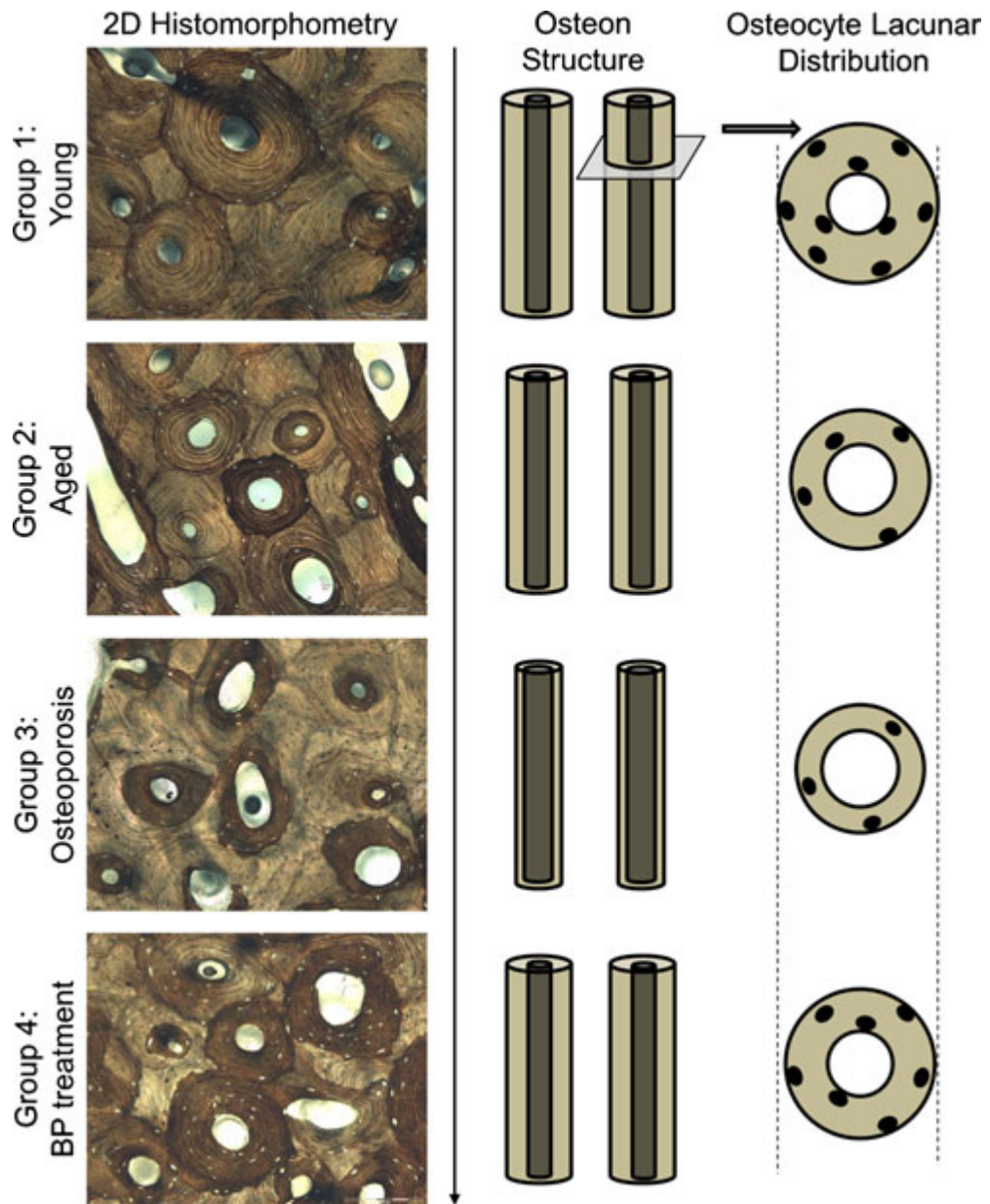


Figure 2.8 Microscopic images with schematic presentation of the osteon structure and lacunar distribution of femoral cortical bone in young, aged, osteoporosis, bisphosphonate-treatment (Bernhard et al., 2013).

2.5 Summary

- In order to understand the mechanical and biological functions of bone. It is important to study its hierarchical structure at various level.
- Bone as a living material has mechanical and biological functions. The remodelling process of bone could maintain the skeleton integrity by ever basic multicellular unit.
- The cement line is an interface between osteon and interstitial matrix. Its functions in fracture behaviour are still required to investigate.
- The imbalance remodelling process caused by age and disease could influence the hierarchical structure of bone.
- Age and disease could change the nanostructure and microstructure, including mineral phase, collagen matrix, water, porosity and osteon.
- The data of microstructure of bone in four groups, including young group, aged group, diseased group and treated group, is not enough to establish a statistical simulation model.
- Therefore, it is necessary to investigate the characteristics of osteonal microstructure of cortical bone in the different group to improve the computational models.

Chapter 3 Bone mechanics

3.1 Introduction

The cortical bone provides the mechanical support and protection of the body. The failure of cortical bone could influence the daily life. The mechanical properties of cortical bone are important parameters to present the quality and predict the risk of cortical bone fracture. The complex hierarchical structure of cortical bone results in its unique mechanical properties. The mechanical properties of cortical bone were influenced by the many factors, such as gender, species, age and health condition. Especially, age and disease could change the hierarchical structure of cortical bone to increase the risk of bone fracture.

Therefore, in order to understand the effect of age and disease on mechanical properties due to the change of hierarchical structure, the mechanical properties and fracture mechanisms of cortical bone will be illustrated in detail.

3.2 Anisotropic elastic properties of cortical bone

A long bone has two parts, including the diaphysis and the epiphysis. The diaphysis of bone mainly contains cortical bone, while the epiphysis of bone mainly contains trabecular bone. In this chapter, the cortical bone at the diaphysis of a long bone is the research target. Cortical bone is composed of collagen fibres and mineral crystals, which are arranged along the long axis of the bones. This unique structure leads to the orientation dependent mechanical properties of cortical bone (Hasegawa et al., 1994; Sasaki et al., 1989). The anisotropic properties in terms of its elastic properties of cortical bone were measured in a number of studies (Currey, 2012; Dong & Guo, 2004; Evans, 1976; Li et al., 2013; Reilly & Burstein, 1975). Figure 3.1 presents the schematic illustration of three

principal directions of cortical bone, including longitudinal, radial and circumferential directions. In general, the cortical bone could be considered as a transversely-isotropic material, because the elastic properties of circumferential and radial directions are similar in many studies (Ashman et al., 1984; Pithioux et al., 2002; Reilly & Burstein, 1975). The osteonal remodelling process is important role in anisotropic material of cortical bone that this process could change bone from orthotropic into transversely isotropic material (Weaver, 2002). At macroscale, the elastic properties of cortical bone in different directions were measured by uniaxial tension testing or ultrasonic testing (Dong & Guo, 2004; Pithioux et al., 2002; Reilly & Burstein, 1975; Yoon & Lawrence Katz, 1976). The results presented that the elastic properties of the longitudinal direction were higher than that of the transverse direction. At microscale, the nanoindentation technique is a popular method to measure the mechanical properties of microstructure constituents of cortical bone (Abdel-Wahab et al., 2011; Fan et al., 2002; Franzoso & Zysset, 2008; Hofmann et al., 2006; Rho et al., 2001). Fan et al. (2002) measured the elastic properties of human cortical bone by the nanoindentation technique. There were 96 samples based on the angles (0° - 90°) from tibial cortical bone. The elastic modulus of osteon and interstitial matrix in longitudinal direction were higher than that of other directions. It is important to research the mechanical properties of cortical bone in circumferential or radial directions, because the cortical bone in these two directions were easier to fail than that of the longitudinal direction.

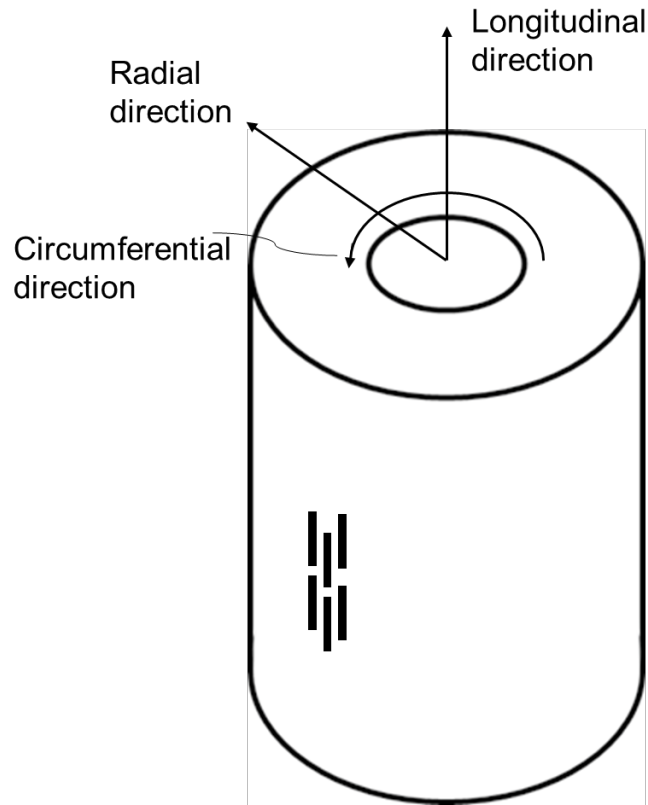


Figure 3.1 Schematic illustration of three direction of cortical bone

3.2.1 Elastic modulus of cortical bone

The elastic modulus or called Young's modulus is the basic mechanical parameter to describe the stiffness of the material. It could be obtained by the slope in the linear region of the stress-strain curve. The elastic modulus of cortical bone were investigated in many studies by the different testing (Ashman et al., 1984; Dong & Guo, 2004; Reilly & Burstein, 1975; Rho, 1996; Knetts, 1977), which were summarized in Table 3.1. The results demonstrated that the elastic properties of human cortical bone were varied, even at the same location, and the testing method used to measure the cortical bone differed. Therefore, the elastic properties of human cortical bone show variability which might depend on many factors.

Table 3.1 Elastic modulus of human cortical bone in longitudinal and transverse directions

Elastic modulus, GPa	Orientation	Bone type	Method	Reference
18.3±4.6	Longitudinal	Human femur	Tension	(Reilly & Burstein, 1975)
14.1±3.4	Transverse			
20.0	Longitudinal	Human femur	Ultrasonic	(Ashman et al., 1984)
12.0	Transverse			
18.7±0.1	Longitudinal	Human tibiae	Tension	(Knets ,1977)
8.7±0.1	Transverse			
20.7±1.9	Longitudinal	Human tibiae	Ultrasonic	(Rho, 1996)
11.2±1.3	Transverse			
16.61±1.83	Longitudinal	Human femur	Tension	(Dong & Guo, 2004)
9.55±1.36	Transverse			
19.411±2.445	Longitudinal	Human tibiae	Tension	(Vincentelli & Grigoroy, 1985)

3.2.2 Poisson's ratio of cortical bone

The Poisson's ratio is the ratio of contraction in transverse direction, to expansion in loading direction. It could be measured by ultrasonic technique or strain gauge glued on specimen during tensile test. Table 3.2 summarizes the Poisson's ratio in previous studies.

Table 3.2 Poisson's ratio of human cortical bone

Poisson's ratio	Bone type	Method	Reference
0.51±0.18	Human femur	Mechanical	(Reilly & Burstein, 1975)
0.376	Human femur	Ultrasonic	(Ashman et al., 1984)
0.307±0.004	Human tibiae	Mechanical	(Knets ,1977)
0.231±0.035	Human tibiae	Ultrasonic	(Rho, 1996)
0.37±0.03	Human femur	Mechanical	(Dong & Guo, 2004)

3.3 Factors affecting elastic properties of cortical bone

In previous section, the wide range of elastic properties of human cortical bone was introduced. Bone as a natural material could not have consistent mechanical properties as the engineering material. Its mechanical properties could be influenced by many factors including species, gender, age and healthy condition. For example, the elastic modulus of bovine cortical bone were from 21.9 to 22.6 GPa in longitudinal direction, which were higher than that of human cortical bone (Lang, 1970; Reilly & Burstein, 1975; Buskirk et al., 2009). Because the bovine has a unique microstructure called plexiform bone, which could provide the higher elastic modulus and ultimate strength in longitudinal directions to withstand the weight of bovine (Currey, 2012). Apart from previous factors, the different anatomic positions of the cortical bone had various mechanical

properties in the previous research. Rho (1996) measured the elastic properties of human tibial cortical bone at the four anatomic positions by ultrasonic technique, including anterior, posterior, lateral and medial positions. The elastic modulus of cortical bone at the posterior position in transverse and longitudinal directions were 12.2 ± 1.2 and 21.2 ± 1.6 GPa, respectively, which were higher than that of three positions. Lai et al. (2005) measured the bone mineral density of cortical bone at different anatomic positions using a highly accurate multislice pQCT. The bone mineral density at the posterior position was 1923 ± 135.3 mg/cm³ which explained the reason of the cortical bone at the posterior position with the highest elastic modulus. The elastic properties of bovine cortical bone at four anatomic positions were also investigated by Li et al. (2012). The results of elastic modulus at four anatomic positions were presented in Fig 3.2. In addition, the author pointed that the fraction of microstructural constituents could influence the elastic modulus of cortical bone. Therefore, it is interesting to investigate the effect of these factors on the mechanical properties of the cortical bone.

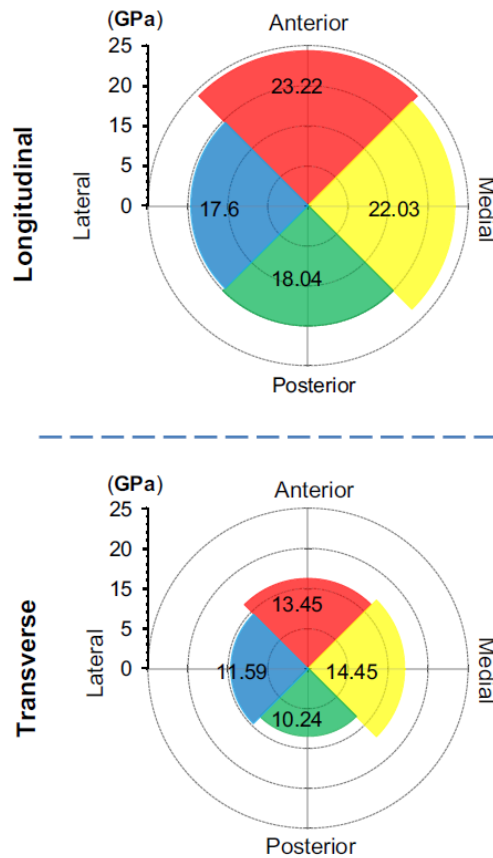


Figure 3.2. Elastic modulus of bovine cortical bone at four anatomic positions in longitudinal and transverse direction (Li et al., 2012).

3.4 Effect of age and disease on elastic properties of cortical bone

Age and disease could influence the hierarchical structure of cortical bone at both microscale and nanoscale which are introduced in the previous sections. In early works, the effect of age and disease on elastic properties of cortical bone was studied by the mechanical test. The elastic properties of human cortical bone were measured by Reilly & Burstein (1975). The elastic modulus of young bone (23-31 years) was higher than that of aged bone (41-71 years). The samples of human cortical bones were divided into three age groups based including young (19-49 years), middle-aged (50-69 years) and elderly (over 70 years). The young group had the maximum elastic properties, which was 11.5 ± 1.99 GPa, while the

elastic modulus of middle-aged and elderly were 11.1 ± 0.78 and 10.7 ± 1.34 GPa. The results presented that age could decrease the elastic modulus of cortical bone (X. Wang et al., 2002). Currey (1998) found a linear relationship between elastic modulus and age that the elastic modulus of bone would decrease with age. However, Wall et al. (1979) and McCalden et al. (1993) did not find the relationship between age and elastic modulus of cortical bone. The osteoporotic cortical bones of human femur were compared with the normal one by tension test. The elastic modulus of osteoporotic and normal bone were 11.55 ± 4.17 and 15.69 ± 2.15 GPa, respectively and the ultimate strength of them were 95.1 ± 33.8 and 117.0 ± 17.3 MPa (Dickenson et al., 2018). The reason that the elastic properties of cortical bone change due to age and disease is attracted with many researchers to investigate based on hierarchical structure of cortical bone.

The bone mineral density is a crucial factor that could influence the elastic properties of cortical bone. Schaffler & Burr (1988) found that the elastic modulus of cortical bone had a power correlation with bone mineral density using tension test. The relationship between elastic modulus and bone mineral density could be by the equation $E = 89.13A^{3.91}$, where E is elastic modulus and A is bone mineral density. The study of elastic modulus of cortical bone by using four points bending test (Keller et al, 1990) also reemphasized the Schaffler & Burr's results. In addition, the results in this study presented that the ultimate strength of cortical bone had a linear correlation with bone mineral density. These results could explain the reason of aged and diseased bone (low mineral density bone) with the low elastic properties.

At microscale, the characteristic of porosity of cortical bone, including fraction and diameter was studied in the early works. The fraction of porosity significantly increased with age (Bousson et al., 2001; McCalden, McGeough, et al., 1993;

Thompson, 1980; Wang & Ni, 2003). In addition, the change of bone remodelling process of cortical bone due to age and disease resulted in the large cavity (Bell et al., 1999; Bell et al., 2001; Parfitt, 1998). Katz et al. (1984) showed that the osteoporosis could result in the large porosity of cortical bone which decreased the elastic modulus of cortical bone. The relationship between elastic properties of cortical bone and porosity in the different aged groups were investigated in a few studies (Dong & Guo, 2004; Martin, 1993; Mitchell B. Schaffler & Burr, 1988; Wachter et al., 2002). Currey (1988) and Schaffler & Burr (1988) found the power law correlation between elastic modulus and porosity that the increase of porosity could decrease the elastic modulus of cortical bone. Dong & Guo (2004) proposed the linear relationship between elastic modulus and porosity. Apart from porosity, the osteons and the interstitial matrix are two main microstructural constituents in cortical bone. The elastic modulus of microstructural constituents in human cortical bone, including osteon and interstitial matrix in longitudinal (Rho et al., 1999; Rho et al., 1997; Zysset et al., 1999) and transverse directions (Abdel-Wahab et al., 2012; Budyn & Hoc, 2010; Mirzaali et al., 2016; Wang et al., 2006) were investigated by using the nanoindentation technique. In those study, the interstitial matrix was stiffer than the osteon. The elastic modulus of cortical bone was calculated using formulas based on the volumetric fraction and elastic properties of microstructure constituents in few studies (Hamed et al., 2010; Li et al., 2013b). A modified Voigt-Reuss-Hill average scheme was applied to calculated the elastic modulus of bovine cortical bone based on the volumetric fraction of microstructural constituents, including osteon, interstitial matrix and porosity (Li et al., 2013b). The results had a good agreement with the experimental one.

As a result, the elastic properties of cortical bones are changed due to age and disease. Because age and disease could influence the hierarchical structure of

cortical bone that the aged and osteoporotic cortical bone had the low bone mineral density and the high fraction of porosity. Apart from those two factors, the fraction of osteon and interstitial matrix are also significant to predict the elastic modulus. Therefore, the investigation of hierarchical structure of cortical bone is significant and necessary to study the elastic properties of cortical bone in different groups,

3.4 Fracture toughening mechanisms of cortical bone

The fracture mechanism of cortical bone could improve its ability of fracture resistance to improve the quality. The fracture mechanism of cortical bone could be divided into intrinsic toughening mechanism and extrinsic toughening mechanism, which was concluded by Launey et al. (2010) in Fig 3.3. The intrinsic toughening mechanism are responsible for the crack initiation and the ahead of a crack. They are molecular uncoiling and intermolecular sliding, microcracking and fibrillar sliding at sub-microscale. The extrinsic toughening mechanisms are responsible for the behind crack tip, such as constrain microcracking, crack deflection and twisting, uncracked ligament bridging, collagen fibril bridging.

3.4.1 Intrinsic toughening mechanism

Intrinsic toughening mechanisms caused by the macular structure and sub-microstructure, improve bone's inherent resistance to microstructural damage and cracking, which is important in the crack initiation and the ahead of a crack (Launey et al., 2010). There are several types of intrinsic toughening mechanism, including molecular uncoiling, fibrillar sliding of mineralized collagen fibril, fibrillar sliding of collagen fibre arrays and microcracking, introduced as following:

Molecular uncoiling: In collagen fibrils, molecular stretching connects with

intermolecular sliding and breaking of weak and strong bonds between tropocollagen molecules. The tropocollagen molecules could have large deformation (up to 50% tensile strain), but it will not break (Gautieri et al., 2009). This ability of tropocollagen provides the basis of plastic deformation mechanism. The H-bonds, also called Hydrogen bonds or water bonds, connects collagen with mineral at nano-level and is important for large and permanent deformation of protein molecules. The H-bonds breaks at 10-20% strain of tropocollagen molecules that provides additional energetic mechanics that dissipate energy during deformation of tropocollagen. This mechanism could be reversible when the applied force is removed. The breaking H-bonds is a viscoelastic effect that depend on the rapid loading.

Fibrillar sliding of mineralized collagen fibril: The mineralized collagen fibrils are the basic unit of nanostructure of bone that have higher stiffness and softening at large strain comparing with pure collagen (Gautieri et al., 2009). In fibrillar sliding, the two types of sliding provide deformation mechanics such as the sliding between mineral crystal and collagen and collagen molecular uncoiling. The tropocollagen molecules uncoiling could provide energy dissipation for large deformation once yielding begins as introduced in previous section. In addition, the sliding between collagen molecules and mineral particles could also discharge energy. This toughening mechanism allows the bone to have microcrack at microscale, but not to be failure at macrolevel.

Fibrillar sliding of collagen fibre arrays: The collagen fibre consist of the mineralized collagen fibrils and extrafibrillar matrix. The extrafibrillar matrix, a thin layer (1-2 nm), act as glue to group the mineralized collagen fibrils together (Fantner et al., 2005). The components of extrafibrillar matrix are non-collagenous protein. The tension load on the tissue could be separated into

tensile deformation of mineralized collagen fibrils and shearing deformation of the extrafibrillar matrix (Gupta et al., 2005). The deformation of non-collagenous due to the breaking of the sacrificial bonds dissipates energy, when the fibres have large deformation.

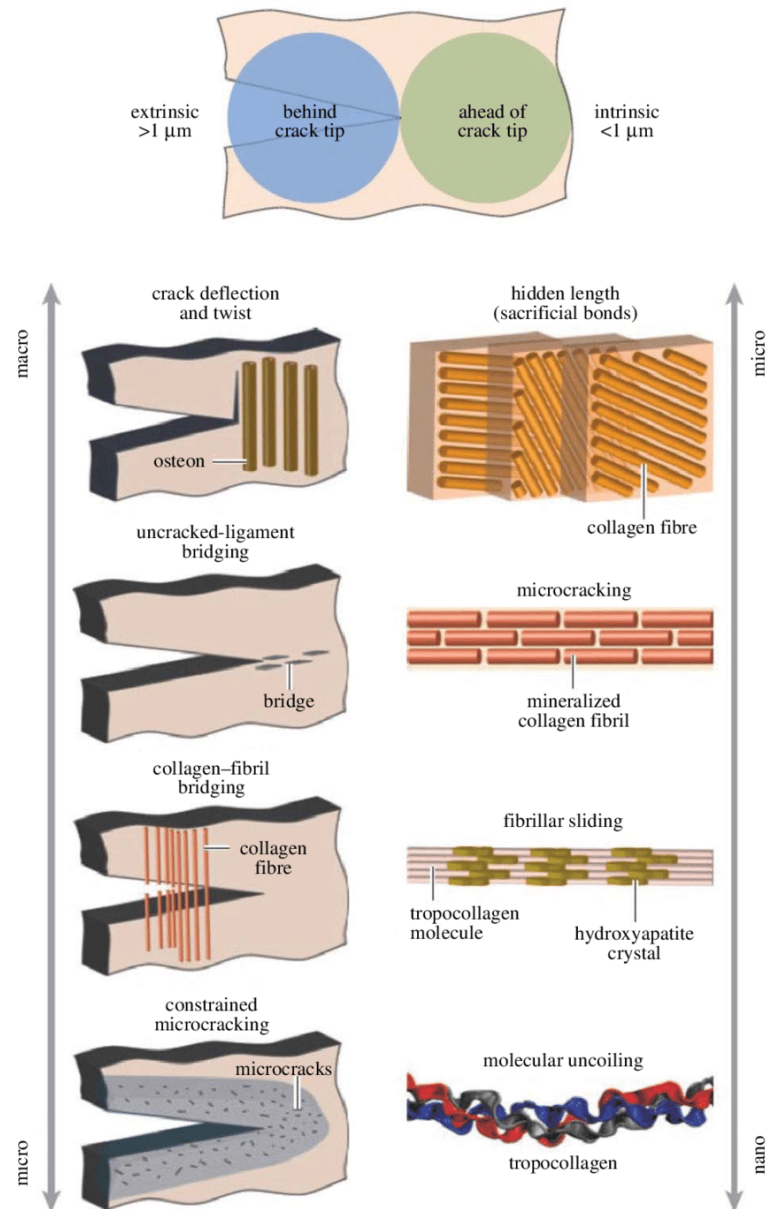


Figure 3.3 Fracture toughening mechanisms of cortical bone, including intrinsic toughening mechanisms and extrinsic toughening mechanism at various scale (Launey et al., 2010)

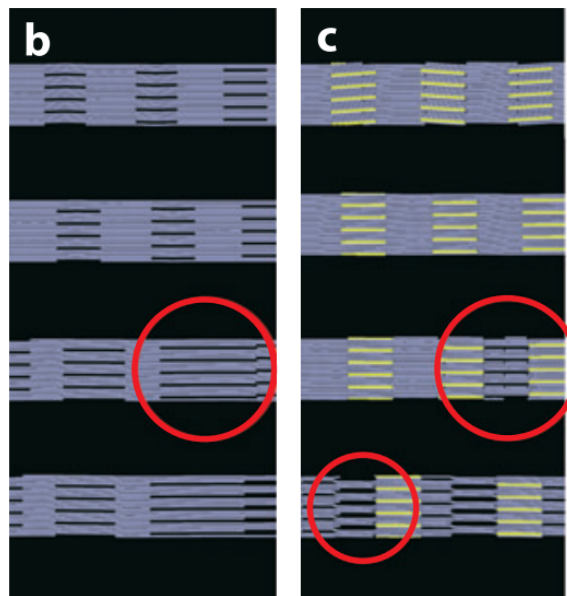
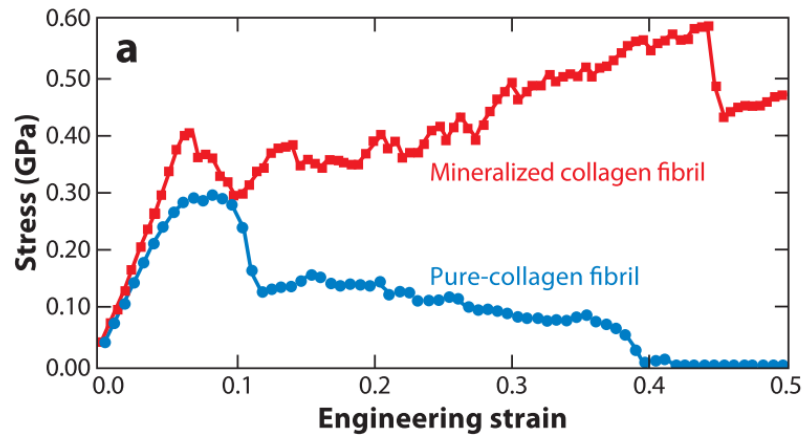


Figure 3.4 (a) Stress–strain response of a mineralized collagen fibril and a non-mineralized, pure collagen fibril. The deformation mechanisms of (b) collagen fibrils and (c) mineral collagen fibril (red circles indicate local area of repeated molecular slip) (Buehler, 2007).

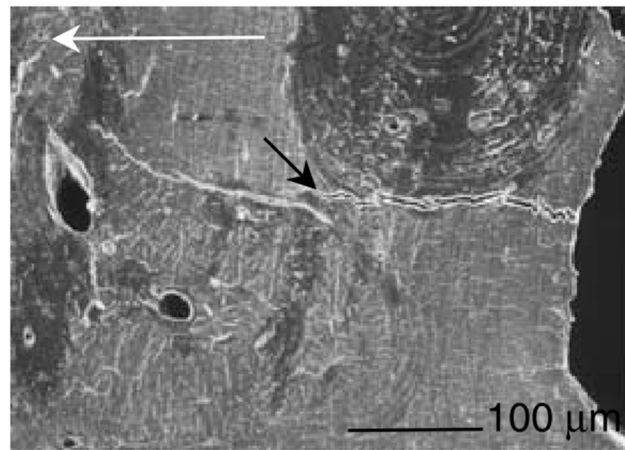
3.4.2 Extrinsic toughening mechanism

On the other hand, the extrinsic toughening mechanism is different from intrinsic toughening mechanism. It operates post-crack (behind the crack tip) during crack propagation and is controlled by the microstructure of the bone (1-100 μm) (Launey et al., 2010). The extrinsic toughening mechanism consists of constrain

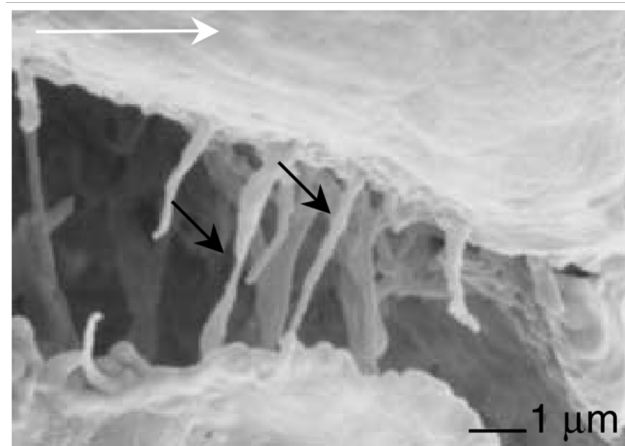
microcracking, crack deflection/twist and crack bridging, presented as following:

Constrained microcracking: Microcrack forms at the region with high local stress concentration near the main crack in the bone. At early study (Vashishth et al., 1997; Vashishth et al., 2003), the microcrack could directly increase the crack-growth toughness of bone during crack propagation. However, the results from Nalla (Nalla et al., 2004; Nalla et al., 2005), indicated that microcracks dissipated little energy for the crack-growth toughness, but it could enhance the formation of crack bridging and crack deflection in bone.

Crack deflection/twist: In ideally brittle materials, the crack growth path follows the direction of maximum strain energy release rate (Zimmermann et al., 2009). But the bone is an anisotropic composite material that the orientation of the maximum strain energy release rate and the path along microstructure with weakest resistance are not aligned with each other (Launey et al., 2010). This conflicts between these two directions results in the crack deflection or twist that provides the bone with high crack-growth fracture toughness. The cement lines arrest the crack as delamination barriers in bone, resulting the crack deflection or twist and rough fracture surface (Launey et al., 2010).



(a)



(b)

Figure 3.5 Micro-images of uncracked-ligament bridging (black arrow indicates the uncracked region) (a) and intact intact collagen fibrils bridging (black arrows indicate the intact collagen fibrils) (b) (Nalla et al., 2005).

Crack bridging: The bone has two type of crack bridging, including uncracked-ligaments bridging and intact collagen fibrils bridging according to the position of bridging respect to the crack tip (Nalla, Stölken, et al., 2005). The microcrack initiates ahead of the crack tip and left uncracked regions in the crack wake that called uncracked-ligament bridging. The uncracked-ligament bridging improves the crack-growth toughness, because its stress intensity factor increase with crack extension (Fig 3.5-a) (Ritchie et al., 2005). The intact collagen fibrils bridging is near the crack tip. The direction of the microcrack is perpendicular to

the long axis of collagen fibrils which could prevent the microcrack growth (Fig 3.5-b) (Yener N. Yeni & Fyhrie, 2003).

The fracture mechanism of the cortical bone enhances the fracture-resistance ability, but the fracture mechanism in different groups, such as young, aged, diseased and treated still need to be investigated.

3.4.3 Fracture toughness

Fracture toughness is an important parameter which assessed the susceptibility of bone to fracture. There are three main three parameters to represent fracture toughness of material, such as the critical stress intensity factor, K_c , and the critical strain energy release rate, G_c , and the critical value of J integral.

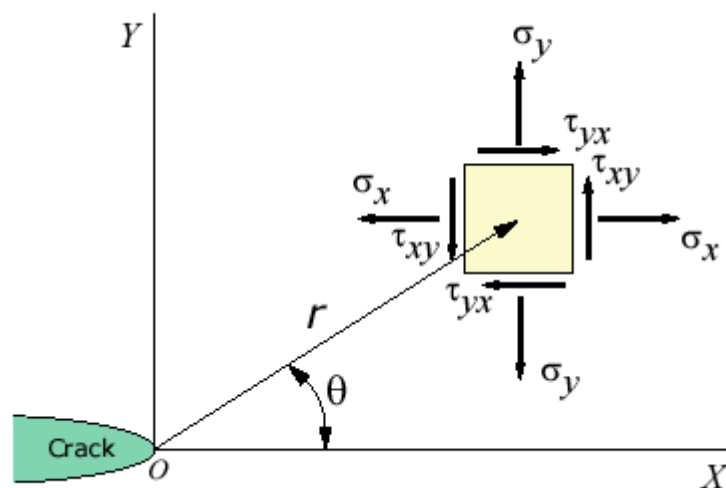


Figure 3.6. Polar coordinate at crack tip (‘eFunda: Stress Intensity Factor, K’, n.d.).

The critical fracture toughness, K_c , represent the toughness to initiate cracking. It is obtained using elastic fracture mechanics (LEFM). The isotropic material is considered to be elastic and with only limited inelastic deformation at a small region of crack tip. The local stress field, σ_{ij} , at a distance r from the crack tip

in Fig 3.6:

$$\lim_{r \rightarrow 0} \sigma_{ij} = \frac{K_c}{\sqrt{2\pi r}} f_{ij}(\theta), \quad (3.1)$$

where K is the stress intensity factor (SIF), θ is the angle with respect to the crack plane and f_{ij} are functions that depend on the crack geometry and loading conditions. K can be described based on fracture mode, including mode-I (tensile mode), mode-II (in plane shear mode) and mode-III (anti-plane shear mode). At fracture, the stress intensity factor, K , reaches a critical value, K_c .

The fracture toughness also could be described by the energy release rate, G . It is defined as the change in potential energy per unit increase in the crack area. For linear elastic isotropic materials, the energy release rate and the stress intensity factor for mixed-mode fracture are expressed:

$$G = \frac{K_I^2}{E^*} + \frac{K_{II}^2}{E^*} + \frac{K_{III}^2}{2\mu}, \quad (3.2)$$

Where G is the strain energy release rate, μ is the shear modulus. For plane strain, $E^* = E/(1 - \nu^2)$, ν is the Poisson ratio, E is the Young's modulus. For plane stress, $E^* = E$. At fracture, the strain energy release rate, G , reaches a critical value, G_c .

The critical value of J integral, J_c also describe the change in potential energy per unit increase in the crack area, while it is obtained using nonlinear fracture mechanics for plasticity and inelastic deformation. If the sample is assumed as elastic material, its critical value of J integral is equal to the critical energy release rate.

Linear elastic fracture mechanics (LEFM) assumes that the material behavior is elasticity and the fracture region is too small comparing with the size of structure.

It could indicate the initiation of crack in bone. But fracture mechanics of bone is complicated. It has many interfaces with various mechanical properties at the same level. Uncracked ligament bridging is also one of important fracture mechanics of bone that this fracture mechanics is difficult to present by LEFM parameters (Currey, 2012). Therefore, R-curve, present how the value of the critical intensity factor increase as a function of the length of crack during fracture process. It is used to examine the process of slow stable crack growth and unstable fracture.

3.5 Effect of age and disease on fracture toughness of cortical bone

Age and disease increase the risk of bone fracture that influence the quality of life. In order to understand the effect of age and disease on fracture toughness of cortical bone, it is important to investigate the difference of cortical bones in fracture mechanics.

At nanoscale, the toughness of cortical bone is dominated by the collagen matrix. Non-enzymatic crosslinks, as connections between collagen fibril, could influence the toughness of cortical bone (Odetti et al., 2005; Tang et al., 2009; Vashishth et al., 2001; Wang et al., 2002). Vashishth et al. (2001) found that the accumulation of non-enzymatic crosslinks could decrease the toughness of cortical bone. Then, Vashishth et al. (2004) pointed out that age could increase the non-enzymatic crosslinks resulting in the decrease of toughness during crack propagation. The effect of non-enzymatic crosslinks on toughness of cortical bone was also investigated by Wang et al. (2002). The aged bone had the higher content of non-enzymatic crosslinks than that of the young bone, so the aged cortical bones loss their quality. The osteoporotic bone had higher content of non-enzymatic crosslinks than that of the health bone, so it had lower toughness

(Oxlund et al., 1996; Mitsuru et al., 2006; Mitsuru et al., 2006).

At microscale, the porosity also influences the toughness of cortical bone. The increase of porosity could result in the decrease of toughness of cortical bone. (Busse et al., 2010; McCalden, McGlough, et al., 1993; Yeni et al., 1997). McCalden et al. (1993) found that age could result in the increase of porosity that decreased the toughness of cortical bone. Later, Yeni & Norman (2000) employed compact tension test to study the effect of porosity on toughness of cortical bone due to age. The results agree with that of McCalden et al. (1993). Burghardt et al. (2010) compared the characteristic of the male and female cortical bone with the age range from 20 to 78 years. The results revealed that the porosity of both two kinds of cortical bone increased with age and the porosity change resulted in the decrease of toughness. The osteoporotic bone with the high porosity had lower toughness of cortical bone compared with that of normal cortical bone (Tjhia et al., 2011).

The osteocyte lacunae were found to be a microcrack-initiation position during tensile or four-point bending test, by scanning the micrograph of equine or bovine cortical bone (G. C. Reilly, 2000; G. C. Reilly & Currey, 1999). Prendergast and Huiskes (1996) adapted the computational method to investigate the stress-concentration area in osteons with osteocytes. The simulation results predicted that the crack propagation might follow the path of lacunae, because these lacunae caused stress concentration. The two-dimensional or three-dimensional computational models with osteocytes, which geometries were circular or elliptical with two angles, also agreed with the previous study (Liu et al., 2018; Rath et al., 2007). Nicolella et al. (2001) used the digital stereoinaging to measure the strain distribution of osteocyte lacunae. The strain at crack tip near the osteocyte lacunae reached 30000 microstrain. The result presented that the

osteocyte lacunae induced the initiation of microcracks. The local strain of cortical-bone specimen without microcracks was also tested, indicating that the strain of osteocyte lacunae was higher than that of microstructural areas with increase in the global strain of cortical bone (Nicolella et al., 2006). Therefore, the osteocyte could be a strain sensor for cortical bone to express the remodelling signal. In addition, the microcracks due to osteocytes might be a barrier to protect the Haversian canal (Da Costa Gómez et al., 2005 and Vashishth, 2004), but the effect of osteocyte on crack propagation still need to be investigated.

Apart from the previous discussion, the microcracks in osteocytes-deficient bone, tend to accumulate resulting in a decrease in the mechanical properties of cortical or trabecular bone, rather than be repaired by the remodelling process (Ma et al., 2008; Qiu et al., 2005; Robert et al., 2010; Schaffler et al., 1995). In another study, Robert et al. (2010) pointed out that the decrease in the osteocyte resulted in the brittleness of bone due to its hypermineralization. Some previous studies presented that the increasing age and disease could result in more microcracks than in the normal bone including cortical or trabecular bone (Bernhard et al., 2013; Qiu et al., 2003; Robert et al., 2010). Qiu et al. (2003) compared the osteocyte density of healthy and osteoporotic iliac cancellous bone. The osteocyte density of healthy bone was 190 mm^{-2} , higher than that of the osteoporotic bone (118 mm^{-2}). The osteocyte densities of osteon surface in cortical bone of four groups including young, aged, diseased and treated were also investigated by Bernhard et al. (2013). The values of them were 374.75, 307.83, 367.20 and 380.33 mm^{-2} . Therefore, the aged and diseased cortical bones do not have the ability of fracture resistance as young one, because fewer osteocytes could not deal with the microcrack accumulation..

The parameters of the osteon, including fraction, density and size, are also a significant role in the toughness of cortical bone. The increase of osteon density and the decrease of osteon size due to age could decrease the toughness of cortical bone (Evans, 1976; Yeni et al., 1997). Granke et al. (2016) analysed osteonal fraction, and initiation and growth fracture toughness of human femoral cortical bone by three points bending test. The results presented that the high fraction of osteonal area of young cortical bone could improve the ability of bone resistance to the crack initiation and propagation, while the porosity had the negative effect on the fracture toughness of cortical bone. The toughness of microstructural constituents were measured by nanoindentation technique. The fracture toughness of the osteon and the interstitial matrix of ovine cortical bone were 0.55 and 0.46 MPa(m)^{1/2}, respectively (Mullins et al., 2009). Abdel-Wahab et al. (2012) employed the same method to obtain the fracture toughness of the osteon (860 N/m) and the interstitial matrix (238 N/m) of bovine cortical bone. However, the knowledge of the fracture toughness of microstructural constituents in human cortical bone, even the change of them due to age and disease are not still investigated.

The cement line, which is the interface between osteon and interstitial matrix, plays an important role in toughness of cortical bone during crack propagation. The cement line could attract crack deflection into it because of its unique composition (Burr, 2002; O'Brien et al., 2005; Skedros, Holmes et al., 2005). Chan et al.(2009) analysed the characteristic of crack propagation in young (48 years) and aged (78 years) cortical bone by using compact tension test and X-ray photoelectron spectroscopy. The crack initiation toughness of young and aged cortical bone were 1.610±0.625 and 0.31±0.083 MPa(m)^{1/2}, respectively. The linear slope of crack growth were 1.960±0.283 and 0.031±0.036 MPa(m)^{1/2}/mm. The low toughness of cortical bone during crack propagation was

caused by crack penetration into the osteons instead of destroying the cement lines. Apart from crack deflection, the uncracked ligament bridging is also a factor affecting the toughness of cortical bone during crack propagation (Nalla, Kinney, & Ritchie, 2003; Nalla, Kruzic, Kinney, & Ritchie, 2005). Nalla et al. (2004 and 2006) used compact tension test to obtain the R-curves of aged and young human cortical bone. The results presented that the initiation value of stress intensity factor of the aged cortical bone ($1.26 \pm 0.22 \text{ MPa(m)}^{1/2}$) was lower than that of the young one ($2.07 \pm 0.11 \text{ MPa(m)}^{1/2}$). In terms of crack propagation process, the value of stress intensity factor increased hardly meaning that the crack easily grew in the aged cortical bone. The growth slopes of the aged and young groups were 0.06 ± 0.04 and $0.37 \pm 0.06 \text{ MPa(m)}^{1/2}/\text{mm}$, respectively. In this study, the much smaller uncracked ligament bridging were observed.

In conclusion, many factors could influence the fracture toughness of the cortical bone due to the age and disease. In this thesis, the effect of the micro-morphology of the cortical bone on crack propagation is the main target.

3.6 summary

- Cortical bone as a natural material could be treated as transversely-isotropic material compared with the engineering material
- The diversity of elastic properties of cortical bone could be influenced by many factors, including species, gender, age and healthy condition.
- Age and disease affect the elastic properties of cortical bone because of the change in the hierarchical structure at nanoscale and microscale. The bone mineral density is a significant factor in elastic properties at nanoscale, while the fraction of porosity, osteon and interstitial matrix affect the elastic properties of cortical bone. However, there is still a lack of understanding on the effect of osteonal microstructure on the elastic

properties of cortical bone.

- The fracture toughening mechanisms, such as intrinsic toughening mechanisms and extrinsic toughening mechanisms are introduced in this chapter.
- Age and disease also influence the toughness of cortical bone. Previous studies focus on the collagen matrix of cortical bone at nanoscale. The change in parameters of porosity and osteon due to age and disease are also crucial factors resulting in the low toughness of cortical bone
- The characteristics of crack deflection and uncracked ligament bridging in aged and young cortical bone are different. However, the relationship between these two extrinsic fracture mechanisms and the morphology of osteonal microstructure is not to be investigated.

Chapter 4 Modelling of bone

4.1 introduction

The computational models have become popular to be employed to understand and predict the complex mechanical behaviours of bone because it is powerful and efficient in visualizations and detail analyses. In this chapter, various kinds of bone models will be introduced to deeply understand of current modelling techniques and their limitation in order to find the methods for the investigation of mechanical behaviours of cortical bone.

4.2 Macroscale bone models

The cortical bone can be considered as homogenous material to study its mechanical behaviours based on classical continuum mechanics theory at macrolevel.

4.2.1 Elastic model

In 1972, A mathematical model of cortical bone was used to study the effect of muscle forces on the cortical bone based on a two-dimensional beam theory (Rybicki et al., 1972). Then, a three-dimensional isotropic model of cortical bone was established by Valliappan et al. (1977). Many experiment results prove that bone is a transversely isotropic material. Therefore, a three-dimensional transversely isotropic model of cortical bone was generated to study the stress distribution of bone under different loading conditions (Vichnin & Batterman, 1986). In recent study, the peripheral quantitative computed tomography (pQCT) was used to generate the computational model of cortical bone (Fig 4.1), to improve the accuracy of the geometry of the whole bone (Pietruszczak et al., 2007). The elastic model is suitable to investigate the elastic properties of the

cortical bone, but it is difficult to study the fracture properties with it.

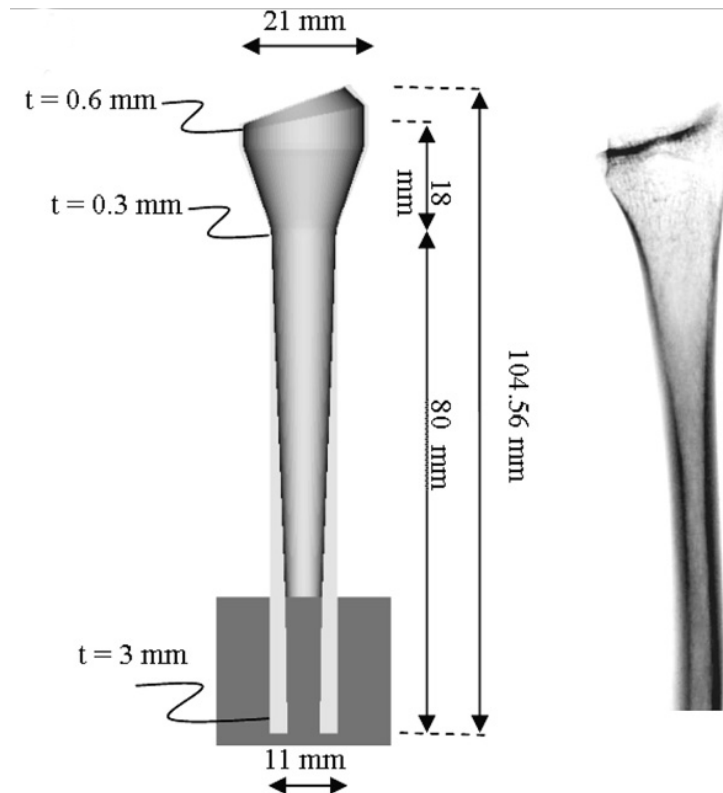


Figure 4.1. Bone model with idealized geometry based on pQCT images (Pietruszczak et al., 2007)

4.2.2 Viscoelastic model

Some studies prove that cortical bone is a time-dependent material (Katsamanis & Raftopoulos, 1990; Lewis & Goldsmith, 1975; Tennyson et al., 1972) In order to mathematically describe this time-dependent features of cortical bone, the viscoelastic model is used. There are two main viscoelastic phenomena including creep and relaxation. If the external loading subject to the material increases linearly and then keep constant, the strain will increase nonlinearly and then increase with time (creep). If the material has a linearly increase in displacement and then keep constant, the stress will increase nonlinearly and then decrease with time (relaxation).

A viscoelastic material can be considered as combinations of viscosity and elasticity components. The elasticity component could be represented as a linear elastic spring. When this component is subject to external loading, its response is to undergo an instantaneous elastic strain with time independency. After removing the external loading, this component also recovers instantaneously and completely. It obeys Hooke's law: $\sigma = E\varepsilon$, where σ is stress, E is elastic modulus and ε is strain. The viscosity component could be represented as a linear viscous dashpot. When this component is subject to external loading, its response is a strain rate proportional to stress (time dependency). This component could not recover after removing the external loading. It obeys Newton's law: $\sigma = \eta \frac{d\varepsilon}{dt}$, where η is the viscosity constant, σ is stress and $\frac{d\varepsilon}{dt}$ is the strain rate. The simple viscoelastic models could be divided into the Kelvin-Vigot model and the Maxwell model, according to the arrangement of spring and dashpot. In Kelvin-Vigot model, the spring and dashpot are in a parallel position. In Maxwell model, the spring and dashpot are in a series position. However, the different lengths of molecular segments result in the various time distributions, these two simple models has limitation to describe the viscoelastic behaviour of material in a wide range of time or frequency. Therefore the complex viscoelastic models were improved to enhance the accuracy, for instance, generalized Maxwell model (Fig. 4.2). The relaxation modulus function $E(t)$ in generalized Maxwell model is based on the following equation:

$$E(t) = E_{\infty} + \sum_{i=1}^n E_i e^{-\frac{t}{\tau_i}} \quad (4.1)$$

where E_{∞} is the long-term modulus, E_i is the modulus of elastic component, τ_i is the relaxation time.

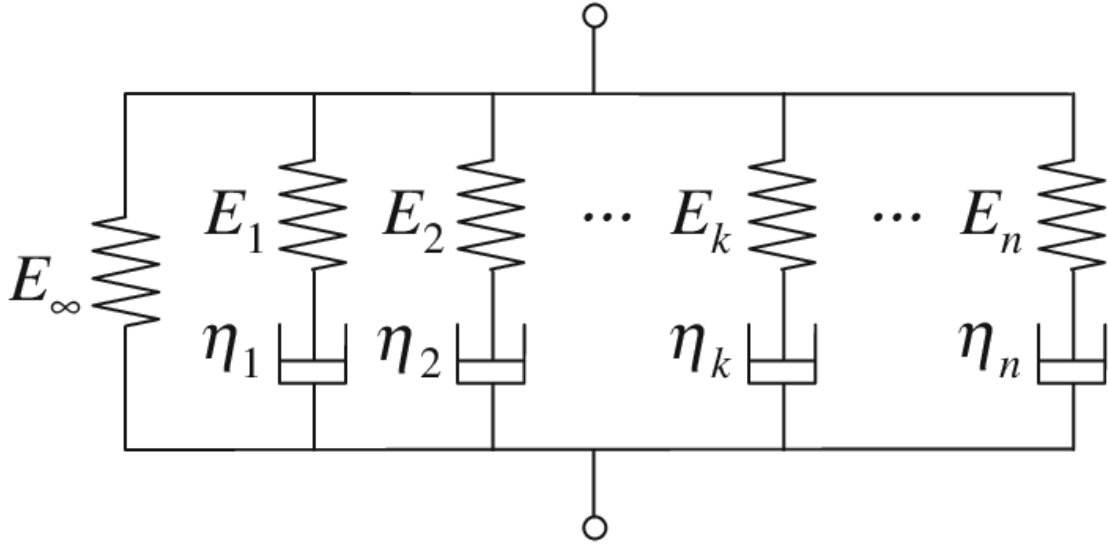


Figure 4.2. Schematic of the generalized Maxwell model

The bovine cortical bone was tested by using the split-Hopkinson pressure bar techniques at strain rates of $10\text{-}450\text{ s}^{-1}$ (Tennyson et al., 1972). The results could be fitted by Kelvin-Vigot model (the long-term elastic constant, E_{∞} , is 18.1 GPa and the viscosity constant, η , is $2.1 \times 10^4\text{ Pa s}$). Lewis and Goldsmith (1975) used the same techniques to test the viscoelastic behaviour of bovine femoral bone. The time constant and the long-term elastic constant in the results are 13 μs and 19.3 GPa, respectively. The viscoelastic behaviour of human cortical bone was studied by Katsamanis and Raftopoulos (1990). The average value of Young's modulus value is 16.2 GPa and the viscosity constant is $3.7 \times 10^4\text{ Pa s}$. Johnson et al. (2010) employed the generalized Maxwell model (three elastic components and two viscosity components) to fit the literature results. The one-dimensional viscoelastic model used in this paper is based on the following equation:

$$\sigma(t) = E_0 \dot{\epsilon} t + \eta_1 \dot{\epsilon} \left(1 - e^{-\frac{E_1 t}{\eta_1}}\right) + \eta_2 \dot{\epsilon} \left(1 - e^{-\frac{E_2 t}{\eta_2}}\right) \quad (4.2)$$

In recent study, Abdel-Wahab et al. (2011) used Instron MicroTester to test the

creep and relaxation behaviour bovine cortical bone. Three stress level ere applied in this experiment, including 17, 19 and 21 MPa. The values of e_1 , e_2 , τ_1 and τ_2 (coefficients of Prony series) are 0.11768, 0.0351218, 7.6998 and 1061.7, respectively. The Young's modulus at strain rates of 10^{-5} and 10^{-3} s^{-1} obtained by uniaxial monotonic tension tests are 12 and 21 GPa, respectively.

The hierarchical structure of bone also affects its viscoelastic properties. There are five main reasons including inhomogeneous deformation, molecular modes in collagen, thermoelastic coupling, piezoelectric-like coupling and motion of fluid in canals in bone (Lakes & Katz, 2018). In this thesis, only elastic behaviour was considered, because all the loading conditions were a quasi-static uniaxial tension or stable compact tension that the dynamic or long-term effects could be ignored.

4.3 Microstructure based model

The hierarchical structure plays an important role in the mechanical behaviour of cortical bone. Therefore, the relationship between the hierarchical structure and the mechanical properties of the cortical bone, have become attractive to be studied. However, the limitations of the experimental techniques restrict to investigate it. For example, the crack growth path is an important parameter in the evaluation of the cortical bone's fracture behaviour, but it is difficult to record the crack growth path on time because of the rapidly crack growth. The microstructured bone model could be useful to gain insights into the relationship between microstructure and the mechanical behaviour of the whole bone. There are three types of microstructured bone models, including osteons model with idealized geometry, a model established based on the micro-images of real bones and a model generated based on the statistical parameter of the four phases measured from the bone's micro-images.

In 1992, Hogan (1992) established a two-dimensional model with a single osteon (idealized circular geometry) to investigate variation in the elastic modulus with porosity. The results showed that the macroscopic mechanical property of simulation model is in good agreement with that of experiments. The single osteon model was improved by Prendergast and Huiskes (1996). The lacuna was embedded into the Haversian system to study the local deformation behaviour around lacuna. The results helped to deeply understand the effect of lacuna on the remodelling process of cortical bone. Raeisi et al. (2007) used a model with a number of osteons to study the interaction between osteons and microcracks and the effect of elastic modulus of cement line on the fracture mechanics. The results pointed out that the fracture mechanics was significantly influenced by the bone microstructural heterogeneity. Later, the two-dimensional model containing microconstituents with orthotropic elastic properties, including interstitial matrix, osteons and cement lines, was developed by Mischinski and Ural (2011) (Fig 4.3). The cement line in this model was as a thin layer described by the zero-thickness cohesive elements. The results indicated that the deflection of crack into cement lines could be caused by the lower strength of the cement lines. This kind of microstructured model containing osteon with idealized geometry is easy to generate the model, but the model cannot represent the real osteon in the cortical bone.

Another type of microstructure based model is generated according to the micro-images of real bones. Budyn and Hoc (2010) captured microscopic images of the transverse section of cortical bone by back scattered electron microscopy (BSEM) observation. The two-dimensional model was duplicated based on the local distribution and shape of four phases in the microscopic images, including osteon, Haversian canal, cement line and interstitial matrix. Giner et al. (2017) used the same method to generate a finite element model to investigate the strain

energy release rate of the cement lines in ovine cortical bone (Fig 4.4). The three-point bending test was employed to obtain the force-displacement curve, to calibrate the numerical results with experimental ones. The strain energy release rate of the cement line is 146 N/m based on the numerical results and experimental results. Mischinski and Ural (2013) also developed a microstructure based model to analyse the crack propagation path in various cortical bones. The two-dimensional model was established based on the microscopic image, while the geometry of osteon is an idealized ellipse (Fig 4.5). In addition, the Haversian canal and resorption cavity were not represented in the model. This kind of model need more time to analyse the microscopic images and the unique geometry of the model is not convenient to do a comparison work.

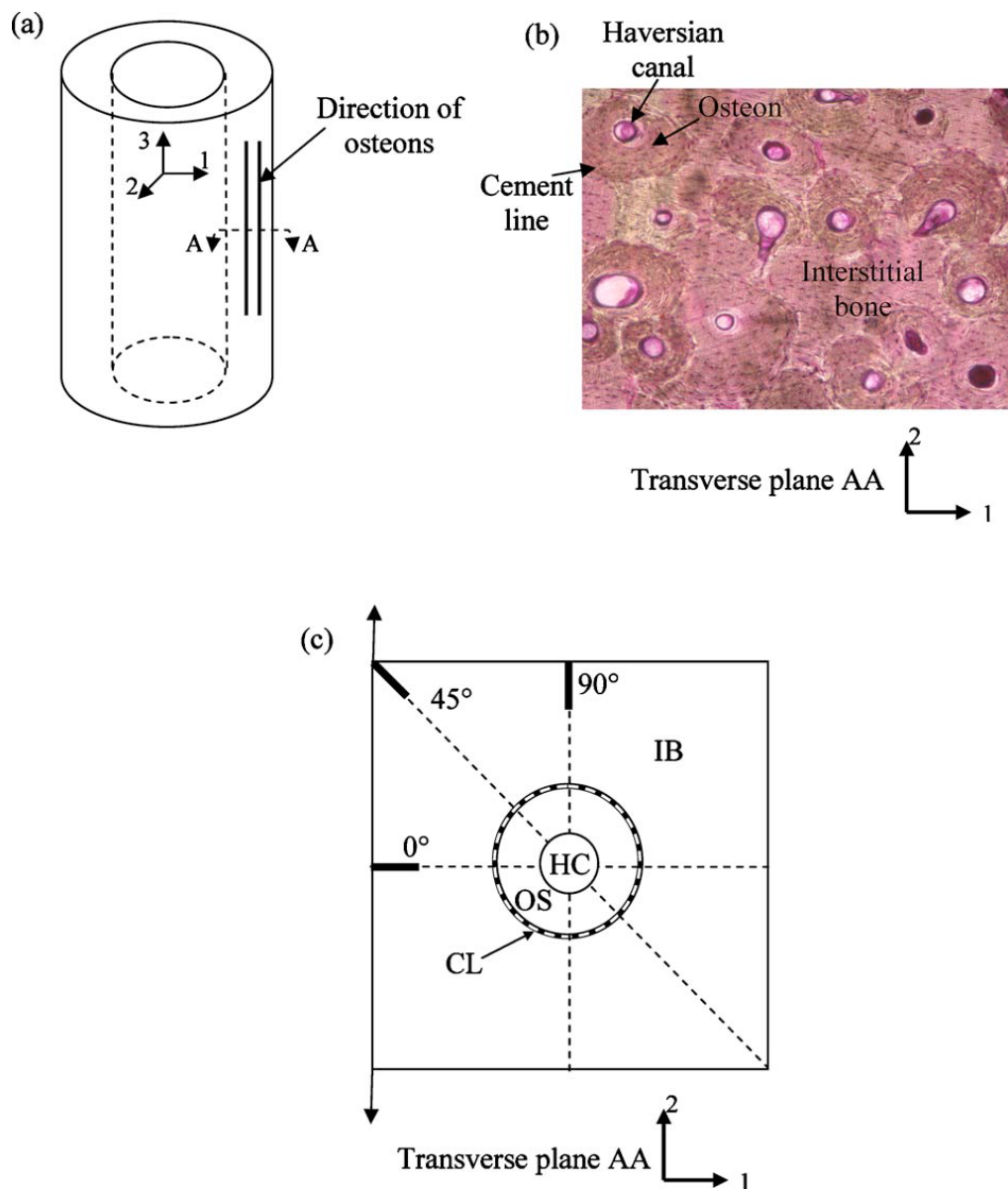
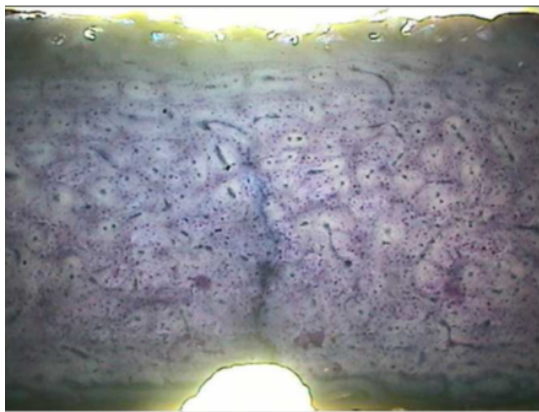
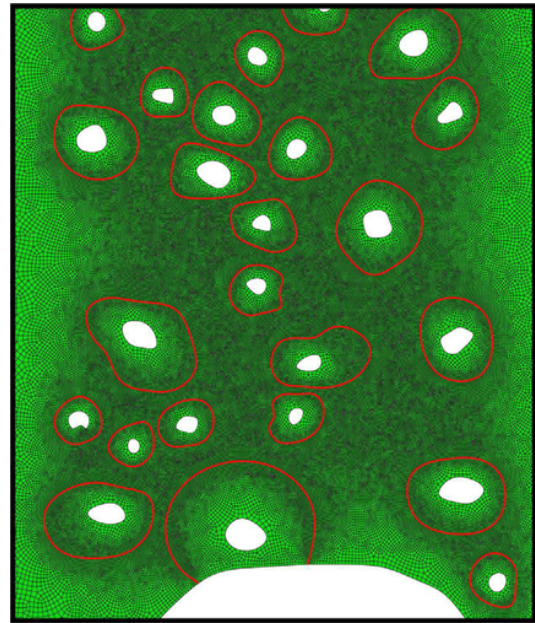


Figure 4.3. Schematics of a cortical bone with the direction of the osteons (a), microscopic image at the radial-transverse direction (b) and osteon with idealized geometry model (HC is Haversian canal, OS is osteon and CL is cement line)(c) (Mischinski & Ural, 2011).

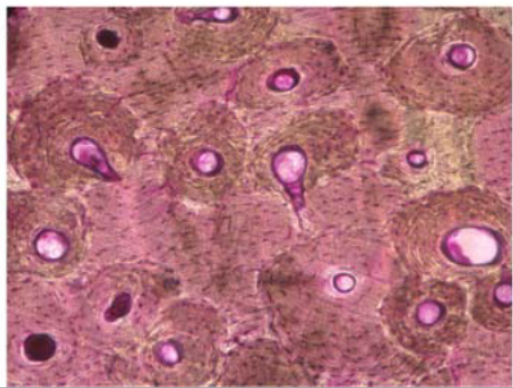


(a)

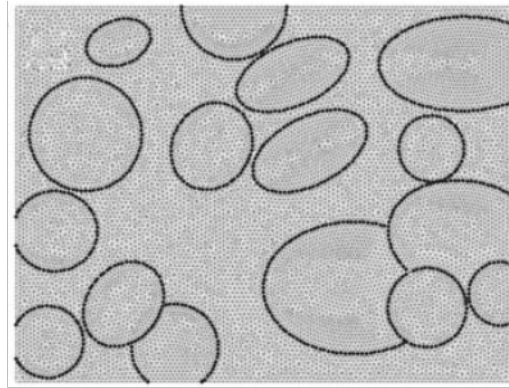


(b)

Figure 4.4. Microscopic image of transverse section of cortical bone (a) and simulation model duplicated based on the microscopic image (b) (Giner et al., 2017).



(a)



(b)

Figure 4.5 Microscopic image of transverse section of cortical bone (a) simulation model duplicated based on the microscopic image (osteon with idealized geometry) (b) (Mischinski & Ural, 2013).

Unlike the generation process of the previous two models, the models in Budyn and Hoc's paper (2007) were generated based on the statistical parameters of

the four phases in the cortical bone. The volumetric fractions and the sizes of the four phases in cortical bone are measured from the microscopic images. The geometry of osteons and Haversian canals are treated as elliptical or circular shape. The mathematical functions are used to obtain the distribution of each measured parameters statistically. Finally, the external software, such as MATLAB, Python, are employed to generate the bone model with randomly distribution microstructural phases. Li et al. (2013) studied the fracture process in cortical bone by using finite element models with different volumetric fractions of the osteonal area and Haversian canal's area (Fig 4.6). The results indicated that the different volumetric fractions of the osteonal area and Haversian canal's area could result in the change in fracture process of the cortical bone. This kind of the microstructure model is a convenient way to describe the characteristics of micro-morphology of different groups, which is adapted in this thesis.

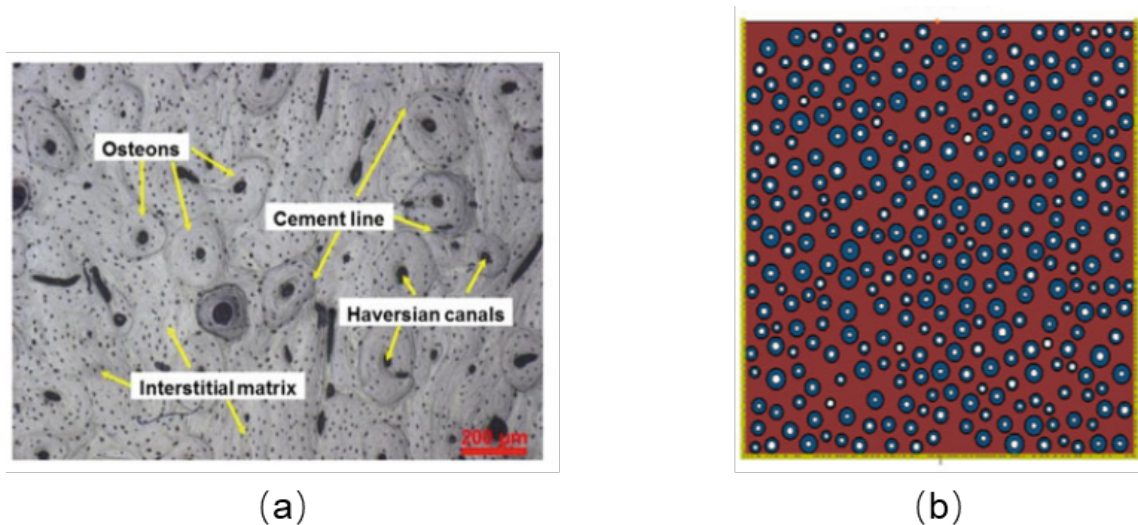


Figure 4.6 Microscopic image of transverse section of cortical bone (a) and simulation model based on statistical parameters of the four phases (b) (Li, Abdel-Wahab, et al., 2013b)

4.4 Fracture mechanics based models of bone

In order to investigate the fracture behaviour of bone, several fracture mechanics theories were employed into the finite element models to obtain the fracture

toughness or fracture process, including linear elastic fracture mechanics models, nonlinear fracture mechanics models (cohesive model and extended finite element model).

4.4.1 Linear elastic fracture mechanics model

Linear elastic fracture mechanics (LEFM), describing the stress field of crack tip, is to quantify the fracture toughness of the material. Therefore, the models based on linear elastic fracture mechanics are utilized to evaluate the fracture behaviour of the cortical bone. A simple osteonal cortical bone model based on linear elastic fracture mechanics theory was utilized to investigate the relationship between osteons and microcracks by Guo et al. (1998) and Najafi et al. (2007). In those studies, the cortical bone was treated as a fibre-matrix composite material. Those studies indicated that the osteon with high stiffness could protect the osteon destroyed by the microcrack. The significant effect of different microcracks morphology and location near the osteon on fracture toughness of the cortical bone using LEFM based model, was studied by Najafi et al. (2007 and 2009). Linear elastic fracture mechanics assume that the material has an elastic behaviour results in small plastic deformation during fracture process so the previous studies focused on the microcrack in cortical bone.

4.4.2 Cohesive model

The cohesive model is a gradual phenomenological model to define the nonlinear behaviour of material at the fracture process zone. In a cohesive model, the fracture process is centered into the crack line and is controlled by a cohesive law that relates traction and displacements jump across cohesive surfaces. The fracture process could be divided into two parts, including traction free area and cohesive zone area. The fracture process can be summarized as Fig 4.7: a linear

elastic material response occurs (1), the crack initiates due to the increase of loading (2), the nonlinear cohesive law controls this part (3), traction free area appears (4) (Alfano et al, 2007).

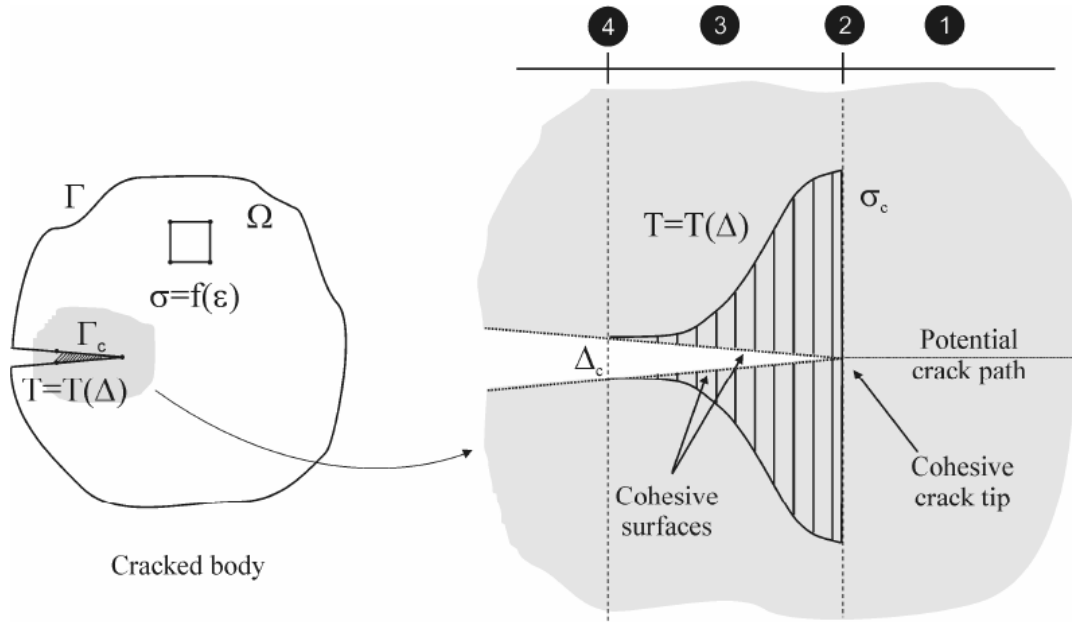


Figure 4.7 Crack initiation and propagation in the cohesive model (Alfano et al, 2007).

The cohesive model was used to study the fracture behaviour of human cortical bone (Cox & Yang, 2007; Yang et al., 2006a, 2006b). In those studies, the line-idealization was employed to describe the discrete damage of cortical bone (a single dominant crack with microcrack and other nonlinear material events). The plane-stress condition was applied in the model and the crack was along a straight front. A bilinear traction law was used to calculate the fracture energy which combined the fracture energy of the crack tip and the crack wake region. In this study, the results of the cohesive model agreed with experimental data, while the model using linear elastic fracture mechanics was an inaccurate model to describe the fracture behaviour of bone (Fig 4.8).

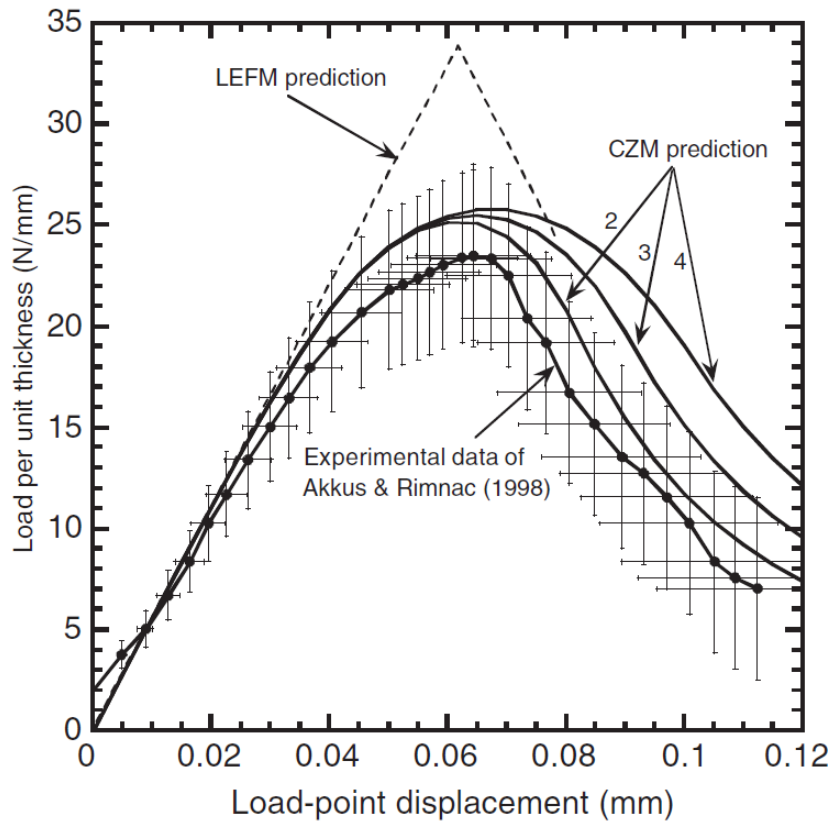


Figure 4.8 Load-displacement curves of experiment, cohesive model and LEFM model.(Yang et al., 2006a)

The cohesive model of the double cantilever beam was employed to study the fracture toughness of cortical bone under pure mode I loading condition (Morais et al., 2010). In this model, the solid in plane stress 8-node element connected with the 6-node two-dimensional cohesive element. The mixed mode cohesive law was used to simulate crack growth. The cortical bone was treated as a transverse isotropic material with 16.61 GPa in longitudinal elastic modulus and 9.55 GPa in transverse elastic modulus. This model in this study could provide a complete curve which is difficult to be obtained by experiment. The fracture characterisation of human cortical bone under mode II loading was also studied using the model of the end-notched flexure test (Silva et al., 2017). A trapezoidal with bilinear softening cohesive law was adjusted to execute numerical analysis. The numerical results showed agreement with experimental ones. Ural et al.

(Ural & Vashishth, 2007; Ural et al., 2011) developed a compact tension model using cohesive zone method to investigate the interaction between fracture behaviour of cortical bone and porosity or strain rate of loading. The three-dimensional models were obtained using micro CT method. The deficient element in the model represented the porosity in the model. The results showed that the increase in porosity due to age increasing and in the strain rate of loading of cortical bone could result in the low initiation and propagation fracture toughness.

The numerical results of the cohesive model in those studies have a good agreement with experimental ones and overcome the limitation of the linear elastic fracture mechanics. However, the cohesive model also has many restrictions. For example, the crack in the cohesive model propagates following the pre-defined path and only a single crack exist in the model, whereas in reality, the multiple random cracks are showed during the fracture process. Therefore, the cohesive model could be applied in the macro-scale models. In order to solve this problem, a novel zero-thickness cohesive element method was proposed by Ural and Mischinski (2013). In this method, the cohesive elements were as an interface connecting all the existing solid elements, while the crack growth path could not be limited at the predefined path. Therefore, the initiation and propagation of cracks were not limited at the pre-defined crack path. Ural and Mischinski (2013) used this simulation method to evaluate the function of the cement lines on the fracture behaviour of bone at multiple scales. Later, the three-dimensional microstructure based model using the cohesive element method was employed to analyse the effect of reduced compositional heterogeneity on fracture resistance of human cortical bone (Demirtas et al., 2016). The increasing heterogeneity of cortical bone could result in the uncracked region which enhances the fracture resistance of cortical bone. In

addition, this cohesive element method also could be used to study the fracture behaviour of ultrastructure of the extrafibrillar matrix in bone (Lin et al., 2017). In this study, the organic interface was represented by the cohesive element between each mineral crystal grain (Fig 4.9). The numerical models with two hydration conditions were tested under tension and compression loading condition. The results indicated that the extrafibrillar matrix is significant in fracture process of bone. Therefore, the improved simulation method, called zero-thickness cohesive element method is adapted to study the crack growth path in the cortical bone.

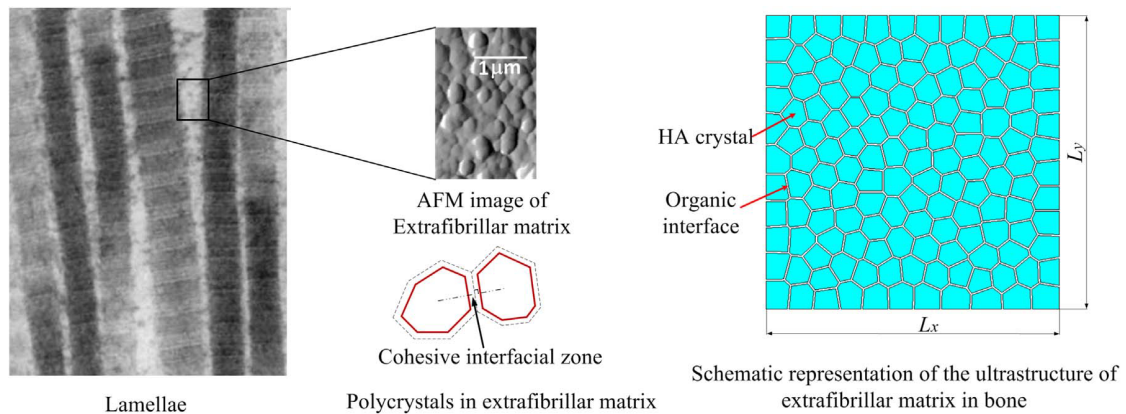


Figure 4.9. Schematic representation of the two-dimensional model of the extrafibrillar matrix in bone lamellae

4.4.3 Extended finite element method model

In the standard finite element method, the crack front region has to be remeshed at each step or a predefined growth path is required, in order to model the crack extension. The extended finite element method (X-FEM) is a numerical technique originated by Belytschko and Black (1999). It models the crack growth independent from current mesh based on the concept of partition of unity by using local enrichment functions to solve the problem of the standard finite element method. In order to simulate the crack, two enrichment functions were employed to describe the singularity of crack tip and the displacement

discontinuity across the crack surface, including asymptotic tip function and displacement jump function. The enriched finite element approximation is as following (Abaqus, V., 2016):

$$u^h(x) = \sum_{I \in N} N_I(x) [u_I + H(x)a_I + \sum_{\alpha=1}^4 F_{\alpha}(x)b_I^{\alpha}] \quad (4.3)$$

Where $N_I(x)$ are the usual nodal shape functions; u_I are the nodal displacement vectors, which is responsible for non-enriched finite-element solution; a_I are the nodal enriched degree of freedom vector related to the discontinuous jump function, which is also called the Heaviside function ($H(x)$) on the crack surface. This part is responsible for the nodes of elements, which are cut by the crack interior; b_I^{α} are the nodal enriched degree of freedom vector related to the asymptotic functions of crack tip, $F_{\alpha}(x)$. This part is in charge of the nodes of elements, which are cut by the crack tip (Fig 4.10) (Dassault, 2016).

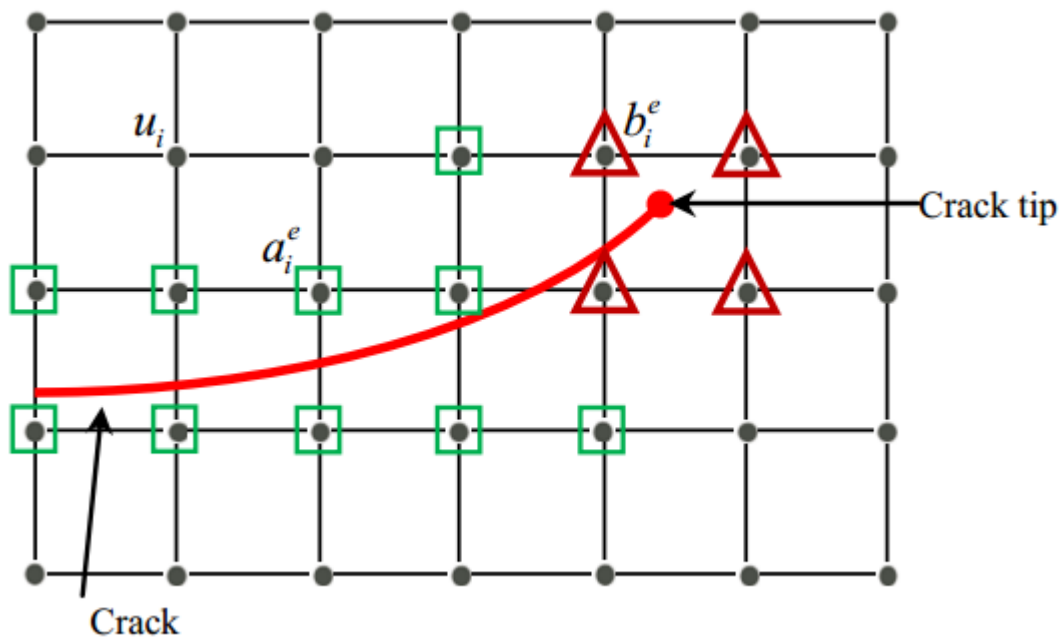


Figure 4.10 X-FEM enrichment method (u_i : continuous element, a_i : split element and b_i : tip element) (Abdelaziz et al., 2011).

The discontinuous jump function, $H(x)$, are presented as the equations:

$$H(x) = \begin{cases} 1 & \text{if } (x - x^*) \cdot \mathbf{n} \geq 0, \\ -1 & \text{otherwise,} \end{cases} \quad (4.4)$$

where x is a sample (Gauss) point, x^* denotes the point on the crack that is the closest to point x and \mathbf{n} is the unit outward normal to the crack at x^* (Dassault, 2016).

The asymptotic crack-tip functions, $F_\alpha(x)$, presented as the equations:

$$F_\alpha(x) = \left[\sqrt{r} \sin \frac{\theta}{2}, \sqrt{r} \cos \frac{\theta}{2}, \sqrt{r} \sin \theta \sin \frac{\theta}{2}, \sqrt{r} \sin \theta \cos \frac{\theta}{2} \right] \quad (4.5)$$

where (r, θ) are the polar coordinate system with its origin at the crack tip, while the crack-tip tangent coincides with $\theta = 0$ (Dassault, 2016).

The extended finite element method (X-FEM) based models were employed to simulate the multiple crack growth in human cortical bone, to analyse the effect of aging, porosity, heterogeneity on mechanical behaviour of cortical bone (Fig 4.11) (Budyn, 2007; Budyn et al., 2008; Budyn & Hoc, 2007a). Those microstructure based models contained four phases, including osteon, Haversian canal, cement line and interstitial matrix. The sizes and volumetric fractions of microstructural constituents were measured based on microscopic images. The models were established based on those statistical analysis data. In order to analyse the multiple crack growth in cortical bone, the models without cracks were stretched until the local zone with strain reaching above 0.4% to determine the positions of crack initiation. Later, Abdel-Wahab et al. (2012) studied the effect microstructure on the characteristic of crack propagation in bovine cortical bone by using the X-FEM models. The macro scale responses and crack propagation paths of three types of models, including the homogenous model, three phases model (without cement lines) and four phased (with cement lines) were compared. The results indicated that the heterogeneity of cortical bone

could improve the ability of crack resistance. Li et al. (2013) focused on the effect of volumetric fractions of osteon and porosity area. The yield strain of 0.6% and the crack initiation strain of 0.65% was chosen to simulate the plastic behaviour and fracture behaviour of cortical bone. The force and displacement curves of the numerical models under three-point bending test demonstrated a good agreement with that of the experiment. The volumetric fraction of osteonal area had a positive correlation with crack resistance of cortical bone, while the one of porosity had a negative correlation. Rodriguez-Florez et al. (2017) analysed the crack propagation paths in healthy and brittle bone by using the X-FEM models. In order to evaluate the effect of porosity on crack propagation of cortical bone, the model just contained the porosity based on CT images and the two types of bones were treated as isotropic linear elastic and homogenous material with the same mechanical properties. The results indicated that the multiple smaller canals of the brittle bone could result in the faster speed of crack propagation. The crack propagation in cortical bone under high speed cutting force was introduced by Sugita et al.(2017). The numerical results showed that the crack penetrated the osteon instead of crack deflection, when the strain rate was high enough.

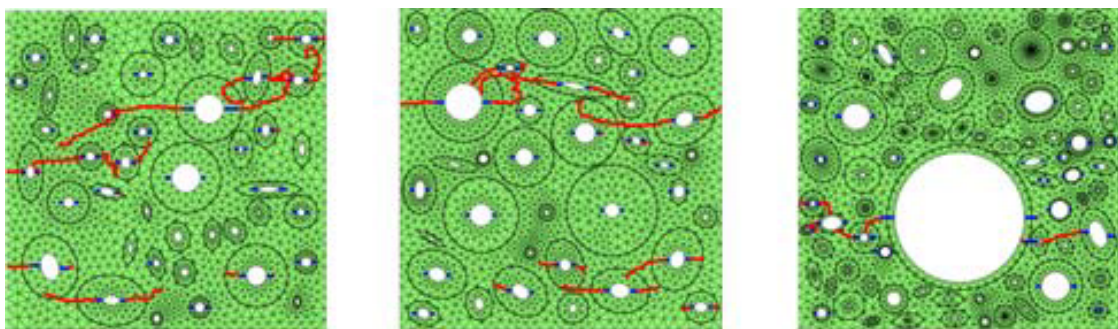


Figure 4.11 X-FEM models with crack initiation (blue) and crack propagation (red) (Budyn et al., 2008)

El Sallah et al. (2016) developed a three-dimensional homogenised X-FEM

model to predict fracture of patient's femur, including cortical bone and trabecular bone. The models were supposed to be an orthotropic or isotropic materials with the same fracture parameters. The model was subjected to 18 KN load on the head of femur in three directions. The numerical results agreed with the experimental ones as Fig 4.12 and presented that the loading direction and the type of material properties could affect the crack initiation and propagation of bone. Sallah et al. (2016) established the three-dimensional numerical model of the two kinds of ceramic pontic tooth, including inlay retained and onlay supported partial denture systems to analyse the crack initiation and propagation by using the extended finite element method. The numerical images of crack initiation and propagation had an agreement with the experimental observation. The results indicated that the loading position could influence the fracture load and cracking path.

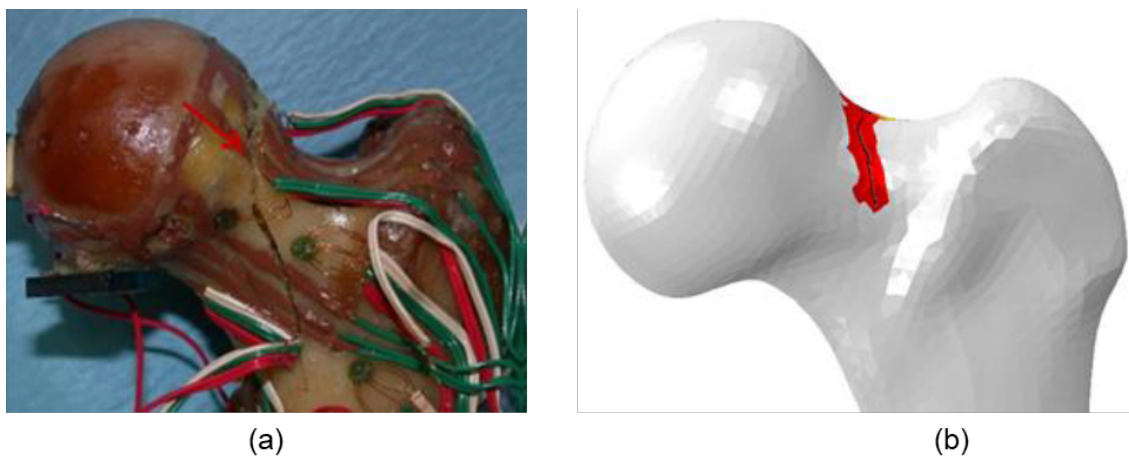


Figure 4.12 Images of crack growth in experimental (a) and simulation (b) results (El Sallah et al., 2016)

The X-FEM model is powerful and efficient to deal with crack growth in bone, while it has the limitations in Abaqus. For examples, the explicit analyse could not be employed to simulate the crack propagation in Abaqus, which could increase the convergence risk. A crack cannot be allowed to turn more than 90

degrees within an element. In order to enhance the accuracy of result, the crack initiation positions have to be predefined. The multiple cracks could exist in the simulation, while the cracks cannot intersect with each other. In addition, a single osteon and multi-osteons finite element models were employed to study the numerical factor, which could influence the accuracy of results (Idkaidek & Jasiuk, 2017; Idkaidek et al., 2017). The finer mesh or smaller analysis increment could influence the convergence and accuracy of the results. Therefore, the optimised mesh density and analysis increment size had to be done to guarantee the accuracy of the results. The X-FEM model is not used in this thesis.

4.5 Summary

- At macroscale, cortical bone can be modelled based on elastic and viscoelastic model to focus on the response or stress distribution of the whole bone.
- At microscale, microstructure based models could be divided in three types, including osteons with idealized geometry, a model established based on the micro-images of real bones and a model generated based on the statistical parameters of the four phases measured from the bone's micro-images.
- Fracture mechanics based models and their limitations were introduced in this chapter, including linear elastic fracture mechanics model, nonlinear elastic fracture mechanics model (cohesive model and extended finite element model).
- A novel zero-thickness cohesive element method and the microstructure based model generated based on the statistical parameters are better choices to compare the fracture behaviour or the characteristics of crack initiation and propagation in various types of cortical bone.

Chapter 5 Methodology for Finite Element Simulation

5.1 Finite element model setup

The effect of geometry and mechanical properties of microstructural constituents in the cortical bone is developed using micro-level finite element model. In addition to previous published method (Budyn et al., 2008; Ural & Mischinski, 2013), a statistical realization of randomly distributed micro-constituents model is used to generate the two-dimensional finite element model. The Haversian canals and osteons are assumed to be in circular and elliptical shapes, respectively. The sizes and volumetric fractions of each constituent are measured using Photoshop and Image-pro software. The statistical database is then embedded into an in-house developed MATLAB program to generate FE ready models. The steps are as below (Fig 5.1):

1. Setting the range of osteon size including long and short axes based on the measured data;
2. Setting the range of Haversian canal size based on the measured data;
3. Setting the range of volumetric fraction of microconstituents including Haversian canals, osteons based on the mean value and standard deviation of each parameter;
4. Setting the range of numbers of osteons based on the measured data;
5. Setting the length and width of the model;
6. Generating randomly the coordination of osteons;
7. Generating the sizes of osteons (the long axis, the angle between long and short axes) and Haversian canals (radius) based on their probability density distributions. The thickness of the cement lines was 5 μm . The

total volume fraction of the osteon and Haversian canal were also satisfied with the setting range of volume fraction of microconstituents of cortical bone

8. Assign the parameters of osteons to each respective coordination;
9. Check whether there are the overlapping osteons.
10. If the model has the overlap osteons, change the permutation of sizes and coordinates of osteons. If there are no the overlapping osteons, the model is generated successfully;
11. If the model still has the overlapping osteons, repeat steps from 6 to 11;
12. Saving the parameters of the model as the python format and inputting this python scripts into Abaqus to automatically generate the model.

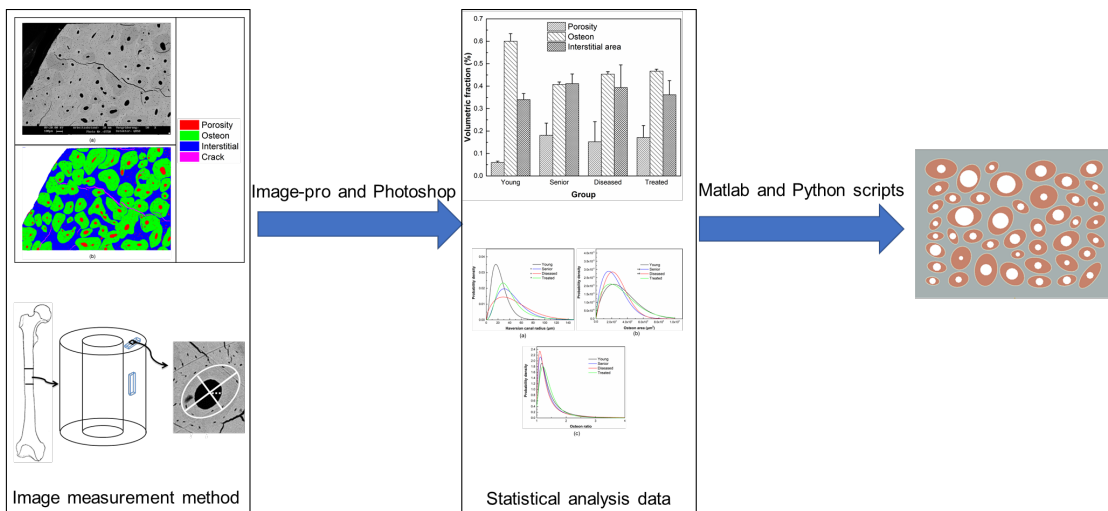


Figure 5.1. Process of finite-element model's setup

5.2 Cohesive element model generation process

The traditional cohesive element method just inserted the cohesive element into one straight path. However, the heterogeneity nature of cortical bone means that the crack propagation path is highly dependent on the local strain or stress concentration. Therefore, the cohesive elements will be implemented into the entire interface between continuum elements domain to facilitate crack

propagation. In order to achieve this target, the MATLAB program is developed to modify the input file generated by Abaqus. The steps are as below:

- 1) Generate the normal input file from Abaqus CAE with defined three microstructural constituents, including the cement lines, the osteons and the interstitial matrix
- 2) Read the numbers of nodes and elements in Abaqus input files using MATLAB
- 3) Create three matrixes in MATLAB so that the element's numbers belonging to each micro-constituent can be saved into individual matrix, respectively
- 4) Renumber the nodes so that each element has its separate nodes (Fig.5.2-b)
- 5) Save the numbers of the new nodes into matrix
- 5) Remove nodes associated with all free edges of the model including edges of the Haversian canal to avoid generate the cohesive elements at these positions
- 6) Perform search to identify all sharing edges of two elements in the model and record their nodes
- 7) Generate a cohesive elements (COH2D4) from every four new nodes of element pair from the search result (Fig.5.2-c)
- 8) Classify the generated the cohesive elements as the cement lines, the osteons and the interstitial matrix, respectively according to the matrix group
- 9) Output the new generated input file with the new nodes and cohesive elements

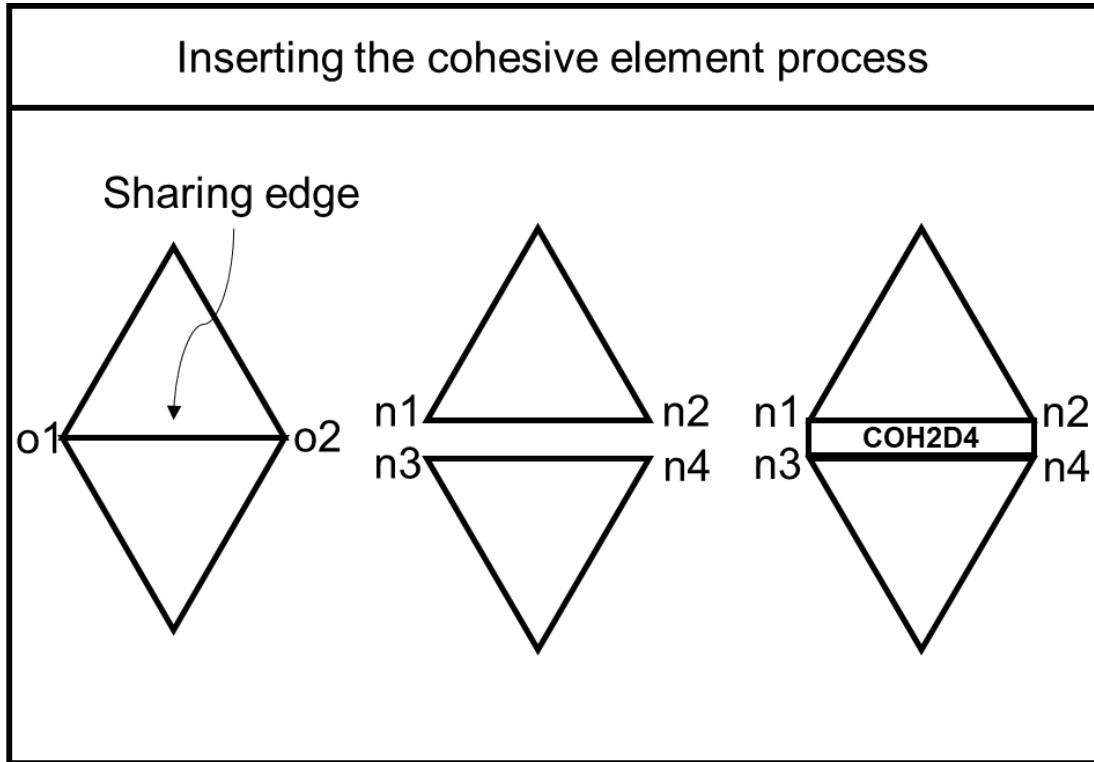


Figure 5.2. Inserting cohesive element process (a) original two elements (b) separate two elements (C) connect two elements by cohesive element-COH2D4

Traction separation law was implemented to govern the separation behaviour of the cohesive elements, as Figure 5.3. T , δ represent the traction and crack opening displacement of cohesive element, respectively. The Zero-thickness cohesive element behaves line elastically upon reaching to the critical point defined by the σ_c and δ_c , after which, crack is assumed to initiate and traction force within the cohesive element reduces until it reaches to the failure point at δ_u . A quadratic nominal strain based damage initiation (initiation the degradation of material response) criteria was applied in the current model (equation 5.1), where ε_n and ε_s are the nominal and shear strains, respectively. After the initiation of damage, the damage evolution was based on linear law. A scalar damage variable, D , whose value was from 0 to 1, dominated stress during the crack process as equation 5.2. The fracture energy release rate, G_f , was used to evaluate the crack opening condition as equation 5.3. When the scalar damage

variable, D , reach 1, it mean that the fracture energy G_f arrive at the critical fracture energy and the crack completely opening.

$$\left\{ \frac{\langle \varepsilon_n \rangle}{\varepsilon_n^o} \right\}^2 + \left\{ \frac{\varepsilon_s}{\varepsilon_s^o} \right\}^2 = 1 \quad 5.1$$

$$t_n = (1 - D)\bar{t}_n \quad 5.2$$

$$G_f = \int \sigma_c d\delta \quad 5.3$$

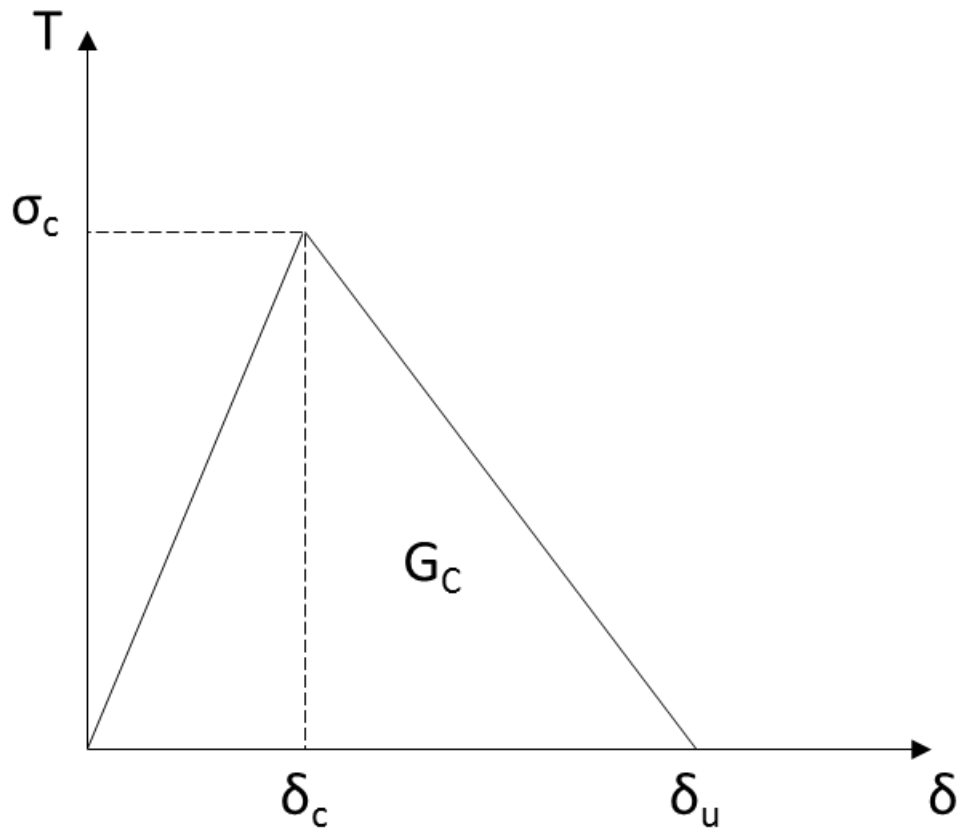


Figure 5.3. Traction–displacement relationship defining the cohesive zone model

5.3 Calculate the percentage of the crack length in microstructural constituents

The percentage of the crack length in different microstructural constituents in the cortical bone is significantly different and dependent on the crack propagation path. In tension and compact tension simulation models, a MATLAB program was developed to automatically calculate these data to avoid the manual calculation error. As previously introduced, the scalar damage variable, D , reaches to 1 when a crack opens completely. Therefore, the condition of the cohesive element of the model could be determined by the D value of the output file. The steps are as below:

- 1) Read the input file to get the number of the cohesive elements in the model.
- 2) Read the input file to get the index of coordinates of the cohesive elements
- 3) Read the input file to get the index of the cohesive elements in three microstructural constituents, including the cement lines, the osteons and the interstitial matrix.
- 4) Read the scalar damage variable, D , and the numbers of the cohesive elements of each step in output file
- 5) Calculate the number of cohesive element which have the D value equal to 1
- 6) Look up the numbers of the pervious cohesive elements in the index of the microstructural constituents to confirm which groups the cohesive elements belong to
- 7) Look up the numbers of the previous cohesive elements in the index of the coordination of the cohesive elements to calculate the length of the crack

- 8) Sum the crack length in different microstructural constituents, respectively
- 9) Calculate the percentage of the crack propagation in microstructural constituents

5.4 Mesh sensitivity study

Mesh convergence study should be done to guarantee the accuracy and computational cost of the model. The mechanical properties of bovine cortical bone were used for validation of mesh convergence due to limitations of experimental data in the literature. Seven mesh sizes were selected for the test, range from 0.01, 0.015, 0.02, 0.025, 0.03, 0.035 to 0.04. The volume fractions of microstructural constituents of the bovine cortical bone in the model were 4.5, 42.7 and 52.8% for the Haversian canal, the osteons and the interstitial matrix, respectively. The mechanical properties of microstructural constituents and homogenised material were selected based on Li's data (2013) as in Table 5.1. The failure of bovine cortical bone was assumed to be at 0.6% maximum principle strain.

Table 5.1. Mechanical properties of microstructural constituents of bovine cortical bone tissue (Li et al., 2013)

Model	Elastic modulus (GPa)	Poisson's ratio	Strain energy-release rate (N/mm)
Osteon	13.50	0.17	0.86
Interstitial matrix	14.60	0.153	0.238
Cement line	10.12	0.49	0.146
Homogenised material	11.18	0.167	0.422

5.4.1 Uniaxial tension

In uniaxial tension model, the mesh element numbers were 31817, 15021, 9386, 6654, 5490, 4552 and 4044 corresponding the previous mesh sizes, respectively (Fig 5.4). For the uniaxial tension simulation, a tensile displacement of 0.04 mm was uniaxially loaded to the edge of the model while the bottom edge was fixed as shown as Fig.6.4. As shown in the figure, the maximum force decreased with the increase of the mesh size, while the maximum forces for mesh sizes of 0.01, 0.015 and 0.02 mm were close to each other. These values were 57.19, 57.09 and 56.93 N, respectively (Fig 5.5-a). The crack-propagation paths in the models of this thesis play a significant role to present the effect of microstructural constituents on crack propagation in the model. Therefore, the sensitive test about crack propagation paths of the models with different mesh sizes should be done to confirm the computational accuracy. In Fig 5.6, the crack-propagation paths in seven kinds of mesh sizes, including 0.01, 0.015, 0.02, 0.025, 0.03, 0.035 and 0.04 mm, were presented. It was clear that the models with 0.01 and 0.015 mm mesh sizes were the same. However, the other kinds of mesh sizes were significantly different from the previous mesh sizes.

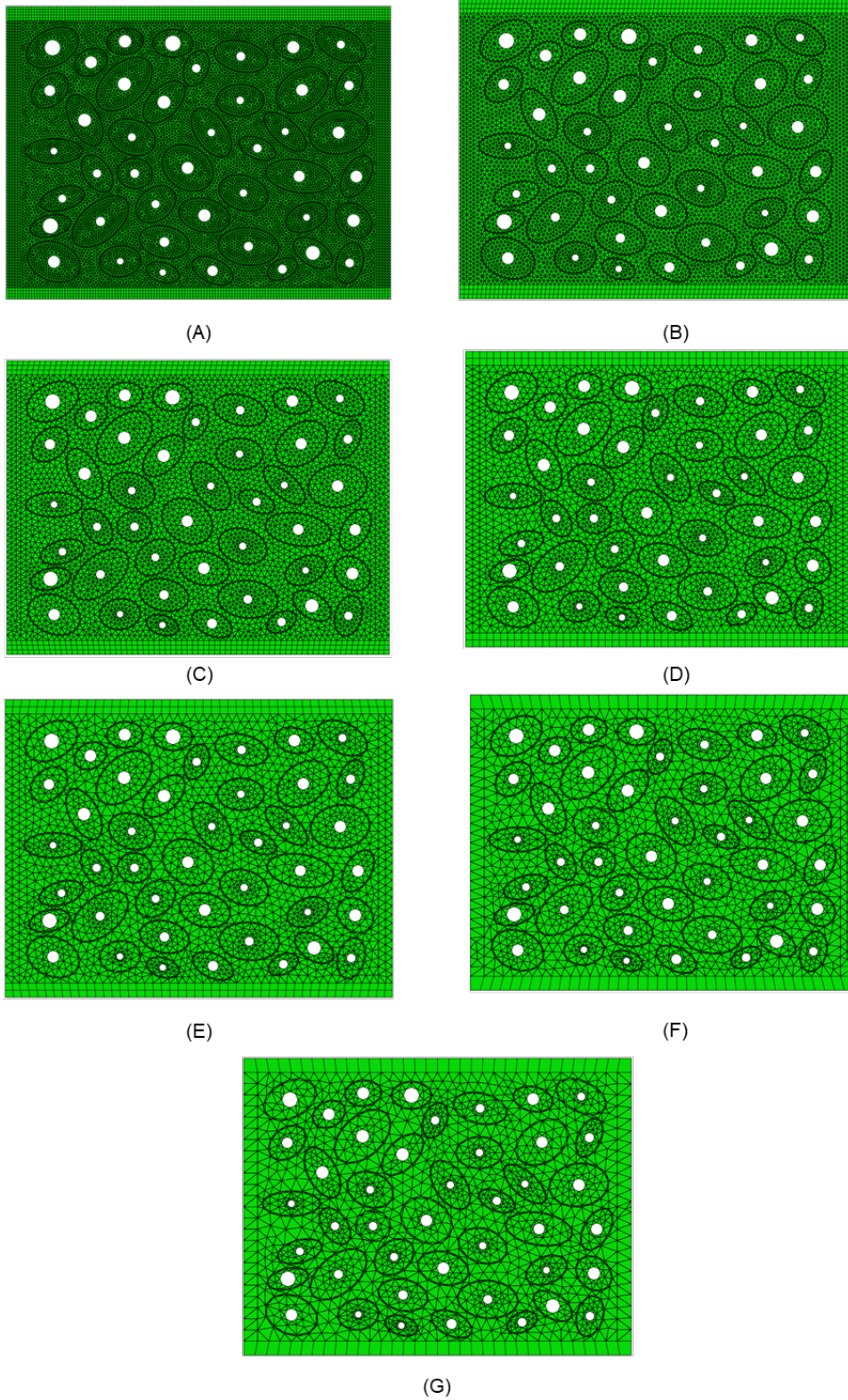
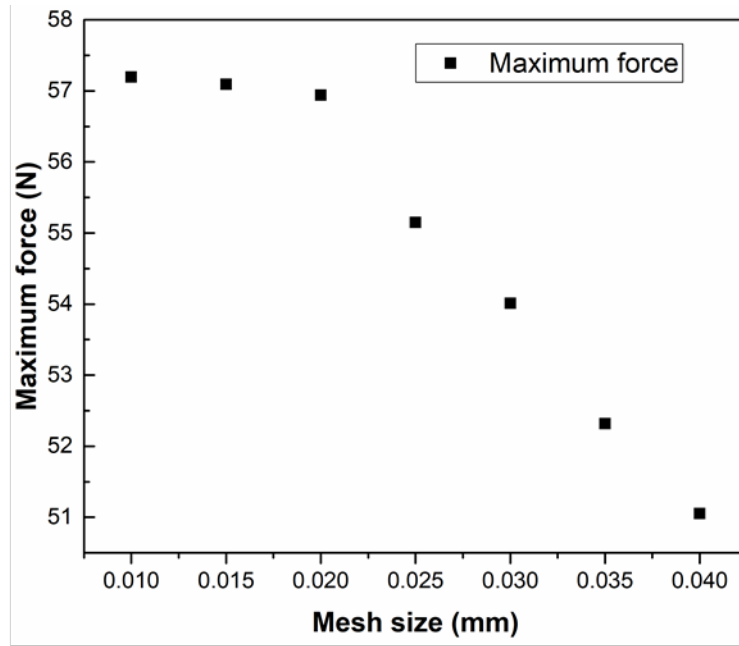
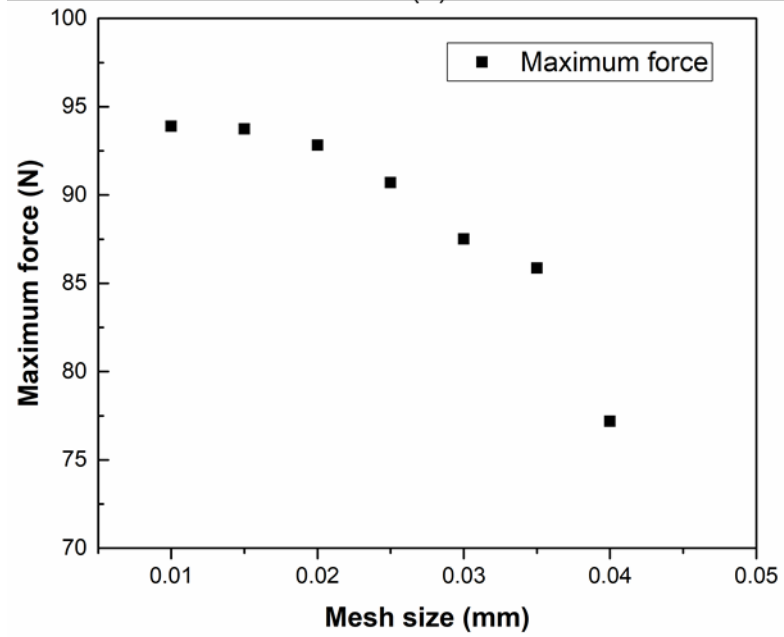


Figure 5.4. Mesh conditions for different mesh sizes including 0.01 (A), 0.015 (B), 0.02 (C), 0.025 (D), 0.03 (E), 0.035 (F) and 0.04 (G)



(a)



(b)

Figure 5.5. Effect of mesh size on maximum force in two loading conditions: (a) uniaxial tension; (b) compact tension

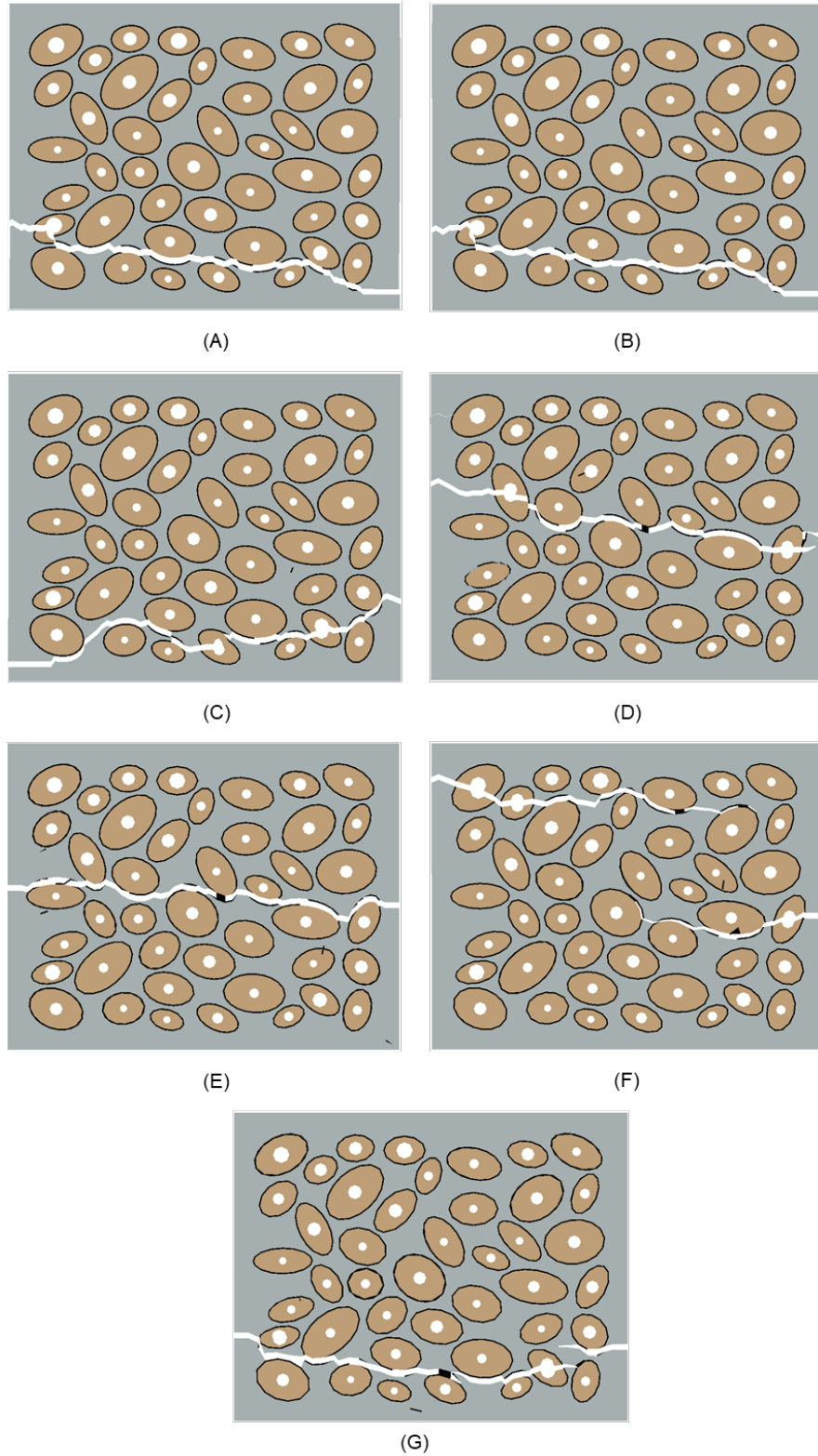


Figure 5.6. Crack propagation in the uniaxial-tension models with different mesh sizes: 0.01 (A), 0.015 (B), 0.02 (C), 0.025 (D), 0.03 (E), 0.035 (F), 0.04 (G) mm.

5.4.2 Compact tension

The mesh element numbers were 78513, 47601, 35599, 28972, 25694, 23136 and 214405 for the compact tension model. The mesh conditions of microstructural area in tension and compact-tension were shown in Fig.5.7. In term of the compact-tension simulation, the width of the models was $W= 13.5$ mm and the initial length of the pre-notch was $a=4.2$ mm. The thickness (B) and thickness between the roots of the side grooves (B_N) of the model were 2.5 mm and 1.5 mm, respectively (An et al., 2011).

In term of the compact-tension model as seen in Fig 5.5-b, the maximum forces for mesh sizes of 0.01, 0.015 and 0.02 were 93.9, 93.74 and 92.82 N, respectively. The maximum forces reduced considerably with with larger mesh sizes.

For the compact-tension models, the models with 0.01 and 0.015 mm mesh sizes had also the same crack propagation paths, while the models with other kinds of mesh sizes had similar crack propagation paths apart from several positions. From the mesh-sensitivity test, the results obtained from the zero-thickness cohesive element modelling approach was affected by the mesh size both in terms of its maximum force and the crack-propagation path. However, for the compact-tension models, the change in mesh sizes did not significantly affect the crack-propagation paths, but the large mesh size resulted in the element distortion (Fig 5.8). In consideration of the balance between the accuracy and the computational time, the mesh size of 0.015 mm was select in the simulation.

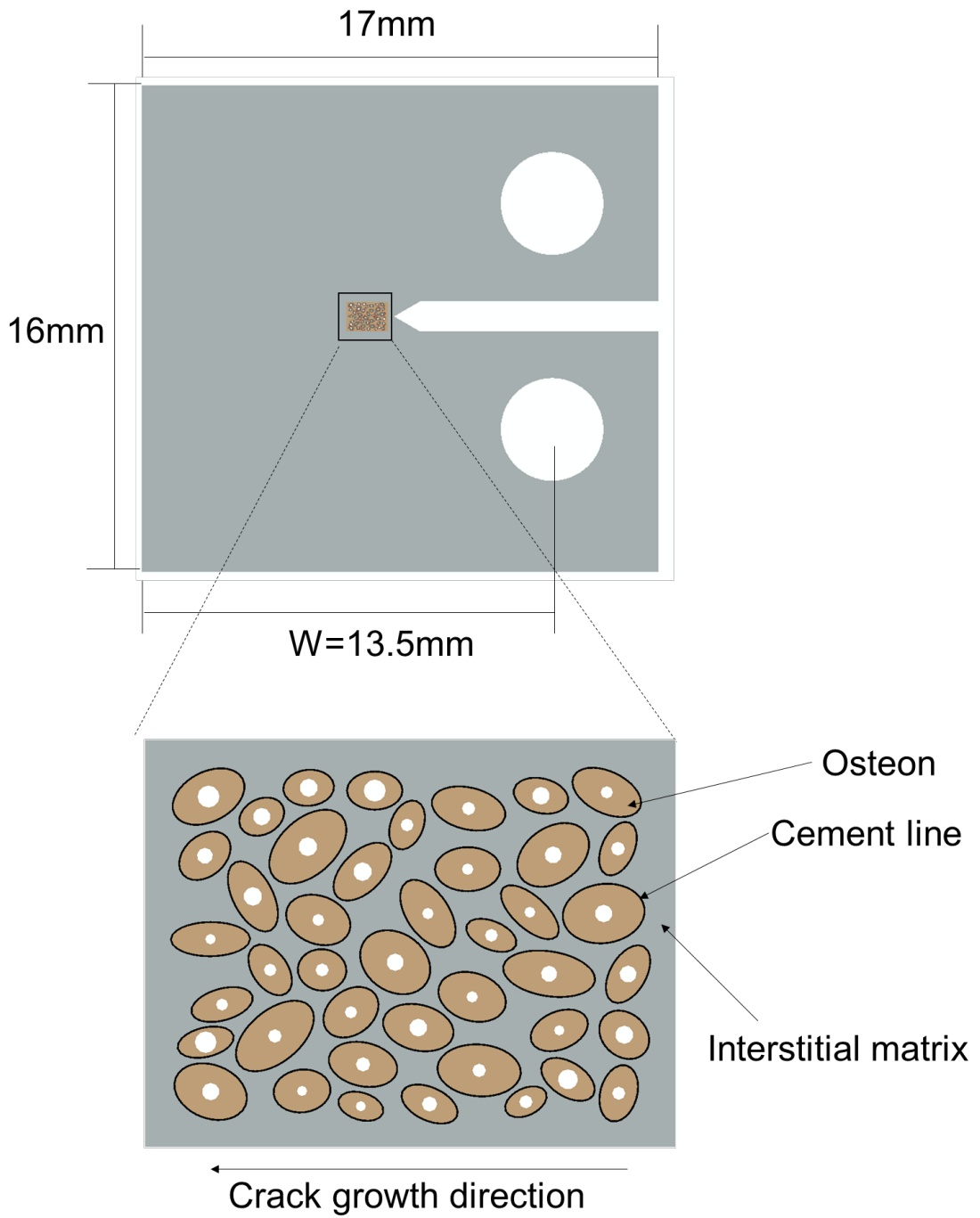


Figure 5.7. Bovine cortical bone under compact-tension loading conditions and example of microstressed domain

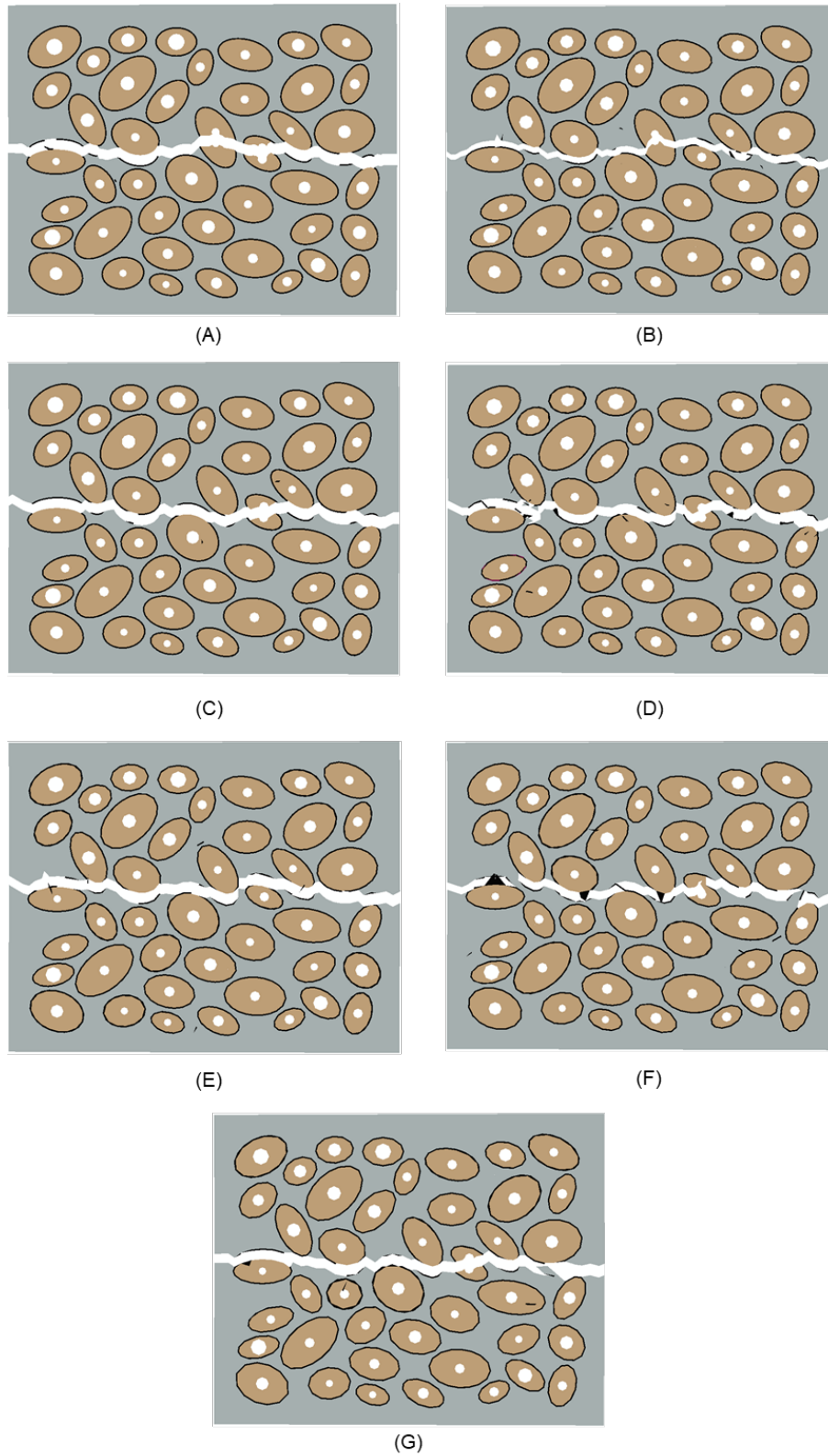


Figure 5.8. Crack propagate in compact-tension models with different mesh sizes: 0.01 (A), 0.015 (B), 0.02 (C), 0.025 (D), 0.03 (E), 0.035 (F), 0.04 (G) mm. (The black triangles are the element distorted due to the large element size in (F))

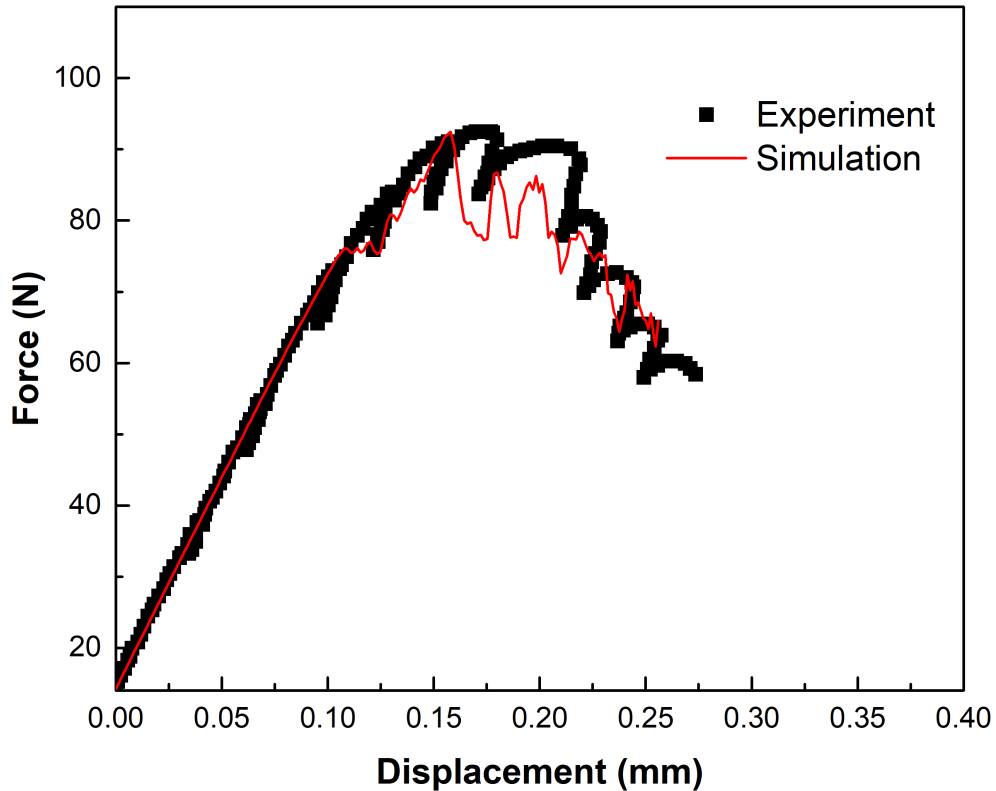


Figure 5.9. Loading force-displacement curve of compact-tension model simulation (Red) and experiment (Black) (An et al., 2011) of bovine cortical bone

To further validate the accuracy of the developed modelling approach, compact-tension test of bovine cortical bone from (An et al., 2011) was used for this study. The loading force against displacement curves from both the experiment and current simulation model were compared in Fig.5.9. The curves of the experiment and simulation did not match in the propagation parts, because the microstructure of the model was not exactly based on the CT image of the specimen, being on the statistical data. However, some parts of the simulation curve still had a good match with the experimental one. The fracture resistance curve (R-curve) from the same study was used to validate the fracture toughness of the cortical bone. The initiation stress-intensity factor of the simulation was $2.51 \text{ MPa m}^{0.5}$, which was in the range of the experimental one ($2.55 \pm 0.36 \text{ MPa m}^{0.5}$). The growth of the stress-intensity factor of the simulation (0.53 MPa

$\text{m}^{0.5}/\text{mm}$) was higher than the average value ($0.25 \text{ MPa m}^{0.5}/\text{mm}$), while it was still in the range ($\pm 0.36 \text{ MPa m}^{0.5}/\text{mm}$). Therefore, the crack-propagation paths in the simulation models could make sure that the simulation models had the similar fracture toughness as the experimental one.

5.5 Conclusion

In this chapter, the development of zero-thickness cohesive element modelling approach and its validation were introduced. In addition, a MATLAB program was developed to automatically calculate the percentage of crack length in each microstructural constituent, avoiding manual errors and enhancing work efficiency.

Furthermore, mesh-sensitivity studies were conducted and the results showed that mesh size of 0.015 mm was the best choice to achieve both accuracy and computational efficiency. Last, the developed modelling approach was validated against experiment data.

Chapter 6 Simulation of crack initiation and growth in human cortical bone: effects of osteonal morphology

6.1 Introduction

Bone fracture caused by ageing and degenerative bone disease such as osteoporosis increase the risk of bone fracture, causing detrimental effects to the normal day-to-day life. The shift in demographic population and ageing society means that there is an increasing number of osteoporosis and ageing-related fracture causing significant public health problem. In UK alone, there are more than half a million new fragility fractures each year, which cost over £3492 million per year. In general, osteoporosis treatment is associated with the use of gold-standard medical diagnosis, dual-energy X-ray absorptiometry (DXA), to measure the bone mineral density, and subsequent pharmacologic therapies, which restrain the excessive loss of bone mineralisation. However, such treatment, as indicated in previous research (Bernhard et al., 2013), also changes micro-morphology of microstructural constituents in cortical bone.

At micro-scale level, a cortical bone tissue could be treated as a natural composite material with four main constituents, namely, osteons, Haversian canals, cement lines and interstitial matrix. Several studies suggested that ageing and bone disease have significant impact on the remodelling process (Karen L. Bell et al., 2001; Mulhern, 2000), hence, change the morphological structure and their constituents: increased porosity and decreased osteonal areas were reported to associate with ageing (Rho et al., 2002; Yoshino et al., 1994). The remodelling process affect not only the heterogeneous distributions of microstructure constituents, but also the mechanical properties of bone tissue

(Rho et al., 2002), altering the local stress and strain distributions and/or crack propagation resistance in cases of fracture (Budyn & Hoc, 2010). However, experimental investigation of crack-propagation characteristics in cortical bones, which originate from different population/patient groups is ethically challenging and experimentally expensive and difficult. In this study, a novel computational method was developed to evaluate the impact of morphological changes on crack-propagation process.

Simulations of crack propagation in cortical bone were achieved previously using either Cohesive Zone Element method or Extended Finite Element method (XFEM). Cohesive and XFEM method have their advantages in simulating crack propagation, i.e. less computational power compare with other FE techniques in the same level of accuracy. However, they suffer from several drawbacks: a predefined crack path in the case of cohesive element method or no crack multiplication and bifurcation in those XFEM models.

In this study, a novel zero-thickness cohesive element method (Su et al., 2010; Ural et al , 2011) combining with randomly distributed microstructured cortical bone model was developed to investigate the effects of micro-morphology and mechanical properties on the crack initiation and growth of human cortical bone in four patient groups: young, senior, diseased (osteoporosis) and treated. The micromorphology parametric of cortical bone were obtained based on experimental studies of the respective patient groups.

6.2 Materials and Measurement

Images taken from four groups of cortical bone specimens (young group: 32 ± 8 years, senior group: 79 ± 9 years; diseased (osteoporosis) group: 81 ± 7 years; and medically treated group: 81 ± 9 years), acquired from proximal femoral diaphysis

of 35 female donors (age from 24 to 88) were analysed (Fig 6.1). The cortical bone specimens of donors were related to death, because of traffic accidents, assaults, suicides and other unnatural causes, without any other diseases like cancer, renal disease or Paget's disease that could influence the microstructure of cortical bone. The cortical bones of diseased (osteoporosis) group had a low bone mineral density, which was at least 2.5 standard deviation below the young groups mean based on the World Health Organization. The medically treated group were treated with the third-generation bisphosphonate alendronate at 70 mg/week and for 6 ± 1.6 years.

First, volumetric fractions of three micro-constituents, osteon, porosity, interstitial, was analysed following the steps listed below as Fig 6.2. Then the parametric distributions of osteonal system, including an osteon (defined as elliptic with two axes and an angle of rotation) and a concentric Haversian canal (assumed to be circular shape) (Fig 6.3) were fitted against morphological data using a best fit function. Finally, a MATLAB programme was developed to generate randomly distributed microstructural models of cortical bone based on analysed parameters of each population group (Fig 6.1-b), A detailed volumetric fractions of micro-constituents for each group were shown in table 1.

1. Identify out-lines and perimeter edges of the bony structure in order to calculate accurate areal fraction of the cortical tissue.
2. Existing micro-cracks were distinguished with other micro-constituents using coloured filter.
3. When the boundary of osteon was not clear, Image Pro software was used to increase the contrast of images, where automatic feature recognition and manual operations were used to segment each micro-constituent with different colours: red, green and blue, representing porosity, osteonal

areas, and interstitial matrix, respectively. The micro-cracks were distinguished as purple colour and the area of them were not included into the area of cortical bone.

4. Compute areal fractions of each micro-constituent by counting the overall number of pixels in different colours.

These statistical data were also used to build the randomly distribution of microconstituents in models introduced in Chapter 5. The volume fractions of microconstituents of the model, including porosity, osteons and interstitial matrix were selected based on the experiment and from the Germany partners.

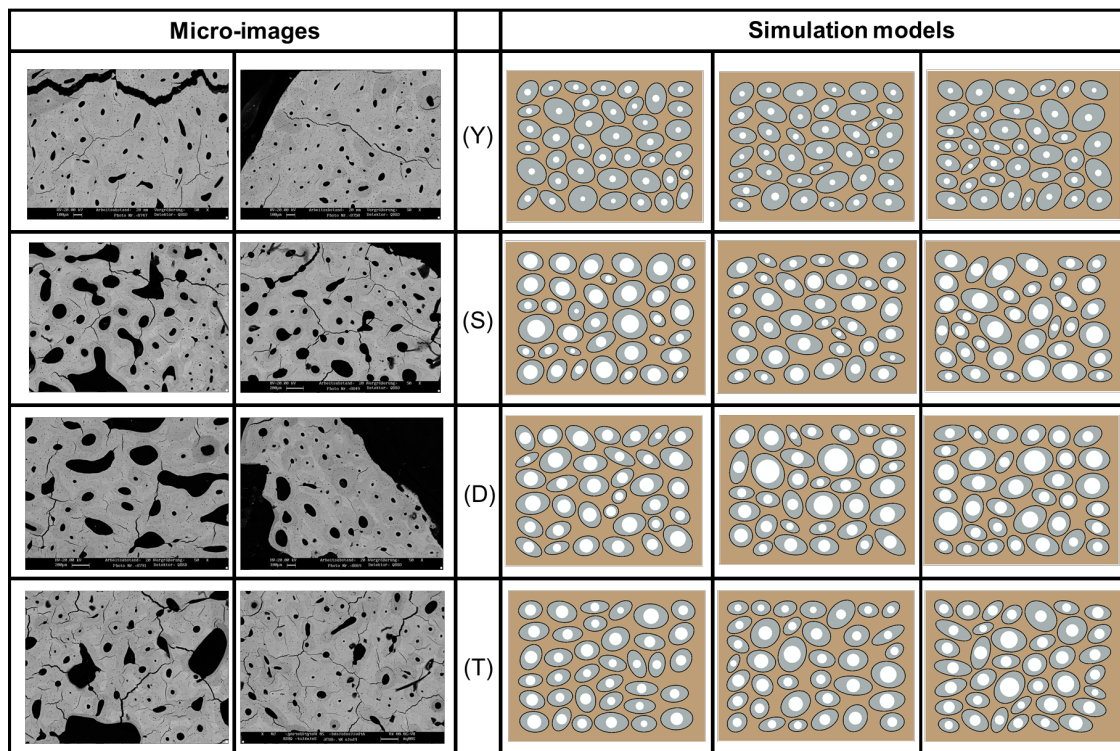


Figure 6.1. Experimental micro-images and randomly distributed microstructural simulation models of human cortical bones in transverse section of four groups (Y-young, S-senior, T-treated, D-diseased)

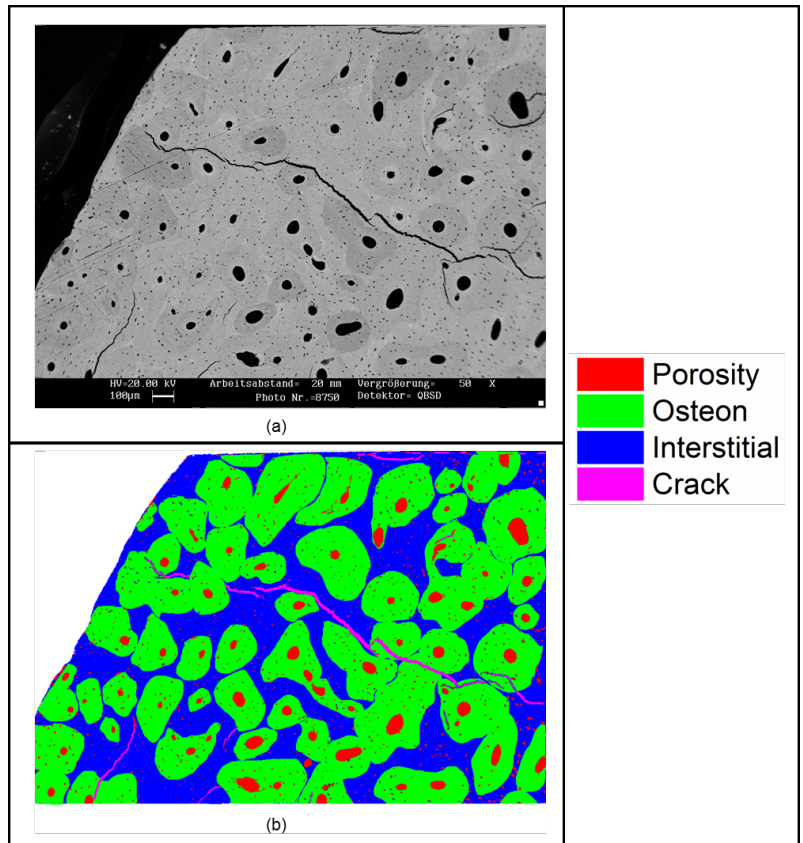


Figure 6.2. Analysis process of micro image volumetric fraction of osteon (green), interstitial area (blue), porosity area (red) and crack area (purple); a is original micro-image and b is analysed image

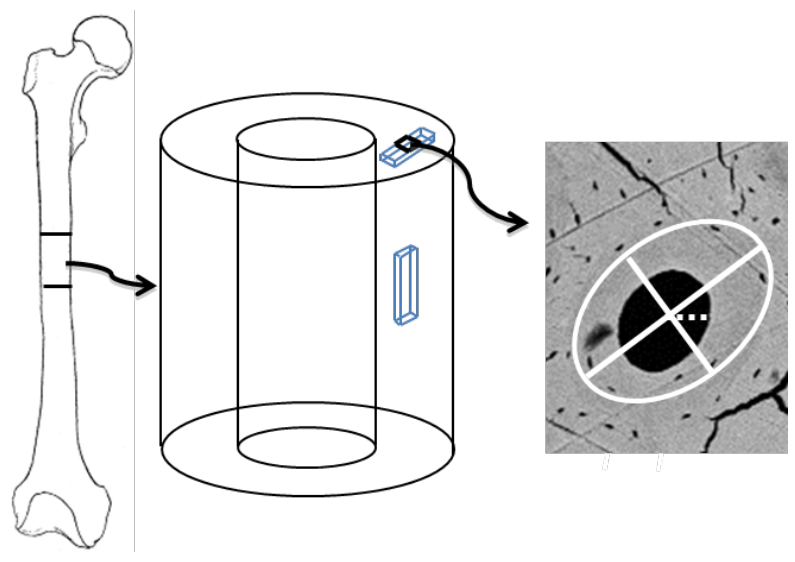


Figure 6.3. Analysis process of parameters of individual osteon as ellipse (long axis and short axis of osteon, radius of Haversian canal)

Table 6.1. Volumetric fraction of micro-constituents of four groups, each group had two simulation models. (The percentages of porosity, osteons and interstitial matrix were selected based on the experiment and from the Germany partners from university medical center Hamburg-Eppendorf (Bernhard et al., 2013))

	Porosity (%)		Osteon (%)		Interstitial area (%)	
	Model	Exp	Model	Exp	Model	Exp
Young	5.94	5.96±0.66	60.01	60.03±3.39	34.05	34.01±2.74
	5.34(specimen)		57.92		36.74	
	5.81	58.31	35.88			
Senior	17.10	18.10±5.46	41.11	40.79±1.11	41.79	41.11±4.53
	12.83		41.54		45.63	
	15.24(specimen)	40.22	44.54			
Diseased	15.71	15.22±8.96	45.38	45.38±1.11	38.91	39.40±10.07
	19.00		44.27		36.73	
	19.98(specimen)	44.62	35.40			
Treated	17.13	17.13±5.34	45.78	46.68±0.92	37.09	36.19±6.26
	13.18		46.68		40.14	
	14.29(specimen)	47.20	38.51			

6.3 Model specification

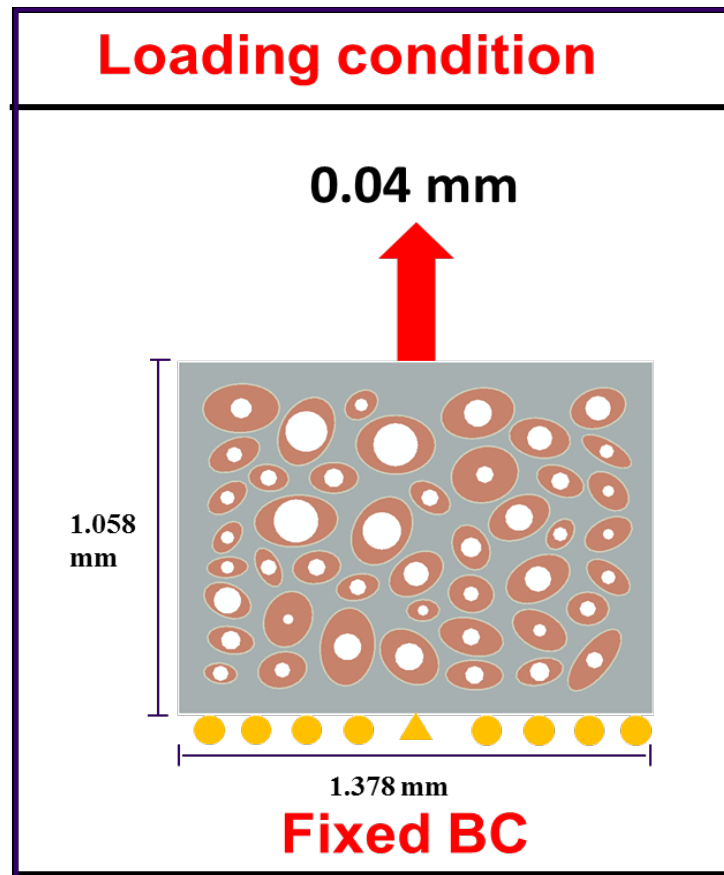


Figure 6.4. Uniaxial tension loading condition and size of model

Four mesh sizes, including 0.01, 0.015, 0.02 and 0.025, was used for mesh convergence study and the average mesh size of 0.015 mm (1%) was used in our current study to balance the accuracy and computational cost. In order to investigate effect of osteonal morphology of cortical bone on crack propagation, mechanical properties of different microstructural constituents, such as osteons, interstitial area, and cement line were adopted based on previous research (Abdel-Wahab et al., 2012; Idkaidek et al., 2017) (Table 6.2). The failure of human cortical bone was assumed to be at 0.4% maximum principle strains. The elastic modulus of cement line was assumed to be 25 percent lower than that of the osteon (Budyn & Hoc, 2007).

Table 6.2. Material properties of microstructural constituents of cortical-bone tissue (Abdel-Wahab et al., 2012; Idkaidek et al., 2017)

Model	Elastic modulus (GPa)	Poisson's ratio	Strain energy-release rate (N/mm)
Osteon	13.50	0.33	0.86
Interstitial matrix	14.60	0.3	0.238
Cement line	10.12	0.41	0.146

In real life, the main force on the cortical bone, caused by supporting the human body, is compression force in the longitudinal direction, while this force also results in tension in the transverse direction at the same time. In this study, the crack propagation in the transverse direction of cortical bone is the main targets. Therefore, a tension loading was applied to the cortical bone. A displacement of 0.04 mm uniaxial tensile load was applied to the top edge of the model while the bottom edge was fixed as shown in Figure 6. The model was running a high performance cluster (HPC) using explicit Abaqus.

6.4. Result and Analysis

6.4.1 Morphological variation

The micro-image analysis confirmed that the micro-morphological properties of cortical bone vary among four groups (Fig 6.5): young (Y) group has the highest average osteonal area ($60.03 \pm 3.39\%$) and lowest porosity ($5.96 \pm 0.66\%$), followed by treated (T) ($46.68 \pm 0.92\%$, $17.13 \pm 5.34\%$), diseased (D) ($45.38 \pm 1.11\%$, $15.22 \pm 8.96\%$) and senior (S) ($40.79 \pm 1.11\%$, $18.10 \pm 5.46\%$) groups, respectively, similar to osteon bone area measured previously (Bernhard et al., 2013). On the other hand, the order of average interstitial area among

groups was completely reversed: highest in senior group ($41.11\pm 4.53\%$) and lowest in young group ($34.01\pm 2.74\%$). Further histogram analysis of micro-constituents confirmed morphological variation among groups: young group has the lowest peak (around $20\ \mu\text{m}$) and narrowest (right skew) spread of Haversian radius among all groups (Fig 6.6-a), while the peak as well as spread continue to increase with diseased group having the widest spread of all. On the other hand, young and treated groups saw a slight wider spread and larger average osteon area compare with senior and diseased groups (Fig 6.6-b). Statistically, Haversian radius and osteon area from young and treated groups are consistently significant ($p < 0.05$) to senior and diseased groups, respectively. However, the aspect ratio measured as the long axis over short axis of an osteon has no significant difference ($p > 0.05$) among groups.

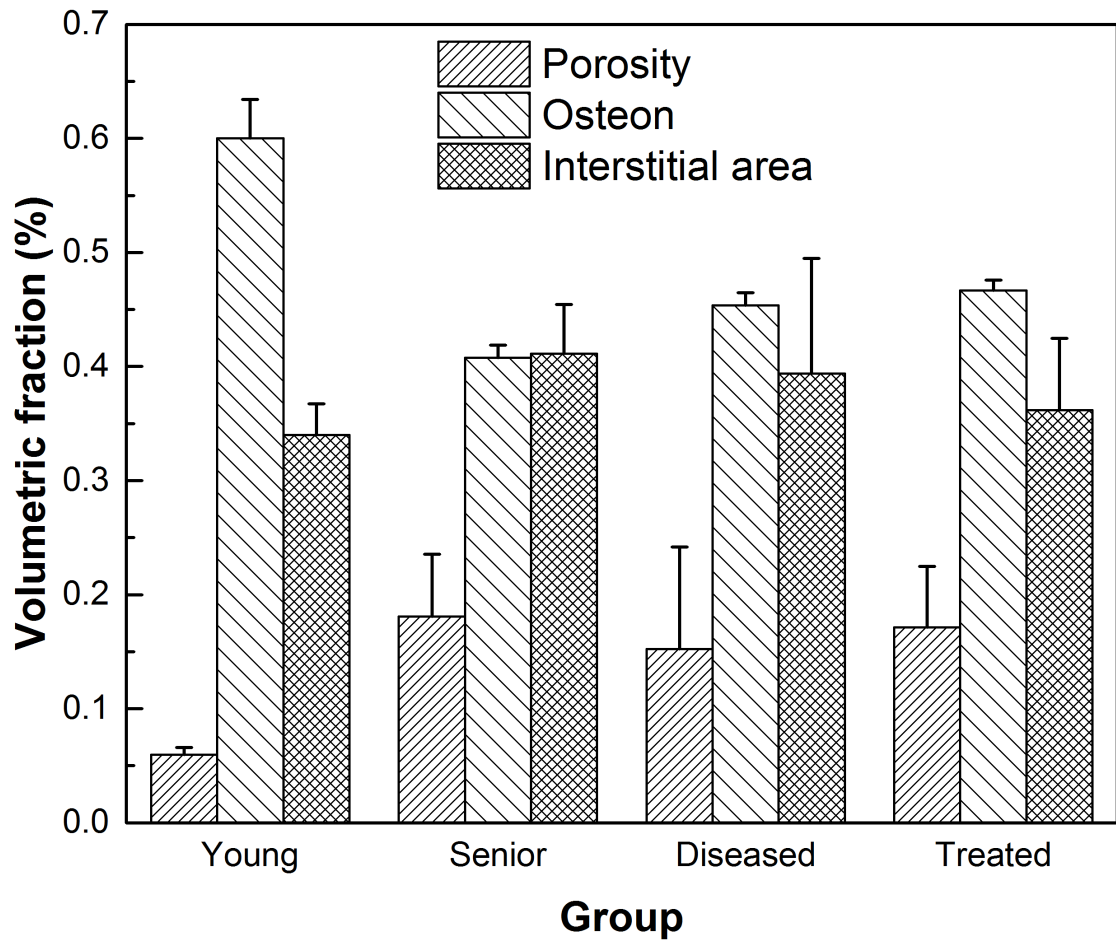


Figure 6.5. Comparison of volumetric fractions of microstructure constituents of human cortical bone between four groups

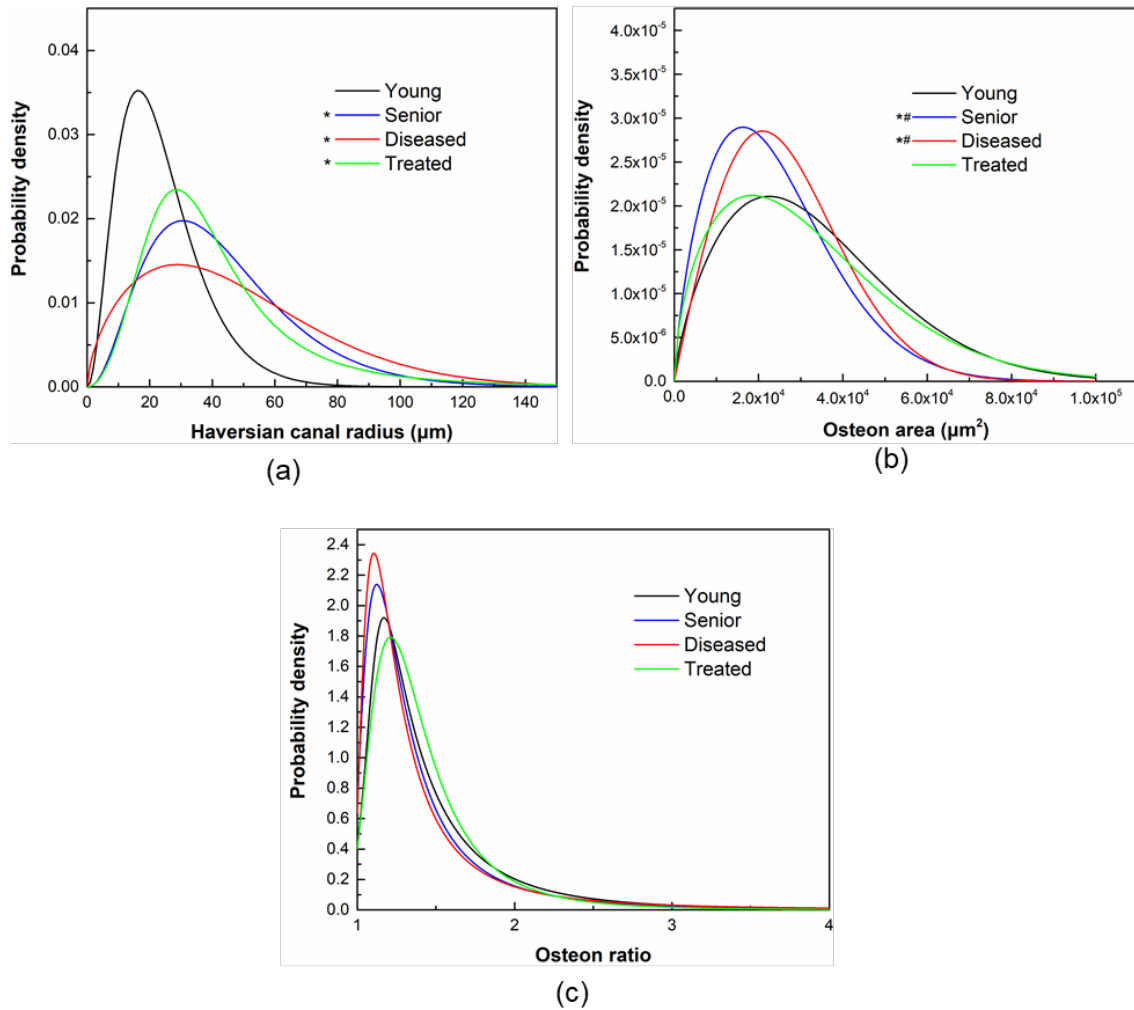


Figure 6.6. Probability density of Haversian canal radius (a), osteon area (b) and osteon ratio-long and short axis (c) in human cortical bone (* and # are that the group with the young and treated group have significant difference <0.05 , respectively)

6.4.2 Mechanical properties

The results obtained from three statistical realised cortical bone models from each group show that human cortical bone behaves as a brittle material when loaded along transversal direction in tension, coincide with experimental observation (Reilly & Burstein, 1975). The average tissue modulus, ultimate strain and ultimate tensile strength for four groups were 10.58 ± 1.13 GPa, $0.367 \pm 0.017\%$ and 32.12 ± 5.11 GPa, respectively, and in agreement with literature values (Li et al., 2013; Reilly & Burstein, 1975). Prior to failure, human

cortical bone models behave linear elastic, with no apparent yielding. Young's modulus for the young group, calculated between zero point and the peak stress, was 12.36 ± 0.08 GPa, significantly higher (20.3%) than the average of the other three groups. On the contrary, diseased group (9.44 ± 0.23 GPa) has the lowest Young's modulus of all, 23.6% lower than that of young group. Treated group (10.39 ± 0.38 GPa) showed ever slight improvement compare with diseased group, but there was no significant difference between treated and senior group. Apart from the modulus difference, the ultimate tensile strengths of human cortical bone between the four groups shared similar trend, with the young and diseased groups being at the two extreme ends of all groups, while the treated group showing slightly improvement compare with diseased group. Statistical ANOVA analysis reviewed that Young's modulus and ultimate strength were statistically significant ($p < 0.05$) among four groups, except that between treated and senior groups. In term of failure strain (the stress would decrease from this point), young group had better performance on it compare with senior and diseased group. The ones of the treated group and diseased group were slightly higher than the diseased group's one.

The curves of normalised stress (the stress over one minus the volumetric fraction of porosity of each group) over strain was shown as Fig 6.8. The results presented that the volumetric fraction of the porosity was not significant role to influence the elastic properties of four groups. The young group was the tough cortical bone, because of the volumetric fractions of the osteon and interstitial matrix. To better illustrate the post-damage mechanical characteristics among four the analysed groups, normalised stress over ultimate tensile strength was plotted against concurrent strain value in Fig 6.9. start at the ultimate tensile stress and end when the first crack-segment is fully opened. It can be seen that both the diseased and senior groups had an early damage initiation strain

compare with the other two groups, with the diseased group having the smallest first crack opening strain of all at 0.393%. The damage process of the senior group took longer to complete than the diseased group, reaching to the same first crack opening strain of the treated group of $0.413 \pm 0.009\%$, respectively. The treated groups, on the other hand, benefited from a delayed damage softening, has a better load bearing capacity at any given strain value. Young group was the most enduring group of all with latest damage initiation and longest damage softening span.

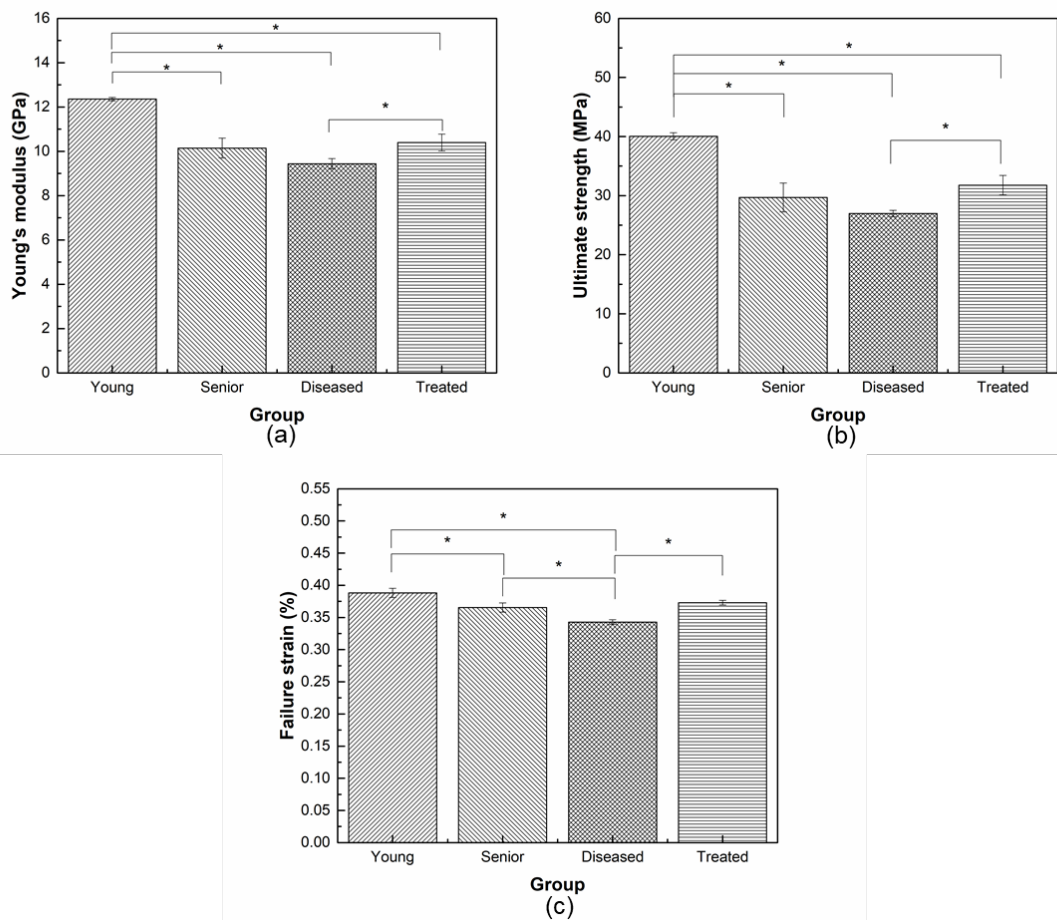
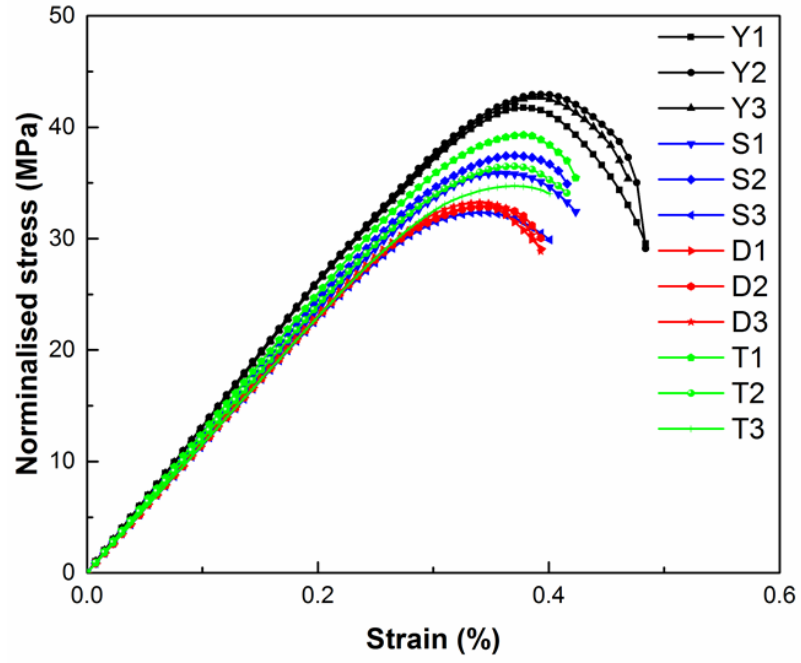
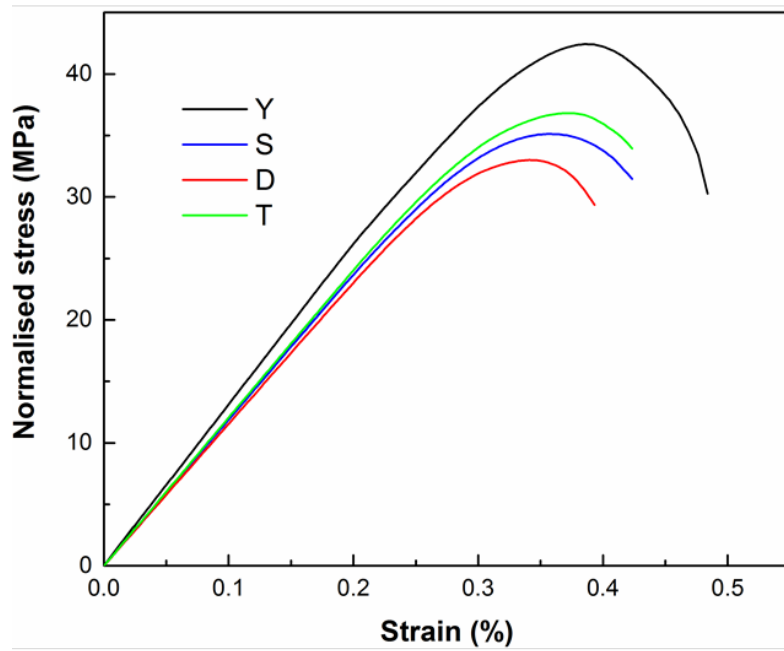


Figure 6.7. Bar charts of Young's modulus (a), Ultimate strength (b) and failure strain (c) (* is significant difference <0.05)

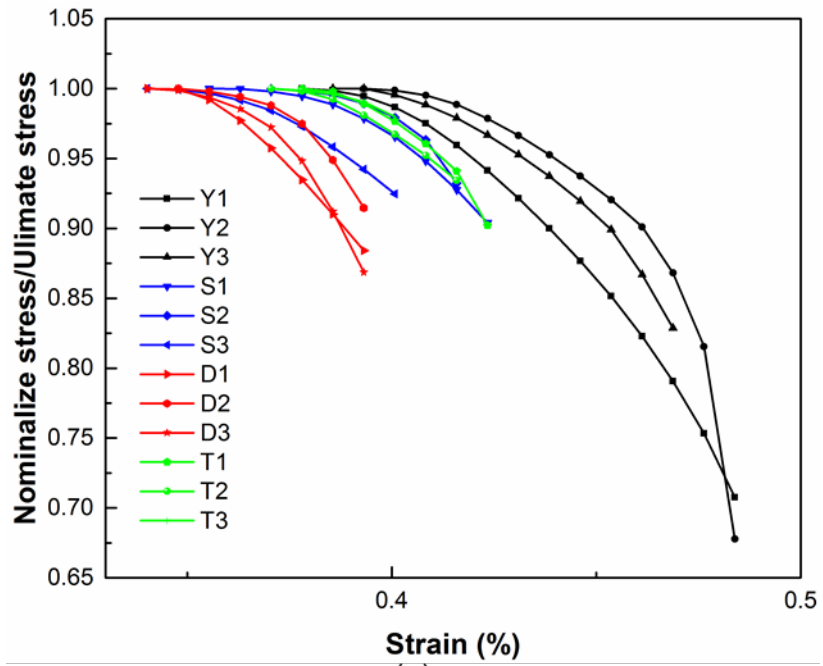


(a)

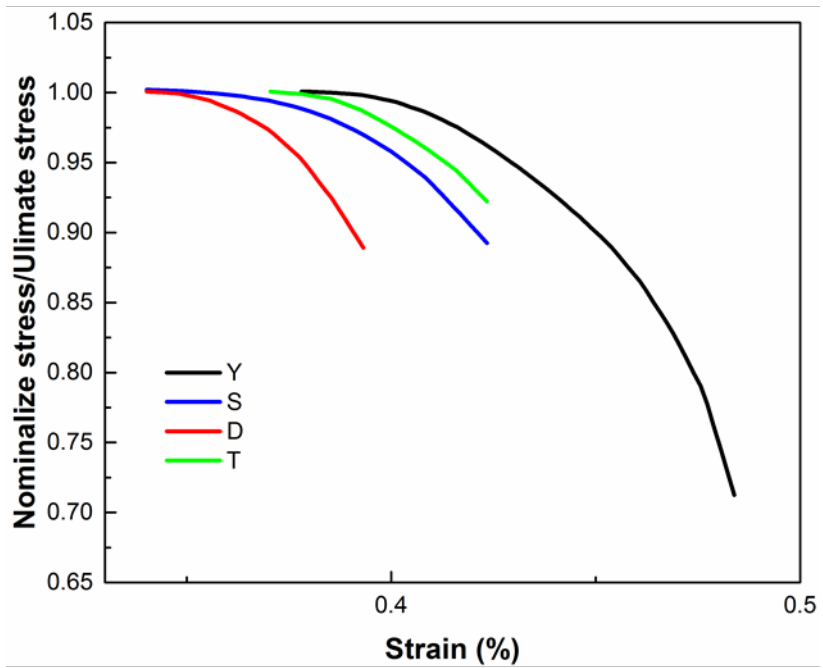


(b)

Figure 6.8. Simulation results (a) and average curves (b) of normalised stress vs strain during elasticity part and crack initiation (the end point of each line is the first crack-segment fully opened)



(a)



(b)

Figure 6.9. Simulation results of nominalize stress/ultimate stress (a) and fitting curve (b) from ultimate strength to crack initiation (the end point of each line is the first crack-segment fully opened)

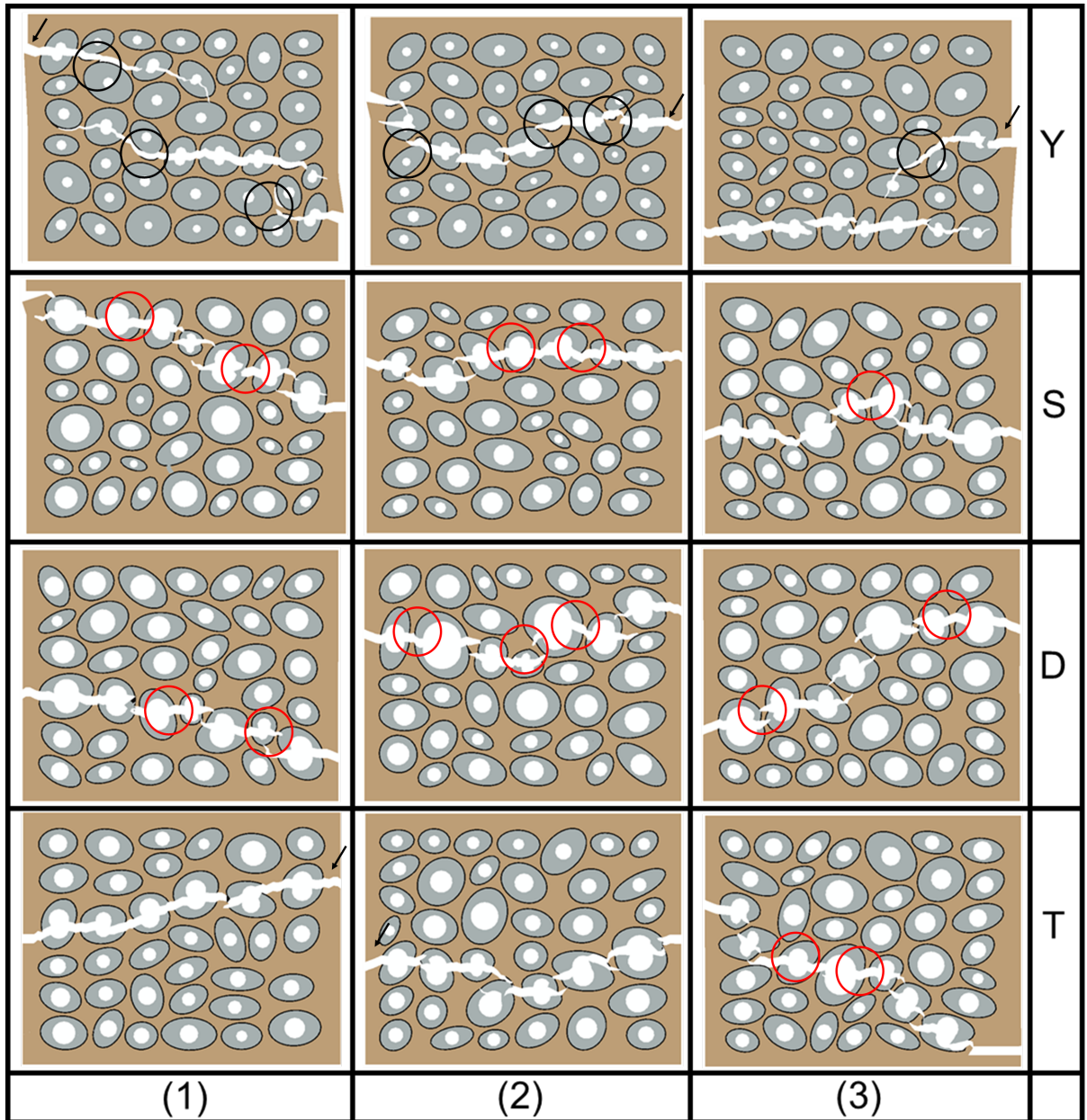
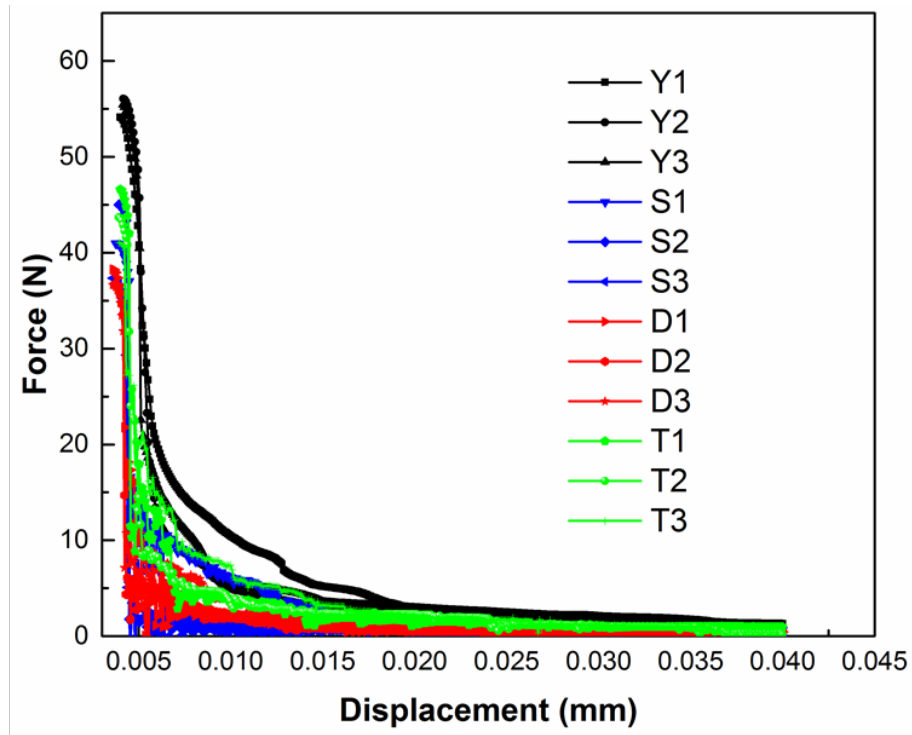
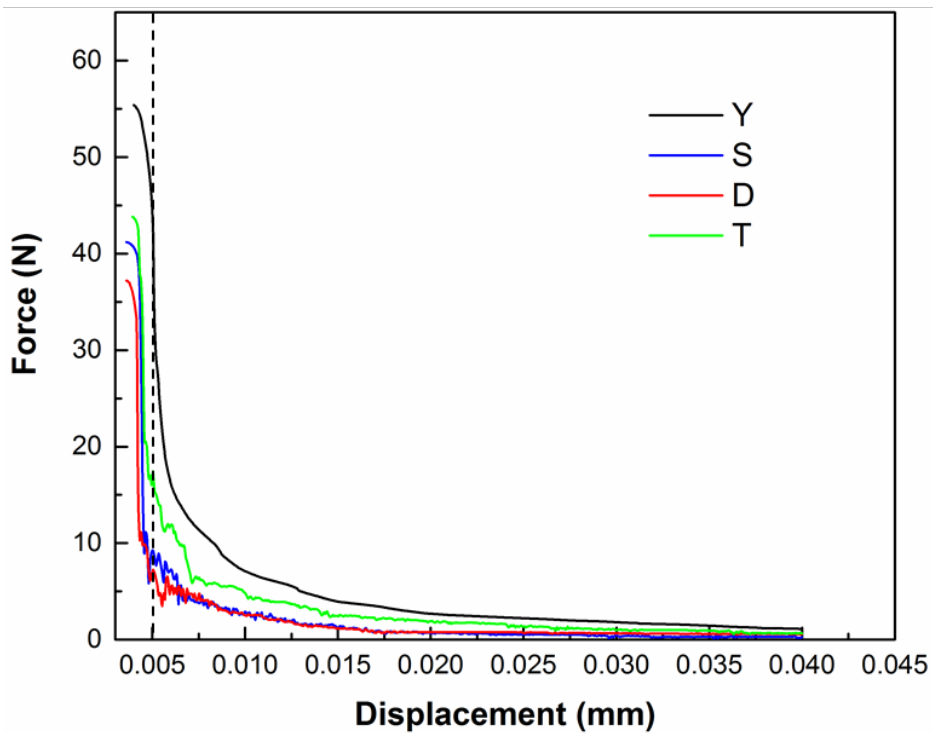


Figure 6.10. Crack propagation in four groups (Y, young; S, senior; D, diseased; T, treated).

The black arrow indicated the crack initiated at free edge, the red circle indicated the crack initiated at large Haversian canal and the black circle indicated the crack grew following the cement line in the young group.

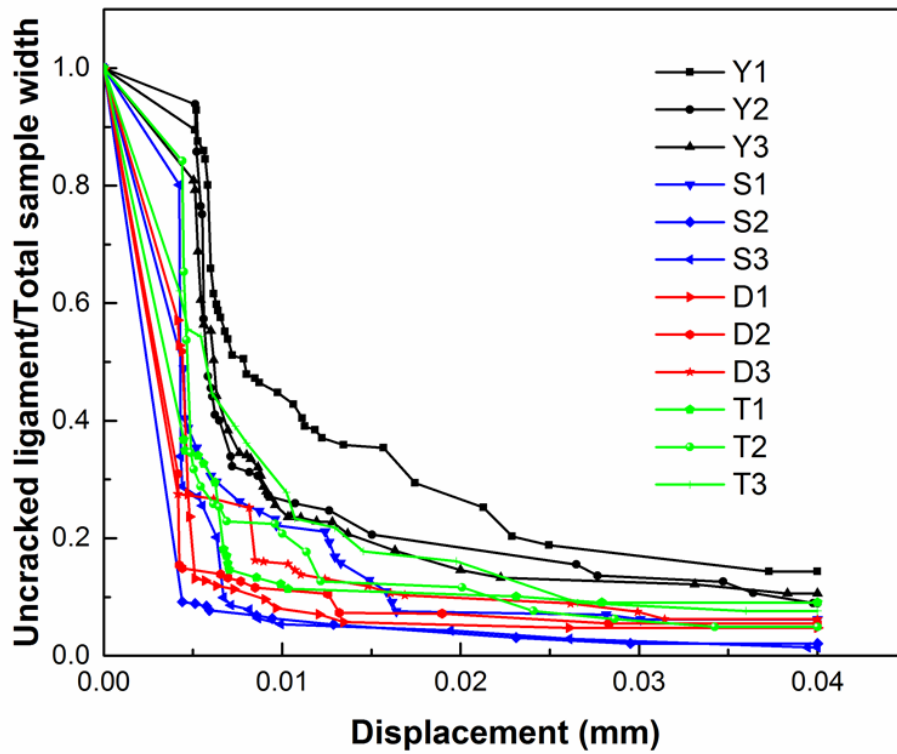


(a)

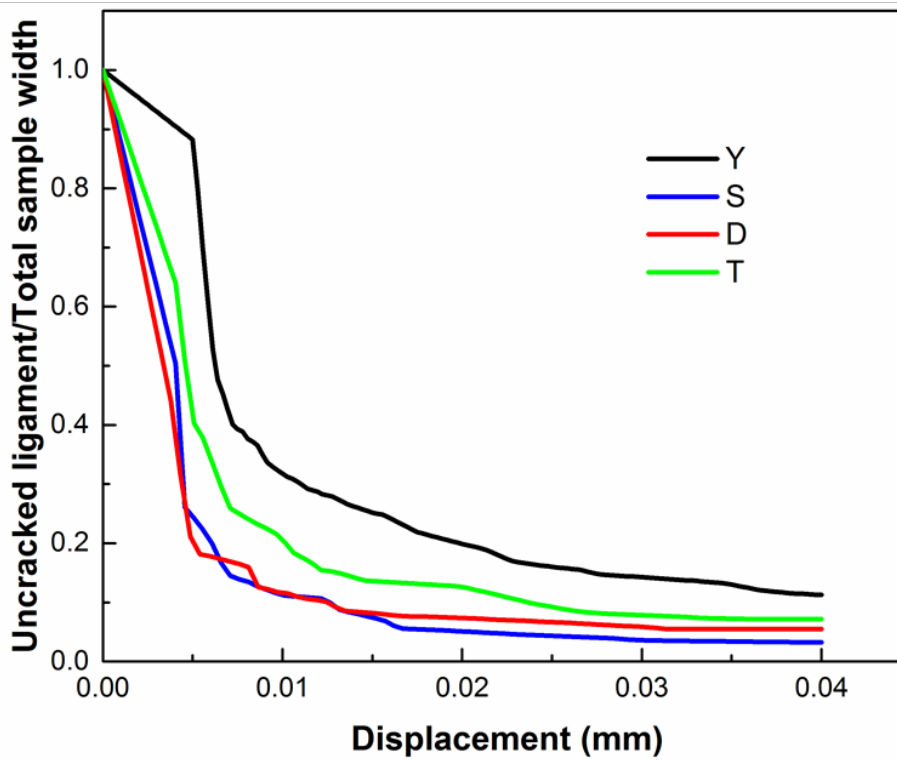


(b)

Figure 6.11. Curves of force over displacement from the ultimate strength point to the end (Y, young; S, senior; D, diseased; T, treated) (the beginning point is the ultimate strength). The dash line showed the loading displacement arrived at 5 μm .



(a)



(b)

Figure 6.12. Analysis of relationship between uncracked ligament/total sample width during loading (a) simulation results (b) fitting curves

To further understand the characteristics of fracture propagation behaviour among groups, crack morphologies of each model (Fig 6.10) and the loading force against concurrent displacement during crack propagation (Fig 6.11) were analysed. In general, the initiation of cracks begin favourably at large porous site of Haversian canal and/or free-edges where onsite strain energy was greatly elevated due to adjacent Haversian canal. This phenomenon was prominently noticeable in diseased group, where more Haversian initiated crack paths were observed at early stage of the fracture process, partially due to its higher average porosity, large Haversian canal and smaller osteon diameter. The propagation of the cracks, however, has shown a complex path with kinks, deflection around microconstituents, crack arresting and bridging which were governed by a variety of localised extrinsic factors such as the young group. In terms of forces against loading displacement, young group has the highest peak force of all groups, followed by groups in the following order $Y > T > S > D$. The trend has maintained so for the young group consistently during the entire crack propagation process. Treated group showed some improvement over senior and diseased groups, with higher initial peak driving force at the beginning of the crack propagation, as well as when tissue displacement reached beyond 5 μm (equivalent to tissue strain of 0.47%). Further analyse of the ratio between uncracked ligaments length (projection of the uncracked tissue width in transversal direction of load) and total specimen width suggested that there was more undamaged tissue per unit width in young and treated groups on average than that of average values in senior and diseased groups (Fig 6.12). These results presented that the osteonal morphology of the young and treated groups could maintain more uncracked ligament to prevent the cortical bone from the crack destroying.

Results from analysing the proportions of the cracks which fall within each of the micro-constituents (Table 6.3 and Fig 6.13) indicated that young group has the

longest cracks of all groups and also has the largest proportional cracks (14.94%) which falls in cement line, almost seven time to next runner up – diseased group which has around 2.32% cement line crack. The treated and senior followed the order and have lower total crack lengths (0.112 mm and 0.016 mm) as well as cement line cracks (9.39% and 2.32 %), respectively. On the other side, diseased group has the largest osteonal cracks of all the groups, occupying 51.64%, so its percentage of interstitial matrix crack were lower than the senior groups' ones; while the average percentage of osteonal cracks in senior and treated groups are around at same level at 43% margin. The results suggested that cracks are greatly influenced by the distribution and areal fractions of micro-constituents, more cracks deflection into cement line seems to associated to higher crack retention force, while osteonal cracks might linked to the lower crack retention as a result. The average osteon areas of young and treated group were 34526.15 and 31870.11 μm^2 . The average the cement line area of aged and diseased group were 2580.33 and 2610.10 μm^2 . These results indicated that young and treated groups had the good fracture resistance because of the large osteon area, and the cement line area might not be a key role in the crack propagation.

From the energy perspective, the energy (area under the force-displacement curve) used to complete fracture the tissue is highest in young group (0.322 mJ), some 43.8% higher than the average of the other three groups, while treated group, having the second most work of energy of 0.224 mJ, was 28.7% higher than senior (0.166 mJ) and diseased groups (0.154 mJ), as shown in Fig 6.14. This result might explain that the cortical bone of diseased group was more fragile.

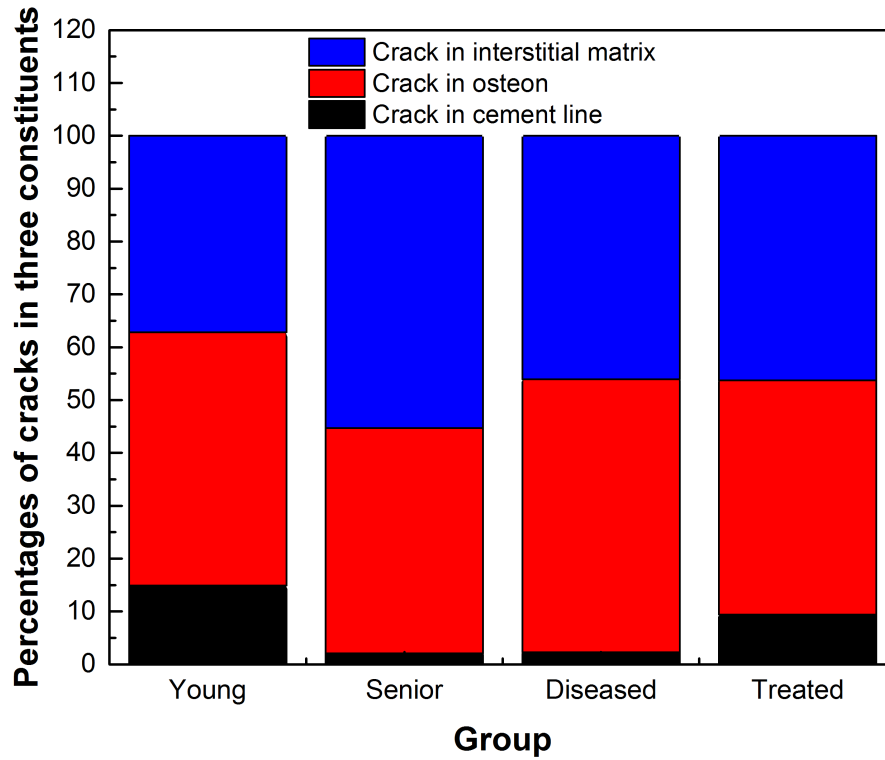


Figure 6.13. Percentages of crack in three constituents in four groups (cement line, osteon and interstitial matrix)

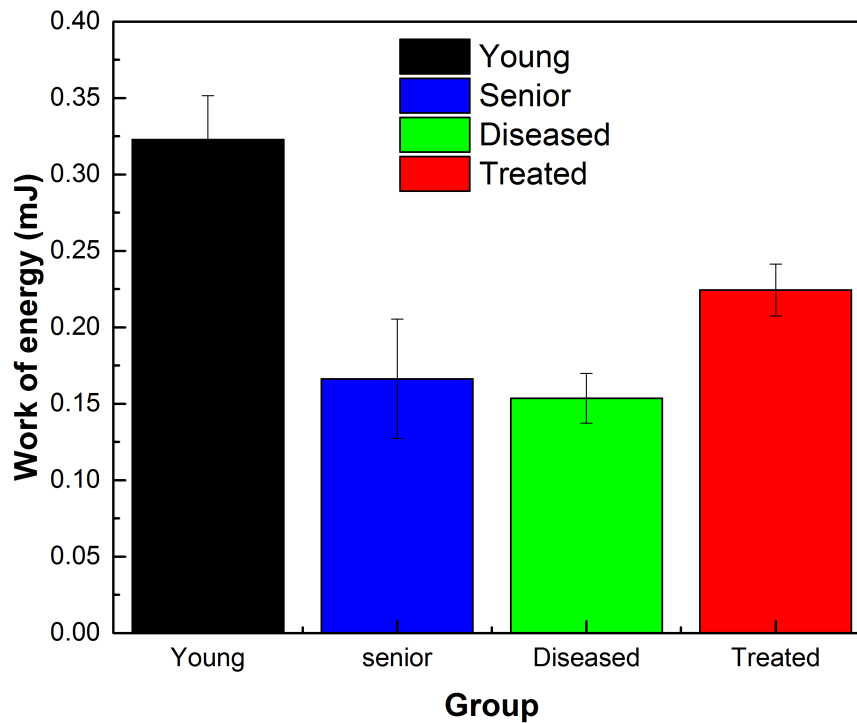


Figure 6.14. Work of energy of four groups during tension process

Table 6.3. Results of crack length of crack destroying cement line and occupy the whole crack length about human models

	Cement line crack length (mm)	Osteon crack length (mm)	Total crack length (mm)	Cement line crack (%)	Osteon crack (%)	Ratio of cement line cracks to areal fraction of cement lines	Average osteon area (μm^2)	Average the cement line area (μm^2)
Young1	0.366	1.106	2.374	14.94	47.86	2.23	34526.15	2424.54
Young2	(± 0.236)	(± 0.119)	(± 0.341)	(± 7.51)	(± 8.93)	(± 1.10)	(± 12628.97)	(± 463.34)
Young3								
Aged1	0.027	0.608	1.442	2.12	42.62	0.35	29005.47	2580.33
Aged2	(min 0.001	(± 0.131)	(± 0.222)	(min 0.04	(± 9.35)	(min 0.01	(± 13338.29)	(± 515.62)
Aged3	max 0.060)			max 4.96)		max 0.081)		
Diseased1	0.016	0.670	1.294	2.32	51.64	0.38	27237.17	2610.10
Diseased2	(± 0.015)	(± 0.092)	(± 0.062)	(min 0	(± 5.52)	(min 0	(± 9640.23)	(± 451.07)
Diseased3				max 5.50)		max 0.89)		
Treated1	0.112	0.765	1.722	9.39	44.38	1.48	31870.11	2489.47
Treated2	(± 0.084)	(± 0.100)	(± 0.072)	(± 2.99)	(± 4.79)	(± 0.44)	(± 12122.02)	(± 496.36)
Treated3								

6.5 Discussion

The diseased group has osteoporosis disease, which could result in low bone mass and structure deterioration due to imbalance of bone modelling, with higher rate of bone resorption than bone formation. While the treated group is the diseased group with oral bisphosphonates treatment could prevent bone resorption rate of cortical bone (Cramer et al., 2007). For the volumetric fraction and size of micro constituents in human cortical bone, it presented diseased and aged factor actually increased volume fraction of size of Haversian, but it decreased volume fraction and size of osteon. So the young group had the largest of volume fraction of osteon, while, the smallest of volumetric fraction and size of Haversian. The balance of remodelling process of cortical bone was changed due to diseased and aged factor that resorption rate was higher than recover rate resulting in Haversian canal size decreasing in other three groups. In McCalden and Bernhard (McCalden et al., 1993) paper, the volumetric fraction of Haversian was decreasing due to age and diseased factor. The histogram results of micro-constituents indicate that ageing process as well as diseases could influence the balance of the remodelling process, which in turn, reflects on perceived changes in morphological parameters of cortical bone (Bernhard et al., 2013).

In term of Young's modulus and ultimate strength of four groups for human, In Reilly's paper (Reilly & Burstein, 1975), the Young's modulus of young group, whose age was around 23 years old, was 13.3 GPa whose error 6.20 % in transversely direction. The experimental result's Young's modulus and ultimate strength of senior group were 10.1 GPa and 40 MPa, among them, the ultimate strength of experimental results had a difference compared with simulation result. This problem may be due to the senior group's age was around 65 years old,

which was lower than simulation model's age. The significant difference of micro-morphology in different groups was volumetric fraction of Haversian and osteon; especially, young group had four times lower than other four groups even more in term of volumetric fraction of Haversian. So, this may result in the young group had the largest value of Young's modulus. In Granke (Granke et al., 2011) and Dong's paper (Dong & Guo, 2004), the Young's modulus in transversely direction had similar trend to describe that larger Haversian could decrease Young's modulus.

The unique micro-morphology of Haversian canal also induces that the crack initiates at the large size of Haversian canal. In Voide (Voide et al., 2009) and Lin (Lin et al., 2016)'s paper, the stress concentration on large size of Haversian canal is higher than other place at bone surface, but, the micro-crack confined in the osteon and seldom are found connected to become a macro-crack. The similar phenomenon could be observation in senior, diseased and treated groups' models.

The cement line, an interface between osteon and interstitial area, is a significant role that guide the direction of crack propagation. The content of cement line, which is an interface between the osteon and interstitial matrix, is a controversial topic according to previous studies. Schaffler and Burr (Burr, et al. 1988; Schaffler et al., 1987) found that the cement line had lower calcium content than that of osteon and interstitial matrix meaning that the cement line is a mineral-deficit tissue. However, the later studies presented that the cement line was a mineral-rich (or called collagen-deficit) tissue, where the cement lines' content was analysed with qualitative Backscattered Electron Imaging (qBEI), quantitative Energy Dispersive X - ray spectroscopy (qEDX) and micro-Raman spectroscopy (μ -Raman) (Milovanovic et al., 2018; Skedros et al., 2005). While the cement line did not have a higher Young' s modulus than the osteon and

interstitial matrix. The Young's modulus and hardness of the cement lines were some 30% lower than that of surrounding tissue tested with the nanoindentation (Conward & Samuel, 2016 and Montalbano & Feng, 2011). Other studies presented that the cement line contained a high-level of noncollagenous protein, while a low level of collagen content (McKee & Nanci, 1996; Skedros et al., 2005). These unique contents make the cement lines more brittle than other surrounding tissues. Dong et al. (2005) found that the shear strength of the cement lines as 8 MPa, which was evaluated by the pushout experiment.

The deflection of crack, caused by break through the cement lines, could increase the fracture resistance of cortical bone. The crack destroying cement lines is caused by the stress concentration area around the tip of the macro-crack (Z. X. Lin et al., 2016). Several researchers (O'Brien et al., 2005)(Burr et al., 1988) found that the cement lines, which is weak interface, have the function of arresting the crack propagation for preventing fracture through osteon. In our study, the crack in the young groups mostly breaks the cement line area comparing with the ones in other three groups. Previous papers (Chan et al., 2007; Chan et al., 2009) illustrated that it depended on initial fracture toughness and deflection tissue fracture toughness. If deflection tissue's fracture toughness was less than half percent of initial fracture toughness, the cracks will growth in this tissue. The tensile force of young group was higher than other groups in the same crack length, so the young group had the highest initial fracture toughness. Therefore, crack in young group will deflect into cement line instead of osteon. The uncracked ligament was also important extrinsic mechanism to improve the toughness of the cortical bone (Nalla et al, 2004; Nalla et al, 2005). The results in this paper also presented that the young group had the more uncracked ligament during tension loading, while diseased had the less one. Therefore, the uncracked ligament and crack deflection into cement line made the young group

was the tough bone, because its unique osteonal morphology.

In this paper, zero thickness cohesive element method is utilized to research the effect of micro-morphology on fracture toughness of cortical bone, described by figure of crack propagation and force-crack length of human cortical bone. At the same time, human's mechanical properties of micro constituents also was implied in simulation model based on force-crack length figure. This latest technique could be without the crack initiation and crack path that ignore the empty area of Haversian canal and describe the crack propagation based on local stress distribution, which is the limitation of X-FEM, cohesive element method.

6.6 Conclusion

This paper researched the effect of micro-morphology of cortical bone on crack propagation by using zero-thickness cohesive element method. Crack propagation result showed that multiple crack could be observed in this simulation through this latest simulation method, because of local stress concentration as real condition. The crack deflection in young and treated group happened frequently that crack growth followed with cement line and remain more uncracked ligament. The cement line's function, which protected osteon, could be presented well. The influence of this phenomenon also was showed in crack length and force curve that young and treated group need more force in the same crack length. In conclusion, the remodeling balance could be changed by diseased and aged, which could affect the micro-morphology to decrease the toughness of whole bone.

Chapter 7- Effect of Micro-morphology of Cortical Bone Tissue on Fracture Toughness and Crack Propagation in Compact-tension Simulation

7.1 Introduction

In Chapter 6, the uniaxial tension test of cortical bone with multiple-crack propagation was analysed with an aim to investigate the effect of morphology of osteonal microstructure on crack propagation. However, the contribution of fracture toughness of each bone constituents to preventing a crack from propagating in cortical bone was not studied. Therefore, the fracture toughness of each group's cortical bone will be thoroughly analysed here based on compact-tension simulations.

Human cortical bone is a nanocomposite material composed of type-1 mineralized collagen fibres, which are up to 15 μm in length and 25-35 nm in radius, and bone apatite nanocrystals with thickness of 2-3 nm. These elements of nanostructure could be arranged parallel to lamellae with thickness of 3-7 μm , which are wrapped around a Haversian canal to form an osteon (Rho et al., 1998). This unique hierarchical structure defines intrinsic and extrinsic toughening mechanisms of cortical bone. Intrinsic toughening mechanisms improve bone's inherent resistance to microstructural damage and cracking, which is important in crack initiation or ahead of a crack, thanks to sub-microstructure. On the other hand, the extrinsic toughening mechanisms operate behind the crack tip. Crack bridging and microcracking play a significant role in these mechanisms, inhibiting the crack growth by reducing the applied stress, because bone acts as a natural

composite material with different kinds of microstructural constituents.

In order to analyse bone's fracture-toughness mechanism clearly, a rising resistance-curve (R-curve), including its parameters - initiation toughness (K_{I0}) and a toughness growth slope - became a popular scientific approach, instead of single fracture parameters such as K_{Ic} or G_c , obtained in cortical bone's fracture experiments (Koester et al., 2011; Malik et al., 2003; Nalla et al., 2006; Vashishth et al., 1997; Vashishth, 2004). Initially, the R-curve approach was adopted to analyse varying fracture toughness of bovine and human cortical bone in a longitudinal direction. The former bone had higher levels of initiation fracture toughness and fracture growth than the ones of the human bone in compact-tension experiments (D. Vashishth et al., 1997). Then, Malik et al. (2003) investigated the character of fracture toughness and crack propagation in equine cortical bone at microstructural level in a transverse direction by the same method as Vashishth's. After identifying the difference of species, the ageing effect on human cortical bone in longitudinal and transverse directions was studied by Nalla et al. (2006) and Koester et al. (2011). It was found that ageing could result in the cortical bone's deterioration, so that both the initiation toughness and toughness growth slope reduced simultaneously.

Numerical modelling can be used to supplement experimental studies of mechanical behaviour of cortical bone. Initially, a cohesive-zone model, which is a kind of nonlinear simulation method, was used to model the fracture of cortical bone with homogeneous mechanical properties (Ural & Vashishth, 2006, 2007; An et al., 2014). Ural and Vashishth (2006 and 2007) utilized a basic cohesive-element model to analyse the aging effect on fracture behaviour of cortical bone. Then, the basic model updated with yield stress was adopted in the cortical bone's models to study the fracture behaviour of bone or bone-like biological

materials (An et al., 2014). As discussed before, extrinsic fracture toughness is related to characteristic features of microstructural constituents, so later simulation models included microstructural constituents, instead of a purely homogeneous material (Ani Ural & Mischinski, 2013). But the original drawback of this model was that the Haversian canals (empty areas inside bone) were not considered in these simulations. The Haversian canals play a significant role in elastic behaviour and fracture development (crack bridging and microcrack); even their volume fraction in bone changes due to such factors as ageing and disease (Nalla et al., 2006).

Therefore, in this chapter, models with random distributions of microconstituents, with inserted zero-thickness cohesive elements, are adopted to discuss the effect of micro-morphology of osteonal structure on fracture behaviour in compact-tension simulation with a pre-notch.

7.2 Models generation

Two-dimensional finite element models of compact tension with random distributions of micro-constituents of cortical bone were generated based on microscopic images obtained from proximal femoral diaphysis of females, including young, senior, diseased and treated groups in Chapter 4. In Nalla's paper (2004), the bone specimens' dimensions (thickness $B=1.2-3.3$ mm, widths $W=13-18.3$ mm, and initial crack length $a=3.0-5.5$ mm) were not only based on the ASTM Standard E399, but also limited by the accuracy of the machine. The compact-tension models with thickness $B=3$ mm, width $W=14$ mm and crack length of pre-notch $a=4.2$ mm, according to ASTM E399 (ASTM, 1997) (Fig.7.1), were developed to calculate fracture toughness of human cortical bone. The level of fracture toughness, K , was calculated based on the following equations:

$$K = \frac{PY_2}{BW^{0.5}}, \quad (7.1)$$

$$Y_2 = \frac{(2+\frac{a}{W})}{(1-a/W)^{3/2}} \{0.866 + 4.64 \left(\frac{a}{W}\right) - 13.36 \left(\frac{a}{W}\right)^2 + 14.72 \left(\frac{a}{W}\right)^3 - 5.6 \left(\frac{a}{W}\right)^4\}, \quad (7.2)$$

where P is the loading force, a is the crack length, B is the model thickness, W is the specimen's width and Y_2 is the shape function.

In this model, a microstructural part (dark rectangle area), with length of 1.378 mm and width of 1.058 mm, was inserted into the model of a compact-tension specimen as shown in Fig.7.1. This domain with homogenized properties adapted CPE4R solid element without any zero-thickness cohesive elements in it and utilized the meshing method that the mesh size of its edges and loading circles were 0.4 mm and 0.1 mm, respectively, to balance the accuracy and the computational cost. The microstructured part was meshed with standard continuum elements (CPE3) with dimensions of 0.015 mm and their surrounding surfaces according to the sensitivity test in Chapter 5; the discontinued surfaces presented cracks or material interfaces were defined by zero-thickness cohesive-zone elements (COH2D4). The total numbers of elements and nodes of the models were around 80000 and 9000, respectively. A Matlab program was developed to insert zero-thickness cohesive-zone element into the existing Abaqus model, using the protocols from (Nguyen, 2014). The mechanical properties of microstructural constituents, including osteons, interstitial matrix and cement lines could be found in Table 6.2. The compact tension part in this study was also as homogenous material, whose Young's modulus was based on previous uniaxial-tensile test simulation results in Chapter 6. Its Poisson's ratio and critical energy-release rate were 0.3 and 0.422 N/mm based on (Abdel-Wahab et al., 2012). The onset of fracture in these simulation models was based on the critical maximum principal strain, which value of 0.4% was chosen as

crack-initiation strain (Élisa Budyn & Hoc, 2007b). This study used displacement-controlled loading method with displacement rate of 0.01 mm/s (Nalla et al., 2004). In this study, the simulation geometry of models was the same as in Chapter 6 for the four studies groups, including young (Y), senior (S), diseased (D) and treated (T); three models were developed for each group. The slopes presented the R-curve of the models where the stress intensity factor was rising with a stable crack extension. The linear regression (free fitting) was chosen based on the R-curve experimental results for human cortical bone in previous papers (Nalla et al. 2005; Ritchie, 1999; Vukicevic et al., 2018).

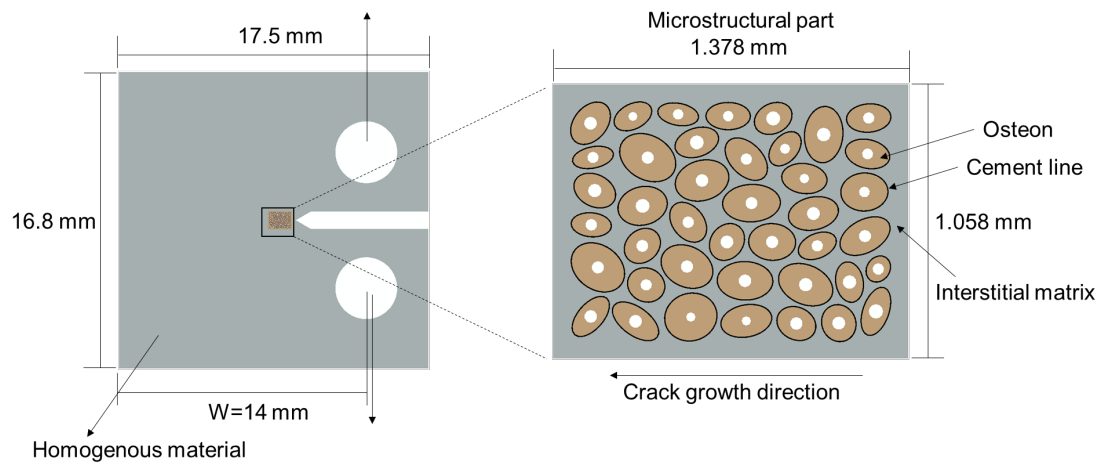


Figure 7.1. Human cortical bone under compact-tension loading conditions and example of microstructured domain

7.3 Results

The compact-tension models in this study were employed to evaluate the stress intensity factor as a function of crack length; the main results are presented as Fig.7.2 and Table.7.1. It was found that group Y had the highest mean initiation stress intensity factor- K_0 values of $2.11 \pm 0.15 \text{ MPa(m)}^{0.5}$ out of the four studied groups. While, group D had the lowest mean K_0 value of $1.35 \pm 0.03 \text{ MPa(m)}^{0.5}$. The levels of K_0 of group S and T were close, which are 1.51 ± 0.18 and $1.54 \pm 0.12 \text{ MPa(m)}^{0.5}$. The mean values of growth slope were 0.63 ± 0.04 , 0.40 ± 0.20 ,

0.31±0.08 and 0.45±0.02 MPa(m)^{0.5}/mm, for group Y, S, D and T, respectively. So, the results presented that ageing and disease affect the micro-morphology, reducing the fracture toughness during the crack initiation and growth.

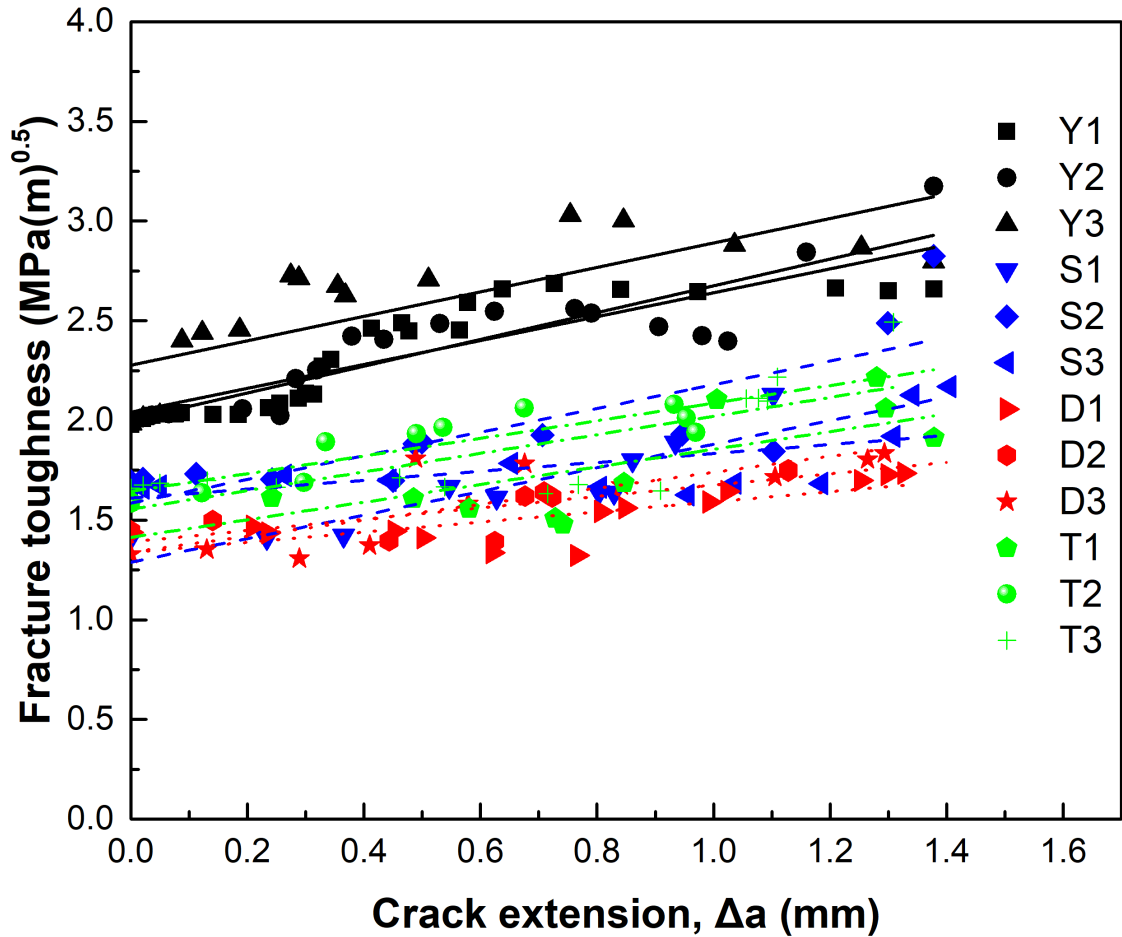


Figure 7.2. R-curves of four groups, including group Y (young), senior group S (senior), diseased group D (diseased) and treated group T (treated)

Table 7.1. Fracture R-curve behaviour of four groups: group Y (young), group S (senior), group D (diseased) and group T (treated)

Groups	Initiation fracture toughness K_{I0} (MPa(m)^{0.5})		Slope (MPa(m)^{0.5}/mm)	
Y1	2.04		0.60	
Y2	2.00	2.11±0.12	0.67	0.63±0.03
Y3	2.28		0.61	
S1	1.30		0.58	
S2	1.63	1.51±0.15	0.42	0.40±0.16
S3	1.59		0.19	
D1	1.34		0.25	
D2	1.39	1.35±0.03	0.28	0.31±0.06
D3	1.33		0.40	
T1	1.41		0.44	
T2	1.64	1.54±0.10	0.44	0.45±0.01
T3	1.56		0.47	

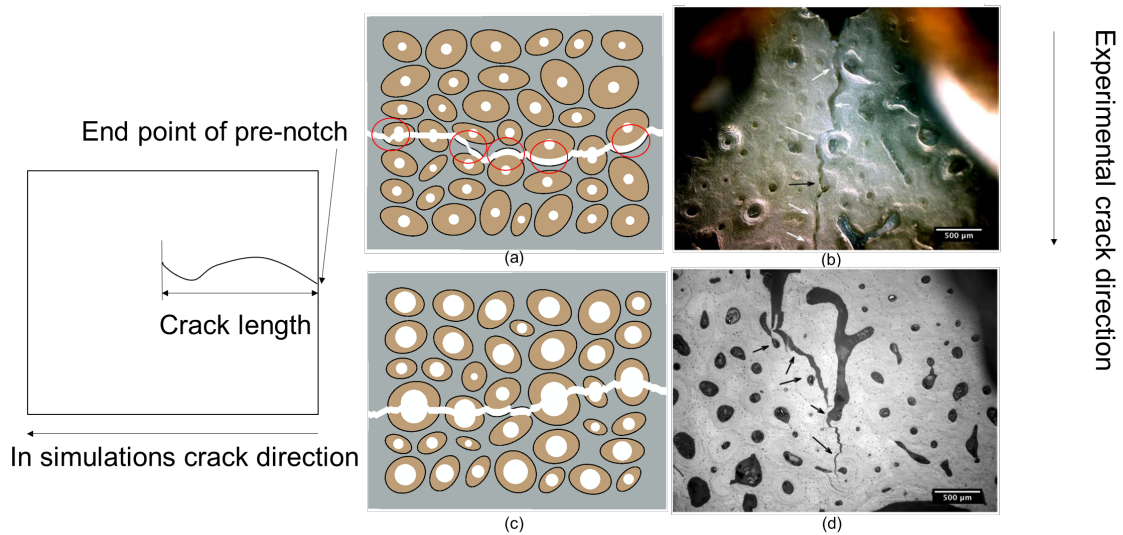


Figure 7.3. Crack growth condition in microstructural area of simulation and experiment: simulation results: (a) young, (c)senior; experimental results (b) young, (d)senior (black arrows indicate the cracks destroying the osteons and white arrow indicate the crack growth following the cement lines) (Chan et al., 2009)

Some examples of crack-propagation paths in human cortical bone are shown in Fig.7.3-a, b where red circles highlight a crack arrested by cement lines in group Y of simulation and experiment's image (white arrows indicate crack propagate through cement lines). Whereas it was found that a crack in group S grew mainly through the osteons instead of the cement lines as simulation and experimental micro-image (black arrows indicate crack penetrate osteons (Fig.7.3-c, d). Therefore, cement lines play an important role in extrinsic toughness. The crack length in cement line along the x direction and its related fraction of the whole crack length were analysed in Table.7.2 to assess relationship between the crack growth through cement lines and the crack-growth fracture toughness. The crack length arrested by cement lines was the longest in group Y, which was 0.454 ± 0.180 mm and $39.7 \pm 11.5\%$. In Fig.7.3-b, the percentage of the crack length arrested by cement lines was 53.4%, which was similar as the Group Y3 and Y1's ones. In contrast, for group D the respective parameters were 0.014 (0-

0.031) mm that occupied 1.0 (0-2.22)%, respectively. Groups S and T had similar percentage of crack length arrested by cement line, their average values were 3.3 ± 2.7 and 4.2 (0.11-9.14)%. The obtained simulation results demonstrate that group Y's micro-morphology of osteons was promoted for crack growth attracted by cement line tissue, that protected osteon from fracture destroying. While, the crack in the other three group mainly penetrated osteons, so that the crack growth fracture toughness in these three groups were lower than group Y's one.

Table 7.2. Analysis of crack growth in cement line as fraction of microstructural area's width

Groups	Crack length along x direction in cement lines (mm)		Percentage (%)	
Y1	0.624		45.3	
Y2	0.265	0.513 ± 0.176	26.5	39.7 ± 9.4
Y3	0.651		47.2	
S1	0.006		0.44	
S2	0.079	0.045 ± 0.030	5.76	3.3 ± 2.2
S3	0.050		3.62	
D1	0.000		0	
D2	0.012	$0.014(0-0.031)$	0.88	$1.0(0-2.22)$
D3	0.031		2.22	
T1	0.001		0.11	
T2	0.044	0.057 ± 0.052	3.23	$4.2(0.11-9.14)$
T3	0.126		9.14	

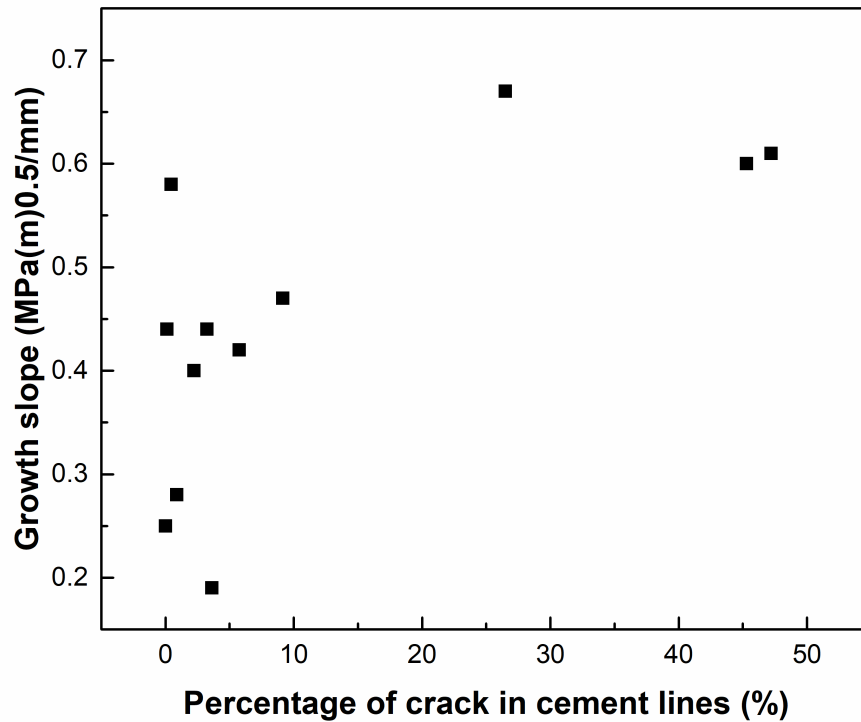


Figure 7.4. Growth slope of stress intensity factor for models as function of percentage of crack in cement lines

The growth slope shows the increase in fracture-resistance ability of the models with crack propagation. Fig 7.4 presents the relationship between percentage of crack in cement lines of the twelve simulation models and crack-growth slope. A positive relationship of them was shown that the growth slope of the model would increase with the increase in percentage of crack in cement lines. This result might present that more crack in cement lines could improve the bone resistance the crack to grow in cortical bone, but this single extrinsic fracture mechanism could not explain the difference of the growth slope in four groups. The uncracked ligament bridging was also observed in the simulation results. The analysis of the uncracked ligament bridging in four groups was presented as follow.

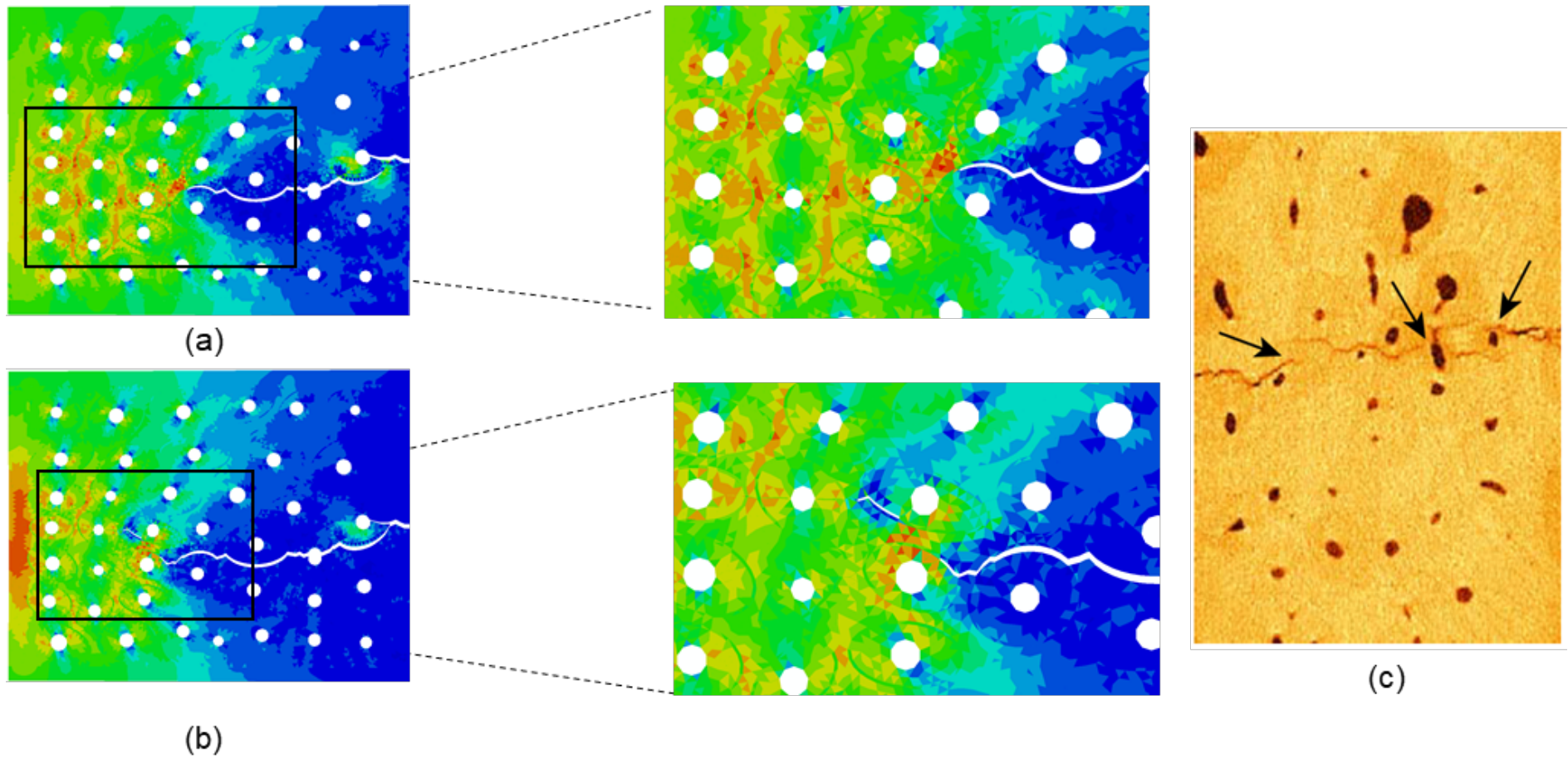


Figure 7.5. Contour plots of maximum principal stress (in MPa) of group Y: (a) first stage; (b) later stage; (c) experimental micro-image: black arrows indicated the uncracked ligament bridging (Nalla, Kruzic, Kinney, et al., 2004)

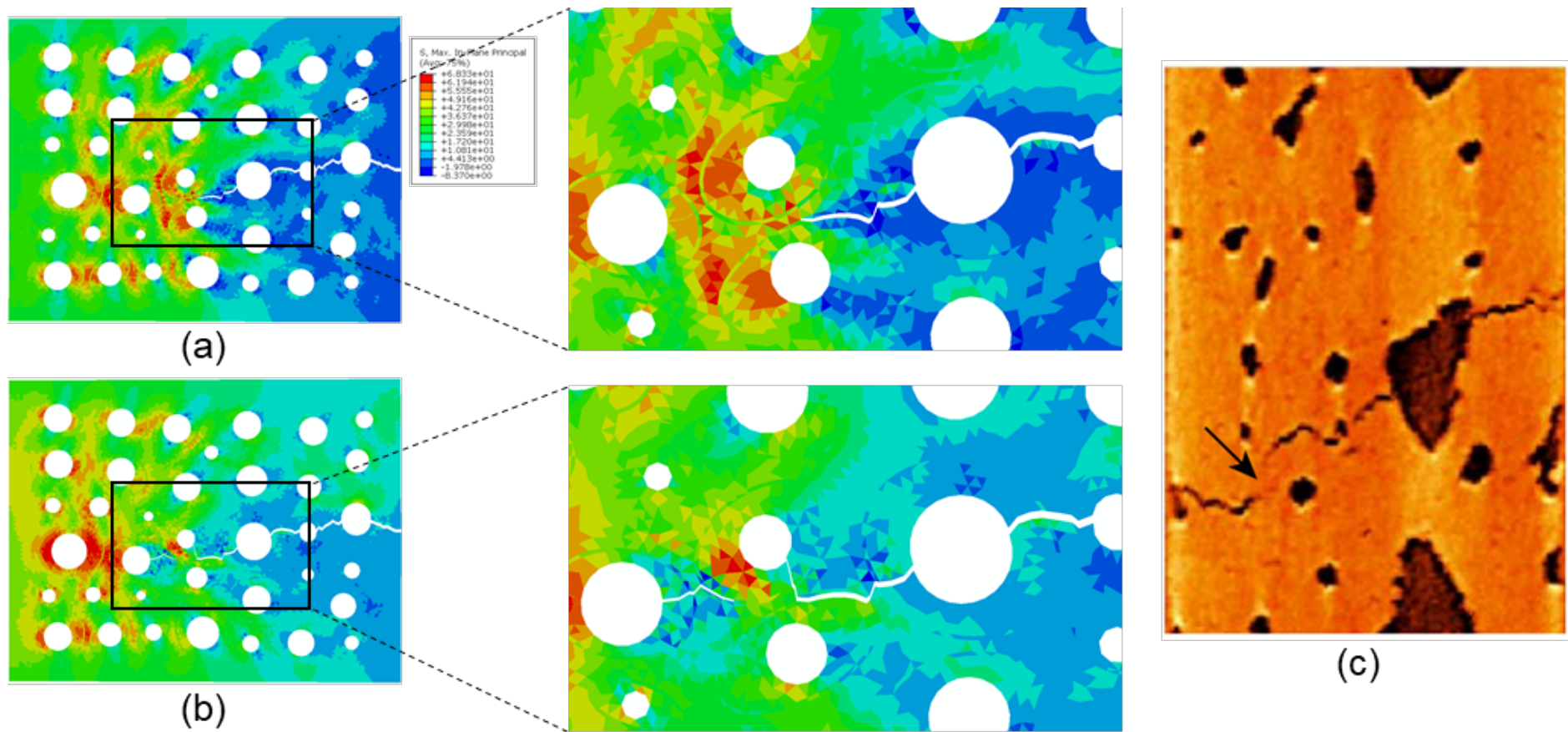


Figure 7.6. Contour plots of maximum principal stress (in MPa) of group S: (a) first stage; (b) later stage; (c) experimental micro-image: black arrows indicated the uncracked ligament bridging (Nalla, Kruzic, Kinney, et al., 2004)

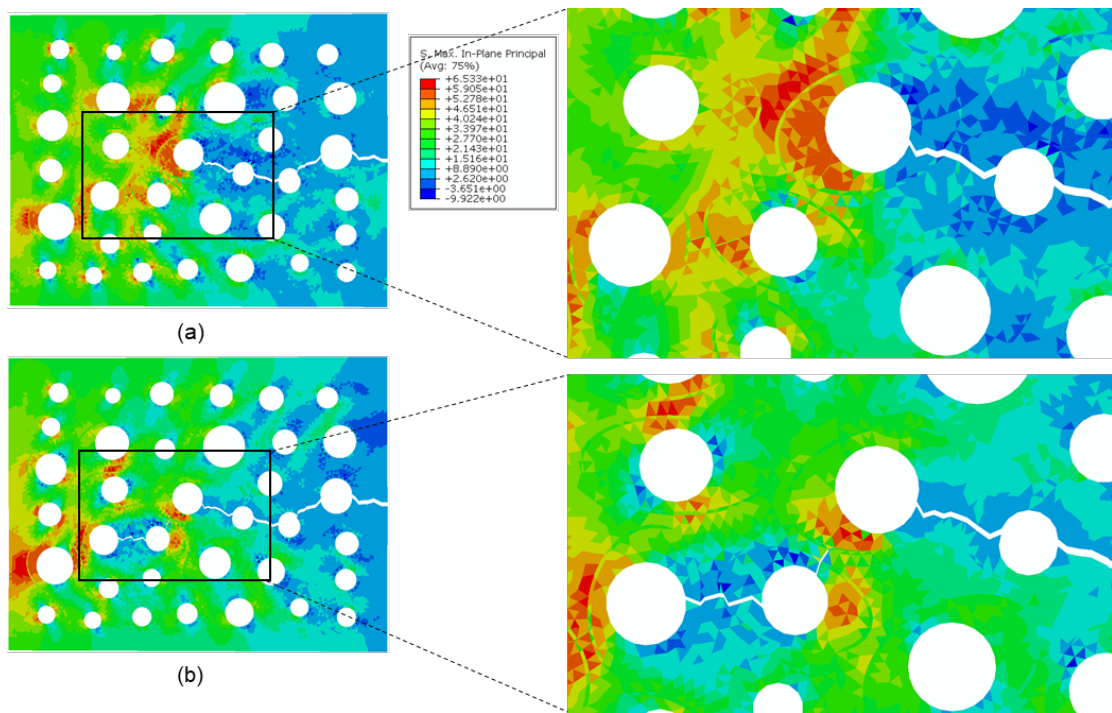


Figure 7.7. Contour plots of maximum principal stress (in MPa) of group D: (a) first stage; (b) later stage

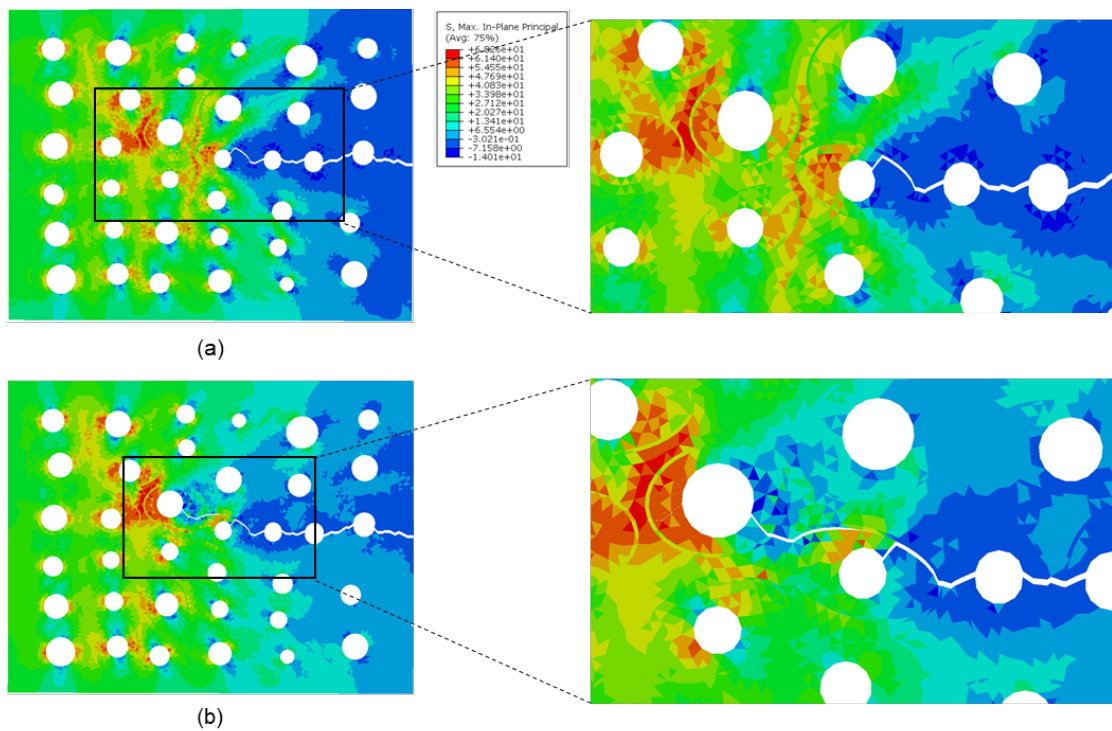


Figure 7.8. Contour plot of maximum principal stress (in MPa) of group T: (a) first stage; (b) later stage

The contour plots of maximum principal stress of four groups are shown in Fig.7.5-7.8, to analyse the effect of osteon morphology on crack-growth fracture toughness. In those contour plots of four groups, the stress concentrations are at the edge of osteon and Haversian-canal areas of the nearest osteons. The crack in group Y grows through the cement-line areas as Fig.7.5-a. Interestingly, after the main crack grew from the pre-notch side, propagating through the cement line, the secondary crack formed at the cement line of another osteon due to high stress concentration joined the main crack form at as Fig.7.5-b. This uncracked ligament bridging indicated by the black arrows in group Y could observed in experimental micro-images as Figure 7.5-c (Nalla et al., 2004). In group S, the main crack was propagating through the cement line after it destroying an osteon as Figure 7.6-a. Then, the main crack penetrated the osteon instead of continually following the cement line due to high stress concentration; while the uncracked ligament bridging was formed between the secondary crack (from another Haversian canal to the cement line) and the main crack in Figure 7.6-b. The micro-image of simulation result of group S was similar to that of experimental micro-image (Figure 7.6-c) (Nalla, Kruzic, Kinney, et al., 2004). Also, the group T had the similar crack growth path as the group S' one in Figure 7.7, therefore, these two groups' crack growth fracture toughness were similar. In contrast, the different uncracked ligament bridging was formed in group D that the main crack was destroying osteon all the time and the secondary crack was penetrating two osteon instead of the cement line from the far side osteon in Figure 7.7. The uncracked ligament bridging of four groups (Y, S, D, T) mentioned above contents were 0.062, 0.046, 0.046 and 0.047 mm, respectively. These value were close to experimental value, which was around tens of micrometers in size (Nalla, Kruzic, Kinney, et al., 2004). The fracture toughness increases from first stage to later stage in four groups were also measured to

quantity these different uncracked ligament bridging. The group Y had the highest value of $0.18 \text{ MPa(m)}^{0.5}$, while the group D had the lowest value of $0.05 \text{ MPa(m)}^{0.5}$. The group S and T had the same value of $0.11 \text{ MPa(m)}^{0.5}$. These values may give four groups different kind growth fracture toughness. Therefore, the micro-morphology of osteon in cortical bone influenced the growth fracture toughness. The uncracked ligament bridging in the group Y was formed in two cement lines which could tough the cortical bone. While, the group S and T had the same uncracked ligament bridging to tough their bone, but this extrinsic fracture toughness was not good as the one in the group Y. Finally, the uncracked ligament bridging in the group D consisted of two crack penetrating osteon that weaken the bone.

7.4 Discussion

R-curves of fracture toughness for the four studied groups of human cortical bone provides information about the crack initiation and growth during fracture process under compact tension loading as Fig.7.2. Experimental R-curves results were investigated by Nalla et al. (2004 and 2005), Vashishth et al. (1997) and Chan et al. (2009), and the current simulation results have similar features with them. Especially, Nalla et al. (2004) who tested young and senior human cortical bone. The crack initiation toughness (K) of young groups, whose age was 41 years, was from 1.69 to $2.23 \text{ MPa(m)}^{0.5}$ while that in the simulation result were $2.11 \text{ MPa(m)}^{0.5}$ i.e. just in this range. The senior group (85 years) had crack initiation toughness similar to that in the simulation, even though four groups in this simulation had the same mechanical properties of their constituents obtained with nano-indentation. At the same time, the crack-growth slopes in the simulation results for group Y ($0.63 \text{ MPa(m)}^{0.5}/\text{mm}$) were somewhat higher than the experimental ones ($0.39 \text{ MPa(m)}^{0.5}/\text{mm}$). The simulation results in the form

of R-curves of the four groups could explain the effect of micro-morphology of osteonal structure of human cortical bone on fracture toughness that ageing and diseased could reduce the crack-initiation and growth fracture toughness level. Here is a brief summary, based on the calculated R-curves (Fig.7.9): The group Y had the highest fracture toughness and crack growth resistance of the four groups, that experimental results (blue and green lines) are in this range. The Groups S and T had similar trends of their fracture behaviour. The initiation fracture toughness of the group D was the lowest, the crack-growth resistances was slightly lower than that of the senior and treated groups. The group T i.e. was diseased groups after treat with bisphosphonates treatment that could cause an increase in the bone mass and the size of osteon (Zimmermann et al., 2016). The improvement of morphology of osteonal structure of the group T could enhance the bone resistance of the crack initiation and growth based on the simulation results. It is important to underline that the same mechanical properties were utilized in these simulations for constituents of all the groups.

The cement lines were a weak interface between osteons and the interstitial matrix. They added as barrier that resulted in crack deflection, protecting osteons from crack penetration and improve fracture toughness of human cortical bone (O'Brien et.al, 2005; Yeni & Norman, 2000). In this study, the length percentage of crack propagation in cement-line areas in the group Y was as 39.7%, higher than in other three group. The Groups S and T had fewer area of cement line demolished by crack. Since the micro-morphology change due to ageing and diseases could decrease the Young's modulus and ultimate strength of cortical bone; therefore, the initiation fracture toughness also declined. Based on theoretical analysis (Qin & Zhang, 2000), the crack deflection into weak layers of composite material was because of higher initiation fracture toughness of cortical bone, accordingly, The group D with initiation fracture toughness of 1.35

MPa(m)^{0.5} had one simulation sample without any crack deflection into cement lines. Moreover, a large diameter of Haversian canal in group D with higher stresses concentrated around them could attract crack to penetrate osteon.

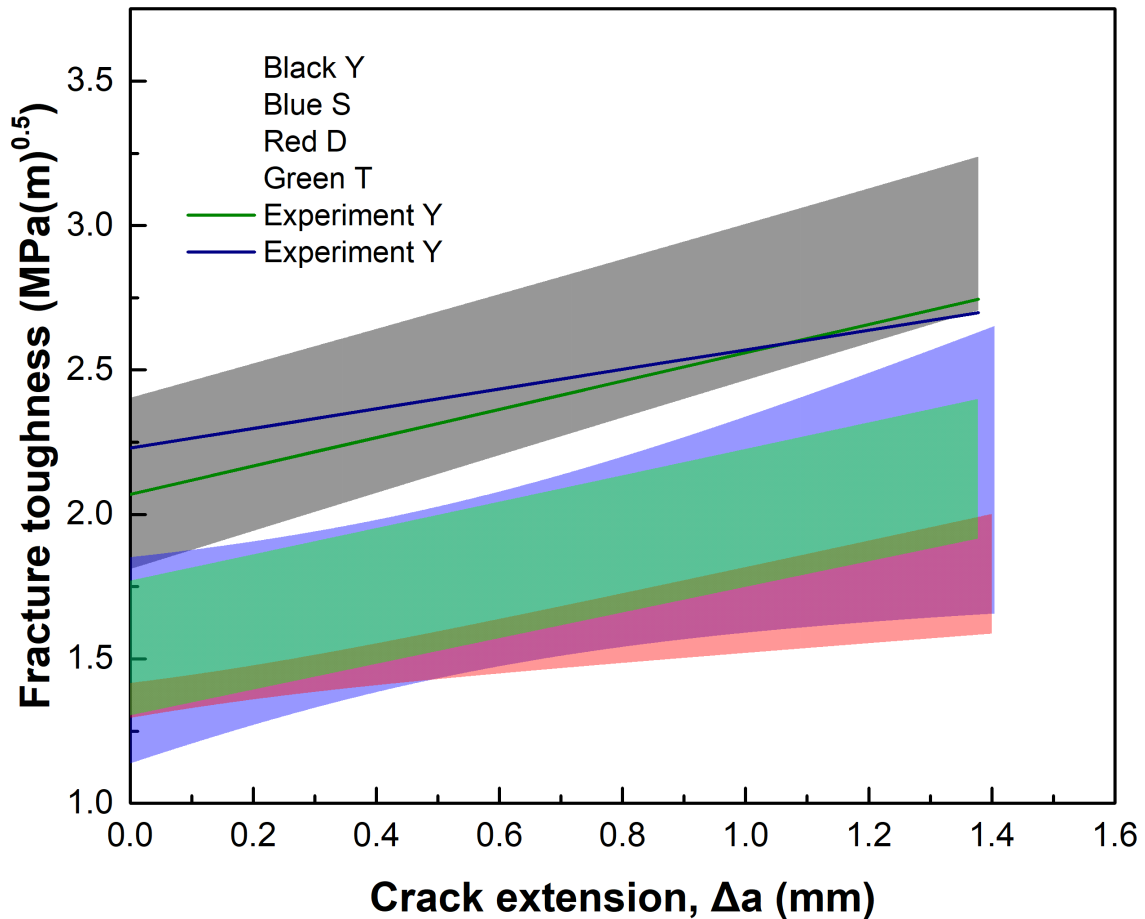


Figure 7.9. Fitting R-curves of four groups, including young (Y), senior (S), diseased (D) and treated (T). (green and blue line present the experimental results) (Nalla et al. 2004)

Uncracked ligament bridging is the fracture mechanism that could inhibit the crack growth since it increases fracture toughness of cortical bone (Zimmermann et al., 2015). In this study, the uncracked ligament bridging is found in the four groups, but the types of them are different. In group Y, the uncracked ligament bridging, offering the highest fracture toughness increase, is formed because of two cement lines breaking. While, the group D has mostly uncracked ligament bridging because two cracks penetrate osteons due to the large size of Haversian

canal. The group S and T had the uncracked ligament bridging consisting of two crack penetrating osteon and cement line. Therefore, the cement lines in cortical bone could protect osteon and also could tough cortical bone.

The random distribution of microconstituents of cortical bone could influence the crack propagation path. In order to deal with this problem, three models of each group were generated based on the statistical data. However, the limited number of samples may result in the difficulty to assess the significance of the statistical outcomes.

7.5. Conclusion

In this study, the zero-thickness cohesive-element method employed in the models of cortical bone with random distributions of its micro-constituents, in order to investigate the effect of micro-morphology of osteonal structure on fracture toughness of human cortical bone. The results demonstrated that aging and diseases could reduce the levels of fracture toughness of cortical bone and the oral bisphosphonates treatment for the diseased group, inhibiting the bone resorption rate, resulted in a rise of the fracture toughness of human cortical bone. The crack deflection into cement lines was a main mechanism of the young groups, because of its unique micro-morphology of osteonal structure, while, the uncracked ligament bridging existed in other three groups are not powerful as the young group's ones to affect on fracture toughness.

Chapter 8 Effect of Fracture Toughness of Micro-constituents of Cortical bone on Crack Propagation

8.1 Introduction

Cortical bone plays an important role in structural support, protection and storage of healing cells, and mineral ion homeostasis (Rho et al., 1998). Therefore, experimental and simulation methods are employed to investigate mechanical behaviour of cortical bone. Especially, an efficient simulation method could provide additional details, which cannot be obtained experimentally. At early stage, macro-scale models of cortical bone were used to study the mechanical properties (Dragomir-Daescu et al., 2011; Hambli et al., 2012). But the relationship between microstructural constituents of cortical bone and the whole cortical bone in the area of mechanical properties at micro-scale, is becoming a hot topic, because of cortical bone's hierarchical structure. For instance, a two-dimensional model of a single osteon, based on linear elastic fracture mechanics (LEFM), was utilized to investigate the osteonal effect on a microcrack (Najafi et al., 2007; Najafi et al., 2009).

However, the fracture process is not bone linear elastic behavior, so a cohesive-element FEM technique and an extended finite-element method (X-FEM) were employed to analyze the fracture behaviour of cortical bone (Abdel-wahab & Silberschmidt, 2011; Budyn & Hoc, 2007b; Li et al., 2013b; Ural & Vashishth, 2006, 2007). But, the cohesive-zone model, which was based on the strain-energy release rate, was mostly used in those two techniques. Initially, the strain-energy release rate of the entire cortical bone, employed in FEM techniques in micro-level, was measured with experimental methods, such as compact tension

(Bonfield, 1987), three-point bending (Ziopoulos & Currey, 1998) or a double-cantilever-beam (DCB) test (Dourado et al., 2013). These experimental methods could not solve the problem of cortical bone's properties of micro-level, so the nanoindentation method was employed to measure the mechanical properties of micro-constituents of cortical bone, such as osteons, interstitial matrix and cement lines. The elastic properties of microstructural constituents in longitudinal and transversely direction were measured (Carnelli et al., 2011; Rho et al., 1997). Then, fracture toughness of microstructural constituents was analyzed by using nanoindentation (Mullins et al., 2009). The obtained levels of fracture toughness of osteons and interstitial matrix were 0.46 and 0.55 MPa m^{0.5}, respectively, which were much lower than that of the whole cortical bone's one (1.6 MPa m^{0.5}). This could be a resulted of the crack length's level: the crack lengths were 5 μm at microlevel and 40 μm at macrolevel. Later, Eugenio et al. (2017) used an inverse investigation method, combing a three-point bending and a FEM simulation method, to investigate the strain-energy release rate of the cement line of cortical bone, but the direct experimental results are still not obtained. Therefore, the fracture toughness of microstructural constituents was still not fully confirmed.

As well-known age-related changes could influence both a collagen network (Wang et al., 2002) and a mineral content (Milovanovic et al., 2015) in bone resulting in the decrease of fracture toughness. On the other hand, the age of microstructural constituents also could influence the mineral content (Milovanovic et al., 2018). However, the effect of different magnitudes of fracture toughness of microstructural constituents on crack propagation in cortical bone is still not investigated. The osteons' geometries and distributions in cortical bone fully vary based on age, disease, species etc., so it is difficult to ignore geometry factors to analyze the effect of fracture toughness of microstructural constituents

on crack propagation with experimental methods. Therefore, in this study, the zero-thickness cohesive-element method was employed for a same geometries and distributions of microstructural constituents but with different magnitudes of fracture toughness of microstructural constituents to evaluate their effect on crack propagation in bone

8.2 Methodology

In this study, the effect of magnitudes of fracture toughness of microstructural constituents in cortical bone was analyzed based on models of compact-tension tests of according to standard ASTM E399 (ASTM, 1997), in order to obtain the fracture toughness of initiation and growth of a crack based on Eqs.7.1 and 7.2. The two-dimensional finite-element model (Y1) presented in Chapter 7 was adapted to guarantee the same geometries and distributions of osteons in cortical bone. The Young's modulus and Poisson ratios of microstructural constituents in this model, including osteons, interstitial matrix and cement lines, were the same as in Table 6.2. The critical maximum principle strain of 0.4%, the same as Chapter 7, was utilized in this model. In this Chapter, the strain energy release rate of cement lines was set as a standard value, which was 0.146 N/mm according with results of Abdel-wahab et al. (2012) and Eugenio et al (2017). The strain energy release rates of osteons and interstitial matrix were changed from being equal to six times of that of the cement line-see Table 8.1. The serial number of models are based on how many times the strain energy release rates of microstructural constituents are higher than that of the cement line (i.e. 0.146 MPa m^{0.5}). The young group had the most cracks propagating in the cement line according to the previous papers' experimental results (Chan et al., 2009; Nalla et al., 2004), while the cracks propagation in the other three groups mostly destroyed the osteons. In order to analyse the effect of fracture toughness of the

osteons and interstitial matrix on crack propagation path in human cortical bone, especially, the crack in cement line and uncracked ligament bridging, only the young group was modelled. The cement line was kept constant, because the high strain energy release rate of the cement line resulted in the crack penetration into the osteon (Fig 8.12), which was not observed in the previous experiment results (Chan et al., 2009; Nalla et al., 2004)

Table 8.1. Strain energy-release rates of microstructural constituents in different groups used in simulations

Model	Cement line (N/mm)	Osteon (N/mm)	Interstitial matrix (N/mm)
111	0.146	0.146	0.146
112	0.146	0.146	0.292
114	0.146	0.146	0.584
116	0.146	0.146	0.876
121	0.146	0.292	0.146
122	0.146	0.292	0.292
124	0.146	0.292	0.584
126 (bovine and human)	0.146	0.292	0.876
141	0.146	0.584	0.146
142	0.146	0.584	0.292
144	0.146	0.584	0.584
146	0.146	0.584	0.876
161	0.146	0.876	0.146
162	0.146	0.876	0.292
164	0.146	0.876	0.584
166	0.146	0.876	0.876

8.3 Simulation Results

8.3.1 Effect of fracture toughness of interstitial matrix and osteon on initiation and growth slope of stress intensity factors

The effects of fracture toughness of microstructural constituents, such as osteon and interstitial matrix, were investigated with the simulation models of compact-tension according to the calculated levels of initiation and growth stress intensity factors (Figure 8.1-8.4). In Figure 8.1, the initiation stress intensity factors of the models increased as the strain energy release rates of the interstitial matrix increased, when the strain-energy release rates of osteon stay at 2 (Figure 8.1-B), 4 (Figure 8.1-C) and 6 (Figure 8.1-D) times higher than that of the cement lines. While the highest value of the initiation stress intensity factor (model 114) was $1.96 \text{ MPa(m)}^{0.5}$ when the strain energy release rates of the osteons and the interstitial matrix were 0.146 and 0.584 N/mm, respectively (Figure 8.1-A). The effect of fracture toughness of osteons on the initiation stress intensity factor could be observed in Figure 8.3. In Figure 8.3-B, the initiation stress intensity factor of model 122 was the highest one ($2.09 \text{ MPa(m)}^{0.5}$), when the fracture toughness of the interstitial matrix was 0.292 N/mm. The initiation stress intensity factors of models were decreasing with the increase of the strain energy release rate of osteon. It was also found that the initiation stress intensity factors of models were increasing as the strain energy release rate of osteon increase, when the one of interstitial matrix stay at the same level in Figure 8.3-B, C and D. Therefore, these results indicated that the initiation stress intensity factors of cortical bone were enhanced by the increase in the strain-energy release rates of both the osteons and the interstitial matrix, even though the crack-initiation positions of models were in the interstitial matrix.

The effect of fracture toughness of the osteons and the interstitial matrix on growth slopes of stress intensity factors of the studied models is illustrated by Figs. 8.2 and 8.4. The growth slopes of the stress intensity factor of the models (Figure 8.2-A) with the strain-energy release rate of the osteon of 0.146 N/mm increased with the increase of the strain-energy release rate of the interstitial matrix. The similar results could be observed in Figure 8.2-A, when the strain-energy release rate of the interstitial matrix stay at the same level. Meanwhile, the initiation stress intensity factors of the models (Figure 8.4-A) with the strain-energy release rate of the interstitial matrix 0.876 N/mm decreased as the strain-energy release rate of the osteons increased. Apart from the previous examples, other results did not have distinct pattern of direct influence of the fracture toughness of microstructural constituents on the crack-growth resistance of cortical bone.

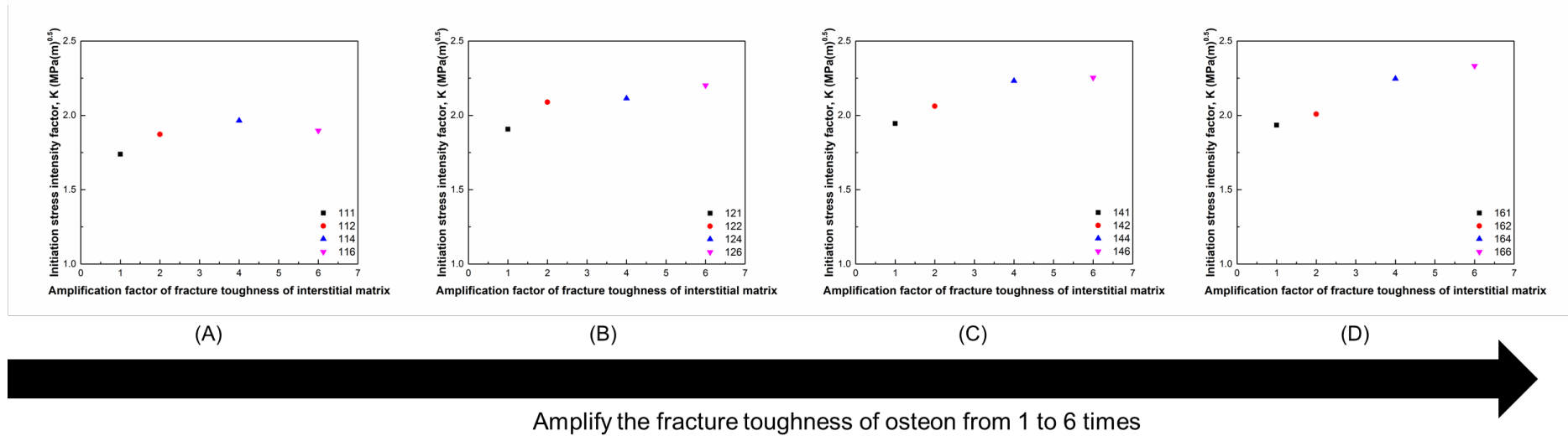
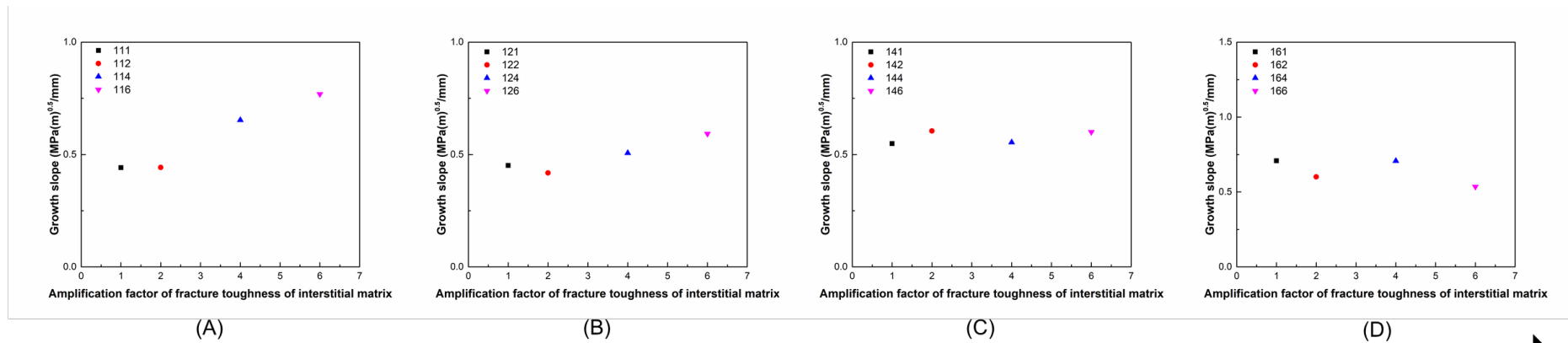


Figure 8.1. Initiation stress intensity factors of models with increasing fracture toughness of interstitial matrix with fracture toughness of osteon amplified 1 (A), 2 (B), 4 (C) and 6 (D).



Amplify the fracture toughness of osteon from 1 to 6 times

Figure 8.2. Growth slopes of models with increasing fracture toughness of interstitial matrix increasing with fracture toughness of osteon amplified by 1 (A), 2 (B), 4 (C) and 6 (D).

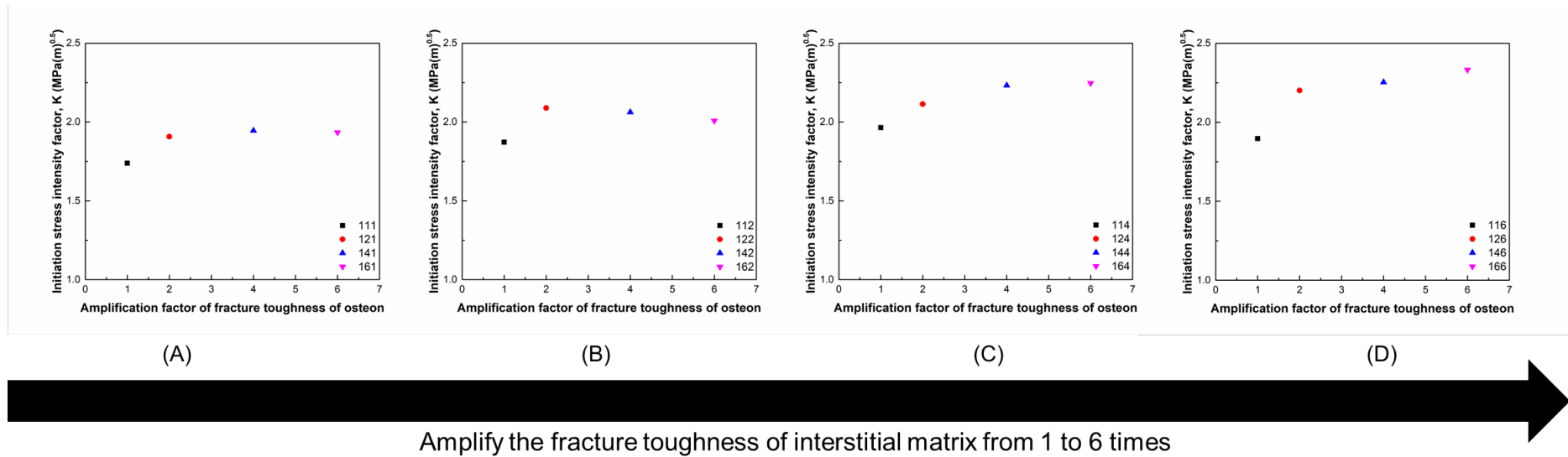


Figure 8.3. Initiation stress intensity factors of models with increasing fracture toughness of osteons with fracture toughness of interstitial matrix amplified by 1 (A), 2 (B), 4 (C) and 6 (D).

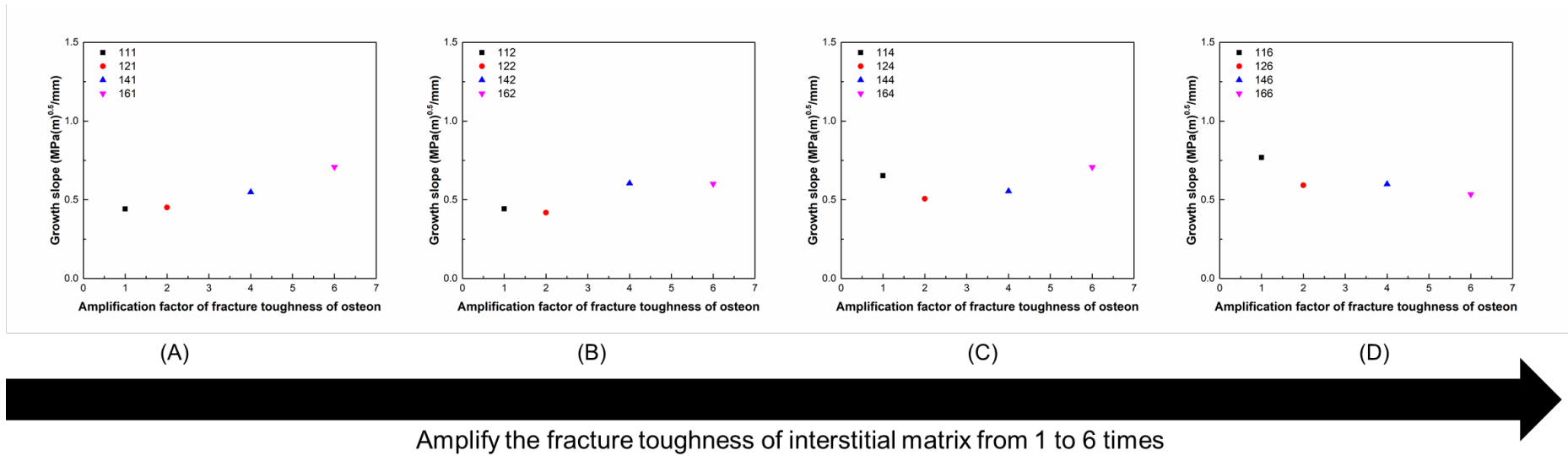


Figure 8.4. Growth slopes of models with increasing fracture toughness of osteons with fracture toughness of interstitial matrix amplified by 1 (A), 2 (B), 4 (C) and 6 (D).

8.3.2 Effect of fracture toughness of interstitial matrix and osteon on fracture mechanics

The fractions of the crack-propagation path in various microstructural constituents are presented in Table 8.2 to analyze the effect of their fracture toughness on the crack growth's path. Furthermore, this analysis would be related to the growth intensity stress factor of the models in Figs. 8.5 and 8.6. In Table 8.2, There was not obvious effect of fracture toughness of microstructural constituents on the percentages of crack in the interstitial matrix, which was $20.8 \pm 1.1\%$. The percentages of crack propagation in osteons and cement lines changed due to their various fracture-toughness levels in the models. For instance, when the strain-energy release rate of the osteons was kept at 0.146 N/mm , the lowest percentage of the crack path in the cement lines for model 111 was 24.6% and the highest one was for model 112- 32.4% that their ranges was almost 7.79% . But the percentage of the crack in the cement lines as slightly enhanced: it was less than 1.9% , when the strain-energy release rate of the osteons was increased from two to six times and kept at the same level. However, if the strain-energy release rate of the interstitial matrix remained at the same level, the crack would increase dramatically in cortical bone's model with the increase of the strain-energy release rate of the osteons- 28.3% , 31.8% and 46.3% , respectively. Apart from previous results, the percentage of the crack path in the cement lines, for the strain energy release rate of osteon was amplified six times, were 45.5% , almost the same as the models with the strain-energy release rate of osteon- 0.584 N/mm .

Table 8.2. Percentages of crack in microstructural constituents, such as cement lines, osteons and interstitial matrix

Models	Percentage of crack in cement line	Percentage of crack in osteon	Percentage of crack in interstitial matrix
111	24.6%	53.5%	21.9%
112	32.4%	45.6%	22.0%
114	27.9%	50.3%	21.8%
116	28.3%	54.1%	17.6%
121	31.0%	47.5%	21.5%
122	31.7%	47.1%	21.1%
124	32.3%	46.9%	20.8%
126	32.3%	46.9%	20.8%
141	45.3%	33.2%	21.5%
142	46.4%	33.5%	20.1%
144	46.4%	33.5%	20.1%
146	47.1%	33.5%	19.3%
161	45.3%	33.2%	21.5%
162	45.3%	33.5%	21.2%
164	46.1%	33.5%	20.4%
166	45.3%	33.6%	21.1%

When the strain energy release rate of interstitial matrix stay at the same level and the one of osteon was amplified from one to six times, the percentages of crack in osteon would dramatically fall, which were 50.9%, 47.1%, 33.5% and 33.5%. These results indicate the strong effect of fracture toughness of the osteons on crack-propagation paths. The crack grew more in the cement lines

instead of the osteons, but there were still limitation for crack propagation in the cement lines. However, the increase of fracture toughness of the interstitial matrix influenced on the crack propagation paths only slightly.

Additionally, the details of crack-propagation paths in cortical bone are presented in Fig 8.5, to analyse the extrinsic fracture-toughness mechanics of cortical bones. The Figures 8.5-A, B, C and D correspond to model 111, 121, 141 and 161 with the strain-energy release rate of the interstitial matrix of 0.146 N/mm and that of osteons were amplified 1, 2, 4 and 6 times, respectively. The red circles in the images indicate the parts of crack growth in the cement lines. It was found that the crack propagated in the cement line when the crack length reached the level of 0.788, 0.865 and 1.143 mm in model 111. The Model 121 had more of crack propagation in the cement lines, when the crack length reached 0.288 mm. Meanwhile, comparing models 141 and 161 with model 121, the cement line was destroyed by the crack, when the latter arrived at the first osteon (0.069 mm). These results showed that higher fracture toughness of the osteons could improve the crack growth in the cement lines near the cracks initiation position, while the lower one just protected the osteon far away from that position from the crack penetration.

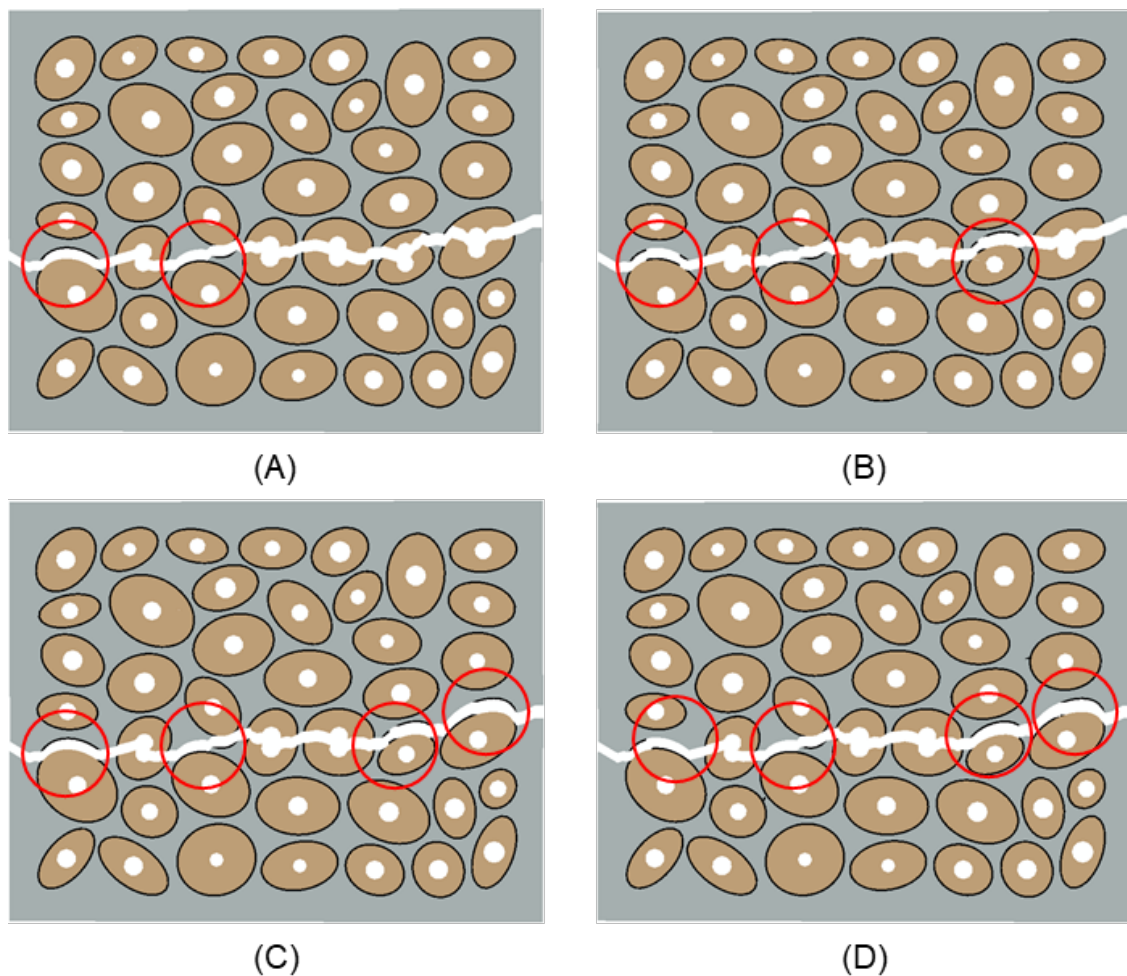
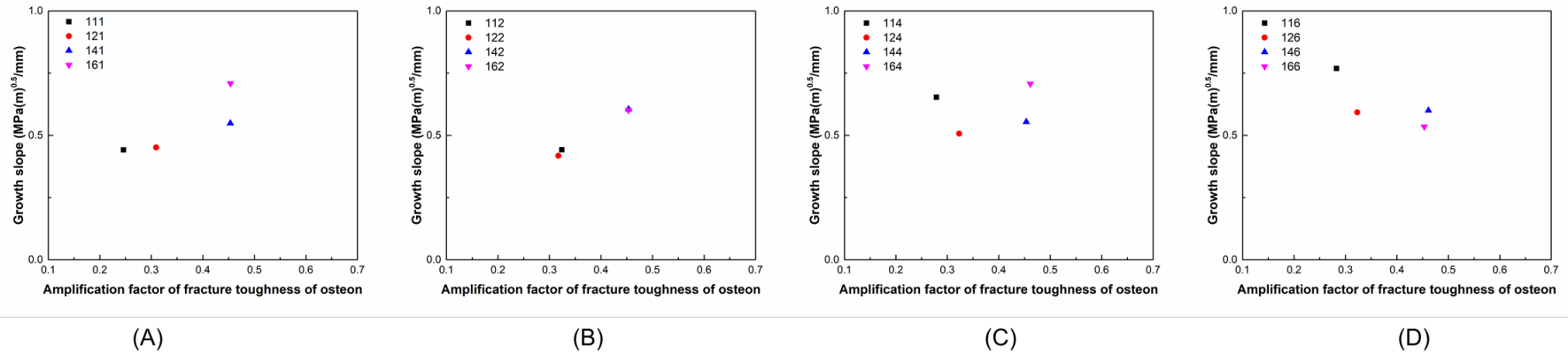
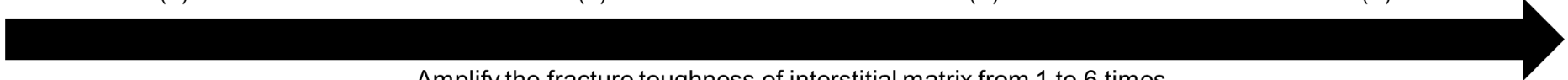


Figure 8.5. Crack propagation of models with the same fracture toughness of interstitial matrix, when fracture toughness of osteon is amplified 1 (A), 2 (B), 3 (C) and 4 (D).

The relationships between the fractions of the crack path in the cement lines or the osteons and the growth slope of stress intensity factor for the studied models are presented in Figs 8.6-8.7 when the strain energy release rate of the interstitial matrix was amplified 1, 2, 4, 6 times. In Fig. 8.6-A and B, the growth slope of stress intensity factors of the models increased with the increase of the crack fraction in the cement lines. While, Fig. 8.6-D shows a falling trend of the growth slope of the stress intensity factor of the models from the lower percentage to 45.3% of the crack in the cement line; after that the growth slope began to increase. But there was no distinct relationship between this fraction and the growth slope in Figure 8.6-C. It was interesting that the 114 and 116 had the high

growth slope, because the high stress intensity factor of interstitial matrix resulted in the uncracked ligament bridging shown as Fig 8.7. The lengths of the uncracked ligament bridging in Fig 8.7-A and B were 0.02 and 0.42 mm, respectively. These results indicated that the increase of the crack fraction in the cement lines could enhance the fracture resistance of cortical bone to the crack propagation when the level of strain-energy release of interstitial matrix was below 0.292 N/mm; while the uncracked ligament bridging due to the stress intensity factor of the interstitial matrix (over 0.292 N/mm) also enhance the fracture resistance of cortical bone.





 Amplify the fracture toughness of interstitial matrix from 1 to 6 times

Figure 8.6. Growth slope of stress intensity factor for models as function of percentage of crack in cement lines, with fracture toughness of osteon is amplified 1 (A), 2 (B), 4 (C) and 6 (D).

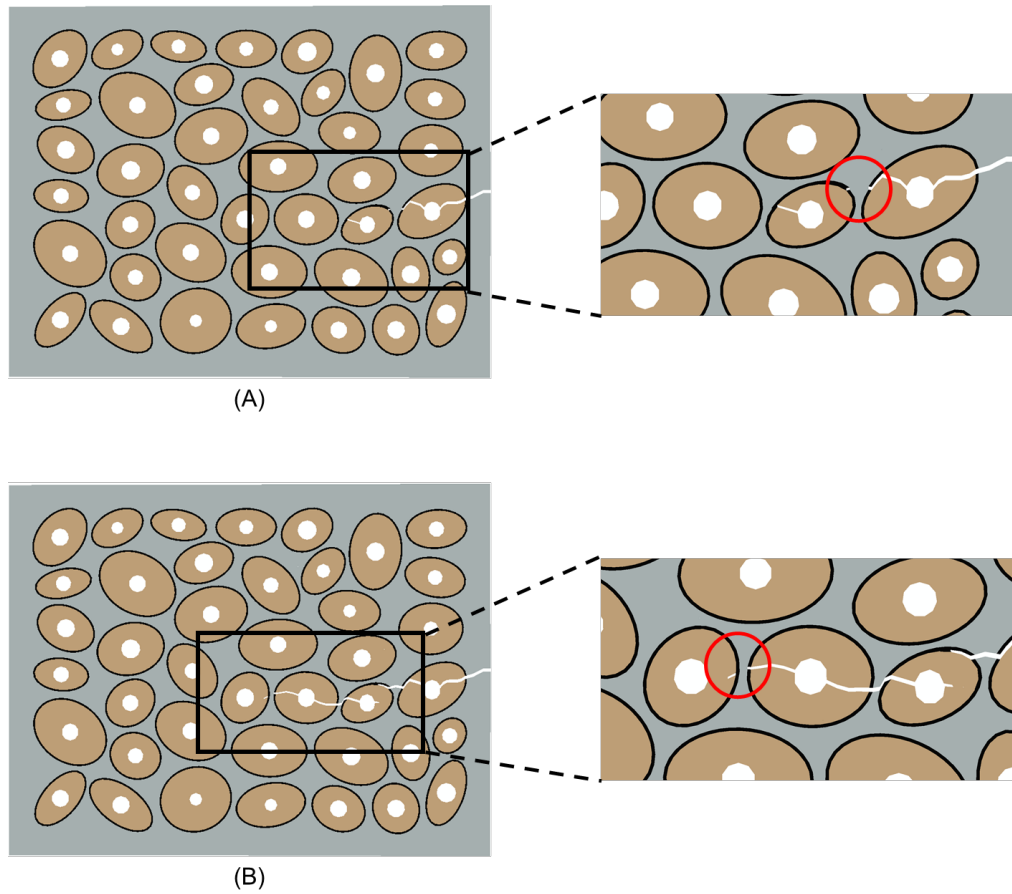


Figure 8.7. Uncracked ligament bridging in 114 model, whose the stress intensity factor of interstitial matrix is amplified 4 times (red circle indicated the uncracked ligament bridging area).

The uncracked-ligament-bridging and crack deflection are significant fracture mechanisms to enhance the fracture toughness of cortical bone during crack propagation. Therefore, R-curves of the cortical bone with the same strain-energy release rate of interstitial matrix (0.146 N/mm) and that of osteons amplified by 1 to 6 times, are presented in Figs 8.8-8.11 to analyse this. Images B-D correspond to the respective ranges of the rising parts of the R-curves in images A: details of the models are shown in zoomed in parts of B-D. In Figure 8.8, there is a slight growth of the stress intensity factor, when the crack propagated through one of an osteon and a cement line. This crack deflection (67.7°) was accompanied by a rise in the stress intensity factor from 1.74 to 1.94 $\text{MPa(m)}^{0.5}$ ($0.20 \text{ MPa(m)}^{0.5}$ in total Figure 8.8-B). The uncracked ligament bridging was observed in Figure 8.8-C to induce the increase of the stress intensity factor from 1.91 to 2.13 $\text{MPa(m)}^{0.5}$, a total of $0.22 \text{ MPa(m)}^{0.5}$, although the microstructural constituents had the same level of the strain-energy release rate. The second rising part for the stress intensity factors could be found in range D, when the crack propagated through the cement line (Fig. 8.8-D). This path was formed by 44.8° deflection of the crack. The stress intensity factor grew from 2.15 to 2.44 $\text{MPa(m)}^{0.5}$ -a total of $0.29 \text{ MPa(m)}^{0.5}$. In the models with the strain-energy release rate of the osteons amplified two times, the stress intensity factor increased from 1.77 to 2.14 $\text{MPa(m)}^{0.5}$, because of the crack destroying the osteon in (Fig. 8.9-B). Then, the uncracked-ligament bridging arrested the crack tip that arrived at the end of microstructural area in Fig. 8.9-C. When the strain-energy release rate of the osteons was amplified four times in Figure 8.10, the crack destroyed the cement line instead of the osteon so that the stress intensity factor increased in total by $0.30 \text{ MPa(m)}^{0.5}$ in Fig. 8.10-B; the crack deflected 59.6° during this process. Then, the crack destroyed the cement line, but there an uncracked ligament bridging during this process. These two simultaneous

fracture mechanisms gave $0.34 \text{ MPa(m)}^{0.5}$ of the increase in the stress intensity factor of the model in Fig. 8.10-C. On the other hand, when the model had the uncracked ligament bridging, the crack destroyed the cement line resulting in a gradual decrease of the stress intensity factor by $0.07 \text{ MPa(m)}^{0.5}$ (Fig. 8.10-D). Fig. 8.11 introduces the model with the strain-energy release rate of osteons was amplified by 6 times. The crack-growth paths were the same as in the model with the four-fold amplification. The rising curve could have ranges B and C, which enhanced the stress intensity factor of the models by 0.39 and $0.33 \text{ MPa(m)}^{0.5}$, respectively. While the falling curve could be also found in range D that the stress intensity factor was slightly decreased from 2.51 to 2.44 of a total $0.07 \text{ MPa(m)}^{0.5}$. In conclusion, the crack deflection could enhance the fracture toughness but it depends on the degree of crack deflection. From the previous results, the magnitude of 45° may be the threshold value. If the degree of crack deflection was higher than 45° , it could enhance the fracture toughness of model. For example, a crack destroying the cement line could help the stress intensity factor of models to reach $2.07 \text{ MPa(m)}^{0.5}$ (Fig. 8.10-B and 8.11-B), which was almost as high as in the case of the crack destroying the osteon with the strain-energy release rate amplified by 2 times ($2.14 \text{ MPa(m)}^{0.5}$) (Fig. 8.9-B). However, if the value was less than 45° , the growth curve of the stress intensity factor growth curve was just as the case of the normal crack growth in the cement line. For instance, the crack propagation followed the cement line (Fig. 8.8-C). The uncracked ligament bridging also could improve the fracture toughness of model. For example, the uncrack bridging ligament could make the stress intensity factor of the model to reach $2.13 \text{ MPa(m)}^{0.5}$. The stress intensity factor of the model in Fig. 8.9-C could be $2.42 \text{ MPa(m)}^{0.5}$ thanks to the uncracked ligament bridging. This value was slightly smaller than the value when the crack arrived at the same position ($2.48 \text{ MPa(m)}^{0.5}$), but the osteon's toughness was amplified by 4 times

in Fig. 8.10. These results also indicated that the increase in the strain-energy release rate of the osteons could not just merely increase the energy of the crack destroying the osteon, but also result in the main crack growing through the cement line instead of the osteon to protect the osteon when the strain energy release rate of osteon was amplified by over 4 times (Fig. 8.10 B-C and Fig. 8.11 B-C).

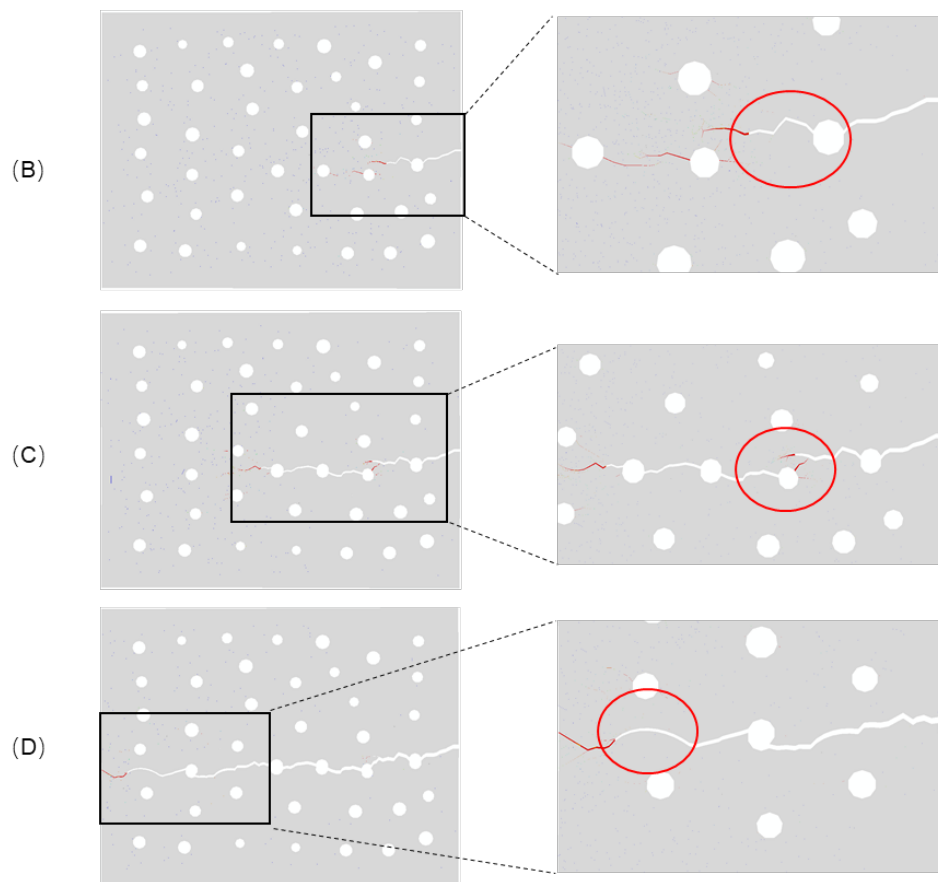
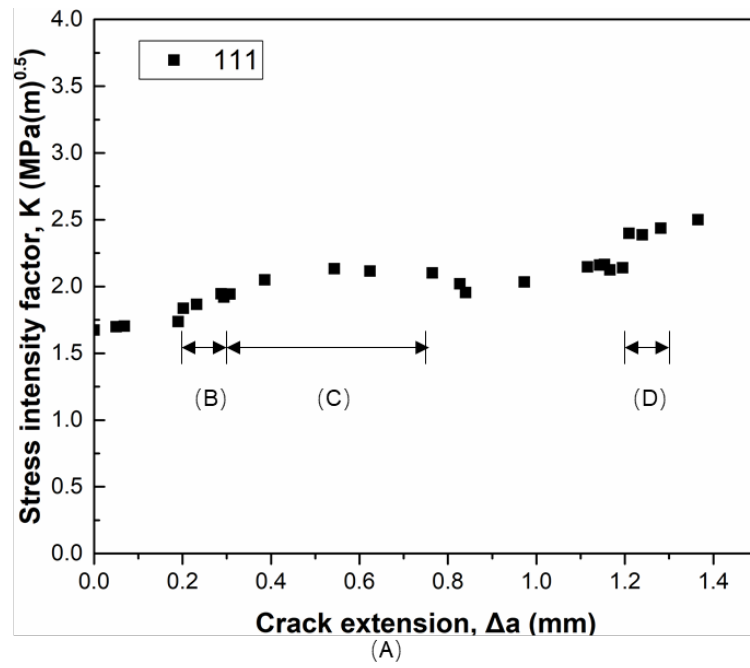
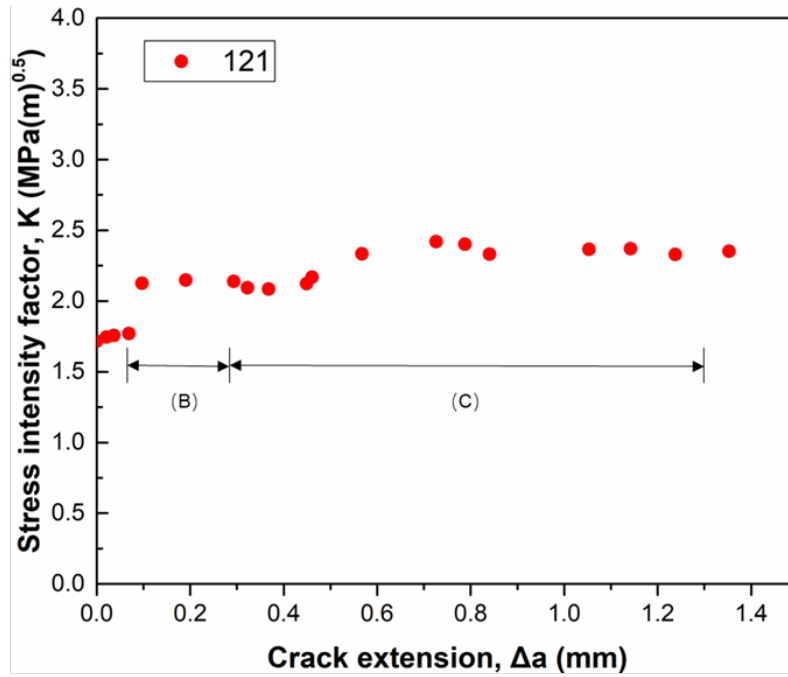


Figure 8.8. R-curve of stress intensity factor of cortical-bone model 111 (A) and crack propagation paths corresponding to ranges (B), (C) and (D) in R-curve (red circles and lines indicate crack deflection into cement line and the uncrack ligament bridging).



(A)

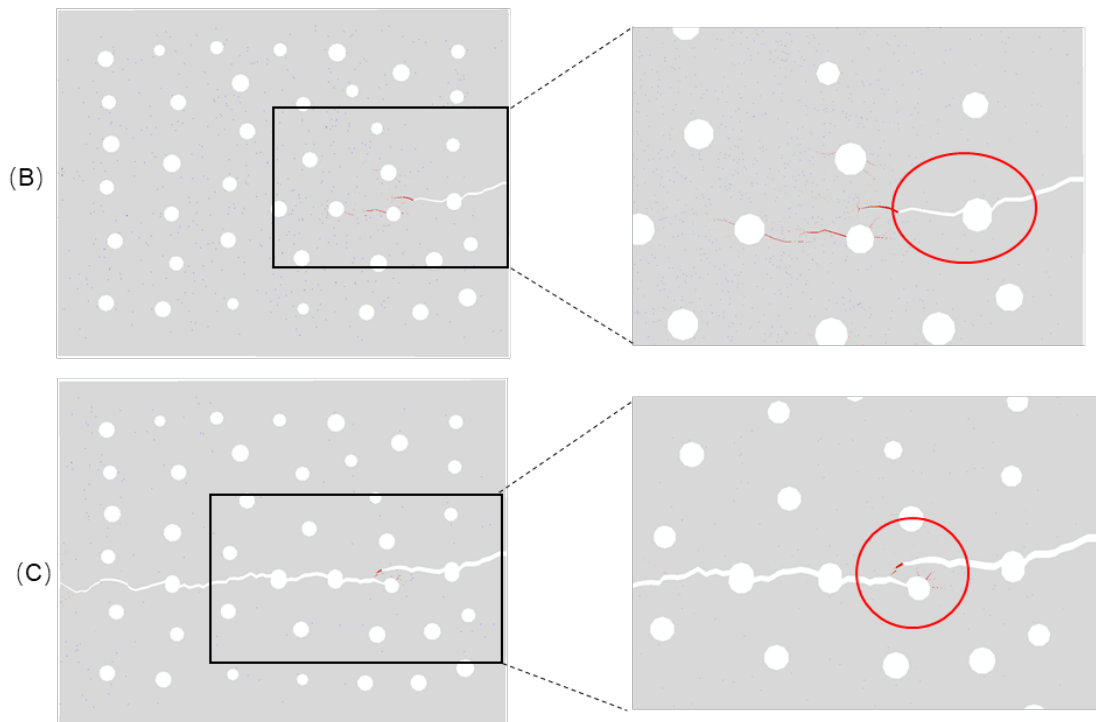
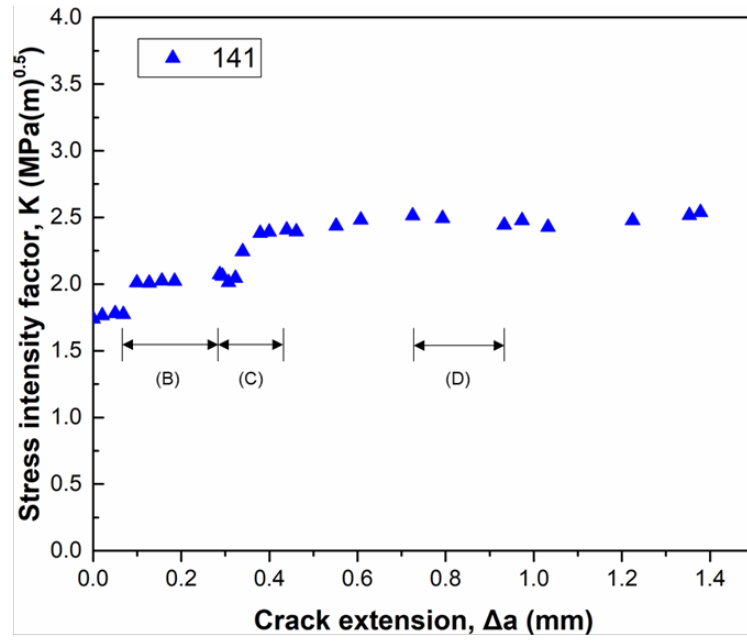


Figure 8.9. R-curve of stress intensity factor of cortical bone model 121 (A) and crack propagation paths corresponding to range (B) and (C) in R-curve. (red circles and lines indicate crack deflection into cement line and the uncrack ligament bridging)



(A)

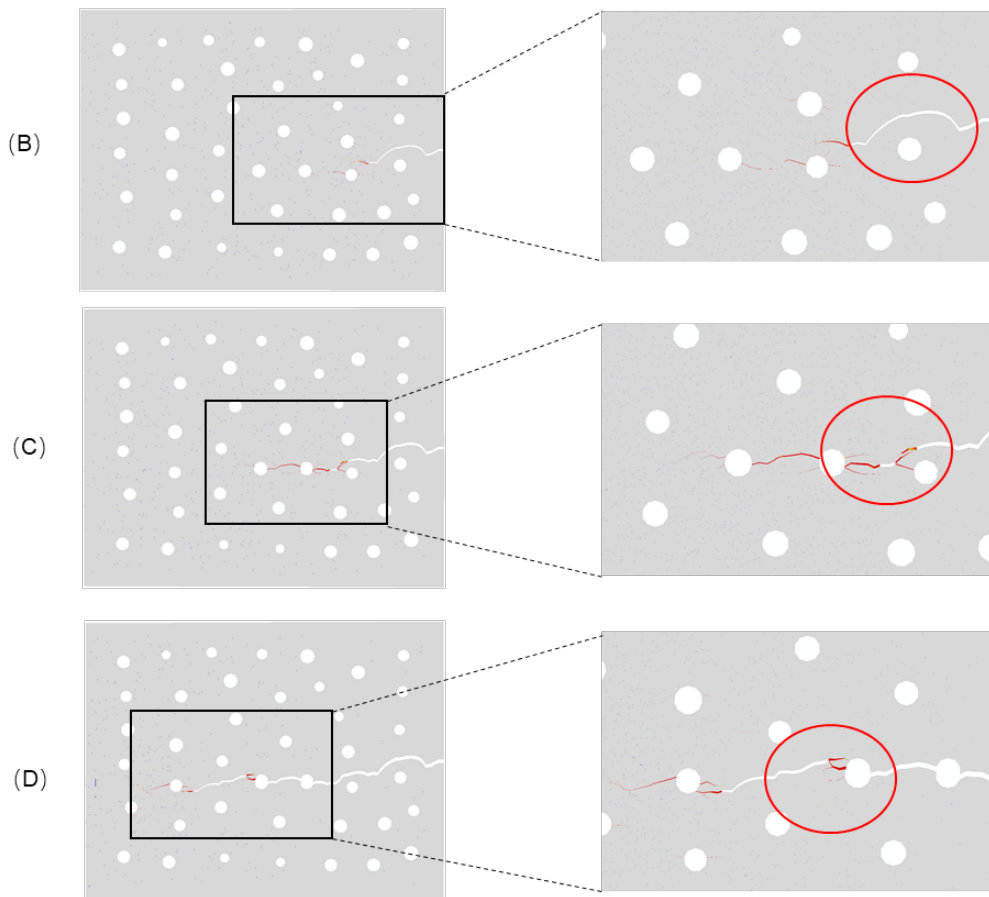


Figure 8.10. R-curve of stress intensity factor of cortical bone model 141 (A) and crack propagation paths corresponding to range (B), (C) and (D) in R-curve. (red circles and lines indicate crack deflection into cement line and the uncrack ligament bridging)

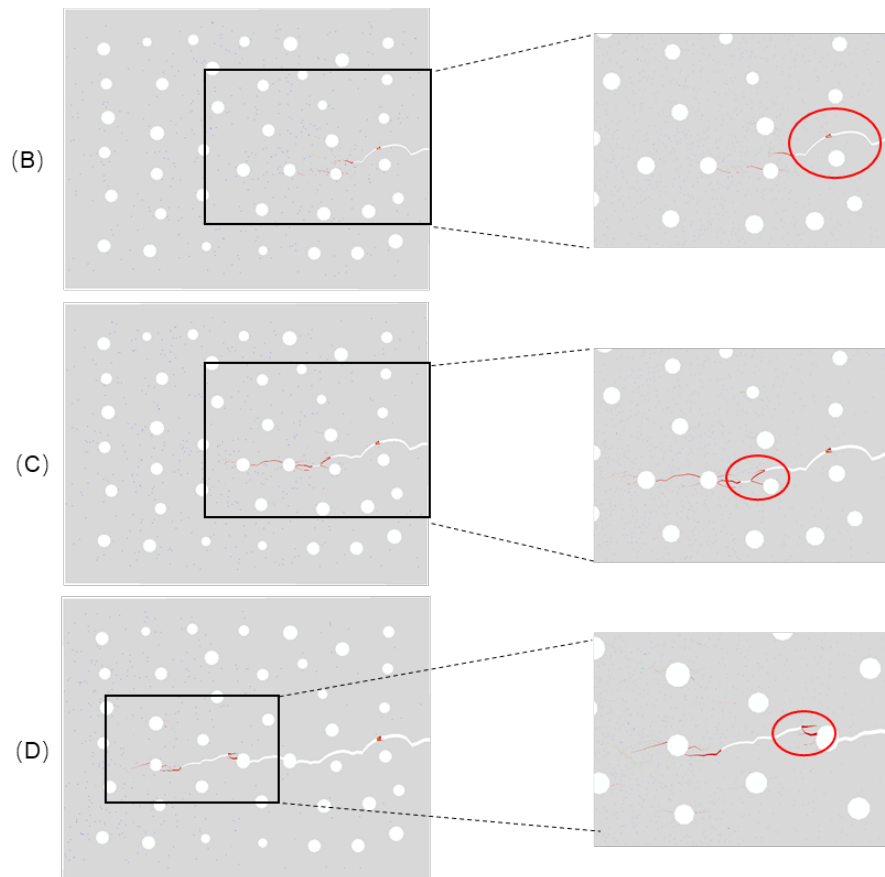
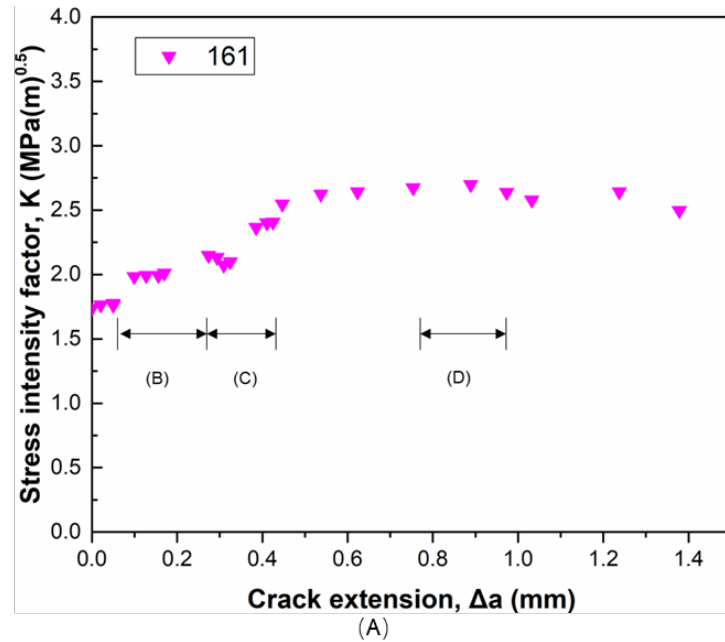


Figure 8.11. R-curve of stress intensity factor of cortical bone model 161 (A) and crack propagation paths corresponding to range (B), (C) and (D) in R-curve. (red circles and lines indicate crack deflection into cement line and the uncrack ligament bridging)

8.4 Discussion

The effect of fracture toughness of microstructural constituents on crack propagation was assessed with finite-element simulations in this chapter. In terms of the initiation stress intensity factor, the increase of the strain-energy release rate of the osteons and interstitial matrix could enhance it for cortical bone, when the Young's modulus and strength of microconstituents did not change. While the fracture toughness of microstructural constituents did not have a linear relationship with the growth slope of the stress intensity factor. It also was found that the increase in the strain-energy release rate of the osteons could induce crack propagation into the cement lines instead of the osteons. The microstructural images with the percentage of the crack growth paths in the cement line was similar to that in the experimental micro-images in Figure 7.3 (Chan et al., 2009).

These results also indicated that the strain energy release rate of the cement lines should be lower than that of other two microstructural constituents to either enhance the growth of fracture toughness of cortical bone or protect the osteon from being destroyed by the crack. In contrast, if the strain-energy release rate of the cement lines is higher than those of the osteons and interstitial matrix for the same mechanical properties of microstructural constituents (Fig 8.12), the crack penetrated osteons instead of cement lines. The cement line was a controversial structure in cortical bone; its mechanical properties were discussed in many papers. Its thickness (about 5 μm) was too small to for direct measurements of its mechanical properties experimentally method; also, the cement line is an interface between the osteons and the interstitial matrix so that the crack caused e.g. by a nano tip could propagate into any of the two constituents (Rho et al., 1998). Therefore, composition of the cement line was

analyzed with X-ray and electric microscopy to investigate its relationship with the osteon and interstitial matrix. Burr, Schaffler, & Frederickson (1988) found that the cement line was a mineral deficit structure, while Boyde and et al. (1990) kept the opposite opinion. The decrease in mineralization discrepancy between osteons and cement lines, so that the strain energy release rate of osteon was close to that of cement line, could result in crack penetration into the osteon (Milovanovic et al., 2018). Mischinski and Ural (2011) also found that lower strength and fracture toughness could improve the crack deflection into cement lines to enhance the cortical resistance to crack propagation. But in that study, a single-circle osteon model was used to analyze the effect, and they did not find that the discrepancy of the strain-energy release rate of microstructural constituents also could induce uncracked ligament bridging.

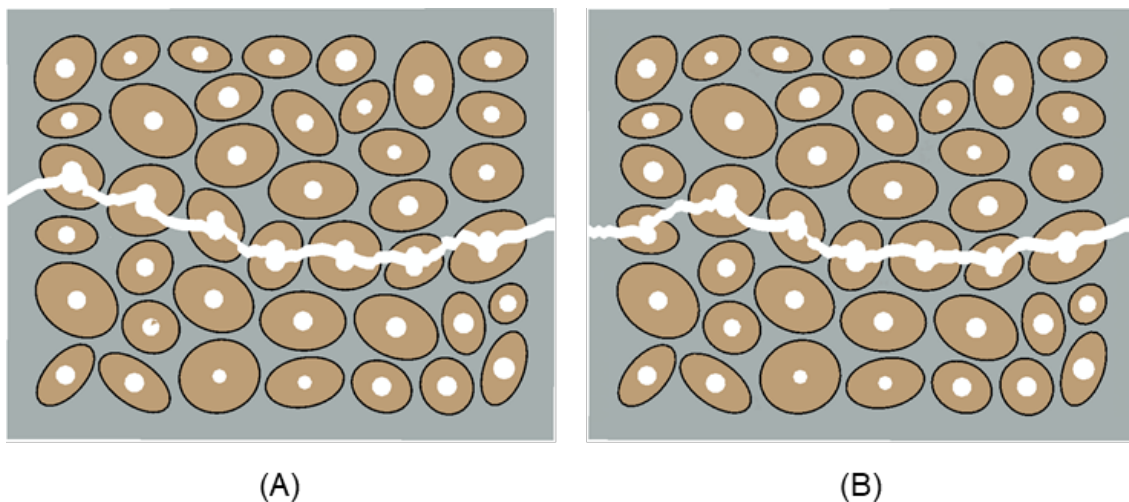


Figure 8.12. Crack-growth paths in cortical bones:(A) different elastic properties of constituents but the cement lines have 2 times higher strain energy release rate (0.292 N/mm) than that of two constituents, (B) the cement lines have the same mechanical properties as that of the osteons.

The results of the analysis demonstrated that the increase in the percentage of the crack paths in the cement lines could enhance the resistance to crack propagation in cortical bone, when the stress intensity factor of interstitial matrix

was below 0.292 N/mm. If the stress intensity factor of interstitial matrix was over 0.292 N/mm, the uncracked ligament bridging due to the interstitial matrix also affected the fracture toughness of cortical bone. However, the microcracks could be always found in the interstitial matrix in the experiments (Boyce et al., 1998; Schaffler et al., 1995). Therefore, the stress intensity factor of interstitial matrix may not be as that of the osteons. The analysis of R-curves and crack-growth paths in cortical bone showed that the strain-energy release rate of the osteons that was over 4 times than the one of the cement lines could result in initiation of uncracked ligament bridging and hinder the crack propagation in the cement line. The crack deviation by over 45° in the cement line act as toughening mechanism of the cortical bone, although the strain-energy release rate of the cement line was the lowest in three microstructural constituents (Fig. 8.8 and 8.9). The uncracked ligament bridging is another mechanism enhancing the bone's resistance ability to the crack propagation. The energy of crack destroying the osteon with the uncracked ligament bridging was almost similar to that of destroying the osteon with the four times higher strain-energy release rate (Fig. 8.9 and 8.10). The same results could be also found in Nalla's study (Nalla, Kruzic, et al., 2005). The higher strain-energy release rates of the osteons may explain that the crack propagated in the cement line and interstitial matrix and did not penetrated osteon in the experimental micro-images (Nalla, Kruzic, Kinney, et al., 2004).

8.5 Conclusion

In this study, the finite-element method was employed to investigate the effect of the fracture toughness of microstructural constituents on the crack propagation. It was found that the significantly higher strain-energy release rate of the osteons induced the crack to propagate into the cement lines instead of the osteon. This

higher value also could make the bone form the uncracked ligament bridging and, hence crack deflection, which could enhance the resistance of cortical bone to crack propagation.

Chapter 9- Conclusions and future work

9.1 General conclusion

The aim of this research project was to investigate the influence of such factors as age and disease on the fracture process in human cortical bone related to its micro-morphology and changes in mechanical properties. To achieved this, the literature review on morphology and mechanical properties of bone tissue was conducted to find the gap of previous research. The cortical bone tissue is the research target of this project because of its importance for daily life of humans since it bears the loading of the body and maintains movements. At micro-level, the cortical bone usually consists of four constituents such as osteons, Haversian canals, cement lines and interstitial area. Different characteristics and functions of microstructure constituents make the cortical bone tough but light. The age and disease change the characteristics of the osteonal microstructure due to the reformation rate. The cortical bone is a natural material that differs with species, genders, individuals, health and location within the body; these factors cause significant variations in distribution of mechanical properties. At macro-level, the basic experiments are tensile, compressive ultrasonic tests, used for assessment of elastic modulus, strength and other parameter of the bone tissue. At micro-level, the nanoindentation test is a popular method to assess the mechanical properties of osteonal microstructural constituents.

Then, the limitations of previous modelling methods were discussed in the literature review. The cohesive-element method and extended finite-element method are two kinds of popular numerical schemes used to simulate the fracture process of human cortical bone. But their limitations make them not suitable to achieve the aim of this thesis. For example, the cohesive-element method must

have a pre-path for crack propagation. The single crack can be treated with the extended finite-element method while multiple cracks are presented in cortical bone in reality. Therefore, the development of new simulation methods was undertaken to improve the quality of the numerical models. The combination of Abaqus software and MATLAB program helped to overcome limitation of the previous approaches. MATLAB programs were developed for inserting the cohesive elements into edges of solid elements, automatically calculation of the percentage of crack length in each microstructural constituents and generation of random distributions of microstructural constituents to enhance work efficiency. The mesh-sensitivity tests were conducted, and the results showed that the mesh size of 0.015 mm was the best choice to provide both the accuracy and computational efficiency of modelling. The developed modelling approach was validated against the experimental data; therefore, the developed cohesive-element method can be considered a reliable computational approach for simulation of the crack-propagation process in cortical bone.

The developed models with several random distributions of osteonal microstructure models were generated based on the experimental data. Numerical simulations of cases with two kinds of loading conditions as well as fixed micro-morphology or mechanical properties provide details of the fracture process for various groups, contributing to the understanding of mechanical behaviour of the cortical bone.

Based on intensive numerical simulations of various types of microstructured cortical bone, the following conclusion can be made:

- Analysis of morphology of various bone types showed that the young group had the smallest value of Haversian radius and a larger osteonal area, while the diseased group had a much larger Haversian-radius

distribution. The treated group demonstrated some improvements compare to the senior group. However, the aspect ratio of osteons measured as the long axis over short axis did not demonstrate any difference between all groups.

- The developed numerical models demonstrated that the young group had the best performance in terms of the Young's modulus, ultimate strength and force falling speed. This indicated that the young group had the highest fracture toughness of bone in four groups, while the diseased group's bones were fragile. The treated and senior groups had a similar performance, with the former slightly better than the latter.
- In general, the initiation of cracks began at the sites where the strain energy of free edges or large Haversian canals made a greater influence. Notably, the diseased group, probably due to higher porosity, had more crack paths initiated from Haversian canals than other groups.
- The numerical results suggested that cracks were greatly influenced by the distribution and areal fractions of micro-constituents. More cracks deflections into cement lines seems to associate with a higher crack retention force, while osteonal cracks might be linked to the lower crack retention as a result.
- The R-curve results reveal that the young group had the highest fracture toughness of initiation and crack-propagation, while the diseased group had the lowest toughness of these two types. The treated and senior groups had similar performance.
- The results presented that the young group's micro-morphology of osteonal structure was promoted the crack growth with crack attracted by cement lines, protecting osteon from fracture. While cracks in three other groups mainly penetrated osteons, their crack growth fracture toughness

was lower than that of the young group.

- The uncracked-ligament bridging in the young group was usually formed by neighbouring two cement lines, acting as toughening mechanism of the cortical bone. While the senior and treated groups had the same uncracked-ligament bridging mechanism to toughen their bone, this extrinsic fracture toughness was less prominent in the young group. Finally, the uncracked-ligament bridging in the diseased group consisted of two crack penetrating osteons and weakening the bone.
- The models with the same distribution of osteonal microstructures but with different strain energy release rates revealed the strong effect of fracture toughness of the osteons on crack-propagation paths. The cracks grew more in the cement lines and not in the osteons, but there were still limitation for crack propagation in the cement lines. However, the increase in fracture toughness of the interstitial matrix influenced the crack-propagation paths only slightly.
- The numerical analysis showed that the higher fracture toughness of the osteons could improve the crack growth in the cement lines near the crack initiation position, while the lower one protected the osteon that the crack-penetration far away from it.
- The crack deflection could enhance the fracture toughness of models but it depended on the degree of the crack deflection. From the previous results, the deflection angle of 45° might be the threshold. Larger angles of crack deflection could enhance the fracture toughness of model.
- The increase in the strain energy release rate of osteons could also enhance the strain energy release rate related to the uncracked-ligament bridging.

9.2 Future work

The cortical bone could be considered as the transversely isotropic material whose mechanical and fracture properties in longitudinal and transversely direction are different due to the orientation of the collagen fibre and Haversian canal. Therefore, it is interesting to investigate the characterisation of the crack propagation of the cortical bone in this direction. In order to reach this target, the three experimental methods could be selected, which will be also used for preparation of computational modelling:

Experimentation:

- Mechanical properties of microstructural constituents of the cortical bone in the longitudinal direction at microlevel.

The mechanical properties of microstructural constituents of the cortical bone could be measured with the nanoindentation testing.

- Characterisation of osteonal micro-morphology of the cortical bone in the longitudinal direction.

The microCT could be utilized in this work. The parameters of micro-morphology of the cortical bone in the longitudinal direction include the size of osteons, the inclination of an osteonal tube to the longitudinal direction and the length of the tubes of the osteons.

- Characterisation of the crack propagation in the cortical bone in the longitudinal direction.

The characterisation of the crack propagation in the cortical bone in the longitudinal direction could be investigated with a high-speed digital camera, which could record the fracture process in the cortical bone.

Finally, the three-dimensional models with the combination of mechanical

properties in two directions will be established to further study complicated characteristics of the fracture process in cortical bone.

Experimentation:

- Analysis of three-dimensional microCT images of the cortical bone at microlevel to help establish 3D numerical microstructured models.

Modelling:

- Development of the three-dimensional cohesive-element method to insert cohesive elements into three-dimensional models.

The three-dimensional cohesive-element could be applied in the three-dimensional models of cortical bone. In order to insert the cohesive elements into this kind of model, the inserting program could be developed in Matlab as extension of the two-dimensional program.

- Development of the three-dimensional model based on the experimental results.

The three-dimensional models could be established directly according to the three-dimensional microCT and the statistical data for osteonal tubes.

The traumatic fracture of cortical bone is usually caused by the high-strain-rate loading conditions, such as sudden falling and sports injuries. The fracture mechanics of cortical bone during such loading condition is a challenging research topic.

Experimentation:

- Analysis of fracture processes in cortical bone loaded at different strain rates in two directions.

The mechanical properties of cortical bone could be influenced by the

loading rates. In order to record the fracture process, the high-speed camera could be used, and the fracture surface of bone could be observed with optical microscope.

Modelling

- Introduction of viscoelastic properties into the finite-element model to investigate the characteristics of fracture process of the cortical bone at different strain rates.

The parameters of viscoelastic properties of cortical bone can be obtained by varying the loading rate in experiments. The computational model could help us to deeply understand the fracture process of the cortical bone.

The osteocyte is a special cell in cortical bone, which is responsible for the signal transmission. The osteocyte lacunae could be found in both trabecular and cortical bone. Previous studies used the experimental and simulation methods to study its function in crack propagation, but there is still a lack of knowledge to understand its function.

Experimentation:

- Characterisation of evolution of osteocyte lacunae of cortical bone in various groups.

The osteocyte lacunae could be observed by scanning the transverse direction of cortical bone, and their function could be analysed by researching their size, orientation and density.

Modelling

- Development of the numerical model with osteocyte lacunae to investigate

their effect on microcrack under various loading conditions.

The model with a single osteon with osteocyte lacunae could be generated with the Matlab program. The characteristics of microcrack or macrocrack propagation due to the distribution of osteocyte lacunae could be studied with the computational method.

9.2 Limitations of the current work

The current models simplify the complex distributions of microconstituents of cortical bone presenting osteon with ellipses. These models helped us to investigate the effect of morphology and fracture toughness of microconstituents on crack propagation, but there is still some limitation in current model.

1. In this thesis, three models of each group were generated based on the statistical analysis data. For four groups, twelve models were analysed employing the computational approach that needed a large quantity of computational time to be calculated from model building to analyse the results. At the same time, twelve models could obtain the difference of four groups, but more models might make this difference clearer.
2. The sensitivity analysis of the location of the pre-notch was not considered in this study. The location of the pre-notch was limited to the middle of the cortical-bone model based on previous papers. These are good research targets, which will be considered in the future work
3. The curves of the experiment and simulation do not completely match in the propagation parts, because the microstructure of the model was not exactly based on the CT image, while just based on the statistical data. However, some parts of simulation curve still had a good match with the experimental one.

References

- Abdel-Wahab, A. A., Alam, K., & Silberschmidt, V. V. (2011). Analysis of anisotropic viscoelastoplastic properties of cortical bone tissues. *Journal of the Mechanical Behavior of Biomedical Materials*, 4(5), 807–820.
- Abdel-Wahab, A. A., Maligno, A. R., & Silberschmidt, V. V. (2012). Micro-scale modelling of bovine cortical bone fracture: Analysis of crack propagation and microstructure using X-FEM. *Computational Materials Science*, 52(1), 128–135.
- Abdel-wahab, A. A., & Silberschmidt, V. V. (2011). Numerical Modelling of Impact Fracture of Cortical Bone Tissue using X-FEM. *Journal of Theoretical and Applied Mechanics*, 49(3), 599–619.
- Abdelaziz, Y., Bendahane, K., & Baraka, A. (2011). Extended Finite Element Modeling: Basic Review and Programming. *Engineering*.
- Abaqus, V. (2016). 6.14 Documentation. Dassault Systemes Simulia Corporation, 651.
- Alfano, M., Furguele, F., Leonardi, A., Maletta, C., & Paulino, G. H. (2007). Cohesive Zone Modeling of Mode I Fracture in Adhesive Bonded Joints. *Key Engineering Materials*.
- An, B., Liu, Y., Arola, D., & Zhang, D. (2011). Fracture toughening mechanism of cortical bone: An experimental and numerical approach. *Journal of the Mechanical Behavior of Biomedical Materials*, 4(7), 983–992.
- An, B., Zhao, X., Arola, D., & Zhang, D. (2014). Fracture analysis for biological materials with an expanded cohesive zone model. *Journal of Biomechanics*, 47(10), 2244–2248.
- Ashman, R. B., Cowin, S. C., Van Buskirk, W. C., & Rice, J. C. (1984). A continuous wave technique for the measurement of the elastic properties of cortical bone. *Journal of Biomechanics*.

- ASTM. (1997). E399-90. Standard test method for plane-strain fracture toughness of metallic materials. *1991 Annual Book of ASTM Standards*, 3(Reapproved), 451–485.
- Bailey, A. J., Sims, T. J., Ebbesen, E. N., Mansell, J. P., Thomsen, J. S., & Mosekilde, L. (1999). Age-related changes in the biochemical properties of human cancellous bone collagen: Relationship to bone strength. *Calcified Tissue International*.
- Bailey, Allen J., Paul, R. G., & Knott, L. (1998). Mechanisms of maturation and ageing of collagen. *Mechanisms of Ageing and Development*.
- Barrera, J. W., Le Cabec, A., & Barak, M. M. (2016). The orthotropic elastic properties of fibrolamellar bone tissue in juvenile white-tailed deer femora. *Journal of Anatomy*, 229(4), 568–576.
- Bell, K. L., Loveridge, N., Jordan, G. R., Power, J., Constant, C. R., & Reeve, J. (2000). A novel mechanism for induction of increased cortical porosity in cases of intracapsular hip fracture. *Bone*.
- Bell, K. L., Loveridge, N., Power, J., Garrahan, N., Meggitt, B. F., & Reeve, J. (1999). Regional differences in cortical porosity in the fractured femoral neck. *Bone*.
- Bell, Karen L., Loveridge, N., Reeve, J., Thomas, C. D. L., Feik, S. A., & Clement, J. G. (2001). Super-osteons (remodeling clusters) in the cortex of the femoral shaft: Influence of age and gender. *Anatomical Record*, 264(4), 378–386.
- Bella, J., Brodsky, B., & Berman, H. M. (1995). Hydration structure of a collagen peptide. *Structure*.
- Belytschko, T., & Black, T. (1999). Elastic crack growth in finite elements with minimal remeshing. *International Journal for Numerical Methods in Engineering*.

- Bernhard, A., Milovanovic, P., Zimmermann, E. A., Hahn, M., Djonic, D., Krause, M., ... Busse, B. (2013). Micro-morphological properties of osteons reveal changes in cortical bone stability during aging, osteoporosis, and bisphosphonate treatment in women. *Osteoporosis International*, 24(10), 2671–2680.
- Black, J., Mattson, R., & Korostoff, E. (1974). Haversian osteons: Size, distribution, internal structure, and orientation. *Journal of Biomedical Materials Research*.
- Bonfield, W. (1987). Advances in the fracture mechanics of cortical bone. *Journal of Biomechanics*, 20(11–12), 1071–1081.
- Boskey, A. L., Gadaleta, S., Gundberg, C., Doty, S. B., Ducky, P., & Karsenty, G. (1998). Fourier transform infrared microspectroscopic analysis of bones of osteocalcin-deficient mice provides insight into the function of osteocalcin. *Bone*.
- Bousson, V., Meunier, A., Bergot, C., Vicaut, E., Rocha, M. A., Morais, M. H., ... Laredo, J. D. (2001). Distribution of intracortical porosity in human midfemoral cortex by age and gender. *Journal of Bone and Mineral Research*.
- Boyce, T. M., Fyhrie, D. P., Glotkowski, M. C., Radin, E. L., & Schaffler, M. B. (1998). Damage type and strain mode associations in human compact bone bending fatigue. *Journal of Orthopaedic Research*.
- Boyde, A., Hendel, P., Hendel, R., Maconnachie, E., & Jones, S. J. (1990). Human cranial bone structure and the healing of cranial bone grafts: a study using backscattered electron imaging and confocal microscopy. *Anatomy and Embryology*, 181(3), 235–251.
- Britz, H. M., Thomas, C. D. L., Clement, J. G., & Cooper, D. M. L. (2009). The relation of femoral osteon geometry to age, sex, height and weight. *Bone*.

- Brodsky, B., & Persikov, A. V. (2005). Molecular structure of the collagen triple helix. *Advances in Protein Chemistry*.
- Budyn, E. (2007). Multiscale Modeling of Human Cortical Bone: Aging and Failure Studies. *Materials Research Society Symposium Proceedings*.
- Budyn, E., Hoc, T., & Jonvaux, J. (2008). Fracture strength assessment and aging signs detection in human cortical bone using an X-FEM multiple scale approach. *Computational Mechanics*, 42(4), 579–591.
- Budyn, É., & Hoc, T. (2010). Analysis of micro fracture in human Haversian cortical bone under transverse tension using extended physical imaging. *International Journal for Numerical Methods in Engineering*, 82(8), 940–965.
- Budyn, É., & Hoc, T. (2007a). Multiple scale modeling for cortical bone fracture in tension using X-FEM. *Revue Européenne de Mécanique Numérique*, 16(2), 213–236.
- Budyn, É., & Hoc, T. (2007b). Multiple scale modeling for cortical bone fracture in tension using X-FEM. *Revue Européenne de Mécanique Numérique*, 16(March 2015), 213–236.
- Budyn, É., & Hoc, T. (2007). Multiple scale modeling for cortical bone fracture in tension using X-FEM. *Revue Européenne de Mécanique Numérique*, 16(March 2015), 213–236.
- Burghardt, A. J., Kazakia, G. J., Ramachandran, S., Link, T. M., & Majumdar, S. (2010). Age- and gender-related differences in the geometric properties and biomechanical significance of intracortical porosity in the distal radius and tibia. *Journal of Bone and Mineral Research*.
- Burnell, J. M., Teubner, E. J., & Miller, A. G. (1980). Normal maturational changes in bone matrix, mineral, and crystal size in the rat. *Calcified Tissue International*.
- Burr, D. B. (2002). The contribution of the organic matrix to bone's material

- properties. *Bone*.
- Burr, David B., Schaffler, M. B., & Frederickson, R. G. (1988). Composition of the cement line and its possible mechanical role as a local interface in human compact bone. *Journal of Biomechanics*, 21(11).
- Busse, B., Hahn, M., Schinke, T., Püschel, K., Duda, G. N., & Amling, M. (2010). Reorganization of the femoral cortex due to age-, sex-, and endoprosthesis-related effects emphasized by osteonal dimensions and remodeling. *Journal of Biomedical Materials Research - Part A*.
- Carnelli, D., Lucchini, R., Ponzoni, M., Contro, R., & Vena, P. (2011). Nanoindentation testing and finite element simulations of cortical bone allowing for anisotropic elastic and inelastic mechanical response. *Journal of Biomechanics*, 44(10), 1852–1858.
- Chan, K. S., Lee, Y. D., Nicoletta, D. P., Furman, B. R., Wellinghoff, S., & Rawls, R. (2007). Improving fracture toughness of dental nanocomposites by interface engineering and micromechanics. *Engineering Fracture Mechanics*, 74(12), 1857–1871.
- Chan, Kwai S., Chan, C. K., & Nicoletta, D. P. (2009). Relating crack-tip deformation to mineralization and fracture resistance in human femur cortical bone. *Bone*, 45(3), 427–434.
- Cosman, F., de Beur, S. J., LeBoff, M. S., Lewiecki, E. M., Tanner, B., Randall, S., & Lindsay, R. (2014). Clinician's Guide to Prevention and Treatment of Osteoporosis. *Osteoporosis International*.
- Cowin, S. C., Moss-Salentijn, L., & Moss, M. L. (1991). Candidates for the Mechanosensory System in Bone. *Journal of Biomechanical Engineering*.
- Cowin, S., & Telega, J. (2003). Bone Mechanics Handbook, 2nd Edition. -. *Applied Mechanics Reviews*.
- Cox, B. N., & Yang, Q. (2007). Cohesive zone models of localization and

- fracture in bone. *Engineering Fracture Mechanics*.
- Cramer, J. A., Gold, D. T., Silverman, S. L., & Lewiecki, E. M. (2007). A systematic review of persistence and compliance with bisphosphonates for osteoporosis. *Osteoporosis International*.
- Currey, J. D. (1988). The effect of porosity and mineral content on the Young's modulus of elasticity of compact bone. *Journal of Biomechanics*.
- Currey, J. D. (2003). The many adaptations of bone. *Journal of Biomechanics*, 36(10), 1487–1495.
- Currey, John D. (2012). The structure and mechanics of bone. *Journal of Materials Science*.
- Currey, John D., Brear, K., & Zioupos, P. (1996). The effects of ageing and changes in mineral content in degrading the toughness of human femora. *Journal of Biomechanics*.
- Da Costa Gómez, T. M., Barrett, J. G., Sample, S. J., Radtke, C. L., Kalscheur, V. L., Lu, Y., ... Muir, P. (2005). Up-regulation of site-specific remodeling without accumulation of microcracking and loss of osteocytes. *Bone*.
- Davies, E., Muller, K. H., Wong, W. C., Pickard, C. J., Reid, D. G., Skepper, J. N., & Duer, M. J. (2014). Citrate bridges between mineral platelets in bone. *Proceedings of the National Academy of Sciences*.
- Demirtas, A., Curran, E., & Ural, A. (2016). Assessment of the effect of reduced compositional heterogeneity on fracture resistance of human cortical bone using finite element modeling. *Bone*, 91, 92–101.
- Dickenson, R., Hutton, W., & Stott. (2018). The mechanical properties of bone in osteoporosis. *The Journal of Bone and Joint Surgery. British Volume*.
- Doblaré, M., García, J. M., & Gómez, M. J. (2004). Modelling bone tissue fracture and healing: A review. *Engineering Fracture Mechanics*.
- Dong, X. N., & Guo, X. E. (2004). The dependence of transversely isotropic

- elasticity of human femoral cortical bone on porosity. *Journal of Biomechanics*, 37(8), 1281–1287.
- Dourado, N., Pereira, F. A. M., De Moura, M. F. S. F., Morais, J. J. L., & Dias, M. I. R. (2013). Bone fracture characterization using the end notched flexure test. *Materials Science and Engineering C*, 33(1), 405–410.
- Dragomir-Daescu, D., Op Den Buijs, J., McEligot, S., Dai, Y., Entwistle, R. C., Salas, C., ... Amin, S. (2011). Robust QCT/FEA models of proximal femur stiffness and fracture load during a sideways fall on the hip. *Annals of Biomedical Engineering*, 39(2), 742–755.
- eFunda: Stress Intensity Factor, K. (n.d.).
- El Sallah, Z. M., Smail, B., Abderahmane, S., Bouiadjra, B. B., & Boualem, S. (2016). Numerical simulation of the femur fracture under static loading. *Structural Engineering and Mechanics*.
- Evans, F. G. (1976). Mechanical properties and histology of cortical bone from younger and older men. *The Anatomical Record*.
- Fan, Z., Swadener, J. G., Rho, J. Y., Roy, M. E., & Pharr, G. M. (2002). Anisotropic properties of human tibial cortical bone as measured by nanoindentation. *Journal of Orthopaedic Research*.
- Fantner, G. E., Hassenkam, T., Kindt, J. H., Weaver, J. C., Birkedal, H., Pechenik, L., ... Hansma, P. K. (2005). Sacrificial bonds and hidden length dissipate energy as mineralized fibrils separate during bone fracture. *Nature Materials*, 4(8), 612–616.
- Ferretti, M., Palumbo, C., Contri, M., & Marotti, G. (2002). Static and dynamic osteogenesis: Two different types of bone formation. *Anatomy and Embryology*.
- Franzoso, G., & Zysset, P. K. (2008). Elastic Anisotropy of Human Cortical Bone Secondary Osteons Measured by Nanoindentation. *Journal of*

Biomechanical Engineering.

- Fratzl, P., Groschner, M., Vogl, G., Plenk, H., Eschberger, J., Fratzl-Zelman, N., ... Klaushofer, K. (1992). Mineral crystals in calcified tissues: A comparative study by SAXS. *Journal of Bone and Mineral Research*.
- Fratzl, Peter, Fratzl-Zelman, N., Klaushofer, K., Vogl, G., & Koller, K. (1991). Nucleation and growth of mineral crystals in bone studied by small-angle X-ray scattering. *Calcified Tissue International*.
- Garnero, P. (2015). The Role of Collagen Organization on the Properties of Bone. *Calcified Tissue International*, 97(3), 229–240.
- Gautieri, A., Buehler, M. J., & Redaelli, A. (2009). Deformation rate controls elasticity and unfolding pathway of single tropocollagen molecules. *Journal of the Mechanical Behavior of Biomedical Materials*.
- Giner, E., Belda, R., Arango, C., Vercher-Martínez, A., Tarancón, J. E., & Fuenmayor, F. J. (2017). Calculation of the critical energy release rate G_c of the cement line in cortical bone combining experimental tests and finite element models. *Engineering Fracture Mechanics*, 184, 168–182.
- Gourion-Arsiquaud, S., Faibish, D., Myers, E., Spevak, L., Compston, J., Hodsman, A., ... Boskey, A. L. (2009). Use of FTIR spectroscopic imaging to identify parameters associated with fragility fracture. *Journal of Bone and Mineral Research*.
- Granke, M., Grimal, Q., Saïed, A., Nauleau, P., Peyrin, F., & Laugier, P. (2011). Change in porosity is the major determinant of the variation of cortical bone elasticity at the millimeter scale in aged women. *Bone*, 49(5), 1020–1026.
- Granke, M., Makowski, A. J., Uppuganti, S., & Nyman, J. S. (2016). Prevalent role of porosity and osteonal area over mineralization heterogeneity in the fracture toughness of human cortical bone. *Journal of Biomechanics*, 49(13), 2748–2755.

- Guo, X. E., Liang, L. C., & Goldstein, S. A. (1998). Micromechanics of Osteonal Cortical Bone Fracture. *Journal of Biomechanical Engineering*.
- Gupta, H. S., Wagermaier, W., Zickler, G. A., Aroush, D. R. Ben, Funari, S. S., Roschger, P., ... Fratzl, P. (2005). Nanoscale deformation mechanisms in bone. *Nano Letters*.
- Hadjidakis, D. J., & Androulakis, I. I. (2006). Bone remodeling. *Ann N Y Acad Sci*, 1092, 385–396.
- Hambli, R., Bettamer, A., & Allaoui, S. (2012). Finite element prediction of proximal femur fracture pattern based on orthotropic behaviour law coupled to quasi-brittle damage. *Medical Engineering and Physics*, 34(2), 202–210.
- Hamed, E., Lee, Y., & Jasiuk, I. (2010). Multiscale modeling of elastic properties of cortical bone. In *Acta Mechanica*.
- Hang, F., Gupta, H. S., & Barber, A. H. (2014). Nanointerfacial strength between non-collagenous protein and collagen fibrils in antler bone. *Journal of the Royal Society Interface*.
- Hasegawa, K., Turner, C. H., & Burr, D. B. (1994). Contribution of collagen and mineral to the elastic anisotropy of bone. *Calcified Tissue International*.
- Hassenkam, T., Fantner, G. E., Cutroni, J. A., Weaver, J. C., Morse, D. E., & Hansma, P. K. (2004). High-resolution AFM imaging of intact and fractured trabecular bone. *Bone*.
- Heaney, R. P., Abrams, S., Dawson-Hughes, B., Looker, A., Looker, A., Marcus, R., ... Weaver, C. (2000). Peak bone mass. *Osteoporosis International*.
- Hillier, M. L., & Bell, L. S. (2007). Differentiating human bone from animal bone: A review of histological methods. *Journal of Forensic Sciences*, 52(2), 249–263.

- Hofmann, T., Heyroth, F., Meinhard, H., Fränzel, W., & Raum, K. (2006). Assessment of composition and anisotropic elastic properties of secondary osteon lamellae. *Journal of Biomechanics*.
- Hogan, H. A. (1992). Micromechanics modeling of Haversian cortical bone properties. *Journal of Biomechanics*.
- Holden, J. L., Clement, J. G., & Phakey, P. P. (1995). Age and temperature related changes to the ultrastructure and composition of human bone mineral. *Journal of Bone and Mineral Research*.
- Hui, S. L., Slemenda, C. W., & Johnston, C. C. (1988). Age and bone mass as predictors of fracture in a prospective study. *Journal of Clinical Investigation*.
- Idkaidek, A., & Jasiuk, I. (2017). Cortical bone fracture analysis using XFEM ??? case study. *International Journal for Numerical Methods in Biomedical Engineering*, 33(4), 1–16.
- Idkaidek, A., Koric, S., & Jasiuk, I. (2017). Fracture analysis of multi-osteon cortical bone using XFEM. *Computational Mechanics*, 1–14.
- Ishtiaq, S., Fogelman, I., & Hampson, G. (2015). Treatment of post-menopausal osteoporosis: Beyond bisphosphonates. *Journal of Endocrinological Investigation*, 38(1), 13–29.
- Jasiuk, I., Sabet, F. A., Najafi, A. R., & Hamed, E. (2015). Modelling of bone fracture and strength at different length scales: a review. *Interface Focus*, 6, 20–30.
- Jee, W. S. S. (2001). Integrated Bone Tissue Physiology: Anatomy and Physiology. In *Bone Mechanics Handbook*.
- Johnson, T. P. M., Socrate, S., & Boyce, M. C. (2010). A viscoelastic, viscoplastic model of cortical bone valid at low and high strain rates. *Acta Biomaterialia*, 6(10), 4073–4080.

- Katsamanis, F., & Raftopoulos, D. D. (1990). Determination of mechanical properties of human femoral cortical bone by the Hopkinson bar stress technique. *Journal of Biomechanics*.
- Keller, T. S., Mao, Z., & Spengler, D. M. (1990). Young's modulus, bending strength, and tissue physical properties of human compact bone. *Journal of Orthopaedic Research*.
- Koester, K. J., Ager, J. W., & Ritchie, R. O. (2008). The true toughness of human cortical bone measured with realistically short cracks. *Nature Materials*, 7(8), 672–677.
- Koester, K. J., Barth, H. D., & Ritchie, R. O. (2011). Effect of aging on the transverse toughness of human cortical bone: Evaluation by R-curves. *Journal of the Mechanical Behavior of Biomedical Materials*, 4(7), 1504–1513.
- Lai, Y. M., Qin, L., Hung, V. W. Y., & Chan, K. M. (2005). Regional differences in cortical bone mineral density in the weight-bearing long bone shaft - A pQCT study. *Bone*.
- Lakes, R. S., & Katz, J. L. (2018). Viscoelastic properties of bone. In *Natural and living biomaterials* (pp. 61–87). CRC Press.
- Landis, W. J., Song, M. J., Leith, A., McEwen, L., & McEwen, B. F. (1993). Mineral and organic matrix interaction in normally calcifying tendon visualized in three dimensions by high-voltage electron microscopic tomography and graphic image reconstruction. *Journal of Structural Biology*.
- Lang, S. B. (1970). Ultrasonic Method for Measuring Elastic Coefficients of Bone and Results on Fresh and Dried Bovine Bones. *IEEE Transactions on Biomedical Engineering*.
- Lanyon, L. E. (1993). Osteocytes, strain detection, bone modeling and

- remodeling. *Calcified Tissue International*.
- Launey, M. E., Buehler, M. J., & Ritchie, R. O. (2010). *On the Mechanistic Origins of Toughness in Bone*. *Annual Review of Materials Research* (Vol. 40).
- Laval-Jeantet, A. M., Bergot, C., Carroll, R., & Garcia-Schaefer, F. (1983). Cortical bone senescence and mineral bone density of the humerus. *Calcified Tissue International*.
- Lawrence Katz, J., Yoon, H. S., Lipson, S., Maharidge, R., Meunier, A., & Christel, P. (1984). The effects of remodeling on the elastic properties of bone. *Calcified Tissue International*.
- Lewis, J. L., & Goldsmith, W. (1975). The dynamic fracture and prefracture response of compact bone by split Hopkinson bar methods. *Journal of Biomechanics*.
- Li, S., Abdel-Wahab, A., Demirci, E., & Silberschmidt, V. V. (2013a). Fracture process in cortical bone: X-FEM analysis of microstructured models. *International Journal of Fracture*, 184(1–2), 43–55.
- Li, S., Abdel-Wahab, A., Demirci, E., & Silberschmidt, V. V. (2013b). Fracture process in cortical bone: X-FEM analysis of microstructured models. In *International Journal of Fracture* (Vol. 184, pp. 43–55).
- Li, S., Demirci, E., & Silberschmidt, V. V. (2013a). Variability and anisotropy of mechanical behavior of cortical bone in tension and compression. *Journal of the Mechanical Behavior of Biomedical Materials*, 21, 109–120.
- Li, S., Demirci, E., & Silberschmidt, V. V. (2013b). Variability and anisotropy of mechanical behavior of cortical bone in tension and compression. *Journal of the Mechanical Behavior of Biomedical Materials*, 21, 109–120.
- Lin, L., Samuel, J., Zeng, X., & Wang, X. (2017). Contribution of extrafibrillar matrix to the mechanical behavior of bone using a novel cohesive finite

- element model. *Journal of the Mechanical Behavior of Biomedical Materials*.
- Lin, Z. X., Xu, Z. H., An, Y. H., & Li, X. (2016). In situ observation of fracture behavior of canine cortical bone under bending. *Materials Science and Engineering C*, 62, 361–367.
- Liu, Y., Yan, G., Chen, S., & Chen, B. (2018). Effects of shape and direction of osteocyte lacunae on stress distribution of osteon. *IOP Conference Series: Materials Science and Engineering*, 423(1).
- Ma, Y. L., Dai, R. C., Sheng, Z. F., Jin, Y., Zhang, Y. H., Fang, L. N., ... Liao, E. Y. (2008). Quantitative associations between osteocyte density and biomechanics, microcrack and microstructure in OVX rats vertebral trabeculae. *Journal of Biomechanics*.
- Malik, C. L., Stover, S. M., Martin, R. B., & Gibeling, J. C. (2003). Equine cortical bone exhibits rising R-curve fracture mechanics. *Journal of Biomechanics*, 36(2), 191–198.
- Martin, B. (1993). Aging and strength of bone as a structural material. *Calcified Tissue International*.
- McCalden, R. W., McGeough, J. A., Barker, M. B., & Court-Brown, C. M. (1993). Age-related changes in the tensile properties of cortical bone. The relative importance of changes in porosity, mineralization, and microstructure. *The Journal of Bone and Joint Surgery. American Volume*, 75(8), 1193–1205.
- McCalden, R. W., McGlough, J. A., Barker, M. B., & Court-Brown, C. M. (1993). Age-related changes in the tensile properties of cortical bone. The relative importance of changes in porosity, mineralization and microstructure. *Journal of Bone and Joint Surgery - Series A*.
- McKee, M. D., & Nanci, A. (1996). Osteopontin at mineralized tissue interfaces

in bone, teeth, and osseointegrated implants: Ultrastructural distribution and implications for mineralized tissue formation, turnover, and repair.

Microscopy Research and Technique.

- Milovanovic, P., Rakocevic, Z., Djonic, D., Zivkovic, V., Hahn, M., Nikolic, S., ... Djuric, M. (2014). Nano-structural, compositional and micro-architectural signs of cortical bone fragility at the superolateral femoral neck in elderly hip fracture patients vs. healthy aged controls. *Experimental Gerontology*.
- Milovanovic, P., vom Scheidt, A., Mletzko, K., Sarau, G., Püschel, K., Djuric, M., ... Busse, B. (2018). Bone tissue aging affects mineralization of cement lines. *Bone*, 110, 187–193.
- Milovanovic, P., Zimmermann, E. A., Riedel, C., Scheidt, A. vom, Herzog, L., Krause, M., ... Busse, B. (2015). Multi-level characterization of human femoral cortices and their underlying osteocyte network reveal trends in quality of young, aged, osteoporotic and antiresorptive-treated bone. *Biomaterials*, 45, 46–55.
- Mirzaali, M. J., Schwiedrzik, J. J., Thaiwichai, S., Best, J. P., Michler, J., Zysset, P. K., & Wolfram, U. (2016). Mechanical properties of cortical bone and their relationships with age, gender, composition and microindentation properties in the elderly. *Bone*, 93, 196–211.
- Mischinski, S., & Ural, A. (2011). Finite Element Modeling of Microcrack Growth in Cortical Bone. *Journal of Applied Mechanics*, 78(4), 041016.
- Mischinski, S., & Ural, A. (2013). Interaction of microstructure and microcrack growth in cortical bone: A finite element study. *Computer Methods in Biomechanics and Biomedical Engineering*, 16(1), 81–94.
- Mitchell, J., & van Heteren, A. H. (2016). A literature review of the spatial organization of lamellar bone. *Comptes Rendus - Palevol*, 15(1–2), 23–31.
- Mohsin, S., O'Brien, F. J., & Lee, T. C. (2006). Osteonal crack barriers in ovine

- compact bone. *Journal of Anatomy*, 208(1), 81–89.
- Morais, J. J. L., de Moura, M. F. S. F., Pereira, F. A. M., Xavier, J., Dourado, N., Dias, M. I. R., & Azevedo, J. M. T. (2010). The double cantilever beam test applied to mode I fracture characterization of cortical bone tissue. *Journal of the Mechanical Behavior of Biomedical Materials*, 3(6), 446–453.
- Mulhern, D. M. (2000). Rib remodeling dynamics in a skeletal population from Kulubnarti, Nubia. *American Journal of Physical Anthropology*, 111(4), 519–530.
- Mullins, L. P., Sassi, V., McHugh, P. E., & Bruzzi, M. S. (2009). Differences in the crack resistance of interstitial, osteonal and trabecular bone tissue. *Annals of Biomedical Engineering*, 37(12), 2574–2582.
- Muschler, G. F., Nakamoto, C., & Griffith, L. G. (2004). Engineering principles of clinical cell-based tissue engineering. *Journal of Bone and Joint Surgery - Series A*.
- Najafi, A. R., Arshi, A. R., Eslami, M. R., Fariborz, S., & Moeinzadeh, M. (2007). Haversian cortical bone model with many radial microcracks: An elastic analytic solution. *Medical Engineering and Physics*, 29(6), 708–717.
- Nalla, R. K., Kinney, J. H., & Ritchie, R. O. (2003). Mechanistic fracture criteria for the failure of human cortical bone. *Nature Materials*, 2(3), 164–168.
- Nalla, R. K., Kruzic, J. J., Kinney, J. H., Balooch, M., Ager, J. W., & Ritchie, R. O. (2006). Role of microstructure in the aging-related deterioration of the toughness of human cortical bone. *Materials Science and Engineering C*, 26(8), 1251–1260.
- Nalla, R. K., Kruzic, J. J., Kinney, J. H., & Ritchie, R. O. (2004). Effect of aging on the toughness of human cortical bone: Evaluation by R-curves. *Bone*, 35(6), 1240–1246.

- Nalla, R. K., Kruzic, J. J., Kinney, J. H., & Ritchie, R. O. (2005). Mechanistic aspects of fracture and R-curve behavior in human cortical bone. *Biomaterials*, 26(2), 217–231.
- Nalla, R. K., Kruzic, J. J., & Ritchie, R. O. (2004). On the origin of the toughness of mineralized tissue: Microcracking or crack bridging? *Bone*, 34(5), 790–798.
- Nalla, R. K., Stölken, J. S., Kinney, J. H., & Ritchie, R. O. (2005). Fracture in human cortical bone: Local fracture criteria and toughening mechanisms. *Journal of Biomechanics*, 38(7), 1517–1525.
- Nguyen, V. P. (2014). An open source program to generate zero-thickness cohesive interface elements. *Advances in Engineering Software*, 74, 27–39.
- NHS. (2015). Osteoporosis - NHS Choices.
- Nicolella, D. P., Moravits, D. E., Gale, A. M., Bonewald, L. F., & Lankford, J. (2006). Osteocyte lacunae tissue strain in cortical bone. *Journal of Biomechanics*, 39(9), 1735–1743.
- Nicolella, D. P., Nicholls, A. E., Lankford, J., & Davy, D. T. (2001). Machine vision photogrammetry: A technique for measurement of microstructural strain in cortical bone. *Journal of Biomechanics*, 34(1), 135–139.
- Nikel, O., Laurencin, D., McCallum, S. A., Gundberg, C. M., & Vashishth, D. (2013). NMR investigation of the role of osteocalcin and osteopontin at the organic-inorganic interface in bone. *Langmuir*.
- Nyman, J. S., Ni, Q., Nicolella, D. P., & Wang, X. (2008). Measurements of mobile and bound water by nuclear magnetic resonance correlate with mechanical properties of bone. *Bone*.
- O'Brien, F. J., Taylor, D., & Lee, T. C. (2005). The effect of bone microstructure on the initiation and growth of microcracks. *J. Orthop. Res.*, 23(2), 475–

480.

- Odetti, P., Rossi, S., Monacelli, F., Poggi, A., Cirnigliaro, M., Federici, M., & Federici, A. (2005). Advanced glycation end products and bone loss during aging. In *Annals of the New York Academy of Sciences*.
- Olszta, M. J., Cheng, X., Jee, S. S., Kumar, R., Kim, Y. Y., Kaufman, M. J., ... Gower, L. B. (2007). Bone structure and formation: A new perspective. *Materials Science and Engineering R: Reports*.
- Oxlund, H., Mosekilde, L., & Ørtoft, G. (1996). Reduced concentration of collagen reducible cross links in human trabecular bone with respect to age and osteoporosis. *Bone*.
- Parfitt, A. M. (1998). Osteoclast precursors as leukocytes: Importance of the area code. *Bone*.
- Pietruszczak, S., Gdela, K., Webber, C. E., & Inglis, D. (2007). On the assessment of brittle-elastic cortical bone fracture in the distal radius. *Engineering Fracture Mechanics*.
- Pithioux, M., Lasaygues, P., & Chabrand, P. (2002). An alternative ultrasonic method for measuring the elastic properties of cortical bone. *Journal of Biomechanics*.
- Poundarik, A. A., Wu, P. C., Evis, Z., Sroga, G. E., Ural, A., Rubin, M., & Vashishth, D. (2015). A direct role of collagen glycation in bone fracture. *Journal of the Mechanical Behavior of Biomedical Materials*.
- Poundarik, A., Gundberg, C., & Vashishth, D. (2011). Non-collageneous proteins influence bone crystal size and morphology: A SAXS study. In *2011 IEEE 37th Annual Northeast Bioengineering Conference, NEBEC 2011*.
- Prendergast, P. J., & Huiskes, R. (1996). Microdamage and Osteocyte-Lacuna Strain in Bone: A Microstructural Finite Element Analysis. *Journal of*

Biomechanical Engineering.

- Qin, Q. H., & Zhang, X. (2000). Crack deflection at an interface between dissimilar piezoelectric materials. *International Journal of Fracture*, 102(4), 355–370.
- Qiu, S., Rao, D. S., Palnitkar, S., & Parfitt, A. M. (2003). Reduced iliac cancellous osteocyte density in patients with osteoporotic vertebral fracture. *Journal of Bone and Mineral Research*.
- Qiu, T., Liu, Q., & Wang, J. (2005). Study on technology of recycling oxalic acid and hydrochloric acid in wastewater discharged from rare earth metallurgical factory. *Journal of Rare Earths*, 23(SUPPL. 2), 10–13.
- Raeisi Najafi, A., Arshi, A. R., Eslami, M. R., Fariborz, S., & Moeinzadeh, M. H. (2007). Micromechanics fracture in osteonal cortical bone: A study of the interactions between microcrack propagation, microstructure and the material properties. *Journal of Biomechanics*, 40(12), 2788–2795.
- Raeisi Najafi, Ahmad, Arshi, A. R., Saffar, K. P. A., Eslami, M. R., Fariborz, S., & Moeinzadeh, M. H. (2009). A fiber-ceramic matrix composite material model for osteonal cortical bone fracture micromechanics: Solution of arbitrary microcracks interaction. *Journal of the Mechanical Behavior of Biomedical Materials*, 2(3), 217–223.
- Rath Bonivtch, A., Bonewald, L. F., & Nicoletta, D. P. (2007). Tissue strain amplification at the osteocyte lacuna: A microstructural finite element analysis. *Journal of Biomechanics*.
- Rauch, F., Travers, R., Parfitt, A. M., & Glorieux, F. H. (2000). Static and dynamic bone histomorphometry in children with osteogenesis imperfecta. *Bone*.
- Reilly, D.T., & Burstein, A. H. (1975). The Elastic and Ultimate Properties of Compact Bone Tissue. *Journal of Biomechanics*, 8, 393–405.

- Reilly, Donald T., & Burstein, A. H. (1975a). The Elastic and Ultimate Properties of Compact Bone Tissue. *Journal of Biomechanics*, 8(6), 393–405.
- Reilly, Donald T., & Burstein, A. H. (1975b). The elastic and ultimate properties of compact bone tissue. *Journal of Biomechanics*, 8(6).
- Reilly, G. C. (2000). Observations of microdamage around osteocyte lacunae in bone. *Journal of Biomechanics*, 33(9), 1131–1134.
- Reilly, G. C., & Currey, J. D. (1999). The development of microcracking and failure in bone depends on the loading mode to which it is adapted. *Journal of Experimental Biology*, 202(5), 543–552.
- Rho, JY; Kuhn-Spearing, L; Zioupos, P. (1998). Mechanical properties and the hierarchical structure of bone. *Medical Engineering and Physics*, 20(2), 92–102.
- Rho, J. Y., Zioupos, P., Currey, J. D., & Pharr, G. M. (1999). Variations in the individual thick lamellar properties within osteons by nanoindentation. *Bone*.
- Rho, J. Y., Zioupos, P., Currey, J. D., & Pharr, G. M. (2002). Microstructural elasticity and regional heterogeneity in human femoral bone of various ages examined by nano-indentation. *Journal of Biomechanics*, 35(2), 189–198.
- Rho, J Y, Currey, J. D., Zioupos, P., & Pharr, G. M. (2001). The anisotropic Young's modulus of equine secondary osteones and interstitial bone determined by nanoindentation. *The Journal of Experimental Biology*, 204(2001), 1775–1781.
- Rho, Jae Young. (1996). An ultrasonic method for measuring the elastic properties of human tibial cortical and cancellous bone. *Ultrasonics*.
- Rho, Jae Young, Kuhn-Spearing, L., & Zioupos, P. (1998). Mechanical

- properties and the hierarchical structure of bone. *Medical Engineering and Physics*, 20(2), 92–102.
- Rho, Jae Young, Tsui, T. Y., & Pharr, G. M. (1997). Elastic properties of human cortical and trabecular lamellar bone measured by nanoindentation. *Biomaterials*, 18(20), 1325–1330.
- Ritchie, R. O. (1999). Mechanisms of fatigue-crack propagation in ductile and brittle solids. In *International Journal of Fracture*.
- Ritchie, R. O., Kinney, J. H., Kruzic, J. J., & Nalla, R. K. (2005). A fracture mechanics and mechanistic approach to the failure of cortical bone. *Fatigue and Fracture of Engineering Materials and Structures*.
- Ritchie, Robert O, Djuric, M., & Amling, M. (2010). Decrease in the osteocyte lacunar density accompanied by hypermineralized lacunar occlusion reveals failure and delay of remodeling in aged human bone ", 1065–1075.
- Rodriguez-Florez, N., Carriero, A., & Shefelbine, S. J. (2017). The use of XFEM to assess the influence of intra-cortical porosity on crack propagation. *Computer Methods in Biomechanics and Biomedical Engineering*.
- Rybicki, E. F., Simonen, F. A., & Weis, E. B. (1972). On the mathematical analysis of stress in the human femur. *Journal of Biomechanics*.
- Sabet, F. A., Raeisi Najafi, A., Hamed, E., & Jasiuk, I. (2016). Modelling of bone fracture and strength at different length scales: a review. *Interface Focus*, 6(1), 20150055.
- Saito, M., Fujii, K., Soshi, S., & Tanaka, T. (2006). Reductions in degree of mineralization and enzymatic collagen cross-links and increases in glycation-induced pentosidine in the femoral neck cortex in cases of femoral neck fracture. *Osteoporosis International*.
- Saito, Mitsuru, Fujii, K., & Marumo, K. (2006). Degree of mineralization-related collagen crosslinking in the femoral neck cancellous bone in cases of hip

- fracture and controls. *Calcified Tissue International*.
- Saito, Mitsuru, Marumo, K., Fujii, K., & Ishioka, N. (1997). Single-column high-performance liquid chromatographic-fluorescence detection of immature, mature, and senescent cross-links of collagen. *Analytical Biochemistry*.
- Sasaki, N., Matsushima, N., Ikawa, T., Yamamura, H., & Fukuda, A. (1989). Orientation of bone mineral and its role in the anisotropic mechanical properties of bone-Transverse anisotropy. *Journal of Biomechanics*.
- Schaffler, M. B., Choi, K., & Milgrom, C. (1995). Aging and matrix microdamage accumulation in human compact bone. *Bone*, 17(6), 521–525.
- Schaffler, Mitchell B., & Burr, D. B. (1988). Stiffness of compact bone: Effects of porosity and density. *Journal of Biomechanics*.
- Schaffler, Mitchell B., Burr, D. B., & Frederickson, R. G. (1987). Morphology of the osteonal cement line in human bone. *The Anatomical Record*.
- Schwarcz, H. P., McNally, E. A., & Botton, G. A. (2014). Dark-field transmission electron microscopy of cortical bone reveals details of extrafibrillar crystals. *Journal of Structural Biology*.
- Shea, J. E., & Miller, S. C. (2005). Skeletal function and structure: Implications for tissue-targeted therapeutics. *Advanced Drug Delivery Reviews*.
- Silva, F. G. A., de Moura, M. F. S. F., Dourado, N., Xavier, J., Pereira, F. A. M., Morais, J. J. L., ... Judas, F. M. (2017). Fracture characterization of human cortical bone under mode II loading using the end-notched flexure test. *Medical and Biological Engineering and Computing*.
- Silva, M. J., Brodt, M. D., Wopenka, B., Thomopoulos, S., Williams, D., Wassen, M. H. M., ... Bank, R. A. (2006). Decreased collagen organization and content are associated with reduced strength of demineralized and intact bone in the SAMP6 mouse. *Journal of Bone and Mineral Research*.
- Simmons, E. D., Pritzker, K. P. H., & Grynblas, M. D. (1991). Age-related

- changes in the human femoral cortex. *Journal of Orthopaedic Research*.
- Skedros, J. G., Holmes, J. L., Vajda, E. G., & Bloebaum, R. D. (2005). Cement lines of secondary osteons in human bone are not mineral-deficient: New data in a historical perspective. *Anatomical Record - Part A Discoveries in Molecular, Cellular, and Evolutionary Biology*.
- Su, X. T., Yang, Z. J., & Liu, G. H. (2010). Monte Carlo simulation of complex cohesive fracture in random heterogeneous quasi-brittle materials: A 3D study. *International Journal of Solids and Structures*, 47(17), 2336–2345.
- Sugita, N., Shu, L., Shimada, T., Oshima, M., Kizaki, T., & Mitsuishi, M. (2017). Novel surgical machining via an impact cutting method based on fracture analysis with a discontinuum bone model. *CIRP Annals - Manufacturing Technology*.
- Tang, S. Y., Allen, M. R., Phipps, R., Burr, D. B., & Vashishth, D. (2009). Changes in non-enzymatic glycation and its association with altered mechanical properties following 1-year treatment with risedronate or alendronate. *Osteoporosis International*.
- Tennyson, R. C., Ewert, R., & Niranjana, V. (1972). Dynamic viscoelastic response of bone. *Experimental Mechanics*.
- Thompson, D. D. (1980). Age changes in bone mineralization, cortical thickness, and Haversian canal area. *Calcified Tissue International*.
- Tjhia, C. K., Odvina, C. V., Rao, D. S., Stover, S. M., Wang, X., & Fyhrie, D. P. (2011). Mechanical property and tissue mineral density differences among severely suppressed bone turnover (SSBT) patients, osteoporotic patients, and normal subjects. *Bone*.
- Tobergte, D. R., & Curtis, S. (2013). *Introductory biomechanics from cells to organisms*. *Journal of Chemical Information and Modeling*.
- Tong, W., Glimcher, M. J., Katz, J. L., Kuhn, L., & Eppell, S. J. (2003). Size and

- shape of mineralites in young bovine bone measured by atomic force microscopy. In *Calcified Tissue International*.
- Turunen, M. J., Kaspersen, J. D., Olsson, U., Guizar-Sicairos, M., Bech, M., Schaff, F., ... Isaksson, H. (2016). Bone mineral crystal size and organization vary across mature rat bone cortex. *Journal of Structural Biology*, 195(3), 337–344.
- Uppuganti, S., Granke, M., Makowski, A. J., Does, M. D., & Nyman, J. S. (2016). Age-related changes in the fracture resistance of male Fischer F344 rat bone. *Bone*.
- Ural, A., & Vashishth, D. (2007). Effects of intracortical porosity on fracture toughness in aging human bone: a microCT-based cohesive finite element study. *Journal of Biomechanical Engineering*.
- Ural, Ani, & Mischinski, S. (2013). Multiscale modeling of bone fracture using cohesive finite elements. *Engineering Fracture Mechanics*, 103, 141–152.
- Ural, Ani, & Vashishth, D. (2006). Cohesive finite element modeling of age-related toughness loss in human cortical bone. *Journal of Biomechanics*, 39(16), 2974–2982.
- Ural, Ani, & Vashishth, D. (2007). Anisotropy of age-related toughness loss in human cortical bone: A finite element study. *Journal of Biomechanics*, 40(7), 1606–1614.
- Ural, Ani, Zioupos, P., Buchanan, D., & Vashishth, D. (2011). The effect of strain rate on fracture toughness of human cortical bone: a finite element study. *Journal of the Mechanical Behavior of Biomedical Materials*, 4(7), 1021–1032.
- Valliappan, S., Svensson, N. L., & Wood, R. D. (1977). Three dimensional stress analysis of the human femur. *Computers in Biology and Medicine*.
- Van Buskirk, W. C., Cowin, S. C., & Ward, R. N. (2009). Ultrasonic

- Measurement of Orthotropic Elastic Constants of Bovine Femoral Bone. *Journal of Biomechanical Engineering*.
- Vashishth, D., Behiri, J. C., & Bonfield, W. (1997). Crack growth resistance in cortical bone: Concept of microcrack toughening. *Journal of Biomechanics*, 30(8), 763–769.
- Vashishth, D., Tanner, K. E., & Bonfield, W. (2003). Experimental validation of a microcracking-based toughening mechanism for cortical bone. *Journal of Biomechanics*, 36(1), 121–124.
- Vashishth, D., Gibson, G. J., Khoury, J. I., Schaffler, M. B., Kimura, J., & Fyhrie, D. P. (2001). Influence of nonenzymatic glycation on biomechanical properties of cortical bone. *Bone*.
- Vashishth, Deepak. (2004). Rising crack-growth-resistance behavior in cortical bone: Implications for toughness measurements. *Journal of Biomechanics*, 37(6), 943–946.
- Vichnin, H. H., & Batterman, S. C. (1986). Stress analysis and failure prediction in the proximal femur before and after total hip replacement. *J Biomech Eng*.
- Vincentelli, R., & Grigoroy, M. (1985). The effect of Haversian remodeling on the tensile properties of human cortical bone. *Journal of Biomechanics*.
- Voide, R., Schneider, P., Stauber, M., Wyss, P., Stampanoni, M., Sennhauser, U., ... Müller, R. (2009). Time-lapsed assessment of microcrack initiation and propagation in murine cortical bone at submicrometer resolution. *Bone*, 45(2), 164–173.
- Vukicevic, A. M., Jovicic, G. R., Jovicic, M. N., Milicevic, V. L., & Filipovic, N. D. (2018). Assessment of cortical bone fracture resistance curves by fusing artificial neural networks and linear regression. *Computer Methods in Biomechanics and Biomedical Engineering*.

- Wachtel, E., & Weiner, S. (1994). Small-angle x- ray scattering study of dispersed crystals from bone and tendon. *Journal of Bone and Mineral Research*.
- Wachter, N. ., Krischak, G. ., Mentzel, M., Sarkar, M. ., Ebinger, T., Kinzl, L., ... Augat, P. (2002). Correlation of bone mineral density with strength and microstructural parameters of cortical bone in vitro. *Bone*, 31(1), 90–95.
- Wagermaier, W., Klaushofer, K., & Fratzl, P. (2015). Fragility of Bone Material Controlled by Internal Interfaces. *Calcified Tissue International*, 97(3), 201–212.
- Wall, J. C., Chatterji, S. K., & Jeffery, J. W. (1979). Age-related changes in the density and tensile strength of human femoral cortical bone. *Calcified Tissue International*.
- Wang, X. J., Chen, X. B., Hodgson, P. D., & Wen, C. E. (2006). Elastic modulus and hardness of cortical and trabecular bovine bone measured by nanoindentation. *Transactions of Nonferrous Metals Society of China (English Edition)*.
- Wang, X., Shen, X., Li, X., & Mauli Agrawal, C. (2002). Age-related changes in the collagen network and toughness of bone. *Bone*, 31(1), 1–7.
- Wang, Xiaodu, & Ni, Q. (2003). Determination of cortical bone porosity and pore size distribution using a low field pulsed NMR approach. *Journal of Orthopaedic Research*.
- Wang, Z., Vashishth, D., & Picu, R. C. (2018). Bone toughening through stress-induced non-collagenous protein denaturation. *Biomechanics and Modeling in Mechanobiology*, 17(4), 1093–1106.
- Weaver, D. S. (2002). Skeletal tissue mechanics. *American Journal of Physical Anthropology*.
- Weiner, S., & Wagner, H. D. (1998). THE MATERIAL BONE: Structure-

- Mechanical Function Relations. *Annual Review of Materials Science*.
- Yang, Q. D., Cox, B. N., Nalla, R. K., & Ritchie, R. O. (2006a). Fracture length scales in human cortical bone: The necessity of nonlinear fracture models. *Biomaterials*, 27(9), 2095–2113.
- Yang, Q. D., Cox, B. N., Nalla, R. K., & Ritchie, R. O. (2006b). Re-evaluating the toughness of human cortical bone. *Bone*.
- Yeni, Y. N., Brown, C. U., Wang, Z., & Norman, T. L. (1997). The influence of bone morphology on fracture toughness of the human femur and tibia. *Bone*.
- Yeni, Y. N., & Norman, T. L. (2000). Fracture toughness of human femoral neck: Effect of microstructure, composition, and age. *Bone*.
- Yeni, Yener N., & Fyhrie, D. P. (2003). A rate-dependent microcrack-bridging model that can explain the strain rate dependency of cortical bone apparent yield strength. *Journal of Biomechanics*.
- Yeni, Yener N., & Norman, T. L. (2000). Calculation of porosity and osteonal cement line effects on the effective fracture toughness of cortical bone in longitudinal crack growth. *Journal of Biomedical Materials Research*, 51(3), 504–509.
- Yoon, H. S., & Lawrence Katz, J. (1976). Ultrasonic wave propagation in human cortical bone-II. Measurements of elastic properties and microhardness. *Journal of Biomechanics*.
- Yoshino, M., Imaizumi, K., Miyasaka, S., & Seta, S. (1994). Histological estimation of age at death using microradiographs of humeral compact bone. *Forensic Science International*, 64(2–3), 191–198.
- Zhang, L., Richardson, M., & Mendis, P. (2012). Role of chemical and mechanical stimuli in mediating bone fracture healing. *Clinical and Experimental Pharmacology and Physiology*.

- Zimmermann, E. A., Busse, B., & Ritchie, R. O. (2015). The fracture mechanics of human bone: influence of disease and treatment. *BoneKEy Reports*, 4(July), 1–13.
- Zimmermann, E. A., Launey, M. E., Barth, H. D., & Ritchie, R. O. (2009). Mixed-mode fracture of human cortical bone. *Biomaterials*, 30(29), 5877–5884.
- Zimmermann, E. A., Schaible, E., Gludovatz, B., Schmidt, F. N., Riedel, C., Krause, M., ... Busse, B. (2016). Intrinsic mechanical behavior of femoral cortical bone in young, osteoporotic and bisphosphonate-treated individuals in low- and high energy fracture conditions. *Nature Publishing Group*, (October 2015), 1–12.
- Ziopoulos, P., & Currey, J. . (1998). Changes in the Stiffness, Strength, and Toughness of Human Cortical Bone With Age. *Bone*, 22(1), 57–66.
- Ziopoulos, P., Currey, J. D., & Hamer, A. J. (1999). The role of collagen in the declining mechanical properties of aging human cortical bone. *Journal of Biomedical Materials Research*.
- Ziv, V., & Weiner, S. (1994). Bone crystal sizes: A comparison of transmission electron microscopic and x-ray diffraction line width broadening techniques. *Connective Tissue Research*.
- Zysset, P. K., Edward Guo, X., Edward Hoffler, C., Moore, K. E., & Goldstein, S. A. (1999). Elastic modulus and hardness of cortical and trabecular bone lamellae measured by nanoindentation in the human femur. *Journal of Biomechanics*.
- Abdel-Wahab, A. A., Alam, K., & Silberschmidt, V. V. (2011). Analysis of anisotropic viscoelastoplastic properties of cortical bone tissues. *Journal of the Mechanical Behavior of Biomedical Materials*, 4(5), 807–820.

- Abdel-Wahab, A. A., Maligno, A. R., & Silberschmidt, V. V. (2012). Micro-scale modelling of bovine cortical bone fracture: Analysis of crack propagation and microstructure using X-FEM. *Computational Materials Science*, 52(1), 128–135.
- Abdel-wahab, A. A., & Silberschmidt, V. V. (2011). Numerical Modelling of Impact Fracture of Cortical Bone Tissue using X-FEM. *Journal of Theoretical and Applied Mechanics*, 49(3), 599–619.
- Abdelaziz, Y., Bendahane, K., & Baraka, A. (2011). Extended Finite Element Modeling: Basic Review and Programming. *Engineering*.
- Alfano, M., Furguiele, F., Leonardi, A., Maletta, C., & Paulino, G. H. (2007). Cohesive Zone Modeling of Mode I Fracture in Adhesive Bonded Joints. *Key Engineering Materials*.
- An, B., Liu, Y., Arola, D., & Zhang, D. (2011). Fracture toughening mechanism of cortical bone: An experimental and numerical approach. *Journal of the Mechanical Behavior of Biomedical Materials*, 4(7), 983–992.
- An, B., Zhao, X., Arola, D., & Zhang, D. (2014). Fracture analysis for biological materials with an expanded cohesive zone model. *Journal of Biomechanics*, 47(10), 2244–2248.
- Ashman, R. B., Cowin, S. C., Van Buskirk, W. C., & Rice, J. C. (1984). A continuous wave technique for the measurement of the elastic properties of cortical bone. *Journal of Biomechanics*.
- ASTM. (1997). E399-90. Standard test method for plane-strain fracture toughness of metallic materials. *1991 Annual Book of ASTM Standards*, 3(Reapproved), 451–485.
- Bailey, A. J., Sims, T. J., Ebbesen, E. N., Mansell, J. P., Thomsen, J. S., & Mosekilde, L. (1999). Age-related changes in the biochemical properties of human cancellous bone collagen: Relationship to bone strength. *Calcified*

Tissue International.

- Bailey, Allen J., Paul, R. G., & Knott, L. (1998). Mechanisms of maturation and ageing of collagen. *Mechanisms of Ageing and Development*.
- Barrera, J. W., Le Cabec, A., & Barak, M. M. (2016). The orthotropic elastic properties of fibrolamellar bone tissue in juvenile white-tailed deer femora. *Journal of Anatomy*, 229(4), 568–576.
- Bell, K. L., Loveridge, N., Jordan, G. R., Power, J., Constant, C. R., & Reeve, J. (2000). A novel mechanism for induction of increased cortical porosity in cases of intracapsular hip fracture. *Bone*.
- Bell, K. L., Loveridge, N., Power, J., Garrahan, N., Meggitt, B. F., & Reeve, J. (1999). Regional differences in cortical porosity in the fractured femoral neck. *Bone*.
- Bell, Karen L., Loveridge, N., Reeve, J., Thomas, C. D. L., Feik, S. A., & Clement, J. G. (2001). Super-osteons (remodeling clusters) in the cortex of the femoral shaft: Influence of age and gender. *Anatomical Record*, 264(4), 378–386.
- Bella, J., Brodsky, B., & Berman, H. M. (1995). Hydration structure of a collagen peptide. *Structure*.
- Belytschko, T., & Black, T. (1999). Elastic crack growth in finite elements with minimal remeshing. *International Journal for Numerical Methods in Engineering*.
- Bernhard, A., Milovanovic, P., Zimmermann, E. A., Hahn, M., Djonic, D., Krause, M., ... Busse, B. (2013). Micro-morphological properties of osteons reveal changes in cortical bone stability during aging, osteoporosis, and bisphosphonate treatment in women. *Osteoporosis International*, 24(10), 2671–2680.
- Black, J., Mattson, R., & Korostoff, E. (1974). Haversian osteons: Size,

- distribution, internal structure, and orientation. *Journal of Biomedical Materials Research*.
- Bonfield, W. (1987). Advances in the fracture mechanics of cortical bone. *Journal of Biomechanics*, 20(11–12), 1071–1081.
- Boskey, A. L., Gadaleta, S., Gundberg, C., Doty, S. B., Ducky, P., & Karsenty, G. (1998). Fourier transform infrared microspectroscopic analysis of bones of osteocalcin-deficient mice provides insight into the function of osteocalcin. *Bone*.
- Bousson, V., Meunier, A., Bergot, C., Vicaut, E., Rocha, M. A., Morais, M. H., ... Laredo, J. D. (2001). Distribution of intracortical porosity in human midfemoral cortex by age and gender. *Journal of Bone and Mineral Research*.
- Boyce, T. M., Fyhrie, D. P., Glotkowski, M. C., Radin, E. L., & Schaffler, M. B. (1998). Damage type and strain mode associations in human compact bone bending fatigue. *Journal of Orthopaedic Research*.
- Boyde, A., Hendel, P., Hendel, R., Maconnachie, E., & Jones, S. J. (1990). Human cranial bone structure and the healing of cranial bone grafts: a study using backscattered electron imaging and confocal microscopy. *Anatomy and Embryology*, 181(3), 235–251.
- Britz, H. M., Thomas, C. D. L., Clement, J. G., & Cooper, D. M. L. (2009). The relation of femoral osteon geometry to age, sex, height and weight. *Bone*.
- Brodsky, B., & Persikov, A. V. (2005). Molecular structure of the collagen triple helix. *Advances in Protein Chemistry*.
- Budyn, E. (2007). Multiscale Modeling of Human Cortical Bone: Aging and Failure Studies. *Materials Research Society Symposium Proceedings*.
- Budyn, E., Hoc, T., & Jonvaux, J. (2008). Fracture strength assessment and aging signs detection in human cortical bone using an X-FEM multiple

- scale approach. *Computational Mechanics*, 42(4), 579–591.
- Budyn, É., & Hoc, T. (2010). Analysis of micro fracture in human Haversian cortical bone under transverse tension using extended physical imaging. *International Journal for Numerical Methods in Engineering*, 82(8), 940–965.
- Budyn, É., & Hoc, T. (2007a). Multiple scale modeling for cortical bone fracture in tension using X-FEM. *Revue Européenne de Mécanique Numérique*, 16(2), 213–236.
- Budyn, É., & Hoc, T. (2007b). Multiple scale modeling for cortical bone fracture in tension using X-FEM. *Revue Européenne de Mécanique Numérique*, 16(March 2015), 213–236.
- Budyn, É., & Hoc, T. (2007). Multiple scale modeling for cortical bone fracture in tension using X-FEM. *Revue Européenne de Mécanique Numérique*, 16(March 2015), 213–236.
- Burghardt, A. J., Kazakia, G. J., Ramachandran, S., Link, T. M., & Majumdar, S. (2010). Age- and gender-related differences in the geometric properties and biomechanical significance of intracortical porosity in the distal radius and tibia. *Journal of Bone and Mineral Research*.
- Burnell, J. M., Teubner, E. J., & Miller, A. G. (1980). Normal maturational changes in bone matrix, mineral, and crystal size in the rat. *Calcified Tissue International*.
- Burr, D. B. (2002). The contribution of the organic matrix to bone's material properties. *Bone*.
- Burr, David B., Schaffler, M. B., & Frederickson, R. G. (1988). Composition of the cement line and its possible mechanical role as a local interface in human compact bone. *Journal of Biomechanics*, 21(11).
- Busse, B., Hahn, M., Schinke, T., Püschel, K., Duda, G. N., & Amling, M. (2010). Reorganization of the femoral cortex due to age-, sex-, and

- endoprosthetic-related effects emphasized by osteonal dimensions and remodeling. *Journal of Biomedical Materials Research - Part A*.
- Carnelli, D., Lucchini, R., Ponzoni, M., Contro, R., & Vena, P. (2011). Nanoindentation testing and finite element simulations of cortical bone allowing for anisotropic elastic and inelastic mechanical response. *Journal of Biomechanics*, *44*(10), 1852–1858.
- Chan, K. S., Lee, Y. D., Nicolella, D. P., Furman, B. R., Wellinghoff, S., & Rawls, R. (2007). Improving fracture toughness of dental nanocomposites by interface engineering and micromechanics. *Engineering Fracture Mechanics*, *74*(12), 1857–1871.
- Chan, Kwai S., Chan, C. K., & Nicolella, D. P. (2009). Relating crack-tip deformation to mineralization and fracture resistance in human femur cortical bone. *Bone*, *45*(3), 427–434.
- Cosman, F., de Beur, S. J., LeBoff, M. S., Lewiecki, E. M., Tanner, B., Randall, S., & Lindsay, R. (2014). Clinician's Guide to Prevention and Treatment of Osteoporosis. *Osteoporosis International*.
- Cowin, S. C., Moss-Salentijn, L., & Moss, M. L. (1991). Candidates for the Mechanosensory System in Bone. *Journal of Biomechanical Engineering*.
- Cowin, S., & Telega, J. (2003). Bone Mechanics Handbook, 2nd Edition. -. *Applied Mechanics Reviews*.
- Cox, B. N., & Yang, Q. (2007). Cohesive zone models of localization and fracture in bone. *Engineering Fracture Mechanics*.
- Cramer, J. A., Gold, D. T., Silverman, S. L., & Lewiecki, E. M. (2007). A systematic review of persistence and compliance with bisphosphonates for osteoporosis. *Osteoporosis International*.
- Currey, J. D. (1988). The effect of porosity and mineral content on the Young's modulus of elasticity of compact bone. *Journal of Biomechanics*.

- Currey, J. D. (2003). The many adaptations of bone. *Journal of Biomechanics*, 36(10), 1487–1495.
- Currey, John D. (2012). The structure and mechanics of bone. *Journal of Materials Science*.
- Currey, John D., Brear, K., & Zioupos, P. (1996). The effects of ageing and changes in mineral content in degrading the toughness of human femora. *Journal of Biomechanics*.
- Da Costa Gómez, T. M., Barrett, J. G., Sample, S. J., Radtke, C. L., Kalscheur, V. L., Lu, Y., ... Muir, P. (2005). Up-regulation of site-specific remodeling without accumulation of microcracking and loss of osteocytes. *Bone*.
- Dassault. (2016). ABAQUS Documentation. *ABAQUS/CAE Documentation*.
- Davies, E., Muller, K. H., Wong, W. C., Pickard, C. J., Reid, D. G., Skepper, J. N., & Duer, M. J. (2014). Citrate bridges between mineral platelets in bone. *Proceedings of the National Academy of Sciences*.
- Demirtas, A., Curran, E., & Ural, A. (2016). Assessment of the effect of reduced compositional heterogeneity on fracture resistance of human cortical bone using finite element modeling. *Bone*, 91, 92–101.
- Dickenson, R., Hutton, W., & Stott. (2018). The mechanical properties of bone in osteoporosis. *The Journal of Bone and Joint Surgery. British Volume*.
- Doblaré, M., García, J. M., & Gómez, M. J. (2004). Modelling bone tissue fracture and healing: A review. *Engineering Fracture Mechanics*.
- Dong, X. N., & Guo, X. E. (2004). The dependence of transversely isotropic elasticity of human femoral cortical bone on porosity. *Journal of Biomechanics*, 37(8), 1281–1287.
- Dourado, N., Pereira, F. A. M., De Moura, M. F. S. F., Morais, J. J. L., & Dias, M. I. R. (2013). Bone fracture characterization using the end notched flexure test. *Materials Science and Engineering C*, 33(1), 405–410.

- Dragomir-Daescu, D., Op Den Buijs, J., McEligot, S., Dai, Y., Entwistle, R. C., Salas, C., ... Amin, S. (2011). Robust QCT/FEA models of proximal femur stiffness and fracture load during a sideways fall on the hip. *Annals of Biomedical Engineering*, 39(2), 742–755.
- eFunda: Stress Intensity Factor, K. (n.d.).
- El Sallah, Z. M., Smail, B., Abderahmane, S., Bouiadjra, B. B., & Boualem, S. (2016). Numerical simulation of the femur fracture under static loading. *Structural Engineering and Mechanics*.
- Evans, F. G. (1976). Mechanical properties and histology of cortical bone from younger and older men. *The Anatomical Record*.
- Fan, Z., Swadener, J. G., Rho, J. Y., Roy, M. E., & Pharr, G. M. (2002). Anisotropic properties of human tibial cortical bone as measured by nanoindentation. *Journal of Orthopaedic Research*.
- Fantner, G. E., Hassenkam, T., Kindt, J. H., Weaver, J. C., Birkedal, H., Pechenik, L., ... Hansma, P. K. (2005). Sacrificial bonds and hidden length dissipate energy as mineralized fibrils separate during bone fracture. *Nature Materials*, 4(8), 612–616.
- Ferretti, M., Palumbo, C., Contri, M., & Marotti, G. (2002). Static and dynamic osteogenesis: Two different types of bone formation. *Anatomy and Embryology*.
- Franzoso, G., & Zysset, P. K. (2008). Elastic Anisotropy of Human Cortical Bone Secondary Osteons Measured by Nanoindentation. *Journal of Biomechanical Engineering*.
- Fratzl, P., Groschner, M., Vogl, G., Plenk, H., Eschberger, J., Fratzl-Zelman, N., ... Klaushofer, K. (1992). Mineral crystals in calcified tissues: A comparative study by SAXS. *Journal of Bone and Mineral Research*.
- Fratzl, Peter, Fratzl-Zelman, N., Klaushofer, K., Vogl, G., & Koller, K. (1991).

- Nucleation and growth of mineral crystals in bone studied by small-angle X-ray scattering. *Calcified Tissue International*.
- Garnero, P. (2015). The Role of Collagen Organization on the Properties of Bone. *Calcified Tissue International*, 97(3), 229–240.
- Gautieri, A., Buehler, M. J., & Redaelli, A. (2009). Deformation rate controls elasticity and unfolding pathway of single tropocollagen molecules. *Journal of the Mechanical Behavior of Biomedical Materials*.
- Giner, E., Belda, R., Arango, C., Vercher-Martínez, A., Tarancón, J. E., & Fuenmayor, F. J. (2017). Calculation of the critical energy release rate G_c of the cement line in cortical bone combining experimental tests and finite element models. *Engineering Fracture Mechanics*, 184, 168–182.
- Gourion-Arsiquaud, S., Faibish, D., Myers, E., Spevak, L., Compston, J., Hodsman, A., ... Boskey, A. L. (2009). Use of FTIR spectroscopic imaging to identify parameters associated with fragility fracture. *Journal of Bone and Mineral Research*.
- Granke, M., Grimal, Q., Saïed, A., Nauleau, P., Peyrin, F., & Laugier, P. (2011). Change in porosity is the major determinant of the variation of cortical bone elasticity at the millimeter scale in aged women. *Bone*, 49(5), 1020–1026.
- Granke, M., Makowski, A. J., Uppuganti, S., & Nyman, J. S. (2016). Prevalent role of porosity and osteonal area over mineralization heterogeneity in the fracture toughness of human cortical bone. *Journal of Biomechanics*, 49(13), 2748–2755.
- Guo, X. E., Liang, L. C., & Goldstein, S. A. (1998). Micromechanics of Osteonal Cortical Bone Fracture. *Journal of Biomechanical Engineering*.
- Gupta, H. S., Wagermaier, W., Zickler, G. A., Aroush, D. R. Ben, Funari, S. S., Roschger, P., ... Fratzl, P. (2005). Nanoscale deformation mechanisms in bone. *Nano Letters*.

- Hadjidakis, D. J., & Androulakis, I. I. (2006). Bone remodeling. *Ann N Y Acad Sci*, 1092, 385–396.
- Hambli, R., Bettamer, A., & Allaoui, S. (2012). Finite element prediction of proximal femur fracture pattern based on orthotropic behaviour law coupled to quasi-brittle damage. *Medical Engineering and Physics*, 34(2), 202–210.
- Hamed, E., Lee, Y., & Jasiuk, I. (2010). Multiscale modeling of elastic properties of cortical bone. In *Acta Mechanica*.
- Hang, F., Gupta, H. S., & Barber, A. H. (2014). Nanointerfacial strength between non-collagenous protein and collagen fibrils in antler bone. *Journal of the Royal Society Interface*.
- Hasegawa, K., Turner, C. H., & Burr, D. B. (1994). Contribution of collagen and mineral to the elastic anisotropy of bone. *Calcified Tissue International*.
- Hassenkam, T., Fantner, G. E., Cutroni, J. A., Weaver, J. C., Morse, D. E., & Hansma, P. K. (2004). High-resolution AFM imaging of intact and fractured trabecular bone. *Bone*.
- Heaney, R. P., Abrams, S., Dawson-Hughes, B., Looker, A., Looker, A., Marcus, R., ... Weaver, C. (2000). Peak bone mass. *Osteoporosis International*.
- Hillier, M. L., & Bell, L. S. (2007). Differentiating human bone from animal bone: A review of histological methods. *Journal of Forensic Sciences*, 52(2), 249–263.
- Hofmann, T., Heyroth, F., Meinhard, H., Fränzel, W., & Raum, K. (2006). Assessment of composition and anisotropic elastic properties of secondary osteon lamellae. *Journal of Biomechanics*.
- Hogan, H. A. (1992). Micromechanics modeling of Haversian cortical bone properties. *Journal of Biomechanics*.

- Holden, J. L., Clement, J. G., & Phakey, P. P. (1995). Age and temperature related changes to the ultrastructure and composition of human bone mineral. *Journal of Bone and Mineral Research*.
- Hui, S. L., Slemenda, C. W., & Johnston, C. C. (1988). Age and bone mass as predictors of fracture in a prospective study. *Journal of Clinical Investigation*.
- Idkaidek, A., & Jasiuk, I. (2017). Cortical bone fracture analysis using XFEM ??? case study. *International Journal for Numerical Methods in Biomedical Engineering*, 33(4), 1–16.
- Idkaidek, A., Koric, S., & Jasiuk, I. (2017). Fracture analysis of multi-osteon cortical bone using XFEM. *Computational Mechanics*, 1–14.
- Ishtiaq, S., Fogelman, I., & Hampson, G. (2015). Treatment of post-menopausal osteoporosis: Beyond bisphosphonates. *Journal of Endocrinological Investigation*, 38(1), 13–29.
- Jasiuk, I., Sabet, F. A., Najafi, A. R., & Hamed, E. (2015). Modelling of bone fracture and strength at different length scales: a review. *Interface Focus*, 6, 20–30.
- Jee, W. S. S. (2001). Integrated Bone Tissue Physiology: Anatomy and Physiology. In *Bone Mechanics Handbook*.
- Johnson, T. P. M., Socrate, S., & Boyce, M. C. (2010). A viscoelastic, viscoplastic model of cortical bone valid at low and high strain rates. *Acta Biomaterialia*, 6(10), 4073–4080.
- Katsamanis, F., & Raftopoulos, D. D. (1990). Determination of mechanical properties of human femoral cortical bone by the Hopkinson bar stress technique. *Journal of Biomechanics*.
- Keller, T. S., Mao, Z., & Spengler, D. M. (1990). Young's modulus, bending strength, and tissue physical properties of human compact bone. *Journal*

of Orthopaedic Research.

- Koester, K. J., Ager, J. W., & Ritchie, R. O. (2008). The true toughness of human cortical bone measured with realistically short cracks. *Nature Materials*, 7(8), 672–677.
- Koester, K. J., Barth, H. D., & Ritchie, R. O. (2011). Effect of aging on the transverse toughness of human cortical bone: Evaluation by R-curves. *Journal of the Mechanical Behavior of Biomedical Materials*, 4(7), 1504–1513.
- Lai, Y. M., Qin, L., Hung, V. W. Y., & Chan, K. M. (2005). Regional differences in cortical bone mineral density in the weight-bearing long bone shaft - A pQCT study. *Bone*.
- Lakes, R. S., & Katz, J. L. (2018). Viscoelastic properties of bone. In *Natural and living biomaterials* (pp. 61–87). CRC Press.
- Landis, W. J., Song, M. J., Leith, A., McEwen, L., & McEwen, B. F. (1993). Mineral and organic matrix interaction in normally calcifying tendon visualized in three dimensions by high-voltage electron microscopic tomography and graphic image reconstruction. *Journal of Structural Biology*.
- Lang, S. B. (1970). Ultrasonic Method for Measuring Elastic Coefficients of Bone and Results on Fresh and Dried Bovine Bones. *IEEE Transactions on Biomedical Engineering*.
- Lanyon, L. E. (1993). Osteocytes, strain detection, bone modeling and remodeling. *Calcified Tissue International*.
- Launey, M. E., Buehler, M. J., & Ritchie, R. O. (2010). *On the Mechanistic Origins of Toughness in Bone. Annual Review of Materials Research* (Vol. 40).
- Laval-Jeantet, A. M., Bergot, C., Carroll, R., & Garcia-Schaefer, F. (1983).

- Cortical bone senescence and mineral bone density of the humerus. *Calcified Tissue International*.
- Lawrence Katz, J., Yoon, H. S., Lipson, S., Maharidge, R., Meunier, A., & Christel, P. (1984). The effects of remodeling on the elastic properties of bone. *Calcified Tissue International*.
- Lewis, J. L., & Goldsmith, W. (1975). The dynamic fracture and prefracture response of compact bone by split Hopkinson bar methods. *Journal of Biomechanics*.
- Li, S., Abdel-Wahab, A., Demirci, E., & Silberschmidt, V. V. (2013a). Fracture process in cortical bone: X-FEM analysis of microstructured models. *International Journal of Fracture*, 184(1–2), 43–55.
- Li, S., Abdel-Wahab, A., Demirci, E., & Silberschmidt, V. V. (2013b). Fracture process in cortical bone: X-FEM analysis of microstructured models. In *International Journal of Fracture* (Vol. 184, pp. 43–55).
- Li, S., Demirci, E., & Silberschmidt, V. V. (2013a). Variability and anisotropy of mechanical behavior of cortical bone in tension and compression. *Journal of the Mechanical Behavior of Biomedical Materials*, 21, 109–120.
- Li, S., Demirci, E., & Silberschmidt, V. V. (2013b). Variability and anisotropy of mechanical behavior of cortical bone in tension and compression. *Journal of the Mechanical Behavior of Biomedical Materials*, 21, 109–120.
- Lin, L., Samuel, J., Zeng, X., & Wang, X. (2017). Contribution of extrafibrillar matrix to the mechanical behavior of bone using a novel cohesive finite element model. *Journal of the Mechanical Behavior of Biomedical Materials*.
- Lin, Z. X., Xu, Z. H., An, Y. H., & Li, X. (2016). In situ observation of fracture behavior of canine cortical bone under bending. *Materials Science and Engineering C*, 62, 361–367.

- Liu, Y., Yan, G., Chen, S., & Chen, B. (2018). Effects of shape and direction of osteocyte lacunae on stress distribution of osteon. *IOP Conference Series: Materials Science and Engineering*, 423(1).
- Ma, Y. L., Dai, R. C., Sheng, Z. F., Jin, Y., Zhang, Y. H., Fang, L. N., ... Liao, E. Y. (2008). Quantitative associations between osteocyte density and biomechanics, microcrack and microstructure in OVX rats vertebral trabeculae. *Journal of Biomechanics*.
- Malik, C. L., Stover, S. M., Martin, R. B., & Gibeling, J. C. (2003). Equine cortical bone exhibits rising R-curve fracture mechanics. *Journal of Biomechanics*, 36(2), 191–198.
- Martin, B. (1993). Aging and strength of bone as a structural material. *Calcified Tissue International*.
- McCalden, R. W., McGeough, J. A., Barker, M. B., & Court-Brown, C. M. (1993). Age-related changes in the tensile properties of cortical bone. The relative importance of changes in porosity, mineralization, and microstructure. *The Journal of Bone and Joint Surgery. American Volume*, 75(8), 1193–1205.
- McCalden, R. W., McGlough, J. A., Barker, M. B., & Court-Brown, C. M. (1993). Age-related changes in the tensile properties of cortical bone. The relative importance of changes in porosity, mineralization and microstructure. *Journal of Bone and Joint Surgery - Series A*.
- McKee, M. D., & Nanci, A. (1996). Osteopontin at mineralized tissue interfaces in bone, teeth, and osseointegrated implants: Ultrastructural distribution and implications for mineralized tissue formation, turnover, and repair. *Microscopy Research and Technique*.
- Milovanovic, P., Rakocevic, Z., Djonic, D., Zivkovic, V., Hahn, M., Nikolic, S., ... Djuric, M. (2014). Nano-structural, compositional and micro-architectural

- signs of cortical bone fragility at the superolateral femoral neck in elderly hip fracture patients vs. healthy aged controls. *Experimental Gerontology*.
- Milovanovic, P., vom Scheidt, A., Mletzko, K., Sarau, G., Püschel, K., Djuric, M., ... Busse, B. (2018). Bone tissue aging affects mineralization of cement lines. *Bone*, *110*, 187–193.
- Milovanovic, P., Zimmermann, E. A., Riedel, C., Scheidt, A. vom, Herzog, L., Krause, M., ... Busse, B. (2015). Multi-level characterization of human femoral cortices and their underlying osteocyte network reveal trends in quality of young, aged, osteoporotic and antiresorptive-treated bone. *Biomaterials*, *45*, 46–55.
- Mirzaali, M. J., Schwiedrzik, J. J., Thaiwichai, S., Best, J. P., Michler, J., Zysset, P. K., & Wolfram, U. (2016). Mechanical properties of cortical bone and their relationships with age, gender, composition and microindentation properties in the elderly. *Bone*, *93*, 196–211.
- Mischinski, S., & Ural, A. (2011). Finite Element Modeling of Microcrack Growth in Cortical Bone. *Journal of Applied Mechanics*, *78*(4), 041016.
- Mischinski, S., & Ural, A. (2013). Interaction of microstructure and microcrack growth in cortical bone: A finite element study. *Computer Methods in Biomechanics and Biomedical Engineering*, *16*(1), 81–94.
- Mitchell, J., & van Heteren, A. H. (2016). A literature review of the spatial organization of lamellar bone. *Comptes Rendus - Palevol*, *15*(1–2), 23–31.
- Mohsin, S., O'Brien, F. J., & Lee, T. C. (2006). Osteonal crack barriers in ovine compact bone. *Journal of Anatomy*, *208*(1), 81–89.
- Morais, J. J. L., de Moura, M. F. S. F., Pereira, F. A. M., Xavier, J., Dourado, N., Dias, M. I. R., & Azevedo, J. M. T. (2010). The double cantilever beam test applied to mode I fracture characterization of cortical bone tissue. *Journal of the Mechanical Behavior of Biomedical Materials*, *3*(6), 446–

453.

- Mulhern, D. M. (2000). Rib remodeling dynamics in a skeletal population from Kulubnarti, Nubia. *American Journal of Physical Anthropology*, 111(4), 519–530.
- Mullins, L. P., Sassi, V., McHugh, P. E., & Bruzzi, M. S. (2009). Differences in the crack resistance of interstitial, osteonal and trabecular bone tissue. *Annals of Biomedical Engineering*, 37(12), 2574–2582.
- Muschler, G. F., Nakamoto, C., & Griffith, L. G. (2004). Engineering principles of clinical cell-based tissue engineering. *Journal of Bone and Joint Surgery - Series A*.
- Najafi, A. R., Arshi, A. R., Eslami, M. R., Fariborz, S., & Moeinzadeh, M. (2007). Haversian cortical bone model with many radial microcracks: An elastic analytic solution. *Medical Engineering and Physics*, 29(6), 708–717.
- Nalla, R. K., Kinney, J. H., & Ritchie, R. O. (2003). Mechanistic fracture criteria for the failure of human cortical bone. *Nature Materials*, 2(3), 164–168.
- Nalla, R. K., Kruzic, J. J., Kinney, J. H., Balooch, M., Ager, J. W., & Ritchie, R. O. (2006). Role of microstructure in the aging-related deterioration of the toughness of human cortical bone. *Materials Science and Engineering C*, 26(8), 1251–1260.
- Nalla, R. K., Kruzic, J. J., Kinney, J. H., & Ritchie, R. O. (2004). Effect of aging on the toughness of human cortical bone: Evaluation by R-curves. *Bone*, 35(6), 1240–1246.
- Nalla, R. K., Kruzic, J. J., Kinney, J. H., & Ritchie, R. O. (2005). Mechanistic aspects of fracture and R-curve behavior in human cortical bone. *Biomaterials*, 26(2), 217–231.
- Nalla, R. K., Kruzic, J. J., & Ritchie, R. O. (2004). On the origin of the toughness of mineralized tissue: Microcracking or crack bridging? *Bone*,

34(5), 790–798.

Nalla, R. K., Stölken, J. S., Kinney, J. H., & Ritchie, R. O. (2005). Fracture in human cortical bone: Local fracture criteria and toughening mechanisms.

Journal of Biomechanics, 38(7), 1517–1525.

Nguyen, V. P. (2014). An open source program to generate zero-thickness cohesive interface elements. *Advances in Engineering Software*, 74, 27–39.

NHS. (2015). Osteoporosis - NHS Choices.

Nicolella, D. P., Moravits, D. E., Gale, A. M., Bonewald, L. F., & Lankford, J.

(2006). Osteocyte lacunae tissue strain in cortical bone. *Journal of Biomechanics*, 39(9), 1735–1743.

Nicolella, D. P., Nicholls, A. E., Lankford, J., & Davy, D. T. (2001). Machine vision photogrammetry: A technique for measurement of microstructural strain in cortical bone. *Journal of Biomechanics*, 34(1), 135–139.

Nikel, O., Laurencin, D., McCallum, S. A., Gundberg, C. M., & Vashishth, D. (2013). NMR investigation of the role of osteocalcin and osteopontin at the organic-inorganic interface in bone. *Langmuir*.

Nyman, J. S., Ni, Q., Nicolella, D. P., & Wang, X. (2008). Measurements of mobile and bound water by nuclear magnetic resonance correlate with mechanical properties of bone. *Bone*.

O'Brien, F. J., Taylor, D., & Lee, T. C. (2005). The effect of bone microstructure on the initiation and growth of microcracks. *J. Orthop. Res.*, 23(2), 475–480.

Odetti, P., Rossi, S., Monacelli, F., Poggi, A., Cirnigliaro, M., Federici, M., & Federici, A. (2005). Advanced glycation end products and bone loss during aging. In *Annals of the New York Academy of Sciences*.

Olszta, M. J., Cheng, X., Jee, S. S., Kumar, R., Kim, Y. Y., Kaufman, M. J., ...

- Gower, L. B. (2007). Bone structure and formation: A new perspective. *Materials Science and Engineering R: Reports*.
- Oxlund, H., Mosekilde, L., & Ørtoft, G. (1996). Reduced concentration of collagen reducible cross links in human trabecular bone with respect to age and osteoporosis. *Bone*.
- Parfitt, A. M. (1998). Osteoclast precursors as leukocytes: Importance of the area code. *Bone*.
- Pietruszczak, S., Gdela, K., Webber, C. E., & Inglis, D. (2007). On the assessment of brittle-elastic cortical bone fracture in the distal radius. *Engineering Fracture Mechanics*.
- Pithioux, M., Lasaygues, P., & Chabrand, P. (2002). An alternative ultrasonic method for measuring the elastic properties of cortical bone. *Journal of Biomechanics*.
- Poundarik, A. A., Wu, P. C., Evis, Z., Sroga, G. E., Ural, A., Rubin, M., & Vashishth, D. (2015). A direct role of collagen glycation in bone fracture. *Journal of the Mechanical Behavior of Biomedical Materials*.
- Poundarik, A., Gundberg, C., & Vashishth, D. (2011). Non-collageneous proteins influence bone crystal size and morphology: A SAXS study. In *2011 IEEE 37th Annual Northeast Bioengineering Conference, NEBEC 2011*.
- Prendergast, P. J., & Huiskes, R. (1996). Microdamage and Osteocyte-Lacuna Strain in Bone: A Microstructural Finite Element Analysis. *Journal of Biomechanical Engineering*.
- Qin, Q. H., & Zhang, X. (2000). Crack deflection at an interface between dissimilar piezoelectric materials. *International Journal of Fracture*, 102(4), 355–370.
- Qiu, S., Rao, D. S., Palnitkar, S., & Parfitt, A. M. (2003). Reduced iliac

- cancellous osteocyte density in patients with osteoporotic vertebral fracture. *Journal of Bone and Mineral Research*.
- Qiu, T., Liu, Q., & Wang, J. (2005). Study on technology of recycling oxalic acid and hydrochloric acid in wastewater discharged from rare earth metallurgical factory. *Journal of Rare Earths*, 23(SUPPL. 2), 10–13.
- Raeisi Najafi, A., Arshi, A. R., Eslami, M. R., Fariborz, S., & Moeinzadeh, M. H. (2007). Micromechanics fracture in osteonal cortical bone: A study of the interactions between microcrack propagation, microstructure and the material properties. *Journal of Biomechanics*, 40(12), 2788–2795.
- Raeisi Najafi, Ahmad, Arshi, A. R., Saffar, K. P. A., Eslami, M. R., Fariborz, S., & Moeinzadeh, M. H. (2009). A fiber-ceramic matrix composite material model for osteonal cortical bone fracture micromechanics: Solution of arbitrary microcracks interaction. *Journal of the Mechanical Behavior of Biomedical Materials*, 2(3), 217–223.
- Rath Bonivitch, A., Bonewald, L. F., & Nicoletta, D. P. (2007). Tissue strain amplification at the osteocyte lacuna: A microstructural finite element analysis. *Journal of Biomechanics*.
- Rauch, F., Travers, R., Parfitt, A. M., & Glorieux, F. H. (2000). Static and dynamic bone histomorphometry in children with osteogenesis imperfecta. *Bone*.
- Reilly, D.T., & Burstein, A. H. (1975). The Elastic and Ultimate Properties of Compact Bone Tissue. *Journal of Biomechanics*, 8, 393–405.
- Reilly, Donald T., & Burstein, A. H. (1975a). The Elastic and Ultimate Properties of Compact Bone Tissue. *Journal of Biomechanics*, 8(6), 393–405.
- Reilly, Donald T., & Burstein, A. H. (1975b). The elastic and ultimate properties of compact bone tissue. *Journal of Biomechanics*, 8(6).

- Reilly, G. C. (2000). Observations of microdamage around osteocyte lacunae in bone. *Journal of Biomechanics*, 33(9), 1131–1134.
- Reilly, G. C., & Currey, J. D. (1999). The development of microcracking and failure in bone depends on the loading mode to which it is adapted. *Journal of Experimental Biology*, 202(5), 543–552.
- Rho, JY; Kuhn-Spearing, L; Zioupos, P. (1998). Mechanical properties and the herarchical structure of bone. *Medical Engineering and Physics*, 20(2), 92–102.
- Rho, J. Y., Zioupos, P., Currey, J. D., & Pharr, G. M. (1999). Variations in the individual thick lamellar properties within osteons by nanoindentation. *Bone*.
- Rho, J. Y., Zioupos, P., Currey, J. D., & Pharr, G. M. (2002). Microstructural elasticity and regional heterogeneity in human femoral bone of various ages examined by nano-indentation. *Journal of Biomechanics*, 35(2), 189–198.
- Rho, J Y, Currey, J. D., Zioupos, P., & Pharr, G. M. (2001). The anisotropic Young's modulus of equine secondary osteones and interstitial bone determined by nanoindentation. *The Journal of Experimental Biology*, 204(2001), 1775–1781.
- Rho, Jae Young. (1996). An ultrasonic method for measuring the elastic properties of human tibial cortical and cancellous bone. *Ultrasonics*.
- Rho, Jae Young, Kuhn-Spearing, L., & Zioupos, P. (1998). Mechanical properties and the hierarchical structure of bone. *Medical Engineering and Physics*, 20(2), 92–102.
- Rho, Jae Young, Tsui, T. Y., & Pharr, G. M. (1997). Elastic properties of human cortical and trabecular lamellar bone measured by nanoindentation. *Biomaterials*, 18(20), 1325–1330.

- Ritchie, R. O. (1999). Mechanisms of fatigue-crack propagation in ductile and brittle solids. In *International Journal of Fracture*.
- Ritchie, R. O., Kinney, J. H., Kruzic, J. J., & Nalla, R. K. (2005). A fracture mechanics and mechanistic approach to the failure of cortical bone. *Fatigue and Fracture of Engineering Materials and Structures*.
- Ritchie, Robert O, Djuric, M., & Amling, M. (2010). Decrease in the osteocyte lacunar density accompanied by hypermineralized lacunar occlusion reveals failure and delay of remodeling in aged human bone *”*, 1065–1075.
- Rodriguez-Florez, N., Carriero, A., & Shefelbine, S. J. (2017). The use of XFEM to assess the influence of intra-cortical porosity on crack propagation. *Computer Methods in Biomechanics and Biomedical Engineering*.
- Rybicki, E. F., Simonen, F. A., & Weis, E. B. (1972). On the mathematical analysis of stress in the human femur. *Journal of Biomechanics*.
- Sabet, F. A., Raeisi Najafi, A., Hamed, E., & Jasiuk, I. (2016). Modelling of bone fracture and strength at different length scales: a review. *Interface Focus*, 6(1), 20150055.
- Saito, M., Fujii, K., Soshi, S., & Tanaka, T. (2006). Reductions in degree of mineralization and enzymatic collagen cross-links and increases in glycation-induced pentosidine in the femoral neck cortex in cases of femoral neck fracture. *Osteoporosis International*.
- Saito, Mitsuru, Fujii, K., & Marumo, K. (2006). Degree of mineralization-related collagen crosslinking in the femoral neck cancellous bone in cases of hip fracture and controls. *Calcified Tissue International*.
- Saito, Mitsuru, Marumo, K., Fujii, K., & Ishioka, N. (1997). Single-column high-performance liquid chromatographic-fluorescence detection of immature, mature, and senescent cross-links of collagen. *Analytical Biochemistry*.
- Sasaki, N., Matsushima, N., Ikawa, T., Yamamura, H., & Fukuda, A. (1989).

- Orientation of bone mineral and its role in the anisotropic mechanical properties of bone-Transverse anisotropy. *Journal of Biomechanics*.
- Schaffler, M. B., Choi, K., & Milgrom, C. (1995). Aging and matrix microdamage accumulation in human compact bone. *Bone*, 17(6), 521–525.
- Schaffler, Mitchell B., & Burr, D. B. (1988). Stiffness of compact bone: Effects of porosity and density. *Journal of Biomechanics*.
- Schaffler, Mitchell B., Burr, D. B., & Frederickson, R. G. (1987). Morphology of the osteonal cement line in human bone. *The Anatomical Record*.
- Schwarcz, H. P., McNally, E. A., & Botton, G. A. (2014). Dark-field transmission electron microscopy of cortical bone reveals details of extrafibrillar crystals. *Journal of Structural Biology*.
- Shea, J. E., & Miller, S. C. (2005). Skeletal function and structure: Implications for tissue-targeted therapeutics. *Advanced Drug Delivery Reviews*.
- Silva, F. G. A., de Moura, M. F. S. F., Dourado, N., Xavier, J., Pereira, F. A. M., Morais, J. J. L., ... Judas, F. M. (2017). Fracture characterization of human cortical bone under mode II loading using the end-notched flexure test. *Medical and Biological Engineering and Computing*.
- Silva, M. J., Brodt, M. D., Wopenka, B., Thomopoulos, S., Williams, D., Wassen, M. H. M., ... Bank, R. A. (2006). Decreased collagen organization and content are associated with reduced strength of demineralized and intact bone in the SAMP6 mouse. *Journal of Bone and Mineral Research*.
- Simmons, E. D., Pritzker, K. P. H., & Grynblas, M. D. (1991). Age-related changes in the human femoral cortex. *Journal of Orthopaedic Research*.
- Skedros, J. G., Holmes, J. L., Vajda, E. G., & Bloebaum, R. D. (2005). Cement lines of secondary osteons in human bone are not mineral-deficient: New data in a historical perspective. *Anatomical Record - Part A Discoveries in Molecular, Cellular, and Evolutionary Biology*.

- Su, X. T., Yang, Z. J., & Liu, G. H. (2010). Monte Carlo simulation of complex cohesive fracture in random heterogeneous quasi-brittle materials: A 3D study. *International Journal of Solids and Structures*, 47(17), 2336–2345.
- Sugita, N., Shu, L., Shimada, T., Oshima, M., Kizaki, T., & Mitsuishi, M. (2017). Novel surgical machining via an impact cutting method based on fracture analysis with a discontinuum bone model. *CIRP Annals - Manufacturing Technology*.
- Tang, S. Y., Allen, M. R., Phipps, R., Burr, D. B., & Vashishth, D. (2009). Changes in non-enzymatic glycation and its association with altered mechanical properties following 1-year treatment with risedronate or alendronate. *Osteoporosis International*.
- Tennyson, R. C., Ewert, R., & Niranjana, V. (1972). Dynamic viscoelastic response of bone. *Experimental Mechanics*.
- Thompson, D. D. (1980). Age changes in bone mineralization, cortical thickness, and Haversian canal area. *Calcified Tissue International*.
- Tjha, C. K., Odvina, C. V., Rao, D. S., Stover, S. M., Wang, X., & Fyhrie, D. P. (2011). Mechanical property and tissue mineral density differences among severely suppressed bone turnover (SSBT) patients, osteoporotic patients, and normal subjects. *Bone*.
- Tobergte, D. R., & Curtis, S. (2013). *Introductory biomechanics from cells to organisms*. *Journal of Chemical Information and Modeling*.
- Tong, W., Glimcher, M. J., Katz, J. L., Kuhn, L., & Eppell, S. J. (2003). Size and shape of mineralites in young bovine bone measured by atomic force microscopy. In *Calcified Tissue International*.
- Turunen, M. J., Kaspersen, J. D., Olsson, U., Guizar-Sicairos, M., Bech, M., Schaff, F., ... Isaksson, H. (2016). Bone mineral crystal size and organization vary across mature rat bone cortex. *Journal of Structural*

Biology, 195(3), 337–344.

- Uppuganti, S., Granke, M., Makowski, A. J., Does, M. D., & Nyman, J. S. (2016). Age-related changes in the fracture resistance of male Fischer F344 rat bone. *Bone*.
- Ural, A., & Vashishth, D. (2007). Effects of intracortical porosity on fracture toughness in aging human bone: a microCT-based cohesive finite element study. *Journal of Biomechanical Engineering*.
- Ural, Ani, & Mischinski, S. (2013). Multiscale modeling of bone fracture using cohesive finite elements. *Engineering Fracture Mechanics*, 103, 141–152.
- Ural, Ani, & Vashishth, D. (2006). Cohesive finite element modeling of age-related toughness loss in human cortical bone. *Journal of Biomechanics*, 39(16), 2974–2982.
- Ural, Ani, & Vashishth, D. (2007). Anisotropy of age-related toughness loss in human cortical bone: A finite element study. *Journal of Biomechanics*, 40(7), 1606–1614.
- Ural, Ani, Zioupos, P., Buchanan, D., & Vashishth, D. (2011). The effect of strain rate on fracture toughness of human cortical bone: a finite element study. *Journal of the Mechanical Behavior of Biomedical Materials*, 4(7), 1021–1032.
- Valliappan, S., Svensson, N. L., & Wood, R. D. (1977). Three dimensional stress analysis of the human femur. *Computers in Biology and Medicine*.
- Van Buskirk, W. C., Cowin, S. C., & Ward, R. N. (2009). Ultrasonic Measurement of Orthotropic Elastic Constants of Bovine Femoral Bone. *Journal of Biomechanical Engineering*.
- Vashishth, D., Behiri, J. C., & Bonfield, W. (1997). Crack growth resistance in cortical bone: Concept of microcrack toughening. *Journal of Biomechanics*, 30(8), 763–769.

- Vashishth, D., Tanner, K. E., & Bonfield, W. (2003). Experimental validation of a microcracking-based toughening mechanism for cortical bone. *Journal of Biomechanics*, 36(1), 121–124.
- Vashishth, D., Gibson, G. J., Khoury, J. I., Schaffler, M. B., Kimura, J., & Fyhrie, D. P. (2001). Influence of nonenzymatic glycation on biomechanical properties of cortical bone. *Bone*.
- Vashishth, Deepak. (2004). Rising crack-growth-resistance behavior in cortical bone: Implications for toughness measurements. *Journal of Biomechanics*, 37(6), 943–946.
- Vichnin, H. H., & Batterman, S. C. (1986). Stress analysis and failure prediction in the proximal femur before and after total hip replacement. *J Biomech Eng*.
- Vincentelli, R., & Grigoroy, M. (1985). The effect of Haversian remodeling on the tensile properties of human cortical bone. *Journal of Biomechanics*.
- Voide, R., Schneider, P., Stauber, M., Wyss, P., Stampanoni, M., Sennhauser, U., ... Müller, R. (2009). Time-lapsed assessment of microcrack initiation and propagation in murine cortical bone at submicrometer resolution. *Bone*, 45(2), 164–173.
- Vukicevic, A. M., Jovicic, G. R., Jovicic, M. N., Milicevic, V. L., & Filipovic, N. D. (2018). Assessment of cortical bone fracture resistance curves by fusing artificial neural networks and linear regression. *Computer Methods in Biomechanics and Biomedical Engineering*.
- Wachtel, E., & Weiner, S. (1994). Small-angle x- ray scattering study of dispersed crystals from bone and tendon. *Journal of Bone and Mineral Research*.
- Wachter, N. ., Krischak, G. ., Mentzel, M., Sarkar, M. ., Ebinger, T., Kinzl, L., ... Augat, P. (2002). Correlation of bone mineral density with strength and

- microstructural parameters of cortical bone in vitro. *Bone*, 31(1), 90–95.
- Wagermaier, W., Klaushofer, K., & Fratzl, P. (2015). Fragility of Bone Material Controlled by Internal Interfaces. *Calcified Tissue International*, 97(3), 201–212.
- Wall, J. C., Chatterji, S. K., & Jeffery, J. W. (1979). Age-related changes in the density and tensile strength of human femoral cortical bone. *Calcified Tissue International*.
- Wang, X. J., Chen, X. B., Hodgson, P. D., & Wen, C. E. (2006). Elastic modulus and hardness of cortical and trabecular bovine bone measured by nanoindentation. *Transactions of Nonferrous Metals Society of China (English Edition)*.
- Wang, X., Shen, X., Li, X., & Mauli Agrawal, C. (2002). Age-related changes in the collagen network and toughness of bone. *Bone*, 31(1), 1–7.
- Wang, Xiaodu, & Ni, Q. (2003). Determination of cortical bone porosity and pore size distribution using a low field pulsed NMR approach. *Journal of Orthopaedic Research*.
- Wang, Z., Vashishth, D., & Picu, R. C. (2018). Bone toughening through stress-induced non-collagenous protein denaturation. *Biomechanics and Modeling in Mechanobiology*, 17(4), 1093–1106.
- Weaver, D. S. (2002). Skeletal tissue mechanics. *American Journal of Physical Anthropology*.
- Weiner, S., & Wagner, H. D. (1998). THE MATERIAL BONE: Structure-Mechanical Function Relations. *Annual Review of Materials Science*.
- Yang, Q. D., Cox, B. N., Nalla, R. K., & Ritchie, R. O. (2006a). Fracture length scales in human cortical bone: The necessity of nonlinear fracture models. *Biomaterials*, 27(9), 2095–2113.
- Yang, Q. D., Cox, B. N., Nalla, R. K., & Ritchie, R. O. (2006b). Re-evaluating

- the toughness of human cortical bone. *Bone*.
- Yeni, Y. N., Brown, C. U., Wang, Z., & Norman, T. L. (1997). The influence of bone morphology on fracture toughness of the human femur and tibia. *Bone*.
- Yeni, Y. N., & Norman, T. L. (2000). Fracture toughness of human femoral neck: Effect of microstructure, composition, and age. *Bone*.
- Yeni, Yener N., & Fyhrie, D. P. (2003). A rate-dependent microcrack-bridging model that can explain the strain rate dependency of cortical bone apparent yield strength. *Journal of Biomechanics*.
- Yeni, Yener N., & Norman, T. L. (2000). Calculation of porosity and osteonal cement line effects on the effective fracture toughness of cortical bone in longitudinal crack growth. *Journal of Biomedical Materials Research*, 51(3), 504–509.
- Yoon, H. S., & Lawrence Katz, J. (1976). Ultrasonic wave propagation in human cortical bone-II. Measurements of elastic properties and microhardness. *Journal of Biomechanics*.
- Yoshino, M., Imaizumi, K., Miyasaka, S., & Seta, S. (1994). Histological estimation of age at death using microradiographs of humeral compact bone. *Forensic Science International*, 64(2–3), 191–198.
- Zhang, L., Richardson, M., & Mendis, P. (2012). Role of chemical and mechanical stimuli in mediating bone fracture healing. *Clinical and Experimental Pharmacology and Physiology*.
- Zimmermann, E. A., Busse, B., & Ritchie, R. O. (2015). The fracture mechanics of human bone: influence of disease and treatment. *BoneKEy Reports*, 4(July), 1–13.
- Zimmermann, E. A., Launey, M. E., Barth, H. D., & Ritchie, R. O. (2009). Mixed-mode fracture of human cortical bone. *Biomaterials*, 30(29), 5877–

5884.

- Zimmermann, E. A., Schaible, E., Gludovatz, B., Schmidt, F. N., Riedel, C., Krause, M., ... Busse, B. (2016). Intrinsic mechanical behavior of femoral cortical bone in young , osteoporotic and bisphosphonate- treated individuals in low- and high energy fracture conditions. *Nature Publishing Group*, (October 2015), 1–12.
- Zioupos, P., & Currey, J. . (1998). Changes in the Stiffness, Strength, and Toughness of Human Cortical Bone With Age. *Bone*, 22(1), 57–66.
- Zioupos, P., Currey, J. D., & Hamer, A. J. (1999). The role of collagen in the declining mechanical properties of aging human cortical bone. *Journal of Biomedical Materials Research*.
- Ziv, V., & Weiner, S. (1994). Bone crystal sizes: A comparison of transmission electron microscopic and x-ray diffraction line width broadening techniques. *Connective Tissue Research*.
- Zysset, P. K., Edward Guo, X., Edward Hoffler, C., Moore, K. E., & Goldstein, S. A. (1999). Elastic modulus and hardness of cortical and trabecular bone lamellae measured by nanoindentation in the human femur. *Journal of Biomechanics*.